A MULTIPHASIC ASSESSMENT OF THE IMPACTS AND FATE OF PRISTINE AND INCIDENTALLY RELEASED SILVER NANOMATERIALS FROM TEXTILES IN MESO-SCALE TREATMENT WETLANDS

UNE ÉVALUATION MULTIPHASIQUE DES IMPACTS ET LE DEVENIR DES NANOMATÉRIAUX D'ARGENT VIERGE ET INCIDENTEL DES TEXTILES DANS DES MARAIS FILTRANTS D'ÉCHELLE MÉSOCOSMES

A Thesis Submitted to the Division of Graduate Studies

Of the Royal Military College of Canada

by

Anbareen Jan Farooq, B.Sc.E in Chemical Engineering

In Partial Fulfillment of the Requirements for the Degree of Doctor of Philosophy

November, 2023

For my parents, Dr. Mohamad Farooq and Dilshad Anjum Farooq

Acknowledgments

I would like to extend my thanks to my supervisor, Dr. Kela Weber, for the support he has shown me as his student. Your mentorship has been invaluable, and I am truly thankful for the opportunities you have provided me to grow both personally and professionally. As I reflect moving forward, I'm truly grateful for the experience I have had at RMC and at ESG under your guidance.

I would like to thank Dr. Iris Koch, Dr. Vincent Gagnon, Dr. Jacques Brisson, and Scott Wallace for their guidance and input with my research.

Thank you to Sarah Wallace, Dani Damasceno Silvera, Dr. Mark Button, and David Patch for your assistance in analyzing my samples.

Thank you to all those at the Environmental Sciences Research Group, whether past or present, who supported me along the way.

I would also like to thank Mhari Chamberlain for her invaluable work with imaging and data analysis. I also want to thank you for your words of encouragement and kindness over the years.

To all the many undergraduate students who assisted in my research. I thank you and wish you all the best.

To my friends, it would have been unimaginable to go through this time without your support.

Finally, I like to thank my family for their patience and encouragement as I worked through my graduate studies. To my parents, Dr. Mohamad Farooq and Dilshad Farooq, your enormous support has helped me through everything.

Abstract

Treatment wetland (TW) systems have become a popular nature-based alternative for decentralized wastewater treatment due to their low-cost, limited energy usage and ease of operation for individual homes and rural areas. The majority of pollutant degradation and transformation in these systems is attributed to the activity and productivity of their diverse microbial communities, primarily housed in biofilms. These systems, though originally designed for the treatment of domestic wastewater, are increasingly being used to treat more complex pollutants and emerging contaminants in wastewater streams, including silver nanomaterials. Silver nanomaterials are released from consumer products through anthropogenic use, enter TWs through wastewater streams, and generally considered toxic to ecological systems based on their antimicrobial properties.

The overall objective of this thesis was to evaluate the impacts and fate of incidental silver nanomaterials from commercial products to the microbial communities in the interstitial water and biofilm matrix in treatment wetlands mesocosms. To that end, a multiphasic study was developed in four phases. For the first phase, a meta-analysis was conducted to assess the current trends and the scalability of mesoscale studies. Following this, biofilm samples were harvested from established TW systems and imaged using both traditional light microscopy and environmental scanning electron microscopy (E-SEM). Morphological characteristics were quantified to develop a conceptual model for microscale TW biofilm dynamics. Thirdly, two in-situ exposure experiments at different concentration (0.1 mg Ag/L and 1 mg/L) were conducted using twenty-four batch-fed subsurface flow TW mesocosms, planted with *Phalaris arundinacea* monitored over a cumulative total of 217 days. Mesocosms were exposed to ionic silver, polyvinylpyrrolidone coated nanoparticles (pristine), or incidental silver nanomaterials released from textiles. The effects of the silver exposures were assessed in terms of the mesocosm water chemistry, water treatment performance, microbial activity/function/structure, and in-situ nanomaterial dynamics. Finally, the overall fate of silver within the mesocosms was determined through destructive sampling of the constructed wetland biofilm, plant roots and aboveground plant biomass. Gravel-associated and rhizospheric microbial biofilm were assessed for structural and function impacts.

The meta-analysis revealed that the global research field of treatment wetlands is expanding and diversifying its use of mesoscale system. Treatment performances of full-scale and meso-scale systems were comparable for the biochemical oxygen demand (BOD) removal rates. In the second phase, E-SEM images of biofilm revealed a structurally heterogenous morphology with features such as water channels and pores, which reached several microns in diameter. Through visual evidence and image analysis, a new more reflective conceptual model was developed to describe microscale TW biofilm dynamics and morphology. During the silver nanomaterial exposure periods, no significant changes were noted to for any metrics at 0.1 or 1 mg Ag/L suggesting the wetland mesocosms were resilient to silver. Following the exposure period, the TW mesocosms were dismantled showing the majority of silver was located in biofilm and predominately in the lower 30 – 60 cm layer. Investigating the microbial biofilm communities showed that functional and structural shifts occurred within the mesocosms due to the varying silver exposures. Although these functional and structural shifts occurred, no major loss of water treatment was seen throughout the study.

Résumé

Les marais filtrants artificiels (MFA) sont devenus une alternative populaire fondées sur la nature pour le traitement décentralisé des eaux usées en raison de leur coût peu élevé, consommation d'énergie limitée et convivialité pour les maisons individuelles et les zones rurales. La majorité de la dégradation et transformation des polluants dans ces systèmes est attribuée à l'activité et à la productivité de leurs diverses communautés microbiennes, principalement trouvées dans des biofilms. Ces systèmes, bien que conçus à l'origine pour le traitement des eaux usées domestiques, sont de plus en plus utilisés pour traiter des polluants complexes et des contaminants émergents, notamment les nanomatériaux d'argent dans les flux d'eaux usées. Les nanomatériaux d'argent sont rejetés des produits de consommation par l'utilisation anthropique et peuvent entrer dans les MFA par les eaux usées et sont généralement considérés comme toxiques pour les systèmes écologiques en raison de leurs propriétés antimicrobiennes.

L'objectif général de cette thèse était d'évaluer les impacts et le devenir des nanomatériaux d'argent fortuits provenant de produits commerciaux sur les communautés microbiennes des interstitielle de l'eau et du biofilm dans les mésocosmes des marais filtrants. À cette fin, une étude multiphasique a été réalisé en quatre phases. L'objectif général de cette thèse était d'évaluer les impacts et le devenir des nanomatériaux d'argent fortuits provenant de produits commerciaux sur les communautés microbiennes des interstitielle de l'eau et du biofilm dans les mésocosmes des marais filtrants. À cette fin, une étude multiphasique a été réalisé en quatre phases. Tout d'abord, une méta-analyse a été réalisée pour évaluer les tendances actuelles et l'évolutivité des études méso-échelle. Par la suite, des échantillons de biofilms ont été prélevés dans des systèmes de MFA établis et imités à l'aide de la microscopie optique traditionnelle et de la microscopie électronique à balayage environnemental (E-SEM). Les caractéristiques morphologiques ont été quantifiées afin d'élaborer un modèle conceptuel pour la dynamique du biofilm TW à l'échelle microscopique. En troisième lieu, deux expériences d'exposition in situ à différentes concentrations (0,1 mg Ag/L et 1 mg/L) ont été réalisées à l'aide de 24 mésocosmes TW d'écoulement souterrain nourris par lots, plantés de Phalaris arundinacea et surveillés pendant un total cumulé de 217 jours. Les mésocosmes ont été exposés à de l'argent ionique, à des nanoparticules revêtues de polyvinylpyrrolidone (vierges) ou à des nanomatériaux argentés incidentel libérés des textiles. Les effets de l'exposition à l'argent ont été évalués en fonction de la chimie de l'eau du mésocosme, du rendement du traitement de l'eau, de l'activité/fonction/structure microbienne et de la dynamique in situ des nanomatériaux. Enfin, le devenir de l'argent dans les mésocosmes a été déterminé par échantillonnage destructif du biofilm des MFAs, des racines végétales et de la biomasse végétale aérienne. Les effets structuraux et fonctionnels des biofilms microbiens associés au gravier et rhizosphériques ont été évalués.

La méta-analyse a révélé que le domaine de recherche mondial des marais filtrants artificiels se développe et diversifie l'utilisation des systèmes à méso-échelle. Les performances de traitement des systèmes à grande échelle et à méso-échelle étaient comparables en ce qui concerne les taux d'élimination de la demande biochimique en oxygène (DBO). Au cours de la deuxième phase, les images E-SEM du biofilm ont révélé une morphologie structurellement hétérogène avec des caractéristiques telles que des canaux d'eau et des pores, qui atteignent plusieurs microns de diamètre. Grâce à des preuves visuelles et à l'analyse d'images, un

nouveau modèle conceptuel plus réfléchi a été réalisé pour décrire la dynamique et la morphologie du biofilm TW à l'échelle microscopique. Pendant les périodes d'exposition aux nanomatériaux d'argent, aucun changement significatif n'a été observé pour les paramètres à 0,1 ou 1 mg Ag/L, ce qui suggère que les mésocosmes des MFA sont résistants à l'argent. Après la période d'exposition, les mésocosmes TW ont été démontés, montrant que la majorité de l'argent se trouvait dans le biofilm et principalement dans la couche inférieure de 30 à 60 cm. L'étude des communautés microbiennes du biofilm a montré que des changements fonctionnels et structurels se sont produits dans les mésocosmes en raison des différentes expositions à l'argent. Malgré ces changements fonctionnels et structurels, aucune perte majeure de traitement de l'eau n'a été observée tout au long de l'étude.

Table of Contents

List of Tables

List of Figures

Abbreviations and Acronyms

Acronym or Abbreviation	Definition
AA	Artificial Aeration
Ag-ENM	Silver Nanomaterials
BOD	Biochemical Oxygen Demand
CEC	Contaminants of Emerging Concern
CLPP	Community Level Physiological Profiling
COD	Chemical Oxygen Demand
CW	Constructed Wetlands
DO	Dissolved oxygen
EC	Electrical Conductivity
EC50	Effective Concentration
ENMs	Engineered Nanomaterials
EPS	Extracellular Polymeric Substances
E-SEM	Environmental Scanning Electron Microscopy
FDA	Fluorescein diacetate
FWS	Free Water Surface
GA	Gum Arabic
HLR	Hydraulic Loading Rate
HRT	Hydraulic Retention Time
HSSF	Horizontal Subsurface Flow
ICP-MS	Inductively Coupled Plasma - Mass Spectrometry
LC50	Lethal Concentration
MIC	Minimum Inhibitory Concentration
NP	Nanoparticles
NM	Nanomaterial
OCT	Optical Coherence tomography
ORP	Oxidative-Reductive (redox) Potential
PEC	Predicted Environmental Concentration
POP	Persistent Organic Pollutants
PVP	Polyvinyl Pyrrolidone
ROS	Radical Oxygen Species
SEM	Scanning Electron Microscope
TEM	Transmission Electron Microscopy
TN	Total Nitrogen
TP	Total Phosphorous
TW	Treatment Wetland
VF	Vertical Flow
WWTP	Wastewater Treatment Plant

1. Introduction

1.1 Background

In recent years, engineered nanomaterials (ENMs) have become widely acknowledged as an emerging contaminant of concern due to their potential release into the environment and wastewater streams through their lifecycle (Li et al., 2022). At the nano-scale (1-100nm), the large specific surface area (surface to volume ratio) of ENMs heightens their reactivity, driving their popular use in a number of products (Horikoshi and Serpone, 2013). The most prevalent type of ENM in use are silver nanomaterials (Ag-ENMs), employed due to their antimicrobial properties, which poses a potential risk for biological wastewater treatment systems, such as treatment wetlands.

Historically, natural wetlands (such as swamps or marshes) were used as convenient sites for wastewater discharge because of their innate ability to transform a wide range of pollutants (e.g. suspended solids, nitrogen, organic carbon, etc.) into harmless by-products as a result of their higher biological activity (Kadlec and Wallace, 2009; Mitsch and Gosselink, 2015). In favour of natural wetland ecosystem preservation, and recognizing the technology potential, the adoption of man-made treatment wetlands (TWs) over the last 60 years has been popularized for decentralized wastewater treatment (Vymazal, 2010). Similar to their natural counterparts, the physical, chemical and biological mechanisms that govern the removal processes in TWs include: adsorption, volatilization, precipitation, filtration, sedimentation, plant uptake, chemical networks, and, most importantly for the majority of pollutants, microbial-mediated pollutant degradation (Kadlec & Wallace, 2009).

TW microbial communities, which are housed in biofilms, are a major sink for Ag-ENMs entering in wastewater streams. Several studies have examine the effects of Ag-ENMs in TW mesocosms, but all thus far have focused on pristine spherical particles (Cao et al., 2021a; Huang et al., 2022). The toxicity of silver nanomaterials to these biofilm microbial communities depends on several factors including nanoparticle properties (e.g. size, coating, and shape); environmental factors (plants, pH, organic matter); and the biofilm itself (Sarkar, 2022). Ag-ENMs released from consumer products have a diverse range of morphologies and size distributions, being released as nanoparticles; aggregates; sheets; or silver ions (Benn et al., 2010; Gagnon et al., 2019). Thuptimdang et al. (2017) found that morphological properties of biofilm (roughness) can enhance the toxic effects of silver nanomaterials to biofilms. However, TW biofilm morphology has not been characterized in the field and is often assumed to a be a fixed film with a small amount of roughness.

1.2 Objectives

In order to address the identified knowledge gaps, several objectives were identified:

A. Evaluate the current trends and relevancy of meso-scale treatment wetlands as a comparative system to the full-scale.

B. Characterize the morphological characteristics of treatment wetland biofilm to more accurately understand pollutant interactions.

C. Examine the in-situ impacts and removal of incidental silver nanomaterials in treatment wetland mesocosms.

D. Assess the impacts and fate of incidental nanomaterials in treatment wetland biofilms.

1.3 Thesis Organization

This thesis is a presented in a manuscript style, consisting of seven chapters plus four appendices, as listed below.

Chapter 1 offers a brief background on the research topic, objectives and organizational structure of the thesis.

Chapter 2 provides a literature review of the relevant background information on treatment wetlands and silver nanomaterials.

Chapter 3 details a meta-analysis describing current global trends, use and potential scalability of meso-scale treatment wetlands used in research.

Chapter 4 provides a detailed assessment of biofilm architecture in treatment wetland mesocosms.

Chapter 5 summarizes the effects and observed nanomaterial dynamics during in-situ silver nanomaterial exposures in treatment wetland mesocosms.

Chapter 6 summarizes the fate and effects of silver nanomaterial exposures on treatment wetland mesocosm biofilm

Chapter 7 summarizes the principal outcomes of the thesis and provides recommendations for future work.

Appendix A contains supplemental information for Chapter 3.

Appendix B contains supplemental information for Chapter 4.

Appendix C contains supplemental information for Chapter 5.

Appendix D contains supplemental information for Chapter 6.

1.4 Co-authorship statement

Chapters 3 through 6 were prepared or submitted for publication in peer-reviewed journals. I am the primary author of the published and submitted chapters, with guidance and assistance of the co-authors indicated below.

Chapter 3 was prepared for publication in *Water Research* and co-authored by Jacques Brisson, Scott Wallace, and Kela Weber. The author contribution statement is included at the end of Chapter 3.

Chapter 4 was published in *Science of the Total Environment* and co-authored by Mhari Chamberlain, Arman Poonja, Kevin G. Mumford, Scott Wallace and Kela P. Weber. The author contribution statement is included at the end of Chapter 4. Reference citation: Farooq, A. J., Chamberlain, M., Poonja, A., Mumford, K. G., Wallace, S., & Weber, K. P. (2023). Peaks, pores, and dragon eggs: Uncovering and quantifying the heterogeneity of treatment wetland biofilm matrices. The Science of the total environment, 855, 158857. https://doi.org/10.1016/j.scitotenv.2022.158857.

Chapter 5 was prepared for publication in *Science of the Total Environment* and co-authored by Laura Jean Ogilvie, Dani Damasceno Silvera, Vincent Gagnon, Mark Button, Sarah Wallace, David J. Patch, Iris Koch, Denis O'Carroll, and Kela P. Weber. The author contribution statement is included at the end of Chapter 5.

Chapter 6 was prepared for publication in *Science of the Total Environment* and co-authored by Dani Damasceno Silvera, Sarah Wallace, David Patch, Denis O'Carroll, and Kela P. Weber. The author contribution statement is included at the end of Chapter 6.

2. Literature Review

2.1 Treatment Wetlands

Treatment wetlands (TWs), also known as constructed wetlands (CWs), are energy-efficient and cost-effective, nature-based systems designed with the main purpose of improving the wastewater quality (Kadlec and Wallace, 2009). Much of the complex wastewater treatment potential in these systems is due to the higher rates of biological activity of their diverse microbial communities. As such, TWs are utilized to treat various types of wastewater including urban runoff, landfill leachate, refinery effluent, explosives, hydrocarbons and agricultural runoff, among others (Vymazal, 2011). The first known use of treatment wetlands was in the 1950s by Dr. Käthe Seidel in Germany, who investigated the role of plants in treatment performance (Kadlec and Wallace, 2009). Since then, this technology has proliferated worldwide; optimizing TW designs to treat numerous different pathogens and pollutants.

2.1.1 Types of Treatment Wetlands

TWs are classified based on two physical traits: hydrology (e.g. water position, flow direction, media saturation, and influent loading type) and vegetation (e.g. sessility, growth form) (Fonder & Headley, 2013; Vymazal & Kröpfelová, 2008). Based on this classification, TWs can be divided into two basic types based on water position: surface flow, commonly referred to as free water surface (FWS) and subsurface flow (SF).

FWS (Figure 2.1) treatment wetlands are shallow open water areas with vegetation whose hydrology mimic a natural wetlands environment; however, these systems have integrated liners, dikes and berms to control the flow of water (Kadlec and Wallace, 2009). Typically, these systems contain up to 40 cm of free-standing water over a 20 – 30 cm layer of rooting soil or sediment (Vymazal, 2010) The water flows horizontally from the inlet, over soil, to the outlet passing between the densely planted emergent, submerged or floating vegetation.

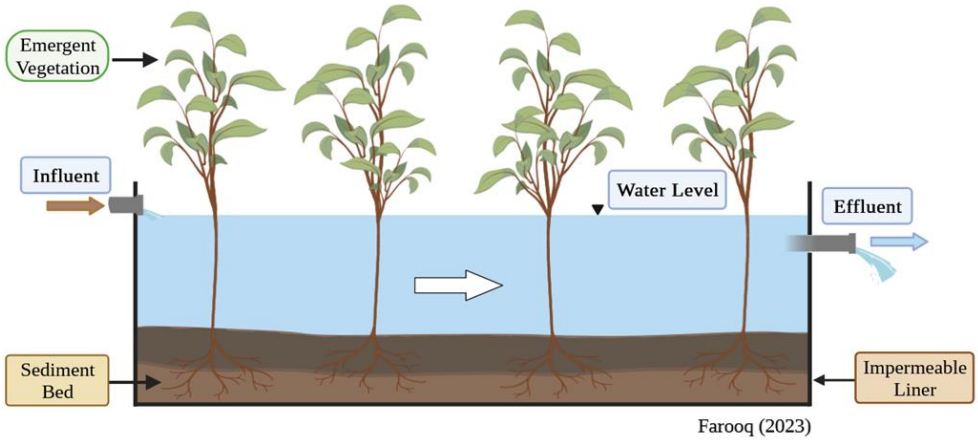

Figure 2.1: Free water surface treatment wetland design (Made in Biorender)

Subsurface systems can be further categorized based on flow direction into horizontal flow (HSSF) and vertical flow (VF). HSSF TWs (Figure 2.2) consist of a media bed (e.g. gravel) planted with emergent macrophytes, such as *Phalaris arundinacea, Phragmites australis, and Typha laitfolia* (Vymazal, 2013). The majority of wastewater flows horizontally beneath the surface of the bed through the porous media (Kadlec and Wallace, 2009). Subsequently, these systems are under primarily more anaerobic conditions as there is minimal oxygen transfer from the atmosphere. However, small aerobic zones occur due to plant-mediated oxygen transfer in the rhizosphere (around the roots) (Brix, 1994, 1993; Jizheng et al., 2019). HSSF TWs are often employed as secondary or tertiary treatment of domestic wastewater for small communities across Europe and North America (Fonder and Headley, 2013; Vymazal, 2009).

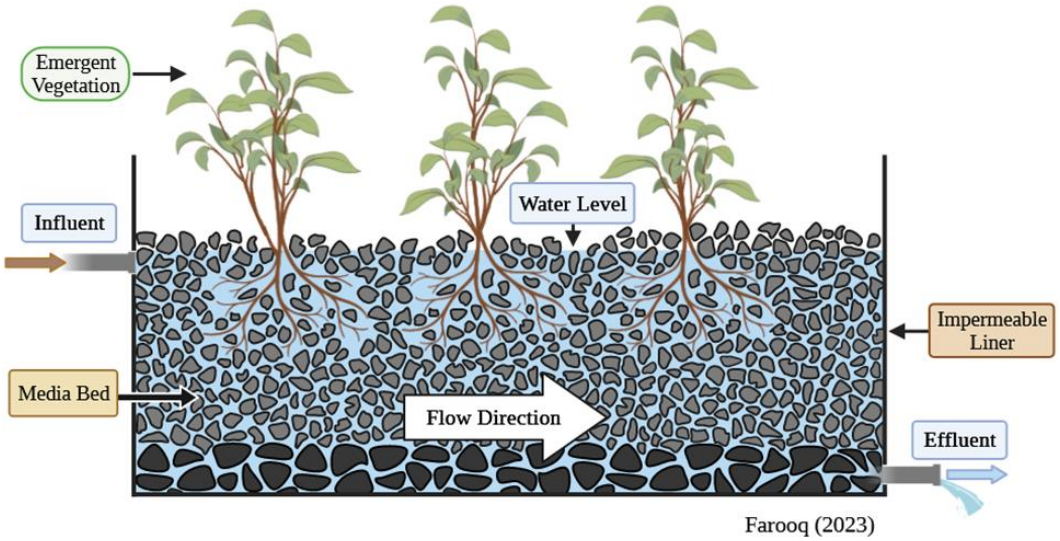

Figure 2.2: Horizontal subsurface flow treatment wetland design (Made in Biorender)

Vertical subsurface flow (VF) TWs (Figure 2.3) are fed intermittently from the top of the system temporarily flooding the surface of the bed. The wastewater then trickles downwards via gravity through the porous media bed (Kadlec and Wallace, 2009). While containing similar features to HSSF TWs, the intermittent feeding allows for greater oxygen transfer, creating an aerobic regime and enhancing the system's nitrification capabilities (Stefanakis et al., 2014; Vymazal, 2010). As such, these systems remain unsaturated most of the time; however, variant designs of VF TWs can be saturated creating biogeochemical conditions similar to anaerobic HSSF TWs (Fonder and Headley, 2013). Compared to FWS TWs, the media in SF TWs provides an increase in available surface area for microbial biofilm development and, in turn, increases the capacity for microbial-based pollutant degradation while reducing its footprint compared to FWS.

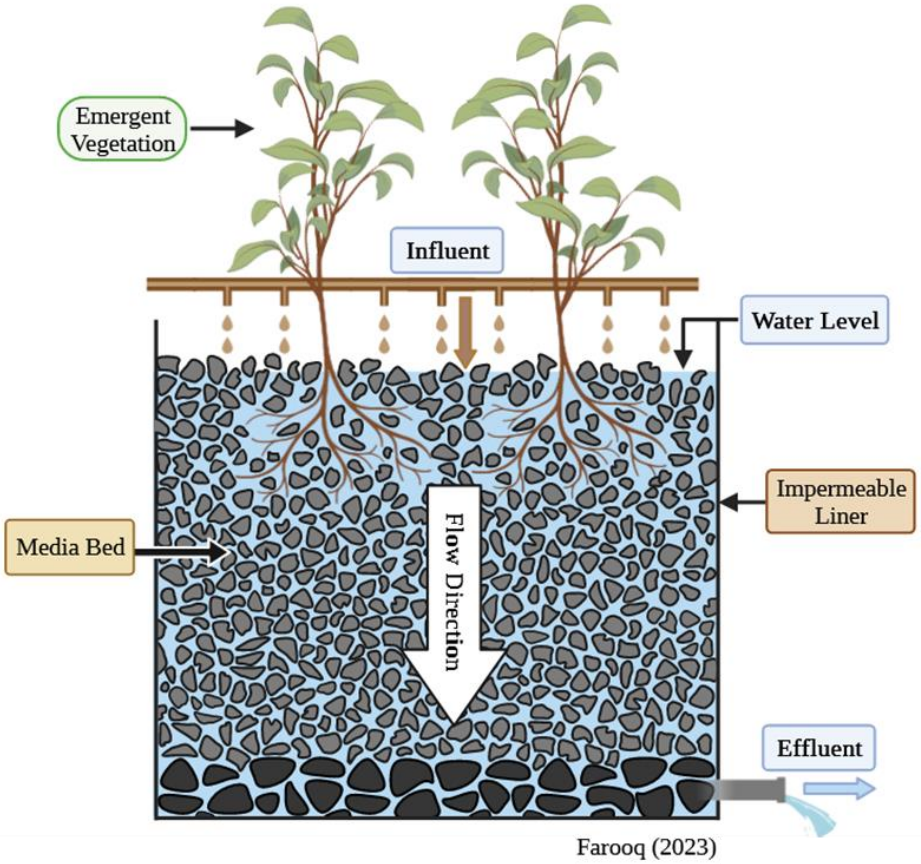

Figure 2.3: Vertical subsurface flow treatment wetland design (Made in Biorender)

In practice, VF and HSSF TWs are frequently combined in series to achieve higher treatment efficiencies, particularly for nitrogen removal to promote the biochemical process of nitrification and denitrification (Ramprasad and Philip, 2018; Vymazal, 2005). The combination of different TW types is referred to as a hybrid system (Kadlec and Wallace, 2009). Furthermore, each type of TW design can be intensified to either promote specific transformations or to improve treatment performance overall through the use of different substrates (Wang et al., 2018) or artificial aeration (Nivala et al., 2014)

2.1.2 Intensification of Treatment Wetland Designs: Artificial Aeration

One limiting factor for wastewater treatment in saturated subsurface TWs is the availability of oxygen in the treatment bed due to the impediment of atmospheric diffusion (Kadlec and Wallace, 2009; Nivala et al., 2013). Studies have found that oxygen transfer rates are notably lower ranging from 0.3 to 3.2 g $O_2 \cdot m^{-2} \cdot d^{-1}$ in HSSF TWs compared to 20.6 to 176 g $O_2 \cdot m^{-2} \cdot d^{-1}$ in conventional unsaturated VF TWs (Dececzaro et al., 2019; Tyroller et al., 2010). Artificial aeration (AA) can be integrated within both subsurface TW designs to increase the transfer of oxygen within the system, which improves the removal of organic carbon, nitrogen, and other pathogens (Boog et al., 2014; Ilyas and Masih, 2017). A combination of a mechanical

blower coupled to a network of tubes enables air to be channeled through the bed (Nivala et al., 2020). Jizheng et al. (2019) studied the implementation of AA in an integrated treatment wetland system containing an aerated VF TW. Artificial aeration enhanced the removal efficiencies of chemical oxygen demand (COD), total phosphorous (TP), and ammonium nitrogen (NH_4-N) by 27%, 30%, and 70%, respectively, compared to the unaerated control. Marked improvements in performance have been noted for both secondary and tertiary treatment of domestic and industrial wastewater in VF and HSSF systems (Ouellet-Plamondon et al., 2006).

Globally, a total of approximately 500 full-scale and pilot-scale aerated TWs are in operation (Nivala et al., 2020). Despite the popularity of aerated TWs, there are still large knowledge gaps that need to be resolved. Therefore, continuing fundamental research into aerated systems of different designs and operational modes is required.

2.1.3 Mechanisms of Pollutant Removal

Similar to their natural counterparts, the physical, chemical and biological mechanisms that govern the removal processes in treatment wetlands include: adsorption, volatilization, precipitation, filtration, sedimentation, plant uptake, chemical networks and, most importantly for the majority of pollutants, microbial-based pollutant removal (Kadlec and Wallace, 2009). These internal processes, summarized in Table 2.1**:** Summary of pollutant removal mechanisms in treatment wetlands (adapted from Kennedy and Mayer (2002) and Stowell et al. (1981))., occur simultaneously within a single TW cell creating a complex, interconnected mosaic of wastewater treatment pathways. The treatment potential of a single pathway is dependent on a number of elements including the system design, operational parameters and environmental factors (Zhang et al., 2023).

Table 2.1: Summary of pollutant removal mechanisms in treatment wetlands (adapted from Kennedy and Mayer (2002) and Stowell et al. (1981)).

Removal Process	Pollutant	Description
Physical		
Sedimentation	Suspended solids, metals, particulate C, N, and P	Gravitational settling of particles and contaminants
Filtration		Mechanical filtering of particles as water flows through substrate, plant litter and roots
Volatilization	Ammonia (NH_3) and volatile organic compounds	Gas absorption with a net flux out of the water surface
Chemical		
Precipitation	Inorganic P, sulfides and metals	Formation of or co-precipitation with insoluble compounds
Adsorption	Dissolved organic compounds, anions (PO_4^{3-}) and cations (metals)	Adsorption on substrate and plant surfaces
Decomposition	Organics, bacterial pathogens	Decomposition or alteration of less stable compounds by UV irradiation, hydrolysis, oxidation/reduction etc
Biological:		
Plant assimilation	N, P, organics, metals	Uptake and in some cases metabolism of nutrients and pollutants in wastewater by plants
Microbial metabolism	BOD, O_2, Nitrogen (NH_4-N, NO_3-N, NO_2-N, Organic N), Organic P, SO_4^2, organic pollutants	Removal of colloidal solids and soluble organics by interstitial bacteria and biofilm, includes nitrification, denitrification, and respiration

2.1.4 Microbial Metabolism

TW microbial communities consume the complex wastewater components compounds through enzymatic reactions, breaking them into harmless by-products (e.g. CO_2, N_2, and H_2O) for either energy (catabolism) or cellular reproduction (anabolism) (Kadlec and Wallace, 2009). Catabolic processes, including respiration and fermentation, are predominately credited for the majority of pollutant transformation and removal in TWs (Weber, 2016). These processes are biochemical oxidation-reduction (redox) reactions, in which the microbes induce a transfer of electrons between a high energy electron donor to an electron acceptor of a lower energy state. In the case of respiration, the terminal electron acceptor is oxygen, whereas for anaerobic respiration, such as fermentation, other inorganic compounds are used as the final electron receptor (Faulwetter et al., 2009).

Studies have shown that internal TW redox conditions have spatial and temporal variability, and are influenced by hydraulic design, depth, presence of plants, influent characteristics, and temperature (Dušek et al., 2008; Faulwetter et al., 2009; García et al., 2003; Wießner et al., 2005). The prevailing microbial metabolism then depends largely on the redox conditions (Table 2.2**:** Selected types of microbial redox reactions (adapted from Faulwetter et al., 2009)). Higher redox potentials (E_h) are linked to more oxidizing conditions favouring aerobic processes and, conversely, lower redox potentials promote more anaerobic processes in a reducing environment. These dynamics create structurally and functionally diverse groups of microbial communities within a single wetland cell, enabling complex treatment (Silveira et al., 2022).

Table 2.2: Selected types of microbial redox reactions (adapted from Faulwetter et al., 2009)

Process	**Electron Acceptor**	**End products**	**ΔG° (kJ/mol e^-)**	**Redox Potential (E_h, mV)**
Aerobic Respiration	O_2	H_2O	-125.1	300 to 700
Denitrification	NO_3^-	N_2, NO_x	-118.8	100 to 350
Manganese reduction	Mn	Mn^{2+}	-94.5	-100 to 300
Sulfate reduction	SO_4^{2-}	S^{2-}	-25.4	-200 to -100
Methanogenesis	CO_2	CH_4, CO_2	-23.2	-350 to -100

Consider nitrogen removal in TWs: it requires both nitrification and denitrification processes for complete removal. Nitrification first transforms ammonium (NH_4^+) into nitrite (NO_2^-) then nitrate (NO_3^-) through oxidation in an aerobic environment by ammonium oxidizing bacteria and nitrite oxidizing bacteria, such as *Nitrosomonas*, *Nitrobacter*, *Nitrosococcus*, and *Nitropira.*(Malyan et al., 2021). Nitrate is then reduced to dinitrogen (N_2) through multistep denitrification under anoxic or anaerobic conditions by mostly heterotrophic bacteria (e.g. *Psydomonas, Agrobacterium*, *Flavobacterium*) (Kadlec and Wallace, 2009). HSSF TWs are predominately reducing environments with micro-pockets of higher redox potential ($E_h \approx 500$ mV) around the roots (rhizosphere) due to plant-mediated O_2 transfer (Kadlec and Wallace, 2009; Stottmeister et al., 2003). This facilitates zones of both nitrification and denitrification

within HSSF design. However, in conventional VF TWs, only aerobic nitrification is possible due to the absence of any anaerobic microenvironments.

In TWs, these microbial communities develop in either the interstitial water, as free-floating bacteria, or by anchoring to any available surface area and forming biofilms through anabolic pathways on the bed media or on plant roots (rhizosphere) (Kadlec and Wallace, 2009; Weber and Gagnon, 2014).

2.1.4.1 Biofilm in Treatment Wetlands

Biofilms are complex structures, sometimes referred to as a "slime" at the macro scale due to their sticky nature. This slime, acts as a bacterial fortress for microbial species, enclosing them in a self-made matrix known as extracellular polymeric substance (EPS) (Boltz et al., 2017; Davey and Toole, 2000; Stoodley et al., 2002). EPS is an integral component of biofilm that offers a stable 3-D structure, aids in adhesion to surfaces, protects from predation, and contributes to the entrapment of nutrients (Flemming and Wingender, 2010; Huang et al., 2019; Murphy et al., 2016). The biofilm structure itself is highly hydrated, containing up to 97% water (Zhang et al., 1998). Without a biofilm, microorganisms will be carried with the flow of water and simply exit the TW system. From a water treatment capacity perspective, this scenario would limit the contact of microorganisms with the pollutants to the length of time that the pollutants are present in the TW system, namely, a maximum of one hydraulic retention time (HRT) worth of effective service. Biofilms, which house microbial communities, are therefore just as important to TW functionality as the microbial communities themselves; however, there are few that have focused on characterizing biofilm at the microscale in treatment wetlands (Weber, 2016).

Movement of pollutants into and out of biofilm is a fundamental step for microorganism mediated water treatment in treatment wetlands. Mass transport of pollutants within TWs has been described through convection-dispersion (Eq. 1):

$$\frac{dC}{dt} = -v \cdot \nabla C + \nabla \cdot (D \nabla C) + R \qquad (1)$$

where C is the concentration of the species (g/m^3), D denotes the molecular diffusivity (m^2/s), R is a reaction rate expression for the species (g/(m^3 s)), and v is the velocity vector (m/s) from the solution. Convective transport accounts for the bulk pollutant movement through the pores and molecular diffusion is attributed as the main mechanism into the biofilm matrix (Kadlec and Wallace, 2009; Murphy et al., 2016; Rajabzadeh et al., 2015).

In TW research, biofilms are described as a relatively uniform film attached to a substrate surface. However, due to the difficulty of obtaining and characterizing TW biofilm samples there are no macroscale studies validating the uniform fixed film morphology assumed in the research field. Any deviations from these assumptions about morphology would directly influence the approach taken when modelling biokinetics and hydraulics in TW systems.

2.1.5 Treatment Wetlands for Wastewater Treatment

TWs designed for a single-family home or larger communities have become increasingly popular around the globe over the last 50 years as a low-cost alternative for conventional wastewater treatment. Vymazal (2023) reported around 200 full scale TWs, primarily HSSF, in operation in the Czech Republic designed for population equivalent (PE) of 235. PE, also known as unit per capita loading, is used to describe the specific organic load per person per day (Kadlec and Wallace, 2009). In the Middle East, the number of full-scale systems is much smaller, estimated to be 10 or fewer per country (Stefanakis, 2020). In France, the number of active systems is over 17 times higher than the Czech Republic, totalling around 3500 TWs (Morvannou et al., 2015). The majority (67%) of systems are configured as two-stage VF TWs designed for capacities between 200 – 2000 PE in rural France. Globally, the number of TWs has not been tallied, but researchers approximate over 12000 systems in use without considering lab scale studies.

For research purposes, TWs are often built at the meso-scale (10 – 1000 L) rather than full-scale or pilot-scale, likely due to practicality. A meso-scale TW, referred to as a mesocosm, offers the ability to perform controlled experiments to confidently investigate fundamental aspects of TW operation, design, and dynamics. Mesocosms are more ecological complex than microscale systems (<10 L), but can be as easily replicated. The design flexibility of mesocosms is such that they can be modified to treat various types of wastewaters (e.g. domestic wastewater, acid mine drainage, agricultural run-off) or even mimic foreign climates (Dordio and Carvalho, 2013; Pedescoll et al., 2013; Weber et al., 2008). Over the past three decades, mesocosm-scale experiments have become essential tools in the TW research field, (Weber, 2016). However, there is limited information on the scalability of these systems to the full or field scale.

Predominately, TWs are used for the treatment of classic wastewater parameters in domestic and municipal wastewater: biochemical oxygen demand (BOD), chemical oxygen demand (COD), total suspended solids (TSS), NH_4^+-N, and TP. However, the popularity of this technology has extended applications to agricultural runoff, storm water, mining, dairy farm effluent, winery, and various other industrial wastewaters.

Recently, studies have begun to focus on the ability of TWs to remediate the increasing number of emerging contaminants found in domestic wastewaters (Petrie et al., 2015). Sauvé & Desrosiers (2014) define contaminants of emerging concern (CECs) as “naturally occurring, manufactured or manmade chemicals or materials which have now been discovered in various environmental compartments and whose toxicity or persistence is likely to significantly alter the metabolism of a living being”. A notable aspect of CECs is a scarcity of information about their associated ecological impacts. The key CECs identified in TWs include pharmaceuticals (Hu et al., 2021; Weber et al., 2014; Zhang et al., 2023), personal care products (Hijosa-Valsero et al., 2016), steroids and hormones (Chen et al., 2021), pesticides (Yang et al., 2022), fire retardants (Liu et al., 2020), and nanomaterials (Huang et al., 2020; Zhang et al., 2016).

2.2 Engineered Nanomaterials

An engineered nanomaterial (ENM) is any solid that has one dimension in the range of 1 – 100 nm (Matović and Bošković, 2007). Under that umbrella falls the term nanoparticle (NP), which is defined as a particle (of any shape) in which 2 or more dimensions fall in 1 – 100 nm (Horikoshi and Serpone, 2013). At such a small size, these particles have unique properties that separate them from their bulk counterparts. This is primarily a result of the high surface area to volume ratios, which means that the smaller the particle, the more available atoms are on the surface giving rise to new physical and chemical properties. Observed changes in hardness, density, lower melting points, higher specific surface areas, specific optical properties, mechanical strengths, and specific magnetizations compared to larger particle sizes, have been noted (Horikoshi and Serpone, 2013; Massarsky et al., 2014). The diversity of these properties has led ENMs to be incorporated in a variety of consumer products such as food additives, drugs, appliances, fuel additives, plastics, sporting goods, and personal care products (Vance et al., 2015). Over the past 60 years, the most popular type in use are silver nanomaterials (Ag-ENMs).

2.2.1 Silver Nanomaterials

The first known production of Ag-ENMs nanomaterials was over 120 years ago, in 1889, with the synthesis of citrate-stabilized Ag-ENMs (Nowack et al., 2011). Soon after, various forms of nanosilver started being incorporated into different medical formulations (e.g. Collargol in 1894) available to consumers (Nowack et al., 2011). New applications for Ag-ENMs are being continually discovered beyond medical supplies, including: electronics and optics, coatings, paints, pigments, cosmetics, and textiles, such as socks (Gottschalk and Nowack, 2011; Keller and Lazareva, 2013). The implementation of Ag ENMs in commercial products is primarily related to their well documented antimicrobial/antibacterial properties (Benn & Westerhoff, 2008; Nowack et al., 2011; Rai et al., 2008) . As previously stated, nanoscale materials, due to their uniquely high surface area to volume ratio, provide a larger reactive surface area to interact with microorganisms compared to their bulk counterparts.

Several online databases have been created to take an inventory of current nanotechnology-based consumer goods and trends including the Nanotechnology Consumer Products Inventory (CPI), StatNano, and Nanowerk.(Talebian et al., 2021; Vance et al., 2015). In 2005, the CPI was launched, detailing a total of 52 products, 30 of which contained Ag-ENMs. By 2023, the CPI comprised a total number of 1833 nanomaterial-based goods, 443 products or 24.2% of those containing silver nanoparticles (Project on Emerging Nanotechnologies, 2023). StatNano, established in 2010, is a much larger global database, most recently listing 1132 different Ag-ENMs products across 44 different countries (StatNano, 2023). Overall, Ag-ENMs are the most frequently used nanomaterial listed and by far the fastest growing sector of engineered nanomaterial market, being valued at $1.3 billion (USD) in 2017; it is expected to grow by 12% to over $3 billion (USD) by 2024 (Verma, 2018). Within the United States, an estimated 2.8 – 20 tonnes of silver nanomaterials are produced per year (Hendren et al., 2011). Global production volumes have ranged between 150 – 500 metric tonnes per year and are expected to reach a maximum 800 tonnes annual by 2025 (Janković and Plata, 2019; Keller et al., 2013; Nowack and Mueller, 2008; Pulit-Prociak and Banach, 2016).

2.2.2 Silver Nanomaterials in the Environment

While Ag-ENMs embedded products provide many benefits, through their production, use and eventual disposal, it is likely that nanomaterials will enter into the environment (Islam et al., 2021; McGillicuddy et al., 2017). Benn and Westerhoff (2008) conducted leaching experiments using socks embedded with Ag-ENMs to restrict the growth of odor causing bacteria. The socks were run through a "real world" washing scenario and were found to release as much as 650 μg of silver (particulate and ionic forms) in 500 mL of distilled water. Additional studies have shown silver nanomaterials released from medical products, toothpaste, shampoo, detergent, children's toys, textiles, and paints with wide ranging concentrations into environmental receptors (Geranio et al., 2009; Kaegi et al., 2010; Mitrano et al., 2014). The released Ag-ENMs enter and participate in environmental cycles and, as a result readily interact with the surrounding organisms, which may directly or indirectly endanger the ecosystem (Sun et al., 2022).

Characterization of Ag-ENMs formed through wear/weathering and incidental release (also referred to as weathered Ag-ENMs) revealed that they are predominately irregular in shape, being released as nanoplates or nano-aggregates, have different compositions, and have a wide variation in size distribution as opposed to their pristine spherical counterparts (Gagnon et al., 2019; Patch et al., 2021; Reidy et al., 2013). These variations in attributes solidify the suggestion that toxicity research should be conducted using realistically weathered Ag-ENMs (See Section 2.2.4 for details on toxic effects of Ag-ENMs). Critically, researchers have noted that the quantity of weathered Ag-ENMs generated tend to be too small to achieve large volumes of high concentrated suspensions. This has proved to be a crucial limitation in the use of weathered silver nanomaterials for ecotoxicological research (Nowack and Mitrano, 2018).

Concerns about ecotoxicological risk have led to the development of several material flow models to predict the final exposure pathways and concentrations in environmental receptors from different points across the Ag-ENMs lifecycle as shown in Figure 2.4 (Sun et al., 2022; Blaser et al., 2008; Gottschalk et al., 2009; Keller et al., 2013; Keller & Lazareva, 2013; Massarsky et al., 2014; Nowack & Mueller, 2008). Although release of ENMs can also result from industrial manufacturing, the main pathway into the environment is from consumer use. There are two main flow pathways from this single point, either entering directly into the influent stream of a wastewater treatment plant (WWTP) or, in the case of municipalities with combined sewer overflow, a bypass stream that discharges directly into surface waters. From the WWTP, Ag-ENMs either exit as a treated effluent stream, or as biosolids, which are applied in agricultural practices or sent to landfills where they can leach back into surface waters.

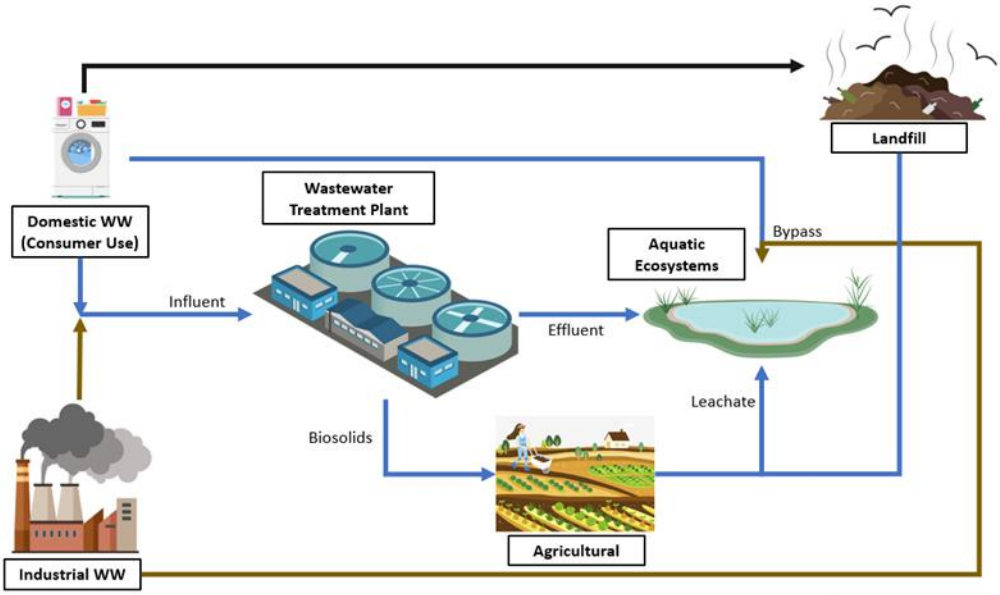

Figure 2.4: Exposure pathways of Ag-ENMs released from production, consumer use and disposal

The predicted environmental concentrations (PECs) of the models presented indicated that 38 – 95% of Ag-ENMs released from consumer products will enter WWTPs before being released into aquatic ecosystems (Gottschalk et al., 2009; Nowack and Mueller, 2008). WWTPs use physical (filtering, sedimentation), chemical (addition of chlorine) and biological (degradation by microbes) processes for the treatment of wastewater streams (Kadlec and Wallace, 2009). The removal efficiencies of Ag-ENMs in WWTP are typically high, upwards of 90%, regardless of size or coating (Ma et al., 2014). TEM imaging showed that the silver nanomaterials were adhered primarily to wastewater biosolids and nearly for the majority had transformed to silver sulfide (Ag_2S) via sulfidation (Kaegi et al., 2011). This transformation is thermodynamically expected as silver binds strongly to sulfur. Moreover, its subsequent form, Ag_2S, has a marked decrease in toxicity due to its lower solubility (Levard et al., 2012).

Keller et al. (2013) predicted that roughly 13% or 63 tonnes Ag-ENMs/year would exit WWTP into surface waters, which equates to a final PEC range of 0.05 to 0.2 ug Ag-ENMs/L. Similarly, Blaser et al. (2008), Nowack & Mueller (2008), Klaine et al. (2008) estimated PECs in the aquatic environment in the range 0.04 to 0.91 ug Ag-ENMs/L. These PECs are in accordance with observed values of Ag-ENMs in Western rivers and streams (Bäuerlein et al., 2017; Li et al., 2016; Peters et al., 2018). It should be noted, however, that these models predominantly examine flows in North America and Europe. Asia is predicted to account for over 50% of the use and release of ENMs globally, and likely will have much higher environmental concentrations (Keller and Lazareva, 2013). To that end, Lazim et al. (2023) and Syafiuddin et al. (2018) reported concentrations of 0.001 to 0.505 mg Ag-ENMs/L and

0.13 to 10.16 mg Ag-ENMs/L, respectively in Malaysian rivers, which reaches over 30 000x higher than the maximum PEC of the Western models.

Once in the aquatic environment, Ag-ENMs can readily interact with their environment, but are subject to a variety of processes including: chemical transformations, homo- and hetero-aggregation to suspended particulate matter, and subsequent sedimentation and dissolution (Markus et al., 2015).

2.2.3 Ecotoxicology of Silver Nanomaterials

The toxicity of Ag-ENMs has been widely researched against individual organisms and more diverse microbial communities. Table 2.3 summarizes a handful of these studies with their key findings.

Table 2.3: Summary of silver nanomaterial toxicity studies

Article	**Organism**	**Concentration or LC_{50}, EC_{50}, MIC**	**Key Findings**
Choi et al. (2008)	Nitrifying bacteria	0.05-1 mg/L	Growth inhibition correlated with Ag ENMs < 5nm
	Escherichia coli	0.5 mg/L	Growth inhibition observed at 0.5 mg Ag-ENMs/L
Kim et al. (2007)	*E. coli*, *Staphylococcus aureus*, yeast	0.2-33 nM	S. aureus more resilient to Ag NP than *E. coli*
Kvítek et al. (2008)	*Bacteria species* (*Staphylococcus aureus, E. coli…*)	MIC: 1.69-13.5 μg/mL	Surface coatings enhanced the antibacterial activity of Ag NPs
Sondi and Salopek-Sondi (2004)	*E. coli*	0-100 μg/mL	Pits were created in the bacterial cell wall
Thuptimdang et al. (2017)	*Pseudomonas putida* biofilm	20 mg/L	Biofilm morphology affected toxicity
Fabrega et al. (2009)	*Pseudomonas putida* biofilm	0-2000 μg/L	Organic matter mitigated toxicity and enhanced uptake into biofilm
Morones et al. (2005)	Bacteria spp	0-100 μg/mL	Ag NPs <10 nm attached to bacterial cells
Navarro et al. (2008)	*Chlamydomas reinhardtii*	EC_{50}: 0.35mg/L (1 h)	Toxicity mediated by Ag^+ dissolution

Kim et al. (2007) reported a minimum inhibitory concentration (MIC; the lowest concentration that will regularly inhibit microbial growth) for Gram negative *E. coli* between 3.3 – 6.6 nM and over 33 nM for Gram positive *S. aureus* in the presence of 13.5 nm silver nanoparticles. This suggests that Gram positive bacterial species are more resilient to the inhibitory action of Ag-ENMs, a finding corroborated by Kvítek et al., (2008) and Sondi and Salopek-Sondi (2004); however, for the latter, a higher concentration of silver nanoparticles was required for *E. coli* inhibition.

Another study reported that synthesized 14 nm polyvinyl alcohol coated Ag-ENMs presented the highest inhibition of growth, 86±3%, on nitrifying bacteria as compared to 46±4% by ionic silver (Choi et al., 2008). The study refocused from autotrophic organisms to heterotrophic ones using *E. coli* as a model organism. Subsequent toxicity tests (using the previously described Ag-ENMs and ionic silver) resulted in the inhibition on *E.coli* growth by 55±8% and 100% respectively at 0.5 mg Ag-ENMs/L. Morones et al. (2005) focused on four Gram negative bacteria, *E. coli*, *V. cholera*, *P. aeruginosa* and *S. typhus* and found no significant growth at 75 μg/mL which was attributed to the Ag NP with a diameter less than 10 nm.

The model organism *Chlamydomonas reinhardtii* was used to determine silver nanoparticle toxicity to freshwater algae (Navarro et al., 2008b). Carbonated-coated nanoparticles, with a median diameter of 40 nm, added to algae have shown to decrease the photosynthetic yield from the control. Additionally, the effects silver nanoparticles on biofilms have also been studied. Fabrega et al. (2009) exposed *Pseudomonas putida* biofilm to 65 nm citrate coated Ag ENMs resulting in a marked decrease in biomass.

2.2.4 Mechanisms of Toxicity of Silver Nanomaterials

Though the toxicity to microbial organisms from Ag ENMs is well-established, there is no consensus on the main mechanism of that toxicity; three commonly described mechanisms have been proposed.

One popular theory is linked to the dissolution of silver ions (Navarro et al., 2008b; Sotiriou and Pratsinis, 2010). Referred to as the "Trojan horse" mechanism, Ag-ENMs themselves are not viewed as toxic; rather they are the vessel of toxic Ag^+ ions released through oxidative dissolution and it is the Ag^+ ions that cause bactericidal action (Liao et al., 2019). The Ag^+ ions readily bind with the thiol group of L-cysteine and cause impairment of enzymatic functions involving this amino acid. This, in turn, disrupts the chain of cellular respiration leading to eventual cell death. Additionally, Ag^+ ions have been shown to penetrate into the bacterial cell decreasing protein expression and compromising chromosomal DNA (Xiu et al., 2012).

The second proposed theory is that Ag-ENM toxicity is due to oxidative stress from the generation by the Ag-ENMs themselves of reactive oxygen species (Bundschuh et al., 2018; Liao et al., 2019). ROS are natural by-products of aerobic metabolism and organisms can typically mitigate the resulting damage through the generation of antioxidant enzymes (Davies, 2000). Numerous studies have reported the generation of ROS from silver

nanoparticles (Auffan et al., 2009; Choi and Hu, 2008; Jiang et al., 2014; Massarsky et al., 2014). The presence of Ag-ENMs enhances the generation of ROS through catalytic redox reactions on the particle surface (Auffan et al., 2009; Massarsky et al., 2014). When exposed to UV light, Ag-ENMs absorb photons causing excitation of electrons, which can then interact with oxygen to create superoxide anion radicals, or with water to form hydroxyl radicals. This has been shown to result in irreversible damage to the cell membrane, DNA and mitochondria and can eventually lead to cell death (Choi and Hu, 2008; Hajipour et al., 2012). This is also thought to be linked to the first mechanism as it is believed that Ag^{+} ions simultaneously released from Ag-ENMs induce the formation of ROS species through their thiol-interaction mechanism (Park et al., 2009).

The third theory of Ag-ENM toxicity attributes the toxicity of Ag-ENMs to their inherent physiochemical properties, Choi et al., (2008), Lin et al. (2013), and Morones et al.(2005) concluded that silver nanoparticles with smaller diameters (< 25 nm) had a higher toxicity towards bacteria compared to their bulk counterparts. Imaging of the uptake of Ag-ENMs in bacterial cells confirmed that smaller nanoparticles were able to bind more readily than aggregates and, in some cases, penetrate the cell. Moreover, Sondi & Salopek-Sondi (2004) observed pitting on the exterior cell wall due to the accumulation of Ag-ENMs. The direct contact of Ag-ENMs could create cytotoxic effects through membrane damage leading to cell death.(Liao et al., 2019). Other properties suggested to influence toxicity include surface coatings, charge, composition, and, of particular concern, shape (El Badawy et al., 2012; Gorka et al., 2015; Kvítek et al., 2008). Pal et al. (2007) found that triangular Ag nanoplates exhibited the highest toxicity against bacteria compared to silver nanospheres and nanorods due to their higher percent of exposed facets. This is important when considering the morphology of Ag-ENMs incidentally released from consumer products as they can be in the form of nanoplates rather than spheres.

2.3 Silver Nanomaterials in Treatment Wetlands

2.3.1 Exposure Pathways of Nanomaterials to Treatment Wetlands

As previously stated, treatment wetlands act as an alternative to conventional WWTPs and, as such, they would receive wastewater streams from the domestic discharge and industrial wastewaters depending on the size of TW system (Figure 2.5). Therefore, the concentrations entering in TWs will be similar to those entering WWTPs rather than the PECs of surface waters (Section 2.2.2).

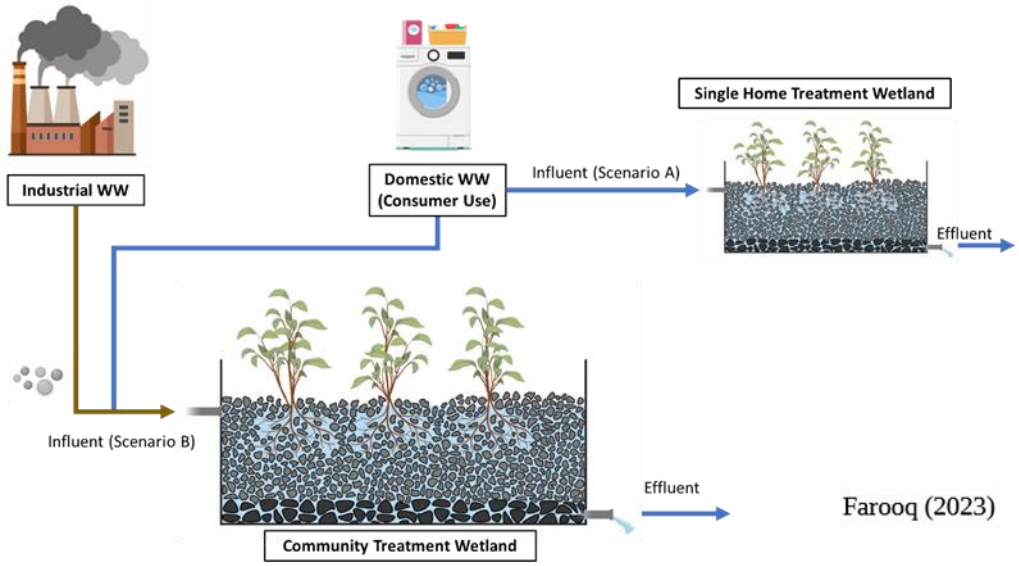

Figure 2.5: Model of Ag-ENMs release into treatment wetlands. Scenario A: Release to a single home treatment wetland; Scenario B: Release into a local community wetland

Button et al. (2016) estimated the influent concentration of Ag ENMs entering a single home TW to be 100 µg Ag-ENMs/L. This calculation was based on Geranio et al. (2009) who observed that 341 to 377 µg Ag/g fabric can be released from a single wash of textiles embedded with Ag-ENM fibers. Assuming a relatively high efficiency washer, one load of Ag-ENM embedded textiles can release a total of 15 mg/L into the single home TW. Averaged over an entire day of water release, the final concentration of 100 µg Ag-ENMs/L is obtained. In the case of TW systems servicing larger communities, the addition of industrial effluent is predicted to reach influent Ag-ENM concentrations as high as 1 mg/L (Liu et al., 2019). Given the biotoxicity of Ag-ENMs, there are concerns that the microbial communities of TWs and, in turn, the treatment performance could be impaired.

2.3.2 Current Research of Silver Nanomaterials in Treatment Wetlands

Several papers have examined the effects, transformations, and fate of Ag-ENMs in TWs (Table 2.4). The first study to examine Ag-ENMs in TWs was conducted by Button et al. (2016a), in which the authors evaluated the impacts of ionic silver and two types of Ag-ENMs, polyvinyl pyrrolidone (PVP)-coated and citrate-coated, on both the interstitial and media-

bound biofilm microbial communities in subsurface CW microcosms. The systems were spiked to a final concentration of 100 µg Ag NP/L and left for 28 days. After one month, no discernable impacts could be determined to the biofilm microbial communities' function or structure from any treatment. A subsequent, *ex-situ* testing at higher concentrations showed significant reductions in activity; therefore, the authors suggested that microbial communities may be robust enough to tolerate low levels of silver in wastewater streams.

Research to date has shown that TWs are highly effective tools for the removal Ag-ENMs from wastewater, reporting high removal efficiencies ranging from 92 to 99% for both meso-scale and pilot-scale planted VF TWs (Huang et al., 2017; J. Huang et al., 2019b). However, under the stress of Ag-ENMs, concentrations as low as 0.02 mg/L have shown the ability, while temporary, to supress the removal capabilities of other parameters by TWs, specifically nitrogen and phosphorus (Huang et al., 2018b). Cao et al. (2022) reported that TN, NH_4^+-N, and TP removals decreased by 15%, 19%, and 14%, respectively, under Ag-ENMs (PVP-coated, 10 – 40 nm) exposures of 0.2 mg/L when compared to the control. Similar findings were reported in previous studies (Cao et al., 2018; Huang et al., 2020).

Complementary metagenomic analysis revealed there were significant microbial shifts in community structure from the addition of Ag-ENMs. Relative abundances of nitrifying and denitrifying bacteria were shown to significantly decrease with Ag-ENMs. However, examining these effects over long-term exposures (120 – 450 d) has shown that TWs were able to recover and restore treatment efficiencies of TN, NH_4^+-N and TP (Cao et al., 2019; Huang et al., 2020; J. Huang et al., 2019a). This has been attributed to functional redundancies in TW microbial communities or the hormesis effect, where sublethal concentrations of Ag-ENMs cause an increase of EPS and upregulation of nitrogen cycling genes (Sarkar, 2022). In the case of TP, while there was a decline in polyphosphate accumulating organisms, the main mechanism for removal was attributed to sorption. Huang et al. (2020) suggested that exposure of Ag-ENMs caused a competition with phosphate ions for binding sites in the soil layer, but, over time (after 360 d), the mechanisms reach a cooperative state.

It should be noted that at higher Ag-ENM exposures (above predicted environmental concentrations), the recovery of TWs performance was not observed. Liu et al. (2019) examined the effects of a 50 mg/L exposure of PVP-coated Ag-ENMs (60 – 80 nm) in planted (*Phragmites australis*) HSSF systems over 60 d. The removal rate constants (k) decreased for both N (0.14 to 0.05) and NH_4^+-N (0.12 to 0.06). The authors noted that this shift was linked to significant reductions in the relative abundance of ammonifers (*Pseudomonas*), nitrifiers (*Nitrosomonas* and *Nitrospira*), and denitrifiers (*Thauera* and *Dechloromas*). Also, the authors noted an increase of lactate dehydrogenase (LDH) release, indicating impairment of the microbial cytomembrane, which would lead to the inhibition of microbial viability.

.

Table 2.4: Selected articles investigating effects and fate of Ag-ENMs in TWs

Article	Type of Ag ENMs	Size (nm)	[ppb]	Focus
Button et al. (2016)	PVP-coated citrate-coated	2030 10	0.1	Evaluated the impacts of different types of Ag-ENMs and ionic Ag^+ on TW on microbial communities associated in interstitial water and biofilm
Auvinen et al. (2017)	citrate-coated	10	0.1	Investigated the ability of differently designed TW microcosms to retain Ag-ENMs and studied their distribution and transformation
Huang et al. (2017)	PVP-coated	10 – 40	0.05, 0.2	Examined long-term impacts of different doses of Ag-ENMs on nutrient removal and changes in microbial community structure in VF TWs mesocosms
Cao et al. (2018)	PVP-coated	10 – 40	0.1	Examined the long-term effects of Ag-ENMs on the nutrient removal efficiencies along the flow path of VF TW mesocosms
Huang et al. (2018a)	PVP-coated	10 – 40	0.1	Investigated the effects of a continuous exposure Ag-ENMs on the removal of COD, nitrogen and phosphorus in lab scale TWs with and without plants
Huang et al. (2018b)	PVP-coated	10 – 40	0.02	Evaluated the long-term (105d) effects of a pilot scale VF TW under an Ag-ENM exposure
Bao et al., (2019)	PVP-coated	94.65	1	Assessed the influence of hydraulic loading, bed depth and plant) on removal efficiency, effect and fate of Ag-ENMs

Table 2.4 (cont'd): Selected articles investigating effects and fate of Ag-ENMs in TWs

Article	Type of Ag ENMs	Size (nm)	[ppm]	Focus
Cao et al. (2019)	PVP-coated	10 – 40	0.1	Examined the effects of two different plant species (*Cyperus alternifolius* and *Arundo donax*) in TW receiving 100 ppb Ag-ENMs
Huang et al. (2019b)	PVP-coated	10 – 40	0.05, 0.2	Investigated the spatial distribution of Ag-ENMs and its impact on microbial communities within VF TWs following a 450-d exposure at different concentrations
Huang et al. (2019a)	PVP-coated	10 – 40	0.05, 0.2	Investigated the effects of a long-term exposure (450d) of Ag-ENMs on nitrogen removal and the abundance of relative functional genes
Huang et al. (2020)	PVP-coated	10 – 40	0.05, 0.2	Evaluate the long-term fate and effects of different does of Ag-ENMs on phosphorous removal and the abundance of relative functional genes
Cao et al. (2021)	PVP-coated Sulphidized	58.1 62.2	0.5, 2	Investigate the effect of Ag^{+}, pristine and sulphidized Ag-ENMs on nitrogen removal and nitrogen functional bacteria
Truu et al. (2022)	Casein-coated	14.6	0.1	Effects of increased Ag-ENMs and Ag^{+} concentrations on the treatment efficiency, microbial community, silver resistome, in a pilot scale hybrid VF-HSSF system
Liu et al. (2023)	PVP coated	10 – 20	0.1, 50	Examined the impact of Ag-ENMs on biofilm formation and biofilm functional activity and the physiological activities of plant roots and leaves

Bao et al. (2019) reported that the presence of plants (*Phragmites australis*) improved removal efficiencies of Ag-ENMs (PVP-coated, 39.2±6.6 nm) from 41% to 78% in gravel bed VF TWs. On the other hand, Huang, Cao, et al. (2018) saw no statistical difference between planted (*Iris pseudacorus*) and unplanted VF systems, achieving removals of greater than 96% for both systems.. Uptake into the plants accounted for about 1% of the total silver mass loaded into the system, thus proving to be a minor sink (Bao et al., 2019; Liu et al., 2019). However, certain plants, such as *Cyperus alternifolius*, have shown to be capable of absorbing more silver via roots and immobilizing Ag-ENMs (Cao et al., 2019).

Overall, the majority of Ag-ENMs were found instead either bound in the soil substrate or the biofilm (Button et al., 2016; Huang, Yan, et al., 2019).In TWs that have soil layers, the silver binds readily to the rich organic matter and, as a result, the Ag-ENMs do not migrate readily throughout the TW. Conversely, in gravel-based TWs, the majority silver is found immobilized in the biofilm due to the electrostatic attraction to the EPS matrix (Auvinen et al., 2016). As Ag-ENMs accumulate in the biofilm, they have been shown to impair its function, decreasing the relative abundance of functional genes involved in forming the EPS, bacterial adhesion, and nitrogen metabolism during high loads of 50 mg Ag-ENM/L (Liu et al., 2023).

Previous research has predominantly focused on Ag-ENMs in classic VF TWs with few studies examining different design modifications. Chen et al. (2023) examined the ability of different substrates (gravel, biochar, pyrite, and biochar/pyrite mix) to alleviate the toxicity of Ag-ENMs in planted (*Cyperus alternifolius*) HSSF TWs receiving doses of PVP-coated Ag-ENMs (10 – 20 nm) at either 0.2 mg/L or 10 mg/L. Following a 60 d exposure, substrates were able to retain 75% – 98% of the Ag-ENMs loaded in the systems. However, only the biochar/pyrite bed was able to significantly mitigate the toxicity of Ag-ENMs by maintaining removal efficiencies of $NH4^+$ (40.8%) and TN (36.5%) that were around 10% higher than in the gravel systems.

Different hydraulic flow regimes (up-flow and down flow) have also been investigated with respect to the impacts of Ag-ENMs (PVP-coated, 10-40nm) on VF TW systems (Cao et al., 2021b). The authors found that up-flow systems were significantly impacted at lower concentration of Ag-ENMs (0.5 mg/L), as TN effluent concentrations increased by 4.8-fold. However, at 2 mg Ag-ENM/L, the up-flow system exhibited more resistance to Ag-ENM toxicity, maintaining larger abundances of functional nitrifying genes (*amoA* and *nxrA*) in the biofilm compared to their downflow counterparts.

Finally, only one study examined the influence of artificial aeration, as well as organic matter content, on the retention of silver nanomaterials in TW planted (*Phragmites australis*) microcosms. Auvinen et al. (2017) spiked 50 µg Ag/week in the form of citrate-coated Ag-ENM (10 nm) in nine 10-L microcosms receiving simulated domestic wastewater, three of which were receiving AA (3.2 mg O_2/L). While there were no discernable impacts from the AA, the addition of organic material increased the TSS output, which was highly correlated with the silver effluent concentration. The organic matter likely increased the available surface area for Ag-ENMs to adhere to and then eventually settled out of the microcosms. As with previous studies, high removal efficiencies (80 –90%) were observed, with most

silver found in the substrate-associated biofilm in the form of Ag_2S. Similarly, rhough not a treatment wetland system, Lowry et al., (2012) examined the transformations and fate of Ag-ENMs in "emergent freshwater" mesocosms, which were representative of natural wetland environments. Following a one-time dose of 4.2 g of pristine PVP coated Ag-ENMs, after 18 months, the majority of silver was found either in the sediments or in terrestrial soils based on the location of the initial dosing. Speciation of Ag NPs indicated that a fraction of dosed particles was oxidized to the form Ag (I) after which they were partially sulfidized to the thermodynamically favoured Ag2S.

In summary, while numerous studies exist examining Ag-ENMs in TWs, their effects and fate are far from known. All previous studies of Ag-ENM in TWs have predominantly focused on pristine NPs manufactured in a laboratory setting. Some researchers included "aged" sulphidized Ag-ENMs; however, these particles were artificially made using their pristine counterparts. As mentioned in Section 2.2.2, it is not these engineered particles that will be ultimately enter the environment, but rather incidentally released Ag-ENMs from the weathering of consumer products (Meyer et al., 2011). To date, no TW studies have yet explored the impacts from realistic incidental or "weathered" Ag-ENMs on treatment wetland systems.

3. Evolution of the mesocosm: Informing treatment wetland research across the globe

Anbareen J. Farooq[†], Jacques Brisson[ǂ], Scott Wallace[§], and Kela P. Weber[†*]

[†]Environmental Sciences Group, Department of Chemistry and Chemical Engineering, Royal Military College of Canada, Kingston, ON K7K 7B4, Canada

[ǂ] Institut de Recherche en Biologie Végétale (IRBV), Département des Sciences Biologiques, Université de Montréal, Montréal, Québec H2X 1Y4, Canada

[§]Naturally Wallace Consulting LLC, Pilot Mountain, North Carolina 27041, USA

*Corresponding author: kela.weber@rmc.ca

3.1 Abstract

In the treatment wetland (TW) field, mesocosm-based studies have increased dramatically over the past decade, being applied across a wide range of different research topics. The use of the meso-scale (10-1000 L) experimental systems is advantageous due to their reduced cost and replicability, while maintaining reasonable ecological complexity. This study endeavoured to examine the global use and applicability of TW mesocosms through a meta-analysis of all peer reviewed journal articles over the period of 1992-2017. A total of 3299 papers were reviewed, of which 542 met the criteria of being within the meso-scale and evaluating at least 3 water quality parameters. Between the two time periods of 1992-2005 and 2005-2017, the number of countries that published meso-scale research increased from 14 to 52, with the majority of studies being performed in Asia. In tandem with this shift, main research topics diversified over time, moving from classic areas of study (plants, media, design) into topics including microbial communities, emerging contaminants, aeration, and novel substrates. Globally, mesocosm research has been primarily conducted using subsurface TWs (both vertical (VF) and horizontal (HSSF) flow), accounting for 74.4% of all unique systems in the meta-analysis. Median sizes of the classic three wetland designs of free-water surface (FWS), HSSF, and VF systems at the meso-scale were 378.5 L, 250 L and 53 L. respectively. Looking at the water quality parameters analyzed across all three systems shows that researchers to be monitoring forms of nitrogen in at least 70% of all studies. Globally, the mesocosm has become an essential research tool in furthering the development and understanding of TWs. In terms of scalability and relevance of mesocosm studies, a comparison of first order BOD removal rate constants between full-scale and meso-scale revealed that the fundamental capabilities seen for full-scale systems are well represented in the smaller meso-scale systems.

Keywords: mesocosm, treatment wetland, meta-analysis, BOD, constructed wetland

3.2 Introduction

Treatment wetlands (TWs) refer to both man-made and natural wetland systems that are intentionally used for the treatment of water pollution. While natural catchments have been receiving wastewater discharge for centuries, the treatment wetland field only began to develop in the last half of the 20th century (Kadlec and Wallace, 2009). Eventually, full-scale systems started being implemented across North America and Europe in the early 1970s, and in Asia during the 1990s for the treatment of domestic wastewater (Vymazal, 2011). Presently, there are thousands of full-scale TW systems worldwide being used to treat numerous different pathogens and pollutants (Morvannou et al., 2015; Vymazal, 2023).

As the TW field developed, three main designs variants have dominated. These designs are classified based on two physical attributes: hydrology (water position, flow direction, saturation of media and influent loading type) and vegetation (sessility and growth form- i.e., emergent, submerged, floating leaved, free-floating) (Fonder and Headley, 2013; Vymazal and Kröpfelová, 2008). Surface flow wetlands, commonly referred to as free water surface (FWS) or more recently as treatment marches, closely mimic natural wetlands with open shallow water areas with flow over a saturated sediment bed and are often employed for the tertiary treatment of domestic wastewater (Dotro et al., 2017). This contrasts the two more popular subsurface flow designs where water flows either horizontally (HSSF) or vertical (VF) through a planted porous media bed. Other configurations such as floating treatment wetlands (FTW) and hybrid (VF-HSSF) designs are used to a lesser degree.

TWs use a complex, interconnected mosaic of internal physical, chemical, and biological processes to treat various pollutants. The potential of a single pathway is dependent on a number of elements including the system design, operational parameters, and environmental factors (Zhang et al., 2023). In operation, TWs are designed to meet specific treatment objectives based on influent loading and guidelines. In many cases these objectives are becoming increasingly more stringent or challenging, prompting improvements to TWs designs through worldwide research. However, constructing full-scale (>100,000 L) or even pilot-scale (1000-100,000 L) TW systems purely for research purposes is not always feasible. Consequently, over the past three decades, smaller mesocosm-scale experiments have become a popular option to evaluate TW design modifications, internal processes, and overall performance (Weber, 2016).

A mesocosm is a controlled experimental tool that introduces an element of ecological complexity that can be easily replicated (Ahn and Mitsch, 2002; Odum, 1984). These tools have been influential in several different fields, bridging the gap between the limited realism of microscale experiments and larger scale systems of higher complexity (Benton et al., 2007; Stewart et al., 2013). Defining the meso-scale varies between disciplines, with a standard range of 10-1000 L being appropriate for treatment wetlands. Its design flexibility is such that they can be implemented to treat many types of wastewaters (e.g. domestic wastewater, acid mine drainage, agricultural run-off) or even mimic foreign climates (Dordio and Carvalho, 2013; Pedescoll et al., 2013; Weber et al., 2008).

The aims of this study are to present an overview of the evolution, usage, and relevancy of the mesocosm within the context of the TW field through a meta-analysis of relevant publications. In tandem, publications were mined for influent and effluent data to determine areal rate constants (k_A) for selected pollutants through the P-k-C* model for comparison to full-scale wetland system data found in Kadlec & Wallace (2009).

3.3 Materials and Methods

3.3.1 Literature Review

The Queen's University (Kingston, ON) Library Omni search engine (previously Library Summon) was used to obtain the relevant literature. This unified academic research tool has access to 80,000+ e-journals containing more than 85,000,000 articles across various databases. In 2018, four unique searches for peer-reviewed articles were conducted using pairings of the following key terms: "constructed wetland" or "treatment wetland", in conjunction with "lab scale" or "mesocosm". All results were pooled together and duplicates were removed yielding a total of 3299 remaining articles. The peer-reviewed publications were filtered against two criteria: (a) the systems' total volume was between 10 L-1,000 L and (b) had monitored at least 3 different types of water quality parameters. Through the filtering of data, a final total of 542 articles were identified to illustrate the evolution of mesocosm-scale research. Articles with missing size dimensions were not included in the final dataset.

3.3.2 Meta-Analysis and Data Collection

Initially, each article was classified by the year of publication, by the continent of origin, focus, and number of mesocosms used for their experiment. For consistency, the continent of origin was selected based on the country associated with the first author of each paper. The focus was identified through the objectives detailed in the introduction of each paper. Next, the article was reviewed using a "per mesocosm" analysis, taking note of characteristics such as: total system volume; type of wetland mesocosm (free-water surface (FWS), horizontal subsurface flow (HSSF), and vertical flow (VF)); type of water treatment (primary, secondary or tertiary); plants (planted or unplanted); and type of wastewater (synthetic or source). For numerous articles, unless explicitly stated, system type was identified based on the characteristics and schematics given in the article including substrate depth, water level, and flow path.

In tandem, inlet-outlet pollutant concentration data (mg/L), hydraulic loading rate (HLR, m^3/m^2d), and hydraulic retention time (HRT, d) were tracked and collated. The key pollutants of interests for analysis were biochemical oxygen demand (BOD), chemical oxygen demand (COD), total suspended solids (TSS), total nitrogen (TN), and total phosphorus (TP). If available, mass loading data (g/m^2d) was extracted as well for the key pollutants. Additionally, the frequency of all parameters (environmental, pollutants, microbial assessment, and plant) analysed were recorded based on information provided in the materials and methods section for each publication.

3.3.3 Comparison of Mesocosm Performance to Full-scale: BOD

In order to evaluate the performance of TW mesocosm studies, a single water quality parameter, BOD, was selected to compare to full scale data from Kadlec & Wallace (2009). Relevant articles were mined for average inlet and outlet BOD data, which was separated into 3 groups based on wetland type: FWS, HSSF, or VF. Key figures were extracted from Kadlec & Wallace (2009) for comparison. Following this, the BOD data from HSSF and VF systems was subdivided into 4 categories based on influent concentrations: primary (0-30 mg BOD/L), secondary (30-100 mg BOD/L), tertiary (100-200 mg BOD/L) or super (>200 mg BOD/L). Median areal removal rates were calculated for each subgrouping using the first order P-k-C* model:

$$\frac{C-C^*}{C_i-C^*} = \frac{1}{\left(1+\frac{k}{Pq}\right)^P} \qquad (1)$$

where, C=outlet concentration (mg/L), C^*=inlet concentration (mg/L), P=number of tanks in series, q=hydraulic loading rate (m/d), and k=aerial removal rate constant (m/d). C* values were based on given influent loadings ranges and P values were assumed based on data from Kadlec & Wallace (2009) (Table A.1 and Table A.2).

3.4 Results and Discussion

3.4.1 What Is Being Published?

3.4.1.1 Study Focus

Figure 3.1 **Figure 3.1:** Specific research foci and article count for treatment wetland mesocosms from 1992 to 2017.summarizes the foci and article count per annum for all available TW mesocosm research from the period of 1992 to 2017. Research output was fairly low until 2005/2006 when the number of meso-scale TW publications began a steady upwards trend. It should be noted that the two key terms used of "constructed wetland" and "treatment wetland" were not popularized in the field until the late 1980s-90s and, as such, this likely excluded any previous research predating this time (Carvalho et al., 2017). The first two peer-reviewed journal articles found through the literature search appeared in 1992 from the Pacific Estuarine Research Laboratory in San Diego, USA, and were published in the same issue of Ecological Engineering. The first paper by Busnardo et al. (1992) details the effect of four different hydroperiods on nitrogen and phosphorous removal in 925 L planted subsurface TW mesocosms. The authors suggested that a pulsed-discharge (or as we now call them tidal flow) TW could provide better pollutant removal and protection to downstream natural salt water marshes by reducing the issue of salinity dilution. Findings showed that fill and drain cycles enhanced phosphorous removal by 20-30% compared to the continuously loaded systems. The second paper by Sinicrope et al. (1992) detailed the same set of systems, examining the effect of different hydroperiods on the removal of metals (Cd, Cr, Cu, Ni, Pb, and Zn) from wastewater. Both articles were categorized under a hydrological focus with the former having an additional focus on nutrients removal and the latter on the removal of metals.

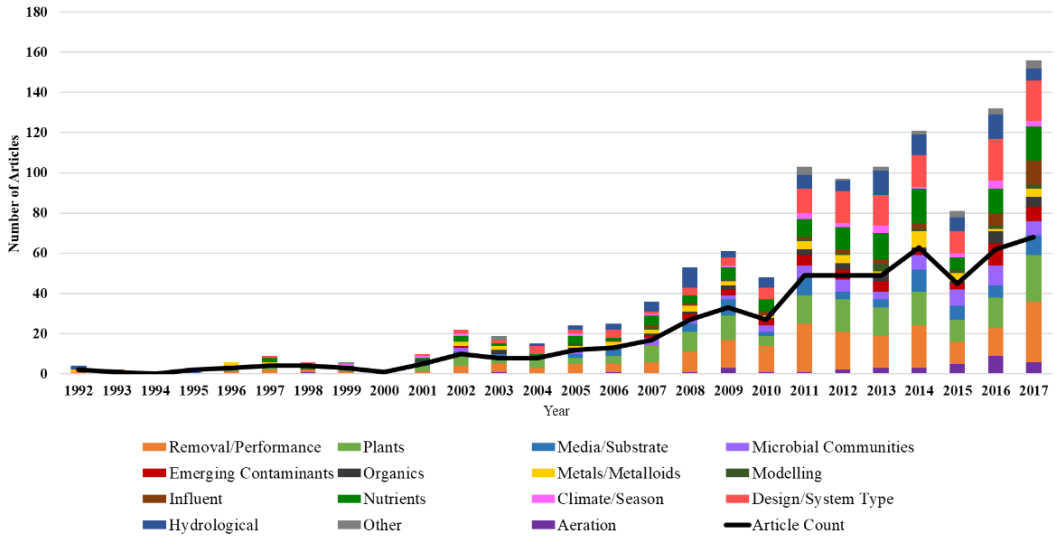

Figure 3.1: Specific research foci and article count for treatment wetland mesocosms from 1992 to 2017. Multiple focus areas were noted for a number of articles.

Over time, as these systems are built for water pollution control, the most prevalent research area was the general performance of the wetland mesocosms. However, this was typically coupled with other TW aspects to further knowledge and optimize treatment potential. In fact, nearly all articles in the present meta-analysis had multiple areas of focus being studied concurrently. Due to the ease of replicability of mesocosms studies, they have become ideal tools to investigate a diverse number of research topics within a single study. The first major focus area was related to the role of plants in TWs. Wetland vegetation is considered one of the key features in TW ecology; however, that can indirectly and directly improve pollutant removal by plant uptake and improving microbial density in the rhizosphere (Brix, 1994; Dotro et al., 2017). This topic encompassed research regarding the comparison of planted vs. unplanted systems, performance of different plants species, planting regimes, plant uptake, and plant development, among others. The most popular plants used across these mesocosm studies were emergent macrophytes of the *Phragmites spp*. and *Typha spp*., similar to full-scale systems (Vymazal, 2013). It should be noted that several recent review articles have called for more extensive studies regarding the role of plants in TWs; however, concerns have been brought up regarding the use of mesocosm scale systems for these investigations due to growth limitations (Kulshreshtha et al., 2022; Vymazal et al., 2021).

The second well-covered focus area of TW mesocosms was related to system design/type. There was a total of 135 different investigations into the performance of specific design modifications (e.g., step-feeding, baffle flow, microbial fuel cells) or comparing wetland types (e.g., HSSF vs. VF). In this meta-analysis artificial aeration was kept as a separate research area from design modifications. This intensification is used to increase the transfer of oxygen within TWs in order to improve organic carbon and nitrogen removal in TW systems (Boog et al., 2014). At the meso-scale, publications began to emerge regarding aeration in 1998, but only started being consistently studied after 2008. Similarly,

investigations into operational modifications of HLR and HRT were categorized separately as hydrologically focused, which accounted for a total of 90 different research articles.

The third most popular focus area that was consistently studied was the removal, transformation, and fate of nutrients in TW mesocosms. The most attention, approximately 53% of all nutrient related studies, focused on nitrogen, which has always been a central pollutant when assessing TW treatment capabilities. A number of these studies concurrently assessed other nutrients (organic carbon or phosphorous) and were viewed through multiple different TW aspects, such as design variations, different C/N loading ratios, microbial community assessments, and influence of substrates. Substrates have a central role participating in the filtration and adsorption of pollutants, and as biofilm carriers (Ji et al., 2022). Subsequently, they are another major area of study globally with a total of 81 related publications focused on the impacts of different substrates in TW beds at the meso-scale. Novel substrates investigated included light expanded clay aggregates (LECA) (Oopkaup et al., 2016), zeolite (Vera et al., 2014), waste rubber chips (Chyan et al., 2013), oyster shell (Sousa et al., 2011), basalt (Iasur-Kruh et al., 2010), crushed limestone (Stark et al., 1996), and tezontle (Zurita et al., 2012).

Notably, from 2011-2017, the number of different focus areas per article dramatically increased as research became more multiphasic. Over the same time period, two smaller research topics emerged as trending foci for TW mesocosms. The first being studies examining the activity, enumeration, structure, and function of TW microbial communities. A full overview by Weber (2016) detailed the development of microbial community analysis used in TW systems. The second trending focus area was emerging contaminants such as pharmaceuticals and personal care products, pesticides, surfactants, and nanomaterials where their effects and fate are widely unknown in TWs. Other research areas included metals, organics, modelling studies, climate/seasonal impacts and influent wastewater composition (i.e., acid mine drainage, landfill leachate, industrial).

3.4.1.2 Wetland Type and Size

Across all publications, of the three main design types, 14.6% were identified as FWS, 38.7% as HSSF and 35.7% as VF mesoscale TWs (Table 3.1). Only a small fraction of articles examined floating treatment wetlands (7.8%) or hybrid (3.2%) designs (data not included). In Figure 3.2, the subsurface systems show relatively well distributed size ranges across the entire mesocosm scale (10-1000 L); whereas, the FWS systems were more frequently in the 500-1000L range. Overall, the median mesoscale FWS were 34% and 86% larger than their HSSF and VF counterparts, respectively. Due to the larger land requirement needed for surface flow systems this may explain the lower occurrence of FWS mesocosm research. Interestingly, a number of mesoscale systems were described in text as either microcosms or as pilot-scale systems; however, met the 10-1000L mesocosm criteria set in this study.

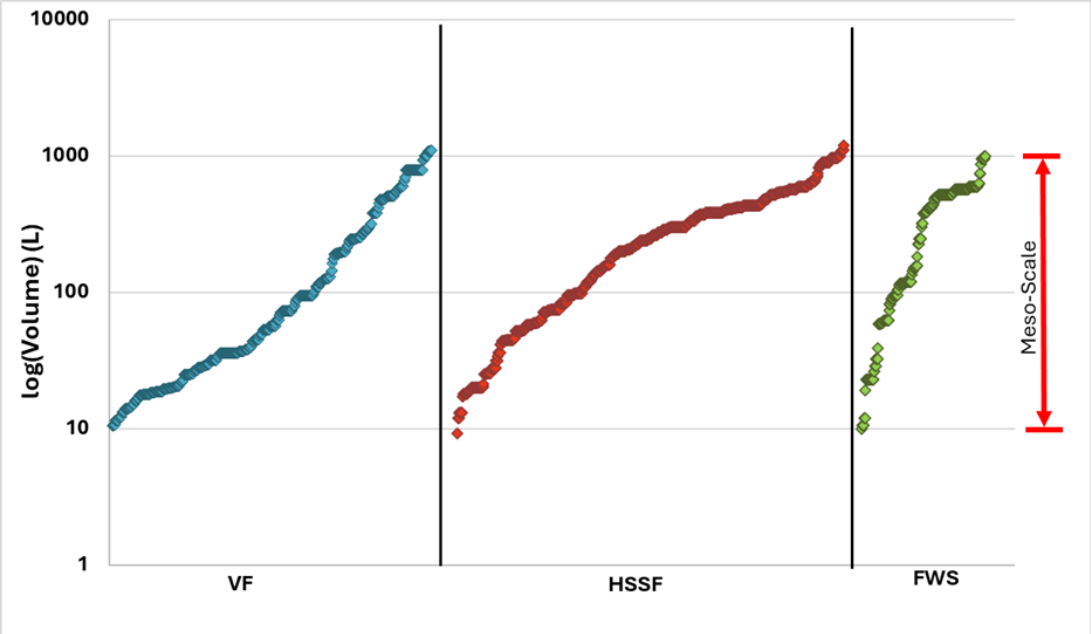

Figure 3.2: Size distribution of the three main design types of treatment wetland mesocosms from 1992-2017. Each point represents the total volume of a unique wetland system (defined by design type, presence of plants, substrate type, influent, and operational mode (batch vs. continuous).

Also, a number of systems across all wetland types can be subcategorized based on specific operational and design modifications used to improve treatment performance. These included the addition of baffles to extend the flowpath/residence time, anodes, and cathodes for microbial fuel cell designs, upflow vs. downflow in VF systems, recycled flow, and step-feeding among others. The most popular operational regime employed was the fill/drain (also referred to as fill/draw and tidal) set-up, which was used for 8.7% of systems as a means of reoxygenating the TW to improve overall performance. Similarly, artificial aeration was investigated in 5.7% of all designs of which 57% of systems were identified as VF and 43% as HSSF.

Of the 1486 unique designs being used globally, only 46.5% had replicate systems, which can be linked to roughly 32% of total published studies in this meta-analysis. In some studies, there was a lack of clarity in the number of systems per studies as there was no mention of replicated systems in the experimental design, but the authors indicated in the results that data was obtained from duplicate or triplicate systems. Some authors opted to use temporal replication for data validation rather physical systems.

Table 3.1: Summary of different wetland designs usage, median size and influent wastewater characteristics of TW mesocosms used in publications from 1992 to 2017.

System Type	Usage Frequency	Median Size (L)	Influent	
			Source	*Synthetic*
FWS	14.6%	378.5	59%	41%
HSSF	38.7%	250.0	58%	42%
VF	35.7%	53.0	55%	45%

3.4.2 What Mesocosms Designs are Being Used and Where?

In this meta-analysis, the final 542 relevant TW mesocosm publications originated in 52 different countries across the globe, representing 1486 unique designs. To investigate geographical shifts in the research field over time, the dataset was subsequently divided into two time periods, 1992-2005 and 2005-2017, for simplicity (Figure 3.3). Prior to 2005, North America, specifically the United States, was the main source of TW mesocosm scale studies globally. In the same time frame, Europe and Asia produced a similar number of articles accounting for a combined total of 36.8% of the meso-scale research generated. The top focus area across the globe from 1992-2017 was related to the treatment performance of the mesocosm systems. Ignoring this category, the next top 3 focus areas were determined for each continent. From 1992-2005, TW plants were one of the top 3 focus areas that was investigated in all continents. In the northern hemisphere, there were a significant number of publications examining metals in TW mesocosms. Authors primarily studied Mn, Zn, and Fe, examining the removal efficiencies under different environmental parameters and hydrological conditions. Other top study areas included nutrients and system design/type.

From 2005 to 2017, Asia dominated the research field accounting for 44% of the papers published using TW mesocosms with the majority (75%) originating from the Republic of China. Europe had the second highest number of publications, followed by North America. Interestingly, South America, which previously did not have any meso-scale studies, now accounted for 3.9% of worldwide research articles. Though the relative global research output decreased from Africa and Oceania, the number of studies in these regions increased between the two time periods. In tandem with the increase in publications, there was also shifts in the top three regional research areas after 2005. While plant-based mesocosm studies still dominated the research field, interest in metals dropped while nutrient and hydrological investigations became more prominent worldwide. Hydrological based studies examined the influence of different HLR or HRT on treatment efficiencies as well as the clogging phenomenon in subsurface systems. The first clogging paper was published by Zhao et al., (2004) from the United Kingdom. The authors examined the difference between anti-size and progressively-sized arrangement of media in reed beds to mitigated clogging in multi-stage VF TW mesocosms receiving authentic animal wastewater. In Africa, the spatial and temporal evolution of TW microbial communities were the second highest focus area in this region. Similarly, in South America there was a specific regional focus on organics primarily out of Colombia.

In North America, Europe, and Asia all three wetland types were equally investigated between 1992-2005. Whereas, in the southern hemisphere subsurface systems were predominately employed. From 2005 to 2017, the number of unique systems being used across the globe increased dramatically. In terms of design, studies focused primarily on subsurface systems with a smaller proportion of meso-scale FWS being reported. Most regions had a relatively even distribution between the use of HSSF and VF designs except for North America where there appeared to be a preference in the use of HSSF systems.

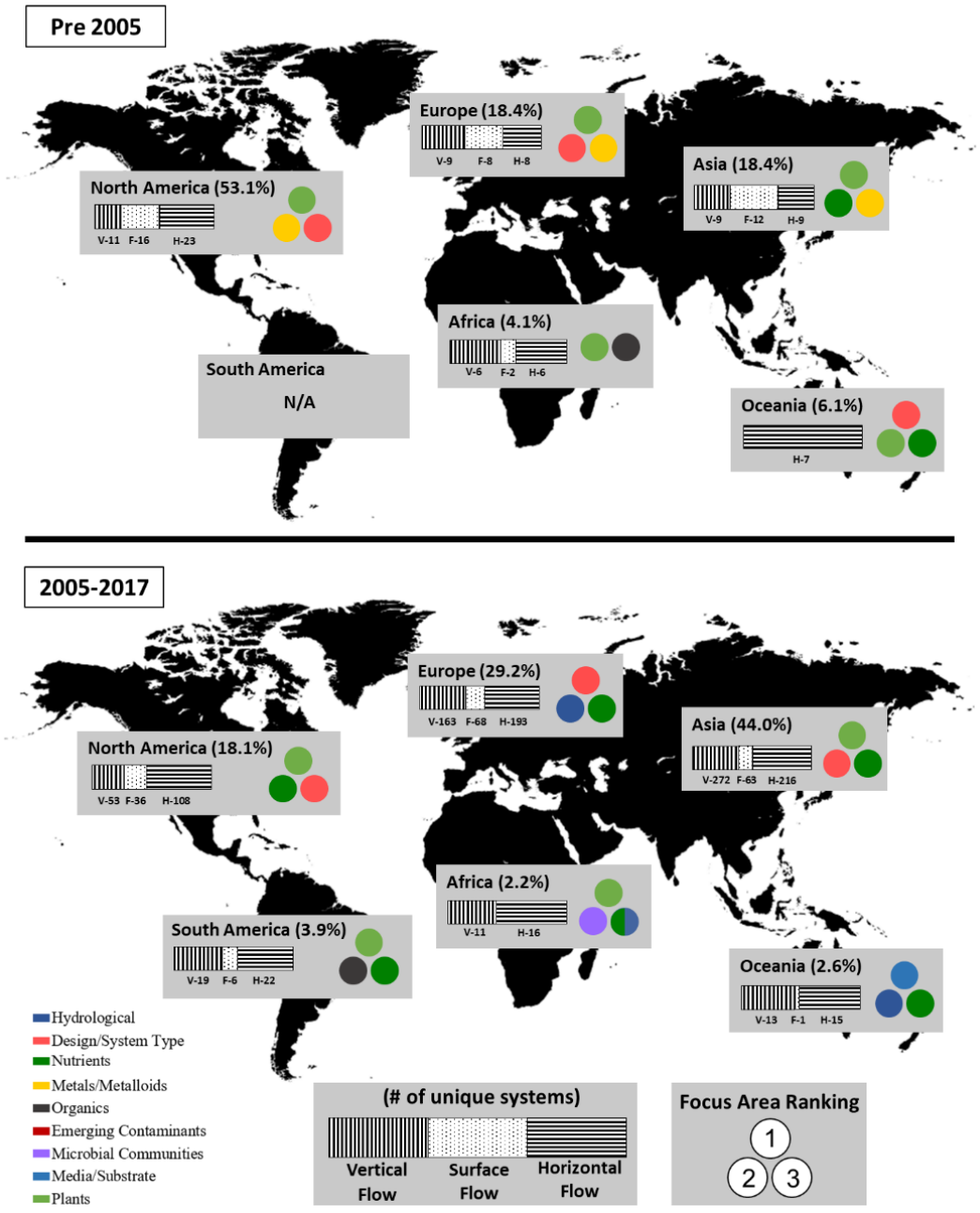

Figure 3.3: Summary of regional trends for treatment wetland mesocosm studies for the periods of 1992-2005 (top); 2005-2017 (bottom). Percentages are based on total number of publications from each geographic location. Dots represent the top 3 study focus areas in each region during the time period.

3.4.3 What Is Being Analyzed?

In this meta-analysis, a wide range of wastewaters types have been applied to TW mesocosms. The most popular include untreated domestic wastewater, secondary wastewater treatment plant effluent, polluted river water, stormwater, urban, dairy, piggery among others. One concern within the TW field is that meso-scale system predominately receive synthetic wastewater, which lacks the complexity of real wastewater creating a large disconnect between laboratory research and full-scale studies (Collison and Grismer, 2013). Based on the current meta-analysis both synthetic and source (or authentic) influent wastewater was applied equally to all 3 TW designs at the meso-scale (Table 3.1).

Figure 3.4 displays the frequency of key water quality parameters used from 2005-2017 based on the TW type. Across all systems, nitrogen was the top pollutant reported at the meso-scale primarily analyzed in the form of ammonium and nitrate in order to assess total nitrogen removal through nitrification and denitrification pathways. The second most popular metric was COD, used to measure organic removal, followed by phosphorous. In terms of environmental parameters, pH, redox potential (ORP), dissolved oxygen (DO), and conductivity were reported in some, but not all publications. This may be due to the fact that the research papers chose not mention these basic metrics and instead focused on other assessments. However, these parameters are critical when discussing TW research as they can heavily influence different microbially mediated removal mechanisms (Rahman et al., 2020). Other parameters of interest included emerging contaminants and assessments of TW microbial communities. Interestingly, VF systems were more frequently used to monitor and evaluate emerging contaminants compared to HSSF and FWS systems. Within the focus of this meta-analysis, microbial communities were rarely monitored in FWS systems; instead, substrate samples were often taken from subsurface systems to complete 16S RNA sequencing on microbial biofilm communities.

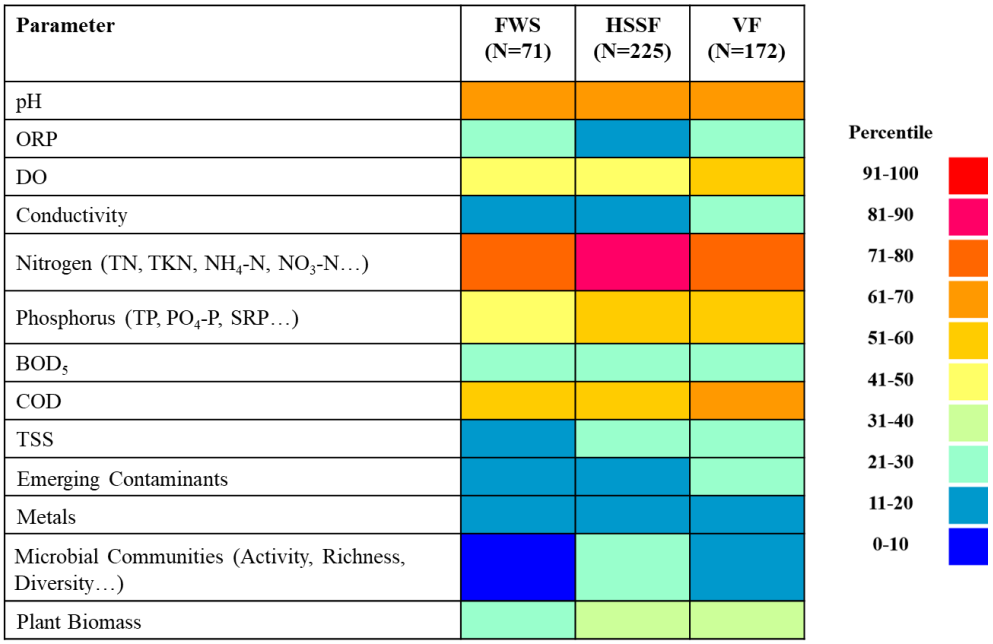

Figure 3.4: Heatmap of top parameters used in 3 main treatment wetland mesocosms designs across the period of 2005-2017, where N=number of articles.

3.4.4 Full-Scale Comparison: BOD

From the large data set obtained through this meta-analysis, a secondary investigation to compare the BOD removal performance of TW mesocosms to their full-scale counterparts was executed. The full-scale data was retrieved from the 2nd Edition of Treatment Wetlands by Kadlec & Wallace (2009). The relationship between influent and effluent BOD data from all relevant TW mesocosms is shown in Figure 3.5 and overlaid on the full-scale data for each system type (The original plots are shown in Figure A.1). This graphical representation of treatment potential illustrated little difference in overall performance between meso-scale and full-scale TW systems even at high influent concentrations (over 1000 mg BOD/L). The data fit relatively well for HSSF and FWS mesocosms, exhibiting a similar log-linear relationship between the inlet and outlet values with 96% of the data above the lower boundary line (denoted by the dashed C* line) of the full-scale systems. In the case of VF systems, while the full-scale inlet and outlet data was poorly correlated (R^2 =0.14), the meso-scale displayed a clear positive trend with increasing inlet concentrations (R^2 =0.78). Additionally, each TW type displayed a high degree of variability between individual wetland systems within their datasets at both scales. This variability at the meso-scale is linked directly to their purpose as flexible TW research tools to examine the effects of different operational and design configurations.

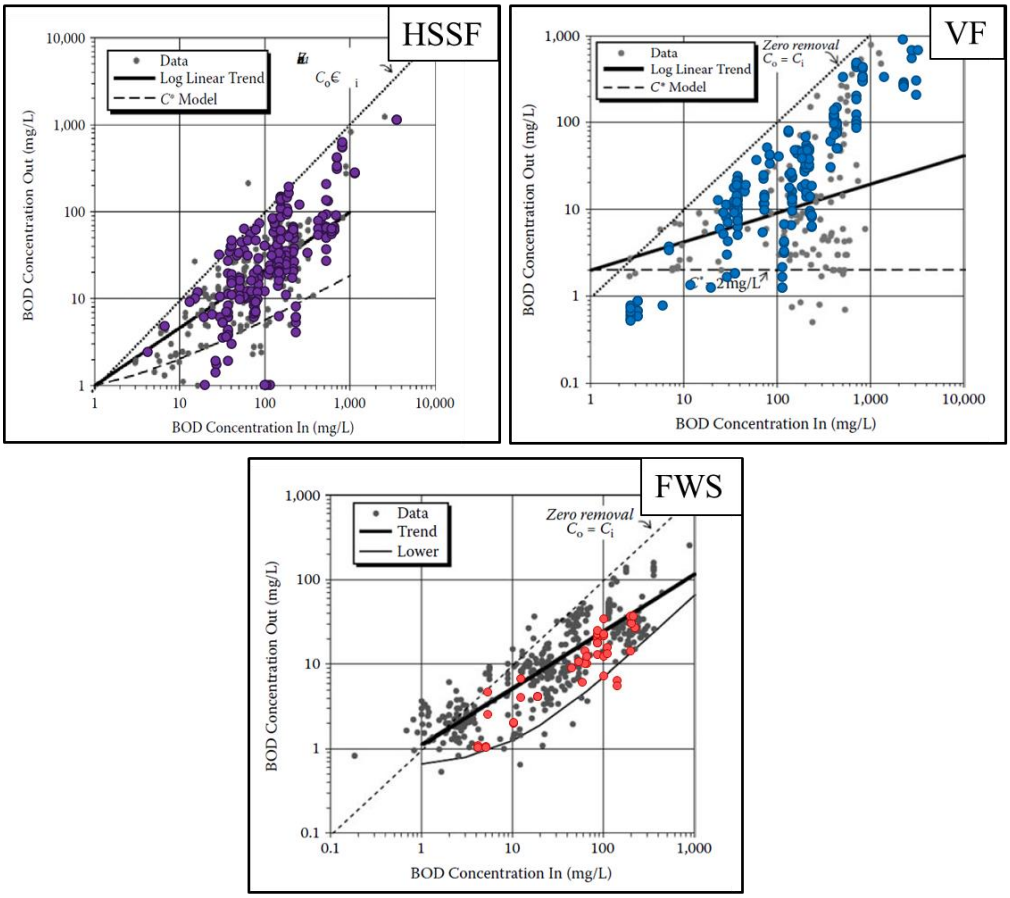

Figure 3.5: BOD input-output concentrations for vertical flow, horizontal flow, and free water surface treatment wetland designs. Base graphs were taken from Chapter 8 of Kadlec & Wallace (2009). The HSSF graph represents data from 202 full scale systems overlaid with data from 210 mesoscale HSSF TWs. The VF graph represents data from 62 full scale TW systems overlaid with data from 189 mesoscale VF TWs. FWS graph represents data from 138 full scale TW systems overlaid with data from 44 mesoscale FWS TWs. The lower bound line excludes approximately 5% of the lower full-scale data points and represents the estimated background concentration (C*). Meso-scale data is represented through colour in each graph.

The median areal removal rate coefficients (k_A) were calculated for the subsurface BOD datasets using the first order P-k-C* model (Eq. 1) under the same assumptions used in Kadlec & Wallace (2009). At different influent concentration levels, the calculated k-values for VF and HSSF TW mesocosms fell predominately within the central range of the full-scale k-distribution (Table 3.2). The overall median k_A values were 158 m/yr and 45 m/yr, respectively for all VF and HSSF meso-scale systems. Even though mesocosms are controlled systems, their overall performance, with respect to BOD, is comparable to realistic full-scale

TW systems with little impact between different scales of operation. It should be noted that the full-scale range is relatively broad representing the seasonal fluctuation and data gathered over long periods. Yet, we can still conclude that TW mesocosm are relatable to full-scale systems. While this data is promising in moving forward when discussing TW scalability, this is only in the context of BOD performance. The removal rate constant will vary by pollutant based on the internal mechanisms of the TW. Further investigation into main water quality parameters, including TN, TP and COD are needed to gain an understanding of the true adaptability of meso-scale systems.

Table 3.2: First-order areal removal rate constant (k_A, m/yr) for HSSF treatment wetlands. [a]Full-scale data retrieve from Kadlec & Wallace (2009). N = number of unique systems.

	BOD	**Tertiary**	**Secondary**	**Primary**	**Super**
	C_i (mg/L)	3-30	30-100	100-200	>200
HSSF	*Percentile*	*Full-Scale[a] k_A (m/yr)*			
	0.4	63	30	23	33
	0.5	86	37	25	66
	0.6	154	39	28	98
	0.7	224	44	44	114
	0.8	287	82	62	210
		Mesocosm Scale k_A (m/yr)			
	N	9	51	28	30
	Median	66	43	56	47
VF	*Percentile*	*Full-Scale[a] k_A (m/yr)*			
	0.4	210	57	153	101
	0.5	471	73	187	143
	0.6	751	91	253	160
	0.7	1025	101	280	246
	0.8	1756	113	343	316
		Mesocosm Scale k_A (m/yr)			
	N	10	16	16	35
	Median	217	91	236	148

3.4.5 Gaps in Research and Future Directions

It is clear that the mesocosm has become an essential research tool in the field of TWs. They are ideal systems to validate concepts and theories within realistic setting that is comparable to the full-scale. This meta-analysis showed that meso-scale based studies are increasing dramatically, from a total of 49 studies published between 1992-2005 to 493 total articles between 2005-2017. In parallel, publications became more multi-focused, spanning topics including the combination of classically studied areas, such as nitrogen removal and plant selection; in combination with novel topics, including microbial fuel cells, artificial aeration, and micropollutants. The diversification of research, in turn, serves to stimulate new discussions and theories on the internal mechanisms of TW.

However, not all TW mesoscale research is the same. Through this meta-analysis, the authors observed that key design information, specifically hydrological information, was missing from publications leading to knowledge gaps. HRT, HLR and flow rate information was missing for 30%, 42%, and 19% of all studies, respectively. Some articles also lacked a description of system dimensions, the presence of plants, and media type and depth which made categorizing and interpreting the results difficult. Additionally, though not presently discussed, the age of the mesocosms prior to the experimental timeframe (the start-up time period) is often not reported in the literature. This is a critical piece of information when completing meso-scale work as microbial communities, which are the main mechanistic driver for the removal of most pollutants, require at least 100 days to reach steady state (Faulwetter et al., 2009; Weber and Legge, 2011). Moreover, microbial communities are also affected by vegetation, which can take several years to be considered established. Due to constraints, some researchers have opted to transplant the vegetation into the system from established wetlands. However, there is no standardize timeframe for the system stabilization in that case. Other publications have grown plants within the systems, but again there is little consistency in the plant establishment period.

While there is still growing concern that meso-scale investigations lack connectivity to the full scale, a lag between small-scale and applied studies is common and expected in ecological research (Benton et al., 2007; Vymazal et al., 2021). The authors agree that more full-scale studies are needed, yet all design modifications and new concepts cannot be tested at the full-scale or even at the pilot-scale. To that end, as the use of the mesocosms in the TW field is not slowing down, the authors recommend that standard design information be included in future treatment wetland studies. This includes, but is not limited to, HLR, HRT, system type, total system dimensions, media size and characteristics, plant descriptions, establishment periods, and feeding strategies. This information will enable researchers to compare and correlate performance between the two scales facilitating the development of scaling factors.

3.5 Acknowledgments

Funding in the form of a NSERC Discovery Grant to KPW is gratefully acknowledged.

3.6 Author Contributions

Anbareen J. Farooq: Conceptualization, Methodology, Investigation, Formal analysis, Data curation, Writing - original draft, Visualization.; **Jacques Brisson:** Conceptualization, Writing – review & editing; **Scott Wallace**: Conceptualization, Writing – review & editing; **KPW:**: Resources, Writing – review & editing, Supervision, Funding Acquisition.

4. Peaks, pores, and dragon eggs: Uncovering and quantifying the heterogeneity of treatment wetland biofilm matrices

Anbareen J. Farooq[†], Mhari Chamberlain[†], Arman Poonja[†], Kevin G. Mumford[‡], Scott Wallace[§] and Kela P. Weber[†*]

[†]Environmental Sciences Group, Department of Chemistry and Chemical Engineering, Royal Military College of Canada, Kingston, ON K7K 7B4, Canada

[‡] Department of Civil Engineering, Queen's University, Kingston, Ontario, K7L 3N6

[§]Naturally Wallace Consulting LLC, Pilot Mountain, North Carolina 27041, USA

*Corresponding author: kela.weber@rmc.ca

4.1 Abstract

Biofilms serve to house diverse microbial communities, which are responsible for the majority of wastewater constituent degradation and transformation in treatment wetlands (TWs). TW biofilm has been generally conceptualized as a relatively uniform film covering available surfaces. However, no direct visual 3D representation of biofilm morphology in TWs has been conducted. This study focuses on imaging the morphology of detached, gravel-associated, and rhizospheric (*Phalaris arundinacea*) biofilms from subsurface TW mesocosms. Images obtained through both traditional light microscopy, environmental scanning electron microscopy (E-SEM) and Wet-SEM revealed that TW biofilms are structurally heterogeneous ranging from corrugated films to clusters of aggregates. Features such as water channels and pores were observed suggesting that pollutant transport inside biofilms is complex, and that the interfacial surface area between water and biofilm is much larger than previously understood. Biofilm thickness generally ranged between 170-240 µm, with internal biofilm porosities estimated as 34 ± 10%, reaching a maximum of 50%. Internal biofilm matrix pore diameters ranged from 1 – 205.2 µm, with a distribution that favored pores and channels smaller than 10 µm, and a mean equivalent spherical diameter of 8.6 µm. Based on the large variation in pore and channel sizes it is expected that a variety of flow regimes and therefore pollutant dynamics are likely to occur inside TW biofilm matrices. Based on the visual evidence and analysis, a new conceptual model was created to reflect the microscale TW biofilm dynamics and morphology. This new conceptual model will serve to inform future biokinetic modelling, microscale hydrology, microbial community assessment, and pollutant treatment studies.

Keywords: biofilm; scanning electron microscopy; bio-aggregates; constructed wetland; microbial community; pores

4.2 Introduction

Treatment wetlands (TWs) are an energy-efficient and cost-effective, nature-based solution for wastewater treatment (Kadlec and Wallace, 2009). Much of the complex wastewater treatment potential in these systems is due to the higher rates of biological activity of their diverse microbial communities (Vymazal, 2011). These microbes develop in either the interstitial water, or by anchoring to any available surface area and forming biofilms on the bed media (gravel-associated) or on plant roots (rhizospheric). Biofilms themselves are complex structures, sometimes referred to as a "slime" at the macro scale due to their sticky nature, that act as bacterial fortresses for microbial species, enclosing them in a self-made matrix known as extracellular polymeric substance (EPS) (Boltz et al., 2017; Davey and O'toole, 2000; Stoodley et al., 2002). The EPS is comprised of polysaccharides, proteins, lipids and extracellular DNA (eDNA), and can account for over 90% of biofilm total dry mass (Nielsen et al., 1997). EPS is an integral component of biofilm that provides a stable 3-D structure, aids in adhesion to surfaces, protects from predation, and contributes to the entrapment of nutrients (Flemming and Wingender, 2010; H. Huang et al., 2019; Murphy et al., 2016). The biofilm structure itself is highly hydrated, containing up to 97% water (Zhang et al., 1998). Without a biofilm, microorganisms will be carried with the flow of water and simply exit the TW system. If this were to occur, the microorganism may offer a limited water treatment capacity while in contact with the pollutants as long as it is present in the TW system, which will be at maximum one hydraulic retention time (HRT) worth of effective service. In actuality, TWs exhibit a range of flow distributions representing different flow paths and removal kinetics not consistent with a clean (biofilm-free) "black box" model. Biofilms, which house microbial communities, are therefore just as important to TW functionality as the microbial communities themselves. In the TW field, many studies have focused on uncovering mechanisms surrounding the "black box" of microorganisms by investigating their activity, function, and structural diversity; however, there are few that have focused on characterizing biofilm at the microscale in treatment wetlands (Weber, 2016).

Over the past few decades, microbial ecologists have begun to use imaging techniques to improve their understanding of biofilm architecture and dynamics. Alongside traditional optical light microscopy, confocal laser scanning microscopy (CLSM), optical coherence tomography (OCT), and scanning electron microscopy (SEM) became popular methods used to characterize biofilm morphology across a variety of different scientific fields. CLSM is often selected as it allows for non-destructive imaging of the internal biofilm structure and 3D structural mapping of a biofilm in its hydrated state. CLSM stacks 2D images, which are taken point by point through localized laser excitation from different focal planes, together to render 3D structures (Canette and Briandet, 2014; Davidovits and Egger, 1969). In conjunction with fluorescent staining, researchers are capable of visualizing specific components within biofilm including nucleic acids, amyloids, and glycoconjugates (Chen et al., 2007; Donelli, 2014; Neu and Lawrence, 2015; Neu et al., 2001; Schlafer and Meyer, 2017). However, this method is limited due to its resolution capabilities and penetration depth. Another non-destructive technique adopted to investigate the structure of biofilms is optical coherence tomography (OCT) (Wagner et al., 2010). OCT uses shorter wavelengths of near-infrared light to produce higher resolution images and increases image penetration into samples to determine both thickness and morphology of a large areas of biofilm (Hou et al.,

2019). In the case of SEM, which is responsible for providing much of the information currently known about biofilms, high-resolution images of the topography and 3D structure of biofilm can be rendered; however, SEM is no longer considered an ideal method of examination. Sample preparation for SEM analysis requires biofilms to undergo a process of fixation, dehydration, and coating with a conductive layer (El et al., 2012). Researchers have found that this does not maintain the structural integrity of biofilm due to the biofilm losing the majority of water before analysis, which tends to cause the collapse of the EPS (Bergmans et al., 2005). Variations of SEM, such as Cryo-SEM and environmental-SEM (E-SEM), are considered optimal alternatives. Specifically, E-SEM imaging became popularized as it does not require any sample preparation, thus conserving the natural hydrated structure of the biofilm (Alhede et al., 2012; Karcz et al., 2012; Little et al., 1991). E-SEM operates with elevated chamber gas pressure rather than under vacuum and, as such, offers an environment which reduces the rate of water loss. This can be improved further by coupling E-SEM with a Peltier sample cooling stage, a method known as Wet-SEM, to control the humidity of the chamber and maintain fully hydrated structures. Other techniques such as nuclear magnetic resonance (Renslow et al., 2017), confocal Raman microscopy (Zhang et al., 2019), and atomic force microscopy (Chatterjee et al., 2014; Huang et al., 2015) have been used in biofilm characterization, but are not favoured for imaging purposes.

Imaging methods have shown that mature microbial biofilms, from single species to more complex environmental samples, are not always uniform in their morphological characteristics; instead, they can display heterogeneity and have complex structures (Neu and Lawrence, 1997; Stewart et al., 1995; Wimpenny et al., 2000). This directly conflicts with the traditional TW biofilm model used in macroscale investigations, which has previously been modelled or conceptualized as a uniform homogeneous entity (Figure 4.1). This is mostly due to the difficulty in obtaining and characterizing a representative sample in a lab environment without destructive sampling. Under this approach, previous TW macroscale models have attributed the main mechanism of substrate transport into the biofilm matrix to diffusion across a relatively homogeneous planar surface layer (Murphy et al., 2016; Rajabzadeh et al., 2015). Although this conceptual understanding may be correct in some instances, there have been no detailed studies completed to test this conceptual assumption. Moreover, any differences in morphology would directly influence the approach taken when modelling biokinetics and hydraulics in TW systems.

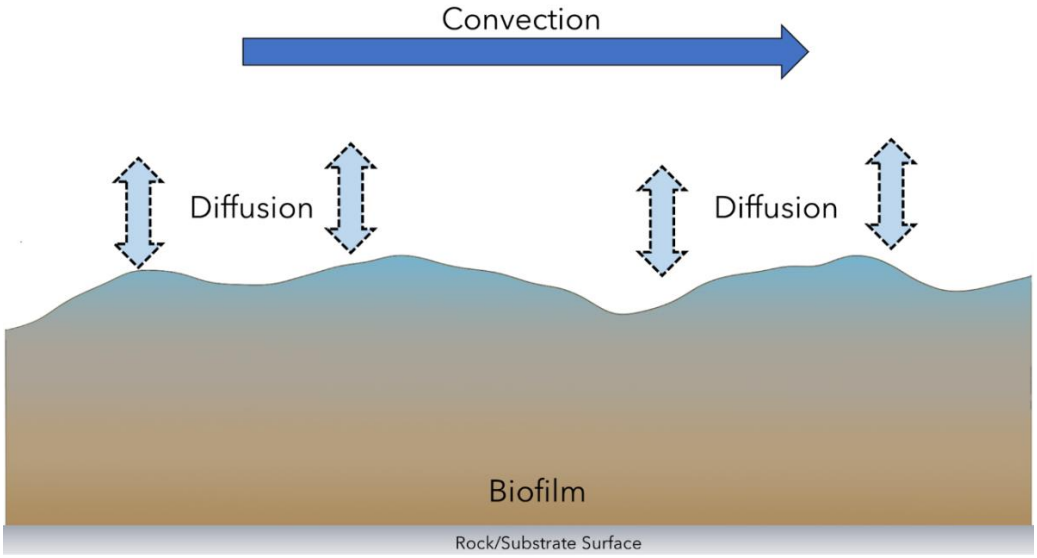

Figure 4.1: Traditional conceptual model of treatment wetland biofilms

In order to more accurately understand the interaction of pollutants with biofilm in TWs an improved understanding of biofilm morphology is required. Therefore, the goal of this study was to examine the morphology of mature detached, gravel-associated, and rhizospheric TW biofilm samples using traditional optical light microscopy, E-SEM and Wet-SEM. To the authors' knowledge, this is the first study to investigate the morphology and architecture of biofilms in TW systems.

4.3 Materials and Methods

4.3.1 Treatment Wetland Design

Biofilm samples were harvested from three batch-fed (7-day HRT) saturated subsurface recirculated flow TW mesocosms that had been in operation for approximately 1 year; one intensified with artificial aeration (M1) and two non-aerated. In the pair of non-aerated systems, one was planted (M2) with reed canary grass (*Phalaris arundinacea*) while the other remained unplanted (M3). *P. arundinacea* was selected as it is a ubiquitous emergent vegetation species found in natural wetlands (Vymazal, 2013). The mesocosms were a modified design of those used in (Weber et al., 2008). Briefly, the mesocosms were built using clear PVC pipes (61.0 cm height x 25.5 cm diameter) and filled to ~55 cm with pea gravel (Ø 5-20 mm) with an initial void volume of 10 L (Figure 4.2A), giving a drainable porosity of 0.35. Water was continuously recirculated through the mesocosms using a magnetic drive pump (Little Giant Pump Company, 1-AA-MD) and distributed below the surface of the gravel through a distribution tee made from ½" clear PVC tubing (Figure 4.2B). The mesocosms were originally seeded with activated sludge (0.5 L/mesocosm) as an inoculum from a local wastewater treatment plant (Cataraqui Bay Wastewater Treatment Plant, Kingston, ON). The activated sludge was applied in three layers (at 15, 30 and 45 cm) during

the gravel filling stage. The mesocosms were batch fed weekly (renewed) with a simulated wastewater solution as described by Weber and Legge (2011) which yielded a final COD:N:P ratio of 100:5:1. Throughout the study, the mesocosms were monitored in laboratory conditions with a relative humidity of 40-60% and ambient temperature of 21-25˚C.

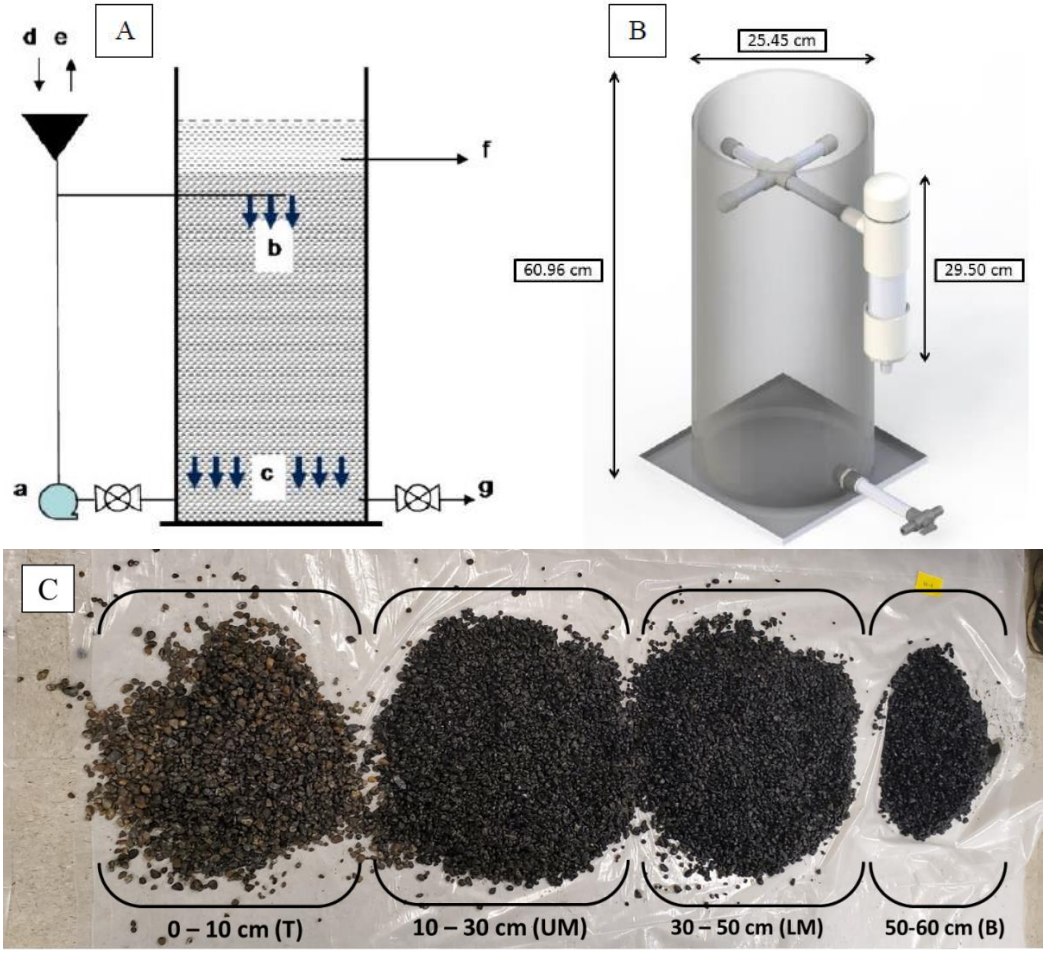

Figure 4.2: (A) Mesocosm schematic: Water is continuously circulated by the pump (a) and distributed into the mesocosm (b) water flows vertically through the mesocosm and is collected at the bottom (c). A port has been affixed to the mesocosm near the water inlet. This is used for injection of tracers (d) and sampling (e). An outlet is positioned at (f) to ensure consistent filling, and at (g) for convenient draining. **(B)** Solid Works render of the mesocosm detailing the build without the tubing and pump. **(C)** Photos of gravel layers increasing in depth from left to right (T -top, UM - upper middle, LM - lower middle, and B - bottom) taken during destructive sampling of M3

4.3.2 Water Chemistry

Water chemistry measurements (temperature, pH, dissolved oxygen (DO), ammonium (NH_4-N), nitrate (NO_3-N), oxidation-reduction potential (ORP), and conductivity) for M1 and M3 were determined via the sampling port using a YSI Professional Plus Multiparameter Water Quality Analyzer (YSI Inc., Yellow Springs, OH) (Table B.1). Water chemistry of M2 was not actively monitored during the operational phases, but M2 was operated under the same feeding and operational schedule as M1 and M3. Water treatment capability was assessed through Total Organic Carbon (TOC) and Total Nitrogen (TN). Samples collected from the simulated wastewater tank (0 hr) and from the sampling port 15, 30, 45 and 60 min after mesocosm renewal were used to determine a TOC/TN kinetic profile. Samples were also taken once a day at 24, 48, 72, 96 and 168 hour post-renewal. TOC/TN samples were kept in a freezer (-4°C) until analysis, where each vial was thawed and subsequently analyzed using the Analytik Jena, TOC/TN (2100s multi N/C Series, Germany).

4.3.3 Biofilm Sampling

Biofilm sampling occurred in three phases (Table B.2). Initially, during operation (phase I), samples of detached biofilm were collected from the top 20 cm of the two unplanted systems (M1 and M3). A serological pipette was inserted roughly 15 cm below the surface and a small amount of agitation was applied before sampling to encourage the detachment of the surrounding biofilm from the gravel. A total volume of 10 mL of a mix of interstitial water and loose biofilm was extracted for imaging. In phase II the unplanted mesocosms were destructively sampled to assess the gravel-associated biofilm architecture at different depths. M1 and M3 were drained and their substrate was removed and divided into four layers: 0-10 cm (top-T), 10-30 cm (upper middle-UM), 30-50 cm (lower middle-LM), and 50-60 cm (bottom-B) (Figure 2C). A total of 20 g of gravel was taken from each layer to be used for E-SEM analysis. An additional 5 mL sample of detached biofilm was retrieved from depth B to be compared to depth T images taken in phase I. This was done to examine to difference, if any, between the top and bottom biofilm morphology in detail. In phase III 5 g of representative root samples were collected from the top 20 cm of the planted mesocosm, M2, to examine the rhizospheric associated biofilm.

4.3.4 Optical Light Microscopy (OM)

Detached biofilm samples were initially examined through light microscopy (2D imaging) to assess morphological characteristics from the unplanted systems, M1 and M3. A total of six slides were prepared per mesocosm. Each slide was loaded with 100 µL of interstitial water with detached biofilm. Three slides from each set of six were either immediately imaged to observe their hydrated state or smeared and heat-fixed prior to imaging. All 2D images were visualized using a Nikon Eclipse 80i microscope (Nikon, Tokyo, Japan). An electron-multiplying charge-coupled device (EMCCD) camera (Luca S, Andor, Belfast, UK) in combination with open-source software Micro-Manager (https://www.micro-manager.org) were used to capture images. The slide area occupied by heat-fixed and hydrated biofilm were visually compared to assess shrinkage due to water loss. No cover slips were used to prevent the compression of biofilm structure during wet imaging.

4.3.5 Scanning electron microscopy: E-SEM and Wet-SEM

Imaging of biofilm architecture was performed using a scanning electron microscope at 30 kV (Quanta FEG 250, ThermoFisher Scientific, OR, USA) in environmental mode. In phases I and II triplicate samples were prepared for imaging from each system first for E-SEM, and then for Wet-SEM analysis. In phase I 100 µL of detached biofilm from M1 and M3 was dispersed on a SEM sample holder stub covered with carbon tape. Relatively flat gravel samples with attached biofilm were selected from the defined depths (T, UM, and LM) of M1 and M3 and were fixed to a sample holder stub using carbon tape before imaging. In phase III a total of 6 root tip and hair samples from M2 were cut (1 cm length) and affixed to a sample holder stub using carbon tape. Carbon tape was used for SEM analysis to provide fixation of the sample to the mounted stub. In phases I and II E-SEM micrographs were initially collected at an ambient air pressure of 300 Pa within 30 minutes of sampling. Following this, the sample cooling stage was installed in the SEM chamber to perform Wet-SEM imaging. To maintain a hydrated biofilm during Wet-SEM imaging the samples were cooled between 1-5˚C at 750 Pa to achieve upwards of 95% humidity within the specimen chamber. Only E-SEM imaging was done in phase III to determine rhizospheric biofilm morphology.

4.3.6 Image Analysis: ImageJ and MATLAB®

Six representative Wet-SEM images of the biofilm morphology were selected for further analysis using a combination of ImageJ and MATLAB® (MATLAB R2022a, Mathworks) software to determine porosity and pore size (Figure B.1). To obtain quantitative pore distributions, the grayscale micrographs were manually thresholded into 2D binary images. The porosity was determined for each image based on the areal proportion of dark (pores) vs white (biofilm) pixels (Buckman et al., 2017). Following this, MATLAB® code was generated to map and quantify the pore diameters of clusters containing 20 or more dark pixels within each image to eliminate noise (Figure 4.3).

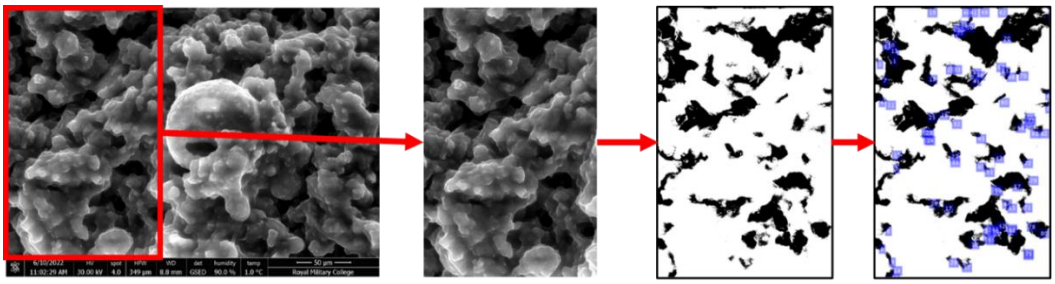

Figure 4.3: E-SEM image processing steps through both ImageJ and MATLAB ® for pore analysis

4.4 Results and Discussion

4.4.1 Biofilm Morphology

A combined total of over 100 images were taken of detached, gravel-associated and rhizospheric subsurface TW biofilm to investigate their three-dimensional structures. No discernable morphological differences were observed between the aerated (M1) and non-aerated (M2 and M3) images in both SEM and OM analyses. Therefore, aerated and unaerated system images were considered interchangeable for analysis.

In phase I images obtained of detached biofilm through conventional optical microscopy revealed a non-uniform thickness in the biofilm matrix with darker regions associated with areas of higher biomass density (Figure 4.4). Additionally, a visual comparison between the heat-fixed (Figure 4.4D-F) and wet slides (Figure 4.4A-C) shows a large reduction in biofilm size, both in width and thickness, from its hydrated state. While these images are 2D representations, the 3D aspect of thickness can be inferred as it is proportional to the vertical displacement of stage as it moves between different focal planes (Bakke and Olsson, 1986). Large blurred sections of the biofilm appeared to come into focus in successive layers suggesting plumes extending from the main body.

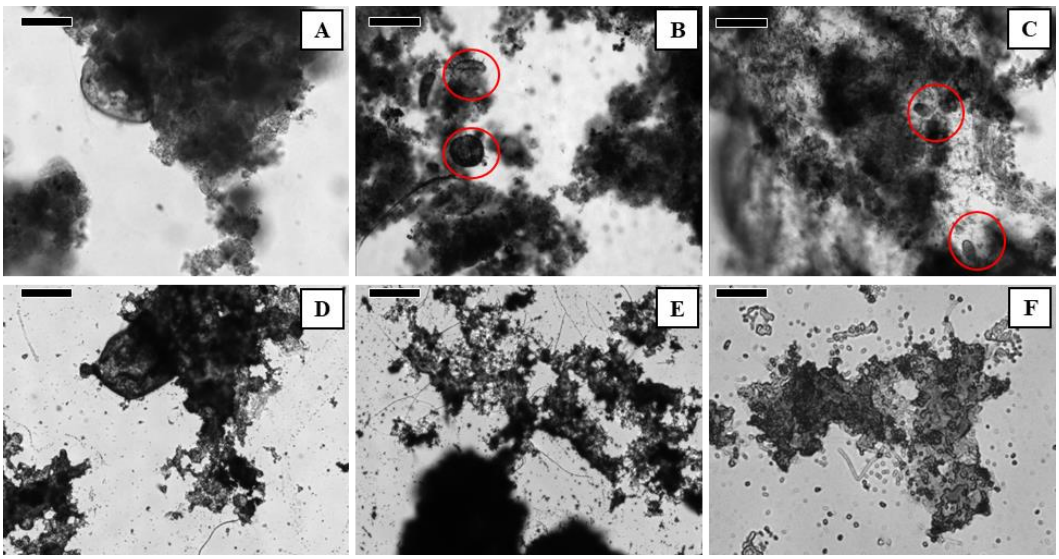

Figure 4.4: Light microscopy images of wet (A-C) and heat fixed (D-F) detached biofilm from depth-T. Organisms noted within the biofilm matrices are circled in red. Image scale bars represent 100 µm in size.

The 3D structure of detached biofilm becomes evident through Wet-SEM images revealing biofilms as porous matrices with visible open channels (Figure 4.5). The grayscale intensity of SEM micrographs can be considered as a reflection of the relative height where lighter pixels represent peaks and darker pixels represent pores (Tavanaei and Salehi, 2015). The topography shows a fairly rough surface with stacked, heterogeneous layers that, at times, resemble small pillars emerging from irregular aggregates. Under E-SEM, the matrix was

partially dehydrated (Figure 4.6A, B) to visualize the underlying architecture of the porous EPS matrix. Upon closer examination of detached biofilms under E-SEM sections of EPS structure appeared as a semi-translucent coating surrounding the microbial communities allowing for partial visualization of the distribution of bacterial cells beneath (Figure 4.6C, D). Clusters of cocci shaped bacteria were observed to be randomly dispersed in the upper layers of the EPS matrix. Their proximity to the biofilm-water interface is likely correlated with a concentration gradient of nutrients and oxygen transporting through the matrix. Further investigations are required to explore the spatial distribution of microbes within the biofilm. Another facet to consider, as the biofilm is detached, the images examined can represent either the surface exposed at the biofilm-water interface or surface adhered to the substrate (i.e., gravel). Under this scenario, the biofilm is not uniformly adhered to substrate surface, but pockets of void space exist between the gravel and biofilm.

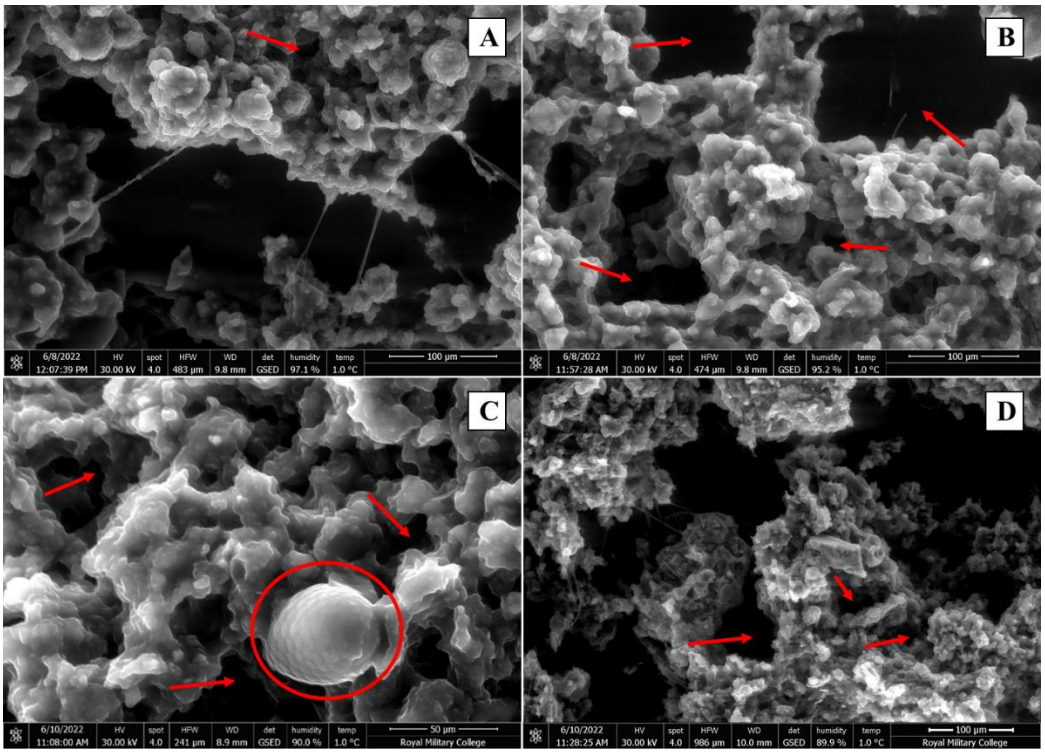

Figure 4.5: Wet-SEM micrographs of detached biofilm taken from depth T (A,B) and depth B (C,D). Pores/water channels observed have been marked with an arrow on the relevant images. A testate amoeba was observed embedded within the biofilm matrix in 6C.

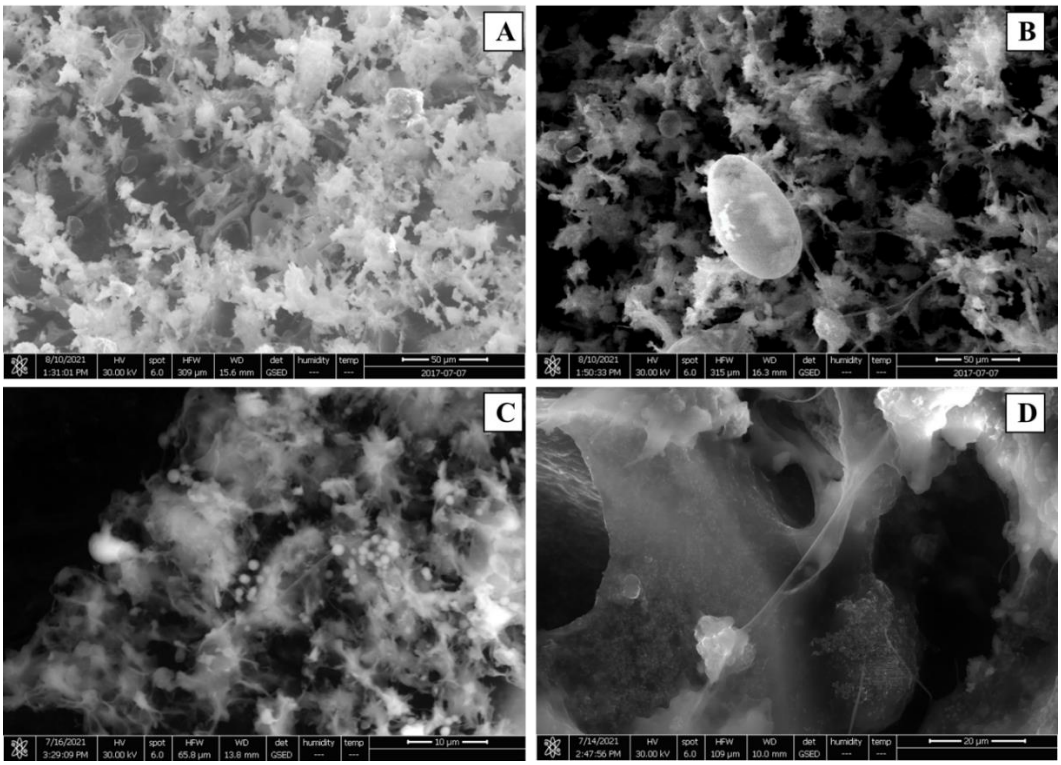

Figure 4.6: E-SEM images of detached partially dehydrated biofilm from depth-B (A, B) and depth-T (C, D).

Similarly, Wet-SEM images of gravel-associated biofilm retrieved from various depths (T, UM, and LM) showed heterogeneous topography of corrugated surfaces or layered stacks with pockets/pores that could increase surface area and reduce convective flow across the biofilm surface (Figure 4.7). For E-SEM images (Figure 4.7C, E) it should be noted that, while there was a gradual dehydration of the gravel-associated biofilm, the inherent structure is identical to the images taken under Wet-SEM (Figure 4.7D, F). Compared to the detached films, the architecture of the gravel-associated biofilm matrix was highly diverse ranging from discrete aggregates to films on the substrate surface; however, the varied architecture appeared across all gravel depths. Overall, biofilm thickness was non-uniform. A maximum thickness observed for the clusters was about 240 µm; whereas the films were slightly smaller, reaching a maximum of roughly 170 µm.

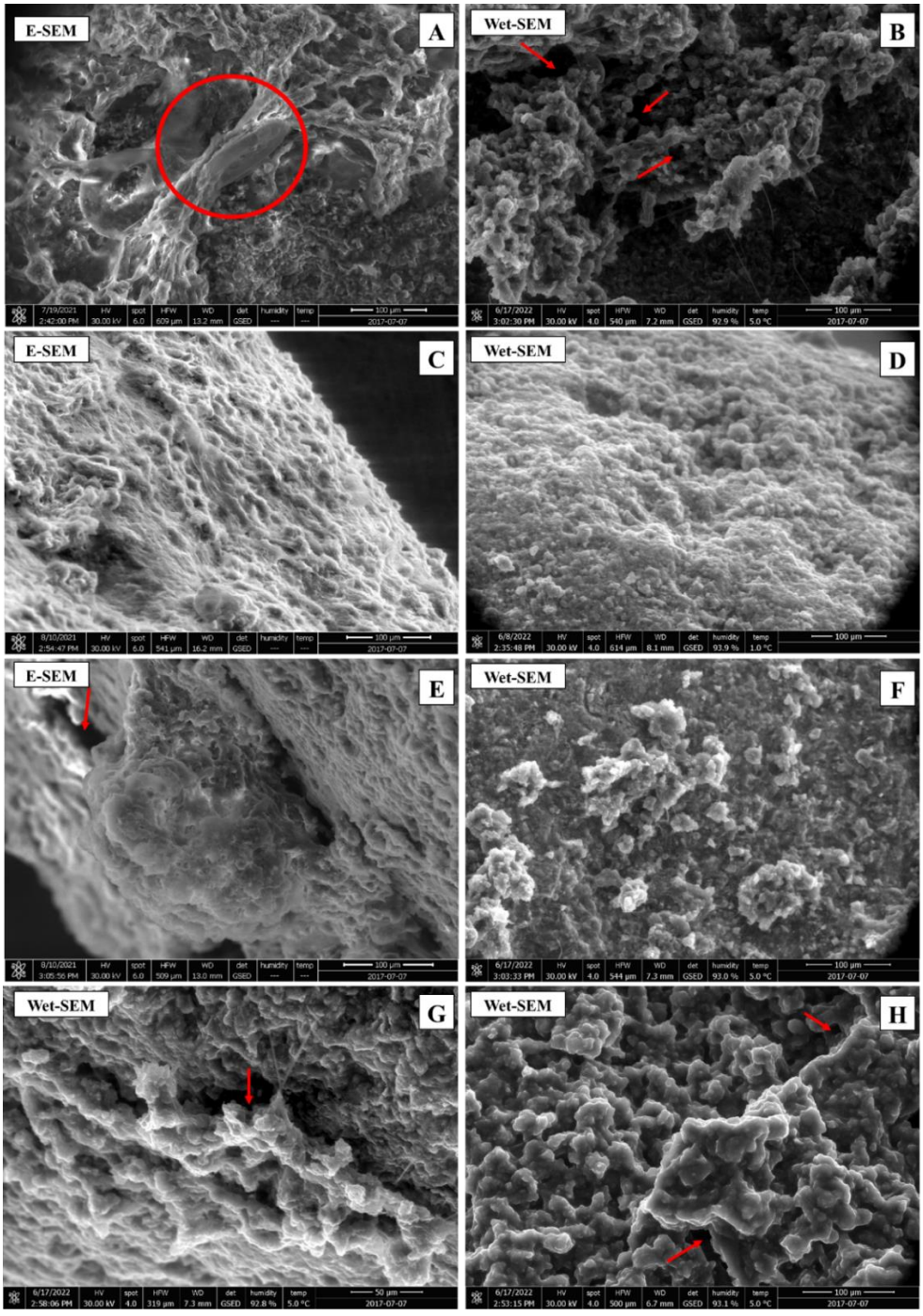

Figure 4.7: Representative E-SEM and Wet-SEM images of gravel-associated biofilm from different depths: T (A, B, G, H), UM (C), and UL (E-G). Water channels have been highlighted with an arrow on the relevant images. Amoebas noted to be embedded within the biofilm matrix in 7A.

Due to the recirculation within these systems, the nutrient load was distributed more evenly, likely leading to minimal differences observed in morphology between the gravel layers. Kim et al. (2010) examined biofilm grown in a porous flow cell on glass beads and found that a combination of flow and nutrient concentrations had a significant impact on the roughness/coarseness (i.e., the structural heterogeneity) alongside the density of biofilms. Limited nutrient availability increases the complexity and roughness of structures as the microbial communities begin to adapt their morphology to search for favourable concentration gradients (Krsmanovic et al., 2021). For example, in static flow environments, as found in batch-loaded TWs, the biofilm structure developed into "pillar-like, filamentous protrusions" due to reduced nutrient flux at its interface (Picioreanu et al., 1998). Specifically, for TWs, spatial variation in biomass density, which has been attributed to nutrient availability, has been frequently reported in subsurface flow systems and is considered a major factor in the phenomenon of biomass accumulation, or "clogging", where inlet regions are characterized by denser biofilm and low hydraulic conductivity, unless appropriate organic loadings are considered during the design process (Button et al., 2015; Deng et al., 2011; Knowles et al., 2011; Nguyen, 2000). It is likely that this change in density is accompanied by morphological adaptation of the biofilm community in full scale TWs.

A key feature observed was the presence of web-like tendrils within the detached and gravel-associated biofilm matrices appearing across 45% of all images taken. These filaments can be seen through and extending out from the EPS matrix (Figure 4.4B-E), appear as fibrous connections between sections of the biofilm matrix itself (Figure 4.5 A, D and Figure 4.7F), and as anchors to the substrate surface (Figure 4.7G). Researchers from fields apart from TWs have identified filamentous structures in biofilm as a combination of the presence of filamentous sheathed bacteria, such as *Sphaerotilus-Leptothrix* (Donelli, 2014; Eaglesham et al., 2004), and streamers, which are morphological features often formed in porous media due to hydrodynamic traction forces under fluid flow (Stoodley et al., 2005). Streamers have a viscoelastic character and oscillate as they extend in length with the direction of flow (Krsmanovic et al., 2021). This unique geometry adds complexity within the biofilm matrix that is still not fully understood. The presence of streamers cannot be confirmed through these images as they initially can have similar thickness as filamentous bacteria and requires further characterization within TWs (Valiei et al., 2012).

This morphology falls in line with visual characteristics seen across the three main conceptual models of biofilm developed outside the TW field. The first was the homogeneous planar model, similar to Figure 4.1, originally developed from SEM images of dental biofilm, which suggested that biofilms form a continuous layer across a substrate with a constant thickness and a small degree of roughness (Nyvad and Fejerskov, 1987). Second, the heterogeneous mosaic model presented by Walker et al. (1995) depicted biofilm from water distribution systems discrete heterogeneous bio-aggregates that can also appear as "column-like" stacks. The final and most popularized model is the mushroom or tulip model from Costerton et al., (1994). Based on CLSM images of natural river biofilms, this model incorporates water channels and pores as key biofilm features through the plume like biofilms. All of the above features were observed in the images of TW biofilm architecture in this study, suggesting that TW biofilm is complex and dynamic. Therefore, no single established model can fully explain TW biofilm morphology. Rather the different models will be more or less appropriate under

different situations. At this current stage of research, we are not able to clearly differentiate differences in biofilm morphology and architecture based on spatial sampling in this study, however this approach can be taken in the future with the objective that trends can be established.

4.4.2 Pore Quantification and Analysis

Another ubiquitous feature seen across both detached and gravel-associated biofilm micrographs are pores within the EPS matrix (Figure 4.5 and Figure 4.7E-H) appearing in close to 74% of all images taken. Research outside of the TW field has attributed these gaps to the presence of water channels and pockets (Boudarel et al., 2018). The general consensus is that these channels are thought to act as additional means of transport for nutrients and oxygen through the structure; whereas the previously noted pockets/cavities are for storage (Quan et al., 2021). The identification of water channels has direct implication for mass transport within the TW conceptual model. This means there is the potential for non-zero velocity within internal sections of the matrix increasing the influence of convective transport within the conceptual model for TW biofilm. With respect to the pockets, these can be considered locations of nutrient reservoirs, potentially leading to areas of higher biofilm density below and within the EPS matrix. For treatment wetlands, these water-filled pockets likely help delay desiccation for fill and drain and tidal operational regimes.

As previously stated, six Wet-SEM micrographs were selected to characterize the porous biofilm matrix using a combination of ImageJ and MATLAB® (Figure B.1). Average areal biofilm porosity was 34±10%, reaching a maximum of 50% for Image 3. Pore sizes ranged from 0.5 µm to 102.6 µm with an average radius of 4.3 µm. Radii less than 0.5 µm were not counted due to challenges in differentiating with background noise. The pore distribution shows that the biofilm matrix is skewed towards smaller pores sizes rather than larger pore sizes (Figure 4.8). Particularly, Image 5 had a high frequency of pores radii below 1 µm.

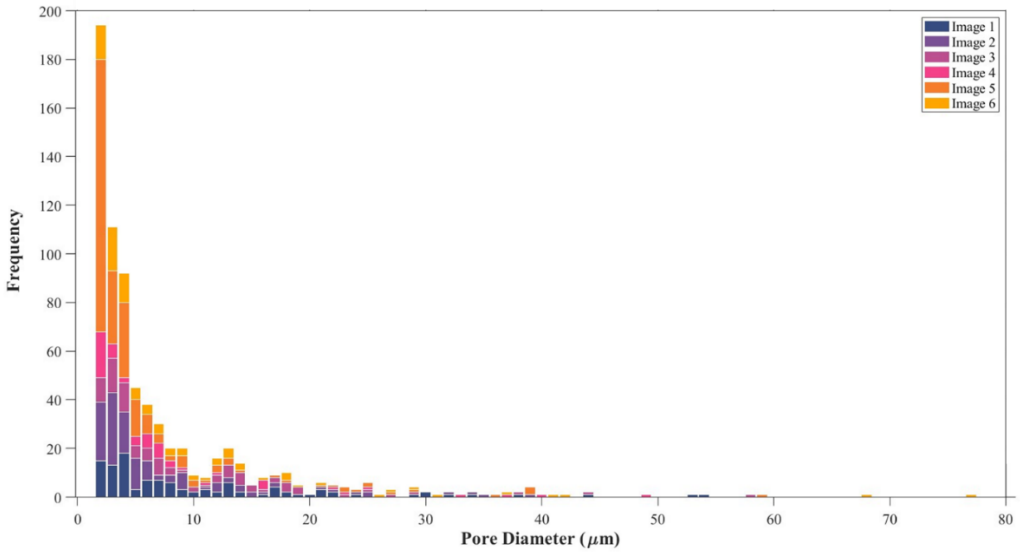

Figure 4.8: Pore size distribution (equivalent spherical diameter) of subsurface TW biofilm

Previously, pollutant transport inside TW biofilm was assumed to be solely based on diffusion. Although diffusion may still be the dominant pollutant transport mechanism into and within the TW biofilm matrix, advective transport needs to be considered and evaluated. As such, the flow regime inside the biofilm cannot be defined at this point. Given the large range of pore and channel sizes, it is expected that a variety of flow regimes, and therefore pollutant transport mechanisms will exist inside the biofilm matrix. From the distribution of pores there appears to be a reasonably clear separation of pore sizes at 10 µm, with a larger number below 10 µm. Until further differentiation is completed, it is suggested that pores below 10 µm are referred to as micropores, and pores larger than 10 µm as macropores. Future work should focus on estimating flow regimes and the degree to which advective transport plays a role in the various pore size ranges. It is expected that the larger macropores may help channel water and therefore promote a different flow regime than the smaller micropores. Approaches estimating Reynolds and Peclet numbers could be helpful in gaining an understanding of whether advective transport inside biofilms could be important, as this concept is not currently incorporated into current conceptual models or numerical models.

4.4.3 Rhizospheric Biofilm Architecture

In the case of the rhizospheric-associated biofilms, the morphology was dominated by heterogeneous aggregates along the root surface (Figure 4.9). Compared to the gravel-associated biofilm, while having a corrugated appearance, the maximum thickness observed was much smaller, falling around 62 µm. Furthermore, biofilm formation along the roots appears to have preferential zones of microbial adhesion. Roots are known to excrete nutrients (root exudates) leading to higher activity and density in rhizospheric-associated microbial communities as compared to gravel-associated biofilm in TWs, in addition to transpiration

flux (water uptake) (Gagnon et al., 2007; Weber & Legge, 2013). Although microbial density is in some ways a separate concept from biofilm thickness, the images taken here do suggests that perhaps there is a spatial distribution of root exudates for *P. arundinacea* resulting in "hotspots" of nutrient availability along the root leading to these localized patches of biofilm aggregates.

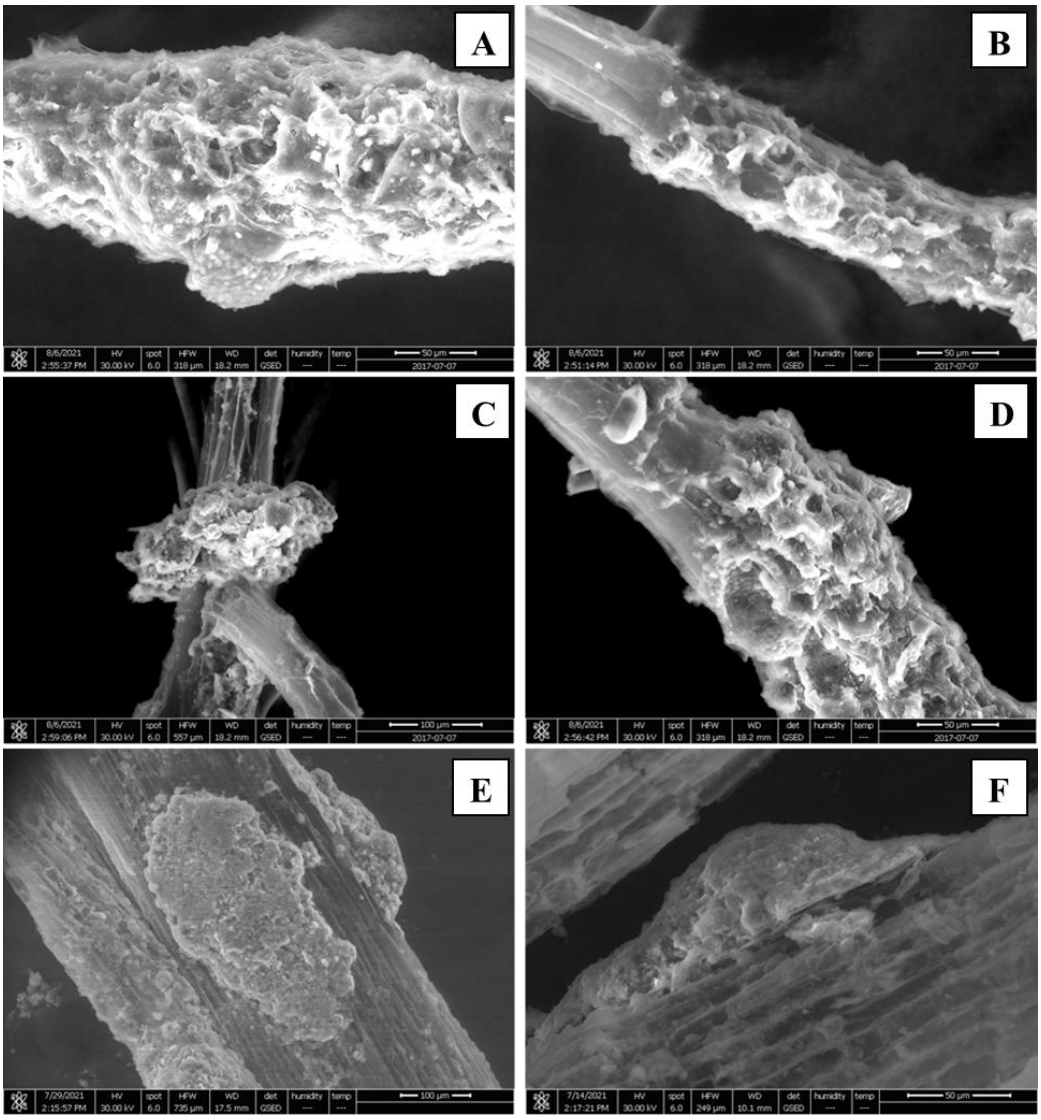

Figure 4.9: Representative E-SEM images of partially dehydrated rhizospheric associated biofilm on P. arundinacea roots retrieved from the top 20 cm of the TW mesocosm

4.4.4 Organisms

An additional aspect to consider in our understanding of the morphology of TW biofilms is the presence of non-bacterial higher-level, and/or physically larger, organisms within the environment (Figure 4.4B, Figure 4.5C, Figure 4.7A). In both SEM and OM images a number of organisms were detected including protists, amoebas, mites, tardigrades, and rotifers (Figure 4.10), which implies a higher "grazing" trophic level. In the matrix structure, organisms were either embedded within the biofilm itself or appeared to move across/underneath it while feeding on the biomass. In Figure 4.10A a tardigrade (water bear) was observed tearing a section of biofilm away from the larger biofilm mass (this is a still image taken from a video), where Figure 4.10B shows a protozoan feeding. Wet-SEM images provided more detailed images of mites covered with biofilm pushing through the pores (Figure 4.10E, F), and amoebas being encased (Figure 4.5C and Figure 4.10F). Notably, several different morphologies of amoebas were observed across SEM micrographs including what appeared to be flat discs, shells, and dragon eggs (Figure B.2). Visual comparison of these morphological attributes to those found in literature indicated that all amoebas seen belong to a polyphyletic group of testate amoebas (Fernández, 2015). Testate amoebas are shelled protozoa often found in rivers, lakes, estuaries and wetland habitats (Mitchell et al., 2008).

Previous studies have shown the acts of predation from protozoa can influence biofilm architecture and growth patterns (Scherwass et al., 2016; Suarez et al., 2015). Aybar et al. (2019) found that under low influent COD (60 mg/L) predation from protozoa played a significant role in increasing the void fraction within the biofilm from 5% to 50%, as compared to the control, creating holes and amplifying the potential for biofilm sloughing. Given the wide range of influent wastewater characteristics in TWs, these higher-level organisms could have a significant impact on the biofilm density, architecture and therefore TW pollutant removal abilities. In order for a complete dynamic model of the biofilm environment to be understood, predation by higher organisms needs to be considered. These organisms play a role in biofilm stability, and in some cases seem to be quite literally incorporated in the biofilm matrix.

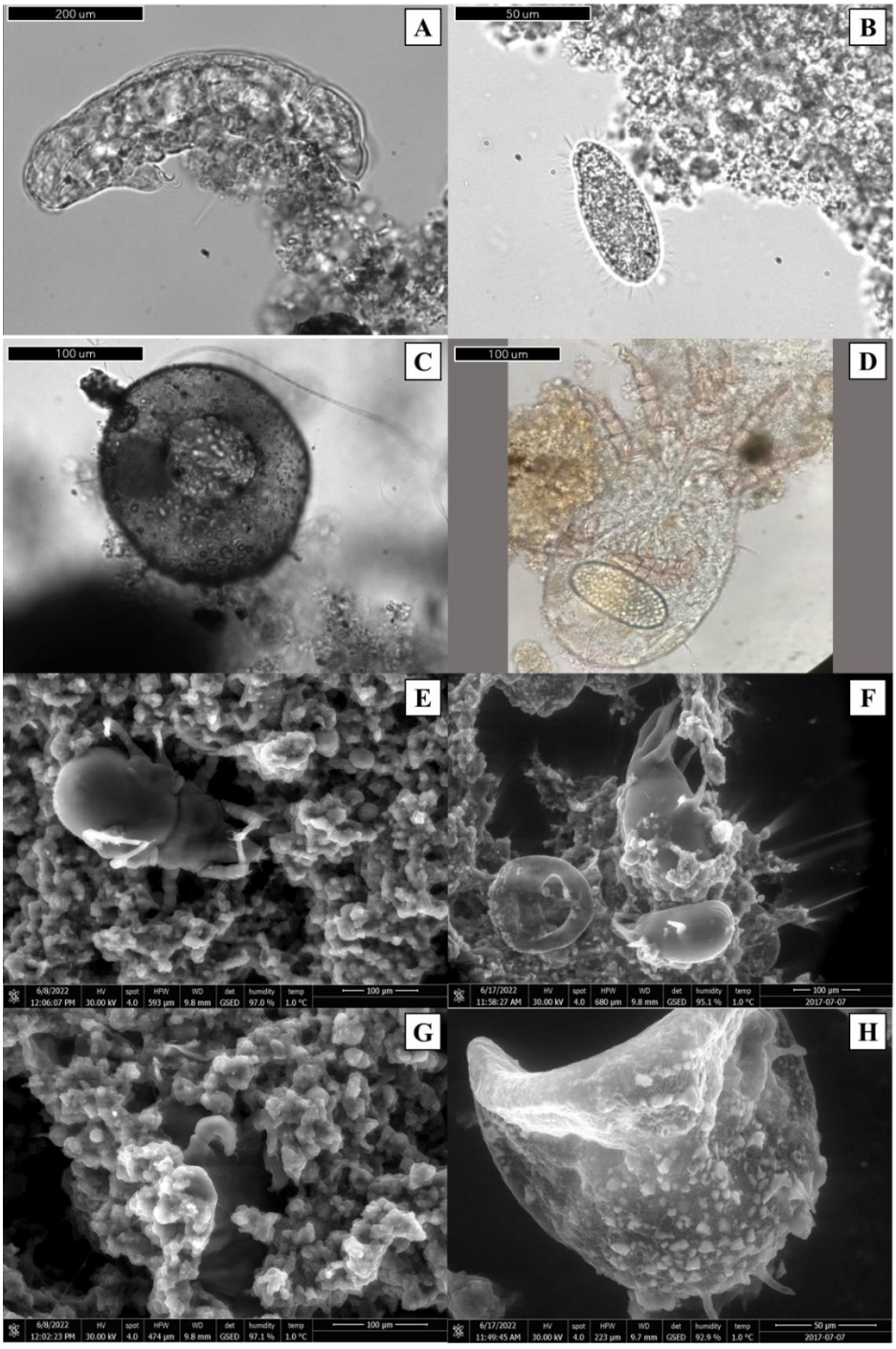

Figure 4.10: Organisms identified in interstitial water through light microscopy: A) tardigrade; B) protist; C) amoebas; D) rotifer. Embedded organisms observed in biofilm through Wet-SEM analysis (E-H).

4.4.5 Implications of a new conceptual model

Based on the images presented here, it is clear that the term "biofilm" does not adequately represent the entirety of the biofilm architecture seen in these treatment wetland systems. Instead of only uniform continuous films, heterogeneous irregular shapes including dense "bio-aggregates" and porous "bio-matrices" with water channels, projected tendrils/plumes, and pores/cavities were formed on the gravel and roots substratum. In fact, Flemming et al. (2021) recently proposed that the term biofilm be removed from research and replaced with instead with a "continuum of aggregates", however given the prevalence of the former term this is unlikely to happen and we continue to use the term biofilm here.

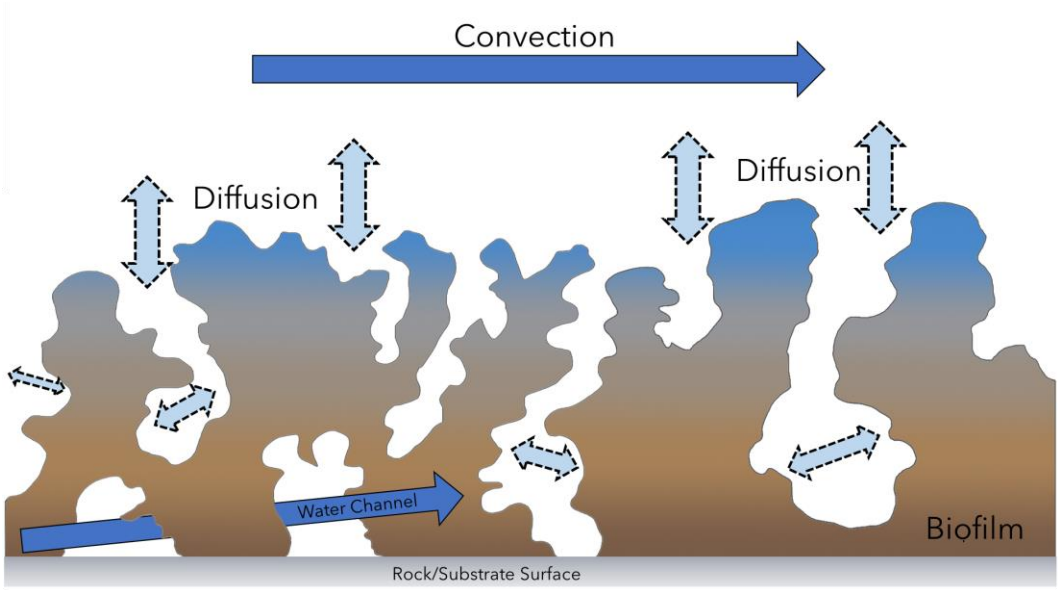

Figure 4.11: Proposed new conceptual model for TW biofilm

With this new understanding of TW biofilm morphology, the previous biofilm conceptual model can be redefined. In the new proposed conceptual model, shown in Figure 4.11, the heterogeneity of the biofilm matrix is reflected through the inclusion of water channels, pores/cavities and emerging stacks from the substrate surface based on the OM and E-SEM imaging conducted. With internal biofilm water pores and channels observed and quantified, previous conceptual models underestimated the interfacial area between the biofilm surface and internal biofilm pore/channel water. The new conceptual model, although more complex, is more accurate and should be used in future studies of biofilm/pollutant interaction in TWs. Movement of pollutants into and out of biofilm is a fundamental step for microorganism-mediated water treatment in TWs. As previously stated, TW macro-scale models have attributed the main mechanism of substrate transport into the biofilm matrix to diffusion (Murphy et al., 2016; Rajabzadeh et al., 2015). While this holds true in the new conceptual model, interfacial area between the biofilm and water is much larger than previously understood, and the additional influence of convective flow within the open channels could potentially enhance the mass transfer processes within the lower depths of the biofilm matrix. Structural heterogeneity at the microscale will result in highly variable, site-specific pollutant

fluxes between water and biofilm dependent on local interfacial surface area, pollutant concentration gradients, and environmental conditions. Moreover, as biofilm thickness is seen to be non-uniform, which in turn will influence biofilm density, thinner films may have higher physical or microbial densities. The effective biofilm diffusion coefficient depends on both the biofilm density as well as the solute physicochemical properties (Stewart, 2003); variations in the biofilm density will result in variable effective diffusion coefficients across TWs and within the highly dynamic biofilm matrix. Given these observed and conceptual biofilm heterogeneities and dynamics, different metabolic processes are likely housed within different areas of the biofilm regulated by the flux of both pollutants and oxygen due to not only depth, but also the morphology. This concept has been seen in a previous study by Lydmark et al. (2006), which examined through CLSM analysis of biofilm micrographs the spatial distribution of nitrifying bacteria in a full-scale nitrifying trickling filter. Two distinct functional regions were observed with ammonia-oxidizing bacteria predominately associated with the biofilm surface; whereas nitrite-oxidizing bacteria were more evenly distributed towards the base of the biofilm regardless of thickness. Rajabzadeh et al. (2015) also noted the possibility of microscale biofilm variation and postulated the need for a biofilm sub-model to explore these biokinetics.

This work serves to align the TW field with current biofilm models across disciplines based on visual evidence from both 2D and 3D imaging techniques. It should be noted, while this study offers a comprehensive first viewing of biofilm morphology in TWs, given the variable nature of TW designs and physicochemical properties, further investigations into the diverse architecture are required to validate this new conceptual model across different TW designs and operational regimes.

4.5 Conclusion

In this work we examined the morphology of gravel-associated, rhizospheric, and detached biofilms through E-SEM, Wet-SEM and optical light microscopy. Images revealed that treatment wetland biofilm architecture is distinctly heterogeneous appearing as continuous films, clusters of aggregates, and as a porous matrix containing features such as filaments, corrugated surfaces, pores/cavities, and water channels. An analysis of pore sizes led to our suggestion that pores with diameters smaller than 10 μm be referred to as micropores, and pores with diameters greater than10 μm be referred to as macropores. It is possible that differing flow regimes and pollutant dynamics will occur in micropores compared to macropores. Based on the characteristics observed, a new conceptual model was proposed to explain microscale morphological dynamics of TW biofilm matrices. It is postulated that the presence of the water channels will enhance the mass transport of dissolved oxygen and pollutants to the internal biofilm structure. Additionally, the presence of organisms, such as amoebas and tardigrades, were observed indicating that predation may be a factor in creating these voids spaces inside TW biofilms. While both Wet-SEM and E-SEM have provided some insight into TWs biofilm morphology, there needs to be a deeper understanding and validation of the new conceptual model proposed. Future studies should consider other imaging techniques, such as CLSM, in combination with staining, which can reveal high resolution images of the biofilm structure including its channels and voids, improve our understanding of the EPS and the microbial community distribution contained within. Additional work

investigating the flow regimes and pollutant transport mechanisms occurring within a range of biofilm pore sizes is also required. These findings have wide ranging implications towards our understanding of biokinetics and pollutant transport in TWs, which is backbone of this technology's treatment potential

4.6 Acknowledgments

Funding in the form of a NSERC Discovery Grant to KPW is gratefully acknowledged.

4.7 CReDiT Authorship Contribution Statement

Anbareen J. Farooq: Conceptualization, Methodology, Investigation, Validation, Formal analysis, Data curation, Writing - original draft, Writing – review & editing, Visualization. **Mhari Chamberlain**: Methodology, Investigation, Software, Writing – original draft. **Arman Poonja**: Investigation, Writing – review & editing. **Kevin Mumford**: Conceptualization, Supervision, Writing – review & editing. **Scott Wallace**: Conceptualization, Writing – review & editing. **Kela P. Weber**: Conceptualization, Resources, Writing – review & editing, Supervision, Funding Acquisition.

5. Limited effects of incidental silver nanomaterials from commercial textiles on treatment wetland mesocosms

Anbareen J. Farooq[1], Laura J. Ogilvie[3], Dani Damasceno Silvera[4], Vincent Gagnon[5], Mark Button[6], Sarah Wallace[1], David J. Patch[1], Iris Koch[1], Denis O'Carroll[2], and Kela P. Weber[1*]

[1]Environmental Sciences Group, Department of Chemistry and Chemical Engineering, Royal Military College of Canada, Kingston, ON K7K 7B4, Canada

[2]School of Civil and Environmental Engineering, UNSW Water Research Laboratory, University of New South Wales Sydney, Manly Vale, NSW, 2093, Australia

[3]Canadian Nuclear Laboratories, Chalk River, ON, K0J 1J0

[4]University of Santa Catarina (UFSC), Campus Universitário, Trindade, CEP 88040-900. Florianópolis, SC, Brazil. daniele.ds@posgrad.ufsc.br

[5]Department of Biology, Champlain College Saint-Lambert, Saint-Lamber, QC J4P 3P2, Canada

[6]Fipke Laboratory for Trace Element Research, Earth, Environmental and Geographic Sciences, University of British Columbia Okanagan, University Way, Kelowna, BC, V1V 1V7, Canada

*Corresponding author: kela.weber@rmc.ca

5.1 Abstract

Recent research has shown that silver nanomaterials (Ag-ENMs), often employed due to their antimicrobial properties, are released from textiles during their use and are entering wastewater streams. However, the effects of incidental (or weathered) Ag-ENMs released from these commercial products, such as textiles, are largely unknown in wastewater treatment systems. The focus of this research is to assess whether a single-home treatment wetland (TW) can remove these weathered Ag-ENMs from wastewater without impairing TW microbial communities. Twenty-four batch-fed, subsurface flow planted wetland mesocosms were developed for this study; twelve were intensified with artificial aeration and twelve were non-aerated. The experiment consisted of four design types: a positive control, a negative control, a pristine Ag-ENM, and an artificially weathered Ag-ENM (released from X-Static® fabric) exposure, all conducted in triplicate. Two separate in-situ exposures at 0.1 mg Ag/L and 1 mg Ag/L were conducted over 189 days and 28 days, respectively. Over both phases, TW systems were able to achieve high removal efficiencies for both the pristine and weathered Ag-ENMs, reaching between 80-99% removal. The presence of 0.1 mg Ag/L in TWs showed no difference for TN and TOC removal across all systems when compared to the control. In the second phase, the addition of 1 mg/L of weathered Ag-ENMs stimulated the removal efficiency of TN in the aerated systems, likely due to inputs of additional carbon with the associated weathered Ag-ENM water matrix. Subsequent investigations into the interstitial microbial community structure and function showed slight variations; however,

there were no appreciable impacts to the overall microbial activity of the fixed regime between the silver treatments and their respective controls, indicating the robustness of the wetland systems.

Keywords: silver nanoparticle, treatment wetland, community level physiological profiling

5.2 Introduction

Silver nanomaterials (Ag-ENMs) are one of the most frequently employed type of engineered nanomaterial found across 44 different countries in over 1132 different products including medical supplies, electronics, cosmetics, and textiles, such as socks (Keller and Lazareva, 2013; StatNano, 2023). The implementation of Ag-ENMs in commercial products is primarily related to their well documented antimicrobial/antibacterial properties (Nowack et al., 2011; Rai et al., 2008; Vance et al., 2015). Current global production volumes are estimated to be around 150 – 500 metric tonnes per year and are expected to reach 800 tonnes annually by 2025 (Janković and Plata, 2019; Nowack and Mueller, 2008; Pulit-Prociak and Banach, 2016). As such, through the production, use and eventual disposal of these products, the majority of incidentally released Ag-ENMs will enter wastewater treatment systems, including treatment wetlands (Gottschalk et al., 2009; Lorenz et al., 2012; Sun et al., 2022).

Treatment wetlands (TWs) are a low-cost, nature-based alternative for decentralized wastewater treatment that has become increasingly employed the last 50 years (Vymazal, 2011; L. Zhang et al., 2018). TWs rely primarily on their diverse microbial communities, both interstitial and housed in biofilms, for the majority of their complex wastewater treatment (Farooq et al., 2023a; Faulwetter et al., 2009; Weber and Gagnon, 2014). Adjusting design factors, such as choice of plants, level of aeration, and loading regimes among others, can promote the development of structurally and functionally different microbial communities to achieve desired water treatment objectives (Silveira et al., 2022). Globally, these systems are popularly employed in rural areas for the treatment of greywater from single family homes or villages (Steer et al., 2002; Wu et al., 2011). For these systems, it is predicted that concentrations can reach up to 0.1 mg /L of Ag-ENMs in treatment wetland systems from the daily use of consumer products (Button et al., 2016a).

Research to date has shown that TWs are highly effective tools for the removal Ag-ENMs from wastewater, reporting treatment efficiencies ranging from 92 to 99% for both meso-scale and pilot-scale planted VF TWs (Huang et al., 2017; Huang et al., 2019b). Upon entering, Ag-ENMs are bound within the soil layers or, in gravel-based systems, the media-bound biofilm (Auvinen et al., 2017). However, under the stress of Ag-ENMs, concentrations as low as 0.02 mg/L have shown the ability, while temporary, to supress the removal capabilities of other parameters by TWs, specifically nitrogen and phosphorus (Huang et al., 2018b). For example, Cao et al. (2022) reported that removal efficiencies of TN, NH_4^+-N, and TP decreased by 15%, 19%, and 14%, respectively, under Ag-ENMs exposures of 0.2 mg/L. Furthermore, these studies have shown that Ag-ENMs caused a reduction in the key functional bacteria, related to the reduced in the overall microbial structure reducing abundances of (Cao et al., 2018; Huang et al., 2020).

While these studies have shown adverse impacts from Ag-ENMs on TW systems, all research thus far has focused on the impacts of pristine or sulphidized Ag-ENMs. However, it is not these engineered particles that will ultimately enter the environment but rather incidentally released Ag-ENMs from the weathering of consumer products (Meyer et al., 2011). Compared to their pristine counterparts, these incidental Ag-ENMs have a diverse range of morphologies and size distribution being released as nanoparticles, aggregates or silver ions (Benn et al., 2010). Gagnon et al. (2019) and Patch et al. (2021) found that the majority (54%) of released particles from textiles embedded with X-STATIC® fibers appeared as thin nano-sheets with 7% as spheres and the remainder irregularly shaped. Moreover, studies have shown that shape and size can influence toxicity exhibited by Ag-ENMs (Gorka et al., 2015). Triangular Ag nanoplates have exhibited the higher toxicity against bacteria compared to silver nanospheres and nanorods due to their higher percent of exposed facets. (Pal et al., 2007). Yet, to date, no studies have been completed examining the effects of incidentally released Ag-ENMs from consumer products in TW systems.

The objectives of this study were to evaluate the impacts from both incidentally released and pristine Ag-ENMs on the interstitial microbial community and treatment performance in both aerated and non-aerated planted subsurface TW mesocosms representing a single-home treatment wetland.

5.3 Materials and Methods

5.3.1 Experimental Design

A total of twenty-four planted (*Phalaris arundinacea*) subsurface flow TW mesocosms (height: 0.61 m, diameter: 0.25 m) systems were used in this study at the Royal Military College of Canada (Figure C.5 and Figure C.6). The mesocosm design used has been previously described by Farooq et al. (2023). Briefly, each mesocosm was filled to approximately 0.55 m with washed limestone pea gravel, and had an initial void volume of 10 L (porosity: 0.32). Twelve of the systems were artificially aerated via individual aeration stones (6") connected to an EcoPlus Air 3 pump (Atlantic Pond Supply; Moncton, NB) by ½" Nalgene tubing. The maximum airflow to each aerated mesocosm was approximately 0.4 L/min. The systems were kept well mixed by a magnetic drive pump (Little Giant Pump Company, 1-AA-MD) that maintains a continuous circulation of the interstitial water. A sampling port constructed from 2" white PVC pipe connected to the side of each mesocosm allowing for interstitial water to be sampled throughout the experiment. The mesocosms were batch fed simulated wastewater (COD:N:P 100:5:1) as described by Weber and Legge (2011) every 7 days. Since the wastewater input is synthetic, to help establish microbial communities, the mesocosms were inoculated with 0.50 L of activated sludge applied in layers from Cataraqui Bay Waste Water Treatment Plant in Kingston, ON. At the start of this experiment, all mesocosms had been established for at least 405 days (porosity at day 405: 0.25).

Four treatments were conducted in triplicate for both aerated (A) and non-aerated (NA) systems: a positive ionic (I) silver control ($AgNO_3$), a pristine (P) Ag-ENM, an artificially weathered (W) Ag-ENM released from textiles (X-Static® fabric), and a negative control (C). In Phase I, which ran for 30 weeks, the exposure scenario was based on the release of laundry wastewater to a single home treatment wetland as described in Button et al. (2016). The

authors estimated that up to 15 mg Ag/L could be discharged into a domestic TW system following one wash cycle achieving a final *in-situ* average concentration over a day of 0.1 mg Ag-ENM/L. All systems were characterized for the first 3 weeks without any silver addition. Following this, systems were spiked weekly, as a pulse load 48h after feeding, for 27 weeks after which the mesocosms were left to recover for 238 days. During Phase I, due to a technical issue the systems were not loading in the week 13 of this phase. After the recovery period, all systems were characterized for 5 weeks in Phase II-A before entering Phase II-B. In this stage, the weekly *in-situ* concentration was increased to approximately 1 mg Ag-ENM/L for a worst-case "shock" scenario over a shorter time period of 4 weeks.

5.3.2 Silver Nanomaterials

5.3.2.1 Pristine Ag-ENM Selection and Preparation

The pristine Ag-ENM (P-Ag-ENM) selected for this study was based on *ex-situ* screening toxicity tests conducted on the catabolic capabilities of aerated and non-aerated interstitial TW microbial communities (139). Using community level physiological profiling (Section 5.3.5.1), dose response curves were made for a variety of pristine Ag-ENMs. Based on the results, polyvinylpyrrolidone (PVP) coated (PVP 0.2 wt%) silver nanoparticles (20-30 nm, Skyspring Nanomaterials, Inc, TX, USA) were selected as they exhibited the lowest toxicity to the aerated interstitial microbial communities. Weekly nanomaterial suspensions were obtained by dispersing the nanopowder in DI water using sonication (Fisher Scientific Model 505 Sonic Dismembrator, Fisher Scientific, NH, USA) at 50 Hz for 60 seconds.

5.3.2.2 Preparation of Weathered Ag-ENM

The incidental or weathered Ag-ENMs (W-Ag-ENMs) used in this study were generated through washing Lululemon's "T.H.E. Sock Silver", an athletic anti-bacterial textile. This process has been previously characterized by Gagnon et al. (2019) and Patch et al. (2021). The socks were used due to their high silver content (37 mg Ag/kg textile) from the incorporation of X-STATIC® fibres, which are nylon fibres that have an electrolytically deposited layer of Ag-ENMs.

In Phase I, the socks were physically stretched then washed in pairs according to a modified version of the International Standard Organization protocol (ISO 105-C06: 1994), identical to the procedure found in Patch et al. (2021), to simulate domestic laundry washing. A total of 300 mL of a 4g/L (Tide® Liquid Original detergent/DI water) soap solution was prepared and then heated to 40˚C. The solution was then added to a 2L high density polyethylene bottle followed by the pair of socks and 10 acrylic spheres (2.5 cm diameter) to stimulate friction. The container was sealed and then shaken at 40˚C and 150 rpm for 45 minutes (Innova 4320 Refrigerated Incubator Shaker). Following the wash procedure, the socks were squeezed to remove the excess water and allowed to air dry. The wash water was then transferred into 1-L Nalgene container and frozen until loaded in the mesocosms.

During Phase II, to achieve higher concentrations the Ag-ENMs, wash solution was dialyzed through a modified method adapted from Vauthier et al. (2008) as detailed in 144. For larger runs, dialysis tubes were left for 8-10h equating to a concentration factor of 10-12. In tandem,

the washing protocol was modified to decrease the soap concentration to 0.4g/L (based off the concentration factor) to replicate the load in Phase I.

5.3.3 Total Silver and Ag-ENM size distribution

Total silver concentrations in the stock solutions and effluent samples were measured through inductively coupled plasma-mass spectrometry (ICP-MS) (Elan DRC II, Perkin Elmer, MA, USA). Samples underwent heated acid digestion prior to analysis using an *aqua regia* solution (1:3 HNO_3 70% and HCl 35%) for 2 hours at 70°C (Kaegi et al., 2013; Lowry et al., 2012). Additional interstitial water samples were taken for total silver analysis at 1, 3, ,5, 8, 10, 20, 30, 60, 180, 300, and 1440 mins after Ag loading to characterize the degradation of Ag-ENMs in the TW mesocosms.

Single particle inductively coupled plasma mass spectrometry (spICP-MS) was used to determine the size distribution and average median particle size of the nanomaterial suspensions and kinetic samples based on mass and assumed spherical shape according to the methodology described in previous work (Gagnon et al., 2019). Samples were diluted in DI water (up to 10000x) to balance the ionic background and the particle signal. Once diluted, samples were analyzed with the Elan DRC II ICP-MS using the Ag^{107} signal in transient acquisition mode at a dwell time of 10 ms during a 60 s run time per sample.

5.3.4 Water Quality and Porosity Measurements

Weekly water quality parameters including pH, oxidation-reduction potential (ORP), temperature, dissolved oxygen (DO), electrical conductivity (EC), ammonium (NH_4^+) and nitrate (NO_3^-) were measured *in-situ* using YSI Professional Plus Handheld Multiparameter Water Quality Meter (YSI Inc., Yellow Springs, USA) via the sampling port. Total organic carbon (TOC) and total nitrogen (TN) concentrations were determined for influent and day 4 water samples using a TOC/TNb analyzer (multi N/C 2100s, Analytik Jena, Germany). Evapotranspiration (ET) was monitored daily using tap water to offset the water losses for each mesocosm and drainable porosity was tracked on a weekly basis following the methods described in Weber & Legge (2011)

5.3.5 Microbial Community Analysis

5.3.5.1 Community Level Physiological Profiling (CLPP)

Community Level Physiological Profiling (CLPP) was used to characterize heterotrophic microbial catabolic activity, substrate richness and function using a 96 well (31 different carbon substrates, and a blank well in triplicate) BIOLOG ® EcoPlate (BIOLOG Inc., CA, USA). Interstitial mesocosm water samples were inoculated in the BIOLOG Ecoplates bi-weekly over the course of Phase I and weekly in Phase II. Together with the carbon substrate, each well contains tetrazolium violet, a redox dye indicator, and when a mixed microbial community sample is inoculated into the well, the production of NADH via cell respiration reduces the tetrazolium dye to formazan. The colour development is tracked over the course of 96 hours with absorbance readings taken at every 4-hour mark by a microplate reader stacker (Eon Microplate Spectrophotometer, BioTek Instruments, Inc., VT, USA) at 595nm. The microbial activity can be determined by the average well color development (AWCD),

which is based on the carbon substrates utilization pattern (CSUP) of a given sample. Substrate richness represents the number of different carbon substrates utilized by a microbial community. The AWCD and richness time point of 52 h was chosen to obtain the most variation within the data set while minimizing the number of over-saturated wells (absorbance units greater than 2.0) (Kela P. Weber and Legge, 2010).

5.3.5.2 Fluorescein Diacetate Assay (FDA)

An indirect measure of overall microbial activity (MA) of each TW mesocosm was observed through an enzymatic assay using fluorescein diacetate (FDA) adapted from Weber et al. (2008). Briefly, the two acetate groups can be enzymatically cleaved transforming FDA to fluorescein, which can be measured photometrically at an excitation wavelength of 490 nm. One mL of a 5mM FDA solution was injected bi-weekly into each mesocosm port. After the injection, water samples were taken every minute for 30 minutes using 96-well plates. Samples were read using a microplate reader stacker (Infinite ® M1000 PRO, Tecan, Switzerland). The final FDA utilization rate was calculated as the average of the incremental slopes between 8 and 15 mins.

5.3.6 DNA Extraction and Sequencing

In tandem with CLPP sampling, 16S ribosomal RNA sequencing was conducted on the interstitial microbial communities throughout the experiment to track structural changes following the procedure outlined in Silveira et al. (2022) . A total of 50 mL of interstitial water was collected per mesocosm and filtered through 0.22 μm filter paper (Millipore, Bedford, MA, USA) using a sterile vacuum filtration. DNA was extracted from the full filter using the FastDNA Spin Kit for Soil (MP Biomedicals, Santa Ana, CA, USA) following the manufacturer's protocol. The DNA concentrations were measured using a Qubit fluorometer and Qubit dsDNA HS assay kit (Invitrogen, ON, CAN). Once quantified, samples taken from the start and end of Phase I and Phase II were selected to track structural and functional changes from the addition of Ag-ENMs.

The variable V3 and V4 regions of the 16S ribosomal RNA gene (16S rRNA) were amplified and purified from each sample following the Illumina 16S Metagenomic Sequencing Library Preparation guide (version B, Illumina Canada Ulc., Victoria, BC, Canada). Each sample was normalized to 4 nM, pooled, denatured, and diluted to 4 pM. Sequencing was performed using the MiSeq Reagent v3 600 cycle kit on the MiSeq (Illumina Canada Ulc., Victoria, BC, Canada) generating paired end 2 x 300 bp reads. A 10% spike in of the PhiX control library was added to monitor the quality of the sequencing run.

QIIME2 version 2021.11 (Caporaso et al., 2010) on VirtualBox (version 7.0) was used to analyze the 16S rRNA sequences. Demultiplexed fastq files were imported and reads were filtered, denoised, and merged with the removal of chimeras using DADA2 (Callahan et al., 2016). Reads were classified using the naive bayes classifier (Bokulich et al., 2018; Robeson et al., 2021) trained on the Silva 138 taxonomic database (99% OTU full length sequences; Quast et al., 2013). The median frequency was 26824 and 30661 reads for Phase I and Phase II, respectively; thus, samples were correspondingly rarefied to 8000 and 10000 reads for diversity analyses. The align-to-tree-mafft-fasttree pipeline was used for phylogenetic dependent analyses. Multiple alpha diversity metrics were estimated including Shannon’s

diversity index, observed OTUs, Faith's phylogenetic diversity, and evenness. Multiple beta diversity metrics were estimated including Jaccard, Bray-Curtis, unweighted UniFrac, and weighted UniFrac distances.

5.3.7 Data Analysis

Analysis of the CLPP data was performed as described by Weber et al. (2007) and Weber and Legge (2010). Principal component analysis (PCA) was performed using the covariance matrix (n-1) of the CSUP data for start and end of Phase I and Phase II to further assess for differences between systems using XLSTAT statistical software (2023.1.2, Addinsoft).. If necessary, datasets were subjected to Taylor series transformation based on assessment of normality, homoscedasticity and linear correlations following the recommendations of Weber et al. (2007). One-way ANOVA was used to identify differences between treatment means in individual measurements while post-hoc Tukey's tests were used to identify significantly different treatment groups.

PCA ordinations were also generated in XLSTAT using the genera abundance data set to compare the differences in the microbial communities within and between each system type. One-way permutational analysis of variance (PERMANOVA) was performed in QIIME 2 with both beta diversity matrices Bray-Curtis and Euclidean distance to assess the differences in microbial composition among samples from different systems. The percent of reads in each sample matching to the top 20 abundant genera were plotted and compared among designs in a heatmap using an average Bray-Curtis metric. All alpha diversity indices and the beta diversity analysis were performed using QIIME 2 software (2019.10).

5.4 Results and Discussion

5.4.1 Silver Removal and Kinetics

The TW mesocosms proved highly effective at retaining the majority of silver loaded, regardless of type or concentration, in both Phase I and Phase II (Table 5.1). This falls in-line with previous studies that have reported between 94 to 99% removal of pristine Ag-ENMs at concentrations up to 10 mg Ag/L in both horizontal and vertical subsurface flow TW systems (Button et al., 2016a; Cao et al., 2021b; Chen et al., 2023). It was observed that the aerated systems had lower and more variable retention compared to their non-aerated counterparts. Auvinen et al. (2017) reported that Ag concentration is highly correlated to the TSS concentration ($R^2 = 0.81$) in the effluent. Though not measured, it was visually observed that the effluent of the aerated systems on Day 7 had higher quantities of total suspended solids, possibly due to shear stress from the aeration, which can explain the variance in removal (Figure C.7)

Table 5.1: Average silver retained in TW mesocosms from Ag-amended treatment wetlands (mean ± standard deviation)

	Phase I		**Phase II**	
Treatment	Aerated	Non-Aerated	Aerated	Non-Aerated
Ionic	86.8 ± 12.4%	95.4 ± 4.6 %	96.6 ± 3.3%	99.9 ± 0.1%
PVP	85.8 ± 11.9%	90.5 ± 8.6%	95.7 ± 4.3%	99.8 ± 0.2%
Weathered	78.9 ± 17.3%	97.3 ± 2.7%	98.1 ± 1.6%	99.9 ± 0.1%

The average median diameter of the P-Ag-ENM and W-Ag-ENM stock solutions were determined to be 76.7±10.8 nm and 89.5 ± 40.4 nm, respectively, through spICP-MS. The concentration and particle distribution were closely monitored following loading of the silver in the systems and were averaged across each phase. The size distribution of both types of Ag-ENMs shifted over time as the larger agglomerations of Ag-ENMs settled out of solution leaving the smaller particles in circulation (Figure 5.1).

The aerated systems removed around 90% of W-Ag-ENMs and P-Ag-ENMs within 2-3 hours during both phases, and achieved near complete of removal after 5h (Figure 5.1; Figure C.8B). In comparison, while the positive Ag^+ control observed the same trend, 90% removal was observed in the first 0.5h in the aerated Ag^+ mesocosms, which was 6 times faster than the Ag-ENM amended mesocosms (Figure C.8A). Free Ag^+ ions can readily interact with organic matter or inorganic ligands (thiols, S_2^-, Cl^-) forming non-soluble complexes, which will settle out of solution, or cause the reformation of secondary smaller Ag-ENMs (Azodi et al., 2016). In this study, following the addition of ionic silver to the mesocosms, a small number of particles were detected 30 mins after loading in the aerated systems with an average median size of 53 ±10 nm. In the non-aerated mesocosms, the nano-scale particles were detected earlier at 10 mins with a larger average median diameter of 78 ± 21nm. The higher TSS in the interstitial water of aerated systems likely increased the availability of organic matter, and in turn created more binding sites for the Ag^+ ions. Moreover, the O_2 rich conditions in the aerated systems, would consistently promote the partial or complete oxidative dissolution of Ag-ENMs into Ag^+ ions (Liu and Hurt, 2010). This dissolution step likely causes the lag time observed between the ionic and Ag-ENMs silver removal kinetics observed in the aerated systems. Conversely, in the non-aerated systems, the limited DO restricts the oxidation, and, consequently, the Ag-ENMs were more persistent only reaching near complete removal 24h post loading. Previous studies have observed that Ag-ENMs remained in the interstitial water for days or weeks before being completely removed in non-aerated systems (Colman et al., 2014; Ward et al., 2019).In the anaerobic systems Ag^+ and Ag-ENMs can also be transformed through sulfidation as Ag_2S shells forming on the surface around the Ag-ENMs (Yonathan et al., 2022).

.

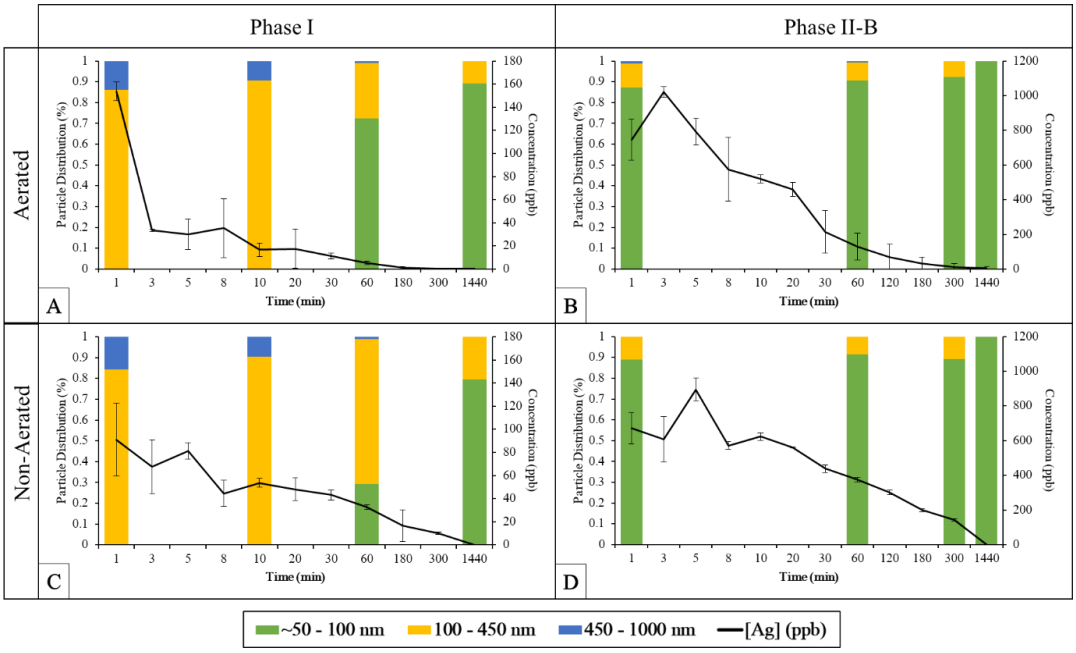

Figure 5.1: Average concentration and particle distribution in treatment wetland mesocosms following loading of weathered Ag-ENMs in Phase I (n = 8): (A) Aerated; (C) Non-aerated; and Phase II (n = 4): (B) Aerated; (D) Non-aerated. Kinetic data presented as means ± standard deviation.

5.4.2 Water Chemistry Parameters

The average water quality data for all systems are shown in Table C.3-Table C.**5**. The water physicochemical characteristics (pH, EC, ET, ORP) were not impacted by the Ag treatments over the 189-d exposure of Phase I and the 28-d exposure of Phase II. Overall, any differences between the water chemistry parameters can be attributed to the intensification of artificial aeration creating two different environmental regimes. The non-aerated systems on average maintained low *in-situ* dissolved oxygen (DO) concentrations of 0.1 ± 0.2 mg/L, which in turn promoted more reducing conditions noted by the negative ORP values in all phases. Interestingly, there was also a marked difference in pH values between the aerated and non-aerated system, which is attributed to the combination of aeration and limestone media. Limestone is composed of calcium carbonate ($CaCO_3$), which is known to increase the alkalinity through the formation of soluble calcium carbonate; in tandem, the artificial aeration can degas the CO_2, both of which increase the pH (Kirby et al., 2009; Tao and Wang, 2009). Additionally, the evapotranspiration (ET) of the non-aerated systems was consistently higher with observed values from 0.5-0.7 L/d across the experiment. Artificial aeration has been reported to have negative effects on the development of plants in treatment wetlands leading to stunted growth and lower root biomass, which, in turn, would lead to the lower ET values (0.3 ± 0.1 L/d) observed in the aerated systems (Nivala et al., 2020).

5.4.3 Treatment Performance: TOC and TN

Internal TOC and TN concentrations were monitored on day 4 of each weekly batch cycle, which corresponding to 2 days post silver loading. In Phase I and Phase II, the P-Ag-ENMs and Ag^+ exposures had no impacts on the removal efficiencies of TOC for both the aerated and non-aerated systems when compared to the controls (Figure C.9A,B; Figure 5.2A, B). The average removal efficiencies of TOC ranged from 93.6 % to 97.1% across the entire experiment. Several studies have shown that concentrations up to 0.5 mg/L of PVP Ag-ENM and $AgNO_3$ have no significant impacts on the removal of organics from both meso-scale and full scale TW systems due to the persistence of heterotrophic bacteria at low silver concentrations (Cao et al., 2021b, 2019; Truu et al., 2022). This same finding is seen in the current study for weathered Ag-ENMs in Phase I, in which, both aerated and non-aerated systems achieved removal efficiencies above 93%, falling in line with the control.

The addition of the W-Ag-ENMs to the TW mesocosms was set-up to replicate the release of wash water to a single home TW system. As such, W-Ag-ENMs were generated in a soap solution to replicate a laundry wash water scenario. For Phase I, the TOC introduced to the mesocosms via loading of weathered nanoparticles was utilized by the system effectively. However, in Phase II, additional TOC content (beyond what was added in phase I) was introduced via the soap in the weathered nanoparticle wash water matrix. Consequently, this increased carbon load resulted in elevated TOC concentrations on day 4 of the batch cycle for the systems receiving weathered nanoparticles (2 days post-wash water loading). It is likely that this elevated day 4 TOC content was comprised mostly of non easily degradable organics. In spite of this, the removal rates across Phase II for TOC did not significantly deviate from the control (as the easily degradable compounds were still utilized), showing that the increase on day 4 was not reflective of a drop in performance, but rather a result of increased soap loading (Figure 5.3).

As such, there is a separate active component in the wash water aside from the W-Ag-ENMs. The quantity of soap in the wash water was adjusted for the dialysis concentration method used in Phase II-B. However, it is clear that even with adjusting for the concentration factor of 10 there was a substantial amount of carbon within the W-Ag-ENM pulse. The same elevated TOC levels at day 4 were not noted for the aerated systems. While it received the same increase in carbon, artificial aeration can stimulate the microbial communities oxidative pathways using the carbon as an electron acceptor, improving nitrogen and organic degradation (Fan et al., 2013), and thus assisting in degrading the non easily degradable compounds.

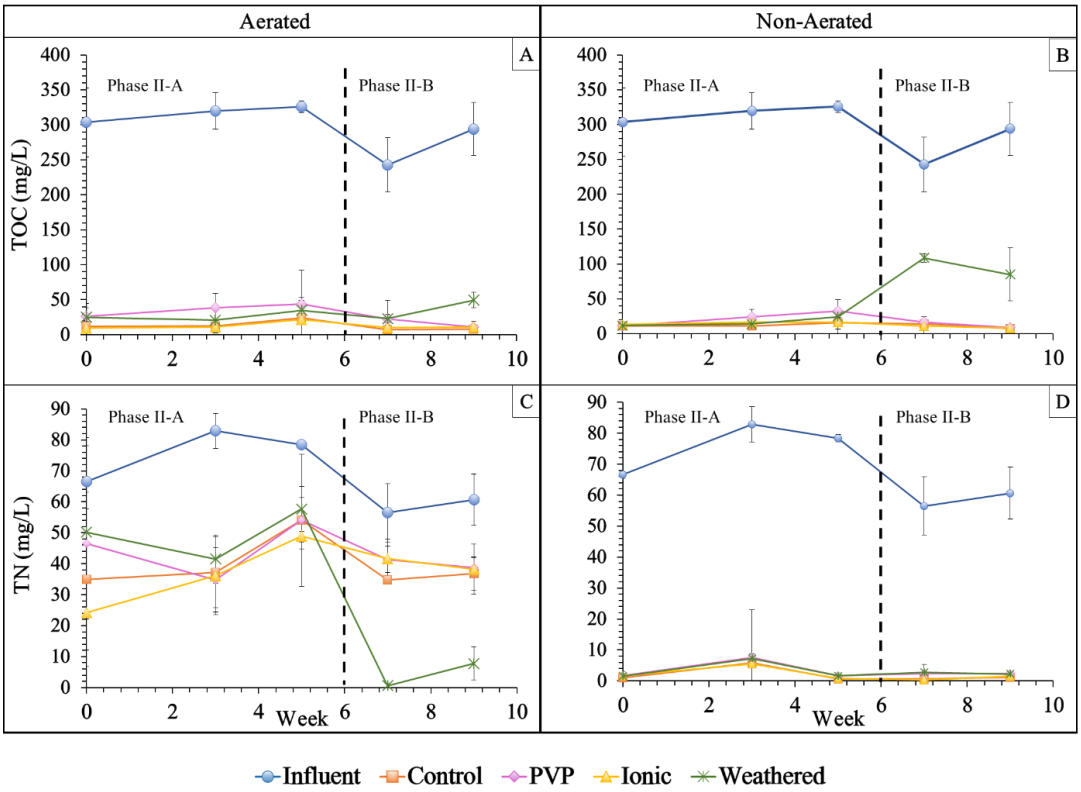

Figure 5.2: Average TOC and TN influent and *in-situ* Day 4 concentrations in aerated (A,C) and non-aerated (B,D) systems during Phase II. Data points are presented as means ± standard deviation of system replicates at each time point, n = 3.

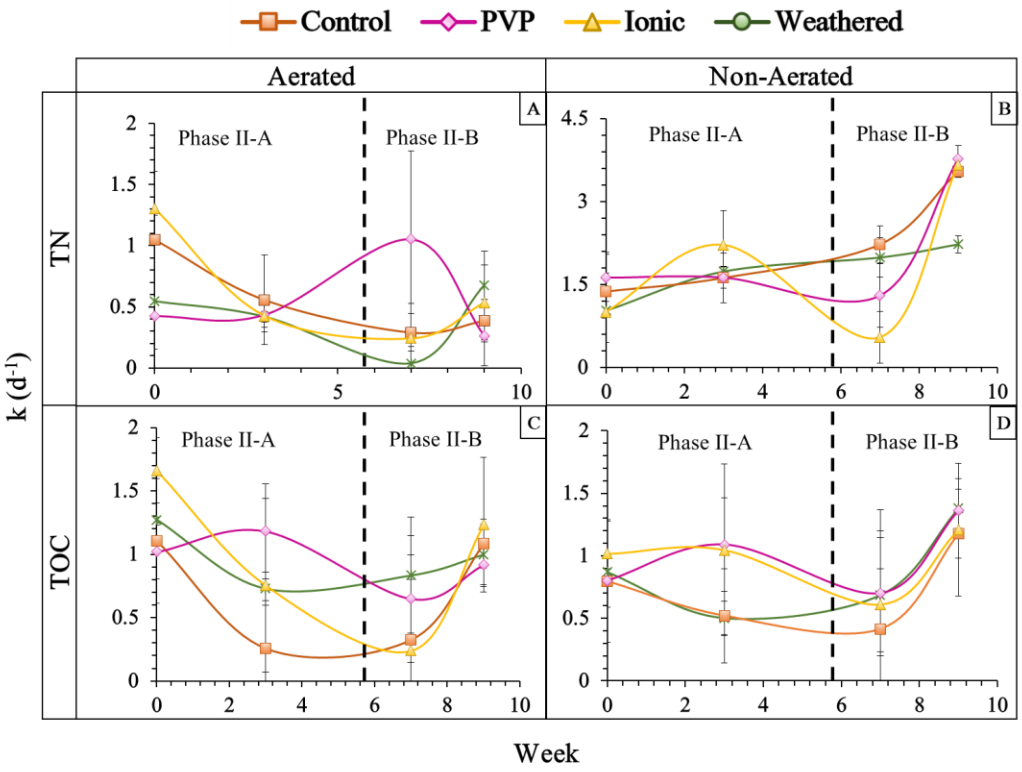

Figure 5.3: Weekly removal rates (k_v, d^{-1}) for TOC and TN for the aerated (A,C) and non-aerated (B,D) during Phase II. Data points are presented as means ± standard deviation of system replicates at each time point, n = 3.

Across the 27-week exposure in Phase I, the TN *in-situ* concentrations of Ag-amended systems showed no significant difference from the controls in the aerated and non-aerated systems sets (ANOVA, $p>0.05$, Figure C.9C, D). Yet, while all systems followed similar temporal trends, a slight inhibition in performance was observed in the Ag^+ and P-Ag-ENMs treatments and a stimulatory one observed in W-Ag-ENMs compared to the controls. In the non-aerated systems, the highest average TN removal efficiency was noted in W-Ag-ENM treatment at 95.5%, followed by control, ionic silver and P-Ag-ENM systems, which were 95.1%, 94.5%, and 93.4%, respectively (Table C.3). For the aerated systems, the average removal efficiencies reached 38.9%, 37.4%, 36.4%, and 36.1%, for WA, CA, PA and IA, respectively. These results agrees with Huang et al. (2019) who found that concentrations between 0.05 – 0.2 mg/L of Ag-ENMs did not significantly alter the performance of TWs only causing slight perturbations in treatment performance.

After the increase in exposure concentration to 1 mg/L in Phase II-B, no statistically significant differences in TN performances were observed in the aerated Ag^+ and P-Ag-ENM mesocosms (ANOVA, $p>0.05$; Figure 5.2C, D). However, from week 5 to week 7 of Phase II, the average TN removal efficiencies initially dropped in IA from 37.6% to 26.3%, and PA from 31.1% to 26.7% before rebounding in week 9 to 37.0% and 36.2%, respectively. All

non-aerated treatments had no significant changes in TN performance maintaining 95-98% removal throughout Phase II. Though, following the addition of 1 mg/L of Ag^+ and P-Ag-ENMs, the removal rates constants of TN were lower than the controls in INA and PNA before rebounded in week 9 (Figure 5.3B). These results contradict previous studies where it was observed that a chronic applications of 1 mg/L of Ag-ENMs in batch-fed subsurface TW mesocosms resulted in a significant inhibitory effects on the TN performance over a period 60d (Liu et al., 2023, 2019).However, Sheng et al. (2018) noted similar contradictory effects in four sequencing batch reactors (SBR) exposed to 1 mg/L of Ag-ENMs and ionic silver. The authors observed no significant changes in performance for COD, NH_4^+ or NO_3^-over time, maintaining around 80-90% removal across all Ag-amended systems. Systems with lower densities of microbial biomass are typically more sensitive to Ag-ENM exposures (Qiu et al., 2016). Microbial biomass in TWs, while lower than SBR, tends to increase over time and, given the age of these system prior to exposure, may have contribute to reduced toxicity.

In the case of WA mesocosm, the average of TN efficiency increased by 73% following the addition of the W-Ag-ENM wash matrix. The results are directly related to the previously observed increase of the in-situ TOC. In aerated systems, denitrification is limited due to the lack of available electrons for the reductive pathway. This process is often enhanced in aerated systems by increasing the C/N ratio as carbon acts as a major electron donor for denitrification (Zhu et al., 2014).

5.4.4 Microbial Activity and Function

During Phase I, from week 4 to week 13, the interstitial catabolic activity, measured through AWCD, and substrate richness of the aerated W-Ag-ENM and ionic silver treatment were noted to have a declining trend with time as the activity of the control increased (Figure C.10A, Figure C.11A). PA showed no observable trends over this time period maintaining a relatively steady state of activity. In week 13, an operational malfunction interrupted the weekly addition of Ag to the systems. In the following weeks, the respective catabolic activities and substrate richness of aerated systems were noted to steadily increase trending along with the control. It is possible that the discontinuous application of Ag created an opportunity for the interstitial microbial communities to recover. For the non-aerated systems, the richness and catabolic activity had no discernable differences in trends from the control during Phase I (Figure C.10B, Figure C.11B).

In Phase II, the W-Ag-ENM load had a significant stimulatory effect increasing the substrate richness. This, in turn, increased the observed AWCD in both the aerated and non-aerated systems compared to the controls, likely as a continued response to the additional carbon in the W-Ag-ENM pulse. While most Ag-ENM treatments had similar trends compared to the controls; in the case of PNA, the addition of 1 mg Ag/L of P-Ag-ENM resulted in an apparent hormetic response of the interstitial microbial communities. The hormesis model typically follows an initial decrease followed by the adaptive overcompensation or rebound (Calabrese and Baldwin, 2001). In TW systems, hormetic responses of microbial communities have been reported as a result of sublethal exposures of Ag-ENMs leading to increased EPS production and an upregulation of nitrogen-cycling genes (Sarkar, 2022).

Overall, TW mesocosms were far more resilient to Ag^{+} and Ag-ENM exposure compared to the pre-screening *ex-situ* test (Figure C.2). Internal microbial dynamics of TW system are far more complex due to the presence of the fixed biological regime, which is housed in biofilm. Biofilms provide an inherent resistance through their multilayered EPS matrix, which acts as barrier to Ag-ENMs providing a higher tolerance compared to free-floating bacteria (Tang et al., 2018). In line with this concept, the microbial activity of the entire microbial regime, determined through the FDA assay, showed little effects from any Ag treatments during Phase I compared to the controls (Figure 5.4A, C). Similarly, in Phase II, 1 mg/L of Ag+ and P-Ag-ENMs did not alter the overall microbial activity in the aerated and non-aerated mesocosms (Figure 5.4B, D). However, the microbial activity of WNA was significantly increased and deviated from the other systems likely in a response to the additional carbon input after 4 weeks of W-Ag-ENMs loading.

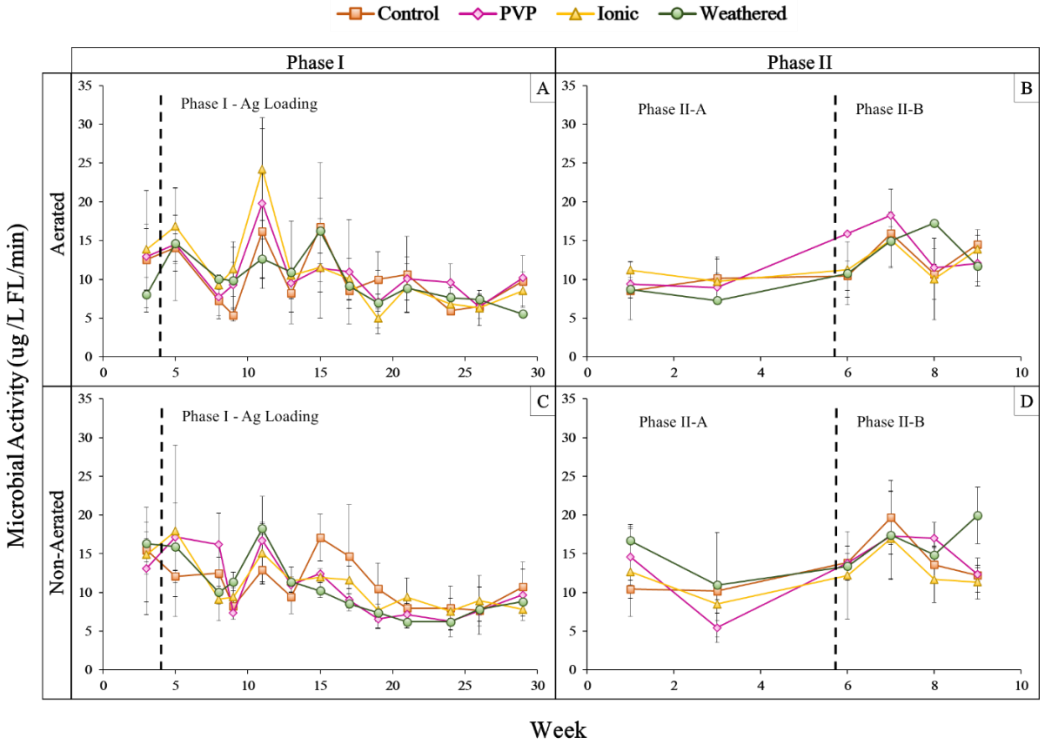

Figure 5.4: Average weekly microbial activity assessed through FDA assay of Phase I (left) and Phase II (right) for the aerated (A,B) and non-aerated system (C,D). Data points presented as means standard deviation (n=3).

Principal component analysis (PCA) was used to examine the functional changes in the carbon source utilization patterns for the beginning and end of each phase. The principal components describe 60.89% and 58.18% of the variance in Phase I and Phase II, respectively. The PCA plots show that there were temporal functional changes for all systems. At the start of Phase I, prior to Ag loading, the non-aerated systems were tightly grouped indicating they initially had similar functional capabilities; whereas, the aerated systems differed from their non-aerated mesocosm and to each other from the start (Figure 5.5A). The aerated system variance is likely a direct result of the artificial aeration being non-uniform, which, in turn, can alter the CSUPs (L. Zhang et al., 2018). Whereas, at the start of Phase II, the PCA ordination revealed all treatments had similar function capabilities only differentiating slightly due to aeration following the recovery period (Figure 5.5B).

In both Phase I and Phase II, following the addition of silver, IA and INA developed similarly to their respective controls indicating little effect of Ag^{+} on the functional potential of the interstitial microbial community. Conversely, Button et al. (2016a) noted that applications of 0.1 mg/L of Ag^{+} resulted in different CSUPs patterns in the microbial communities of TW microcosms compared to controls, while additions of Ag-ENMs had no effect. Though debated, silver ions are considered to have the higher toxicity through the formation of reactive oxygen species and their ability to penetrate into the bacterial cell decreasing protein expression and compromising chromosomal DNA (Xiu et al., 2012). Interestingly, at the end of Phase I, both the W-Ag-ENM and P-Ag-ENM were bound tightly in their aerated and non-aerated pairs, indicating that regardless of aeration and the different physicochemical parameters the functional capabilities of the interstitial microbial communities developed in similar metabolic fingerprints likely due to the addition of the Ag-ENMs. In Phase II, after 9 weeks a similar grouping of the P-Ag-ENM systems was observed while W-Ag-ENMs were less tightly grouped reinforcing this conclusion.

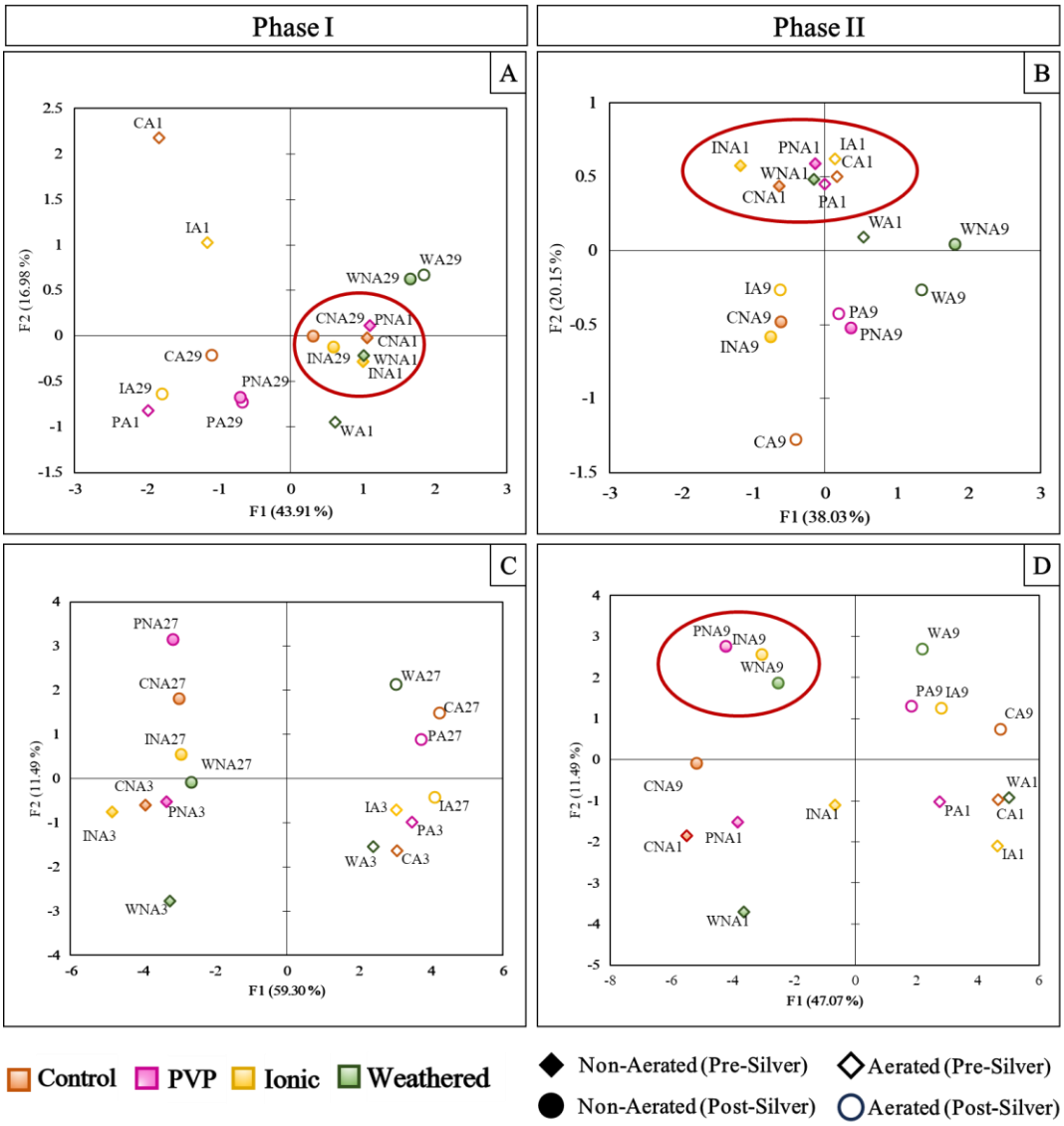

Figure 5.5: Principal component ordinations for transformed carbon source utilization patterns obtained from Biolog Ecoplates for Phase I (A) and Phase II (B); and genera abundance data for Phase I (C) and Phase II (D) where, C= control, P = PVP, I=ionic, W = weathered for the different silver treatments is combined with A=aerated or NA=non-Aerated to denoted the specific system. The number following the treatment abbreviation denotes the respective week the data was collected during each phase. Grouping based on observed visual differences.

5.4.5 Interstitial Microbial Community Diversity and Structure

Microbial communities housed in the biofilm are largely responsible for the breakdown of pollutants within treatment wetlands. Obtaining samples to assess their structure and diversity is difficult to achieve without deconstructing or disrupting the TW itself. As such, tracking temporal changes in community structure is quite difficult. In this study, interstitial water containing a mix of free-floating bacteria and small elements of sheared biofilm (based on constant recirculation) was used as a proxy to analyze the temporal effects of Ag pulses using 16S rRNA sequencing.

The alpha diversity indices, species richness (OTUs), and diversity (Shannon index) of the interstitial microbial communities showed no significant impacts from the high load Ag treatments in Phase II ($p>0.05$; Table C.6). However, following the silver addition, the microbial richness and diversity in the non-aerated systems were observed to slightly decrease in both Ag-ENMs treatments over time, while the control increased both phases. This suggests that the dynamics of the sheared microbial communities in the interstitial water of non-aerated systems were more sensitive to the addition of both types of Ag-ENMs. To further investigate the microbial structure, PCA ordinations were generated based on the average beta diversity measurement (i.e., abundance data) for each treatment in Phase I (Figure 5.5). The principal components of each plot describe 70.79% and 58.56% of the variance in Phase I and Phase II, respectively. In both phases, samples are grouped together along the first principal component (F1) based on level of aeration and then along the secondary axis due temporal changes in the community structure. In week 9 of Phase II, the non-aerated samples from the Ag-amended systems were noted to have developed differently from the non-aerated control.

Taxonomic analysis revealed the top most abundant genera of the interstitial microbial communities were predominately associated with the superphylum *Patescibacteria*, also referred to as candidate phylum radiation (CPR). This phylum is described as highly diverse nanobacteria with reduced redundant metabolic functions involved in carbohydrate, protein, sulfur and nitrogen cycling (Danczak et al., 2017; Tian et al., 2020). Other major phyla observed were *Actinobacteria* and *Proteobacteria* both of which have been associated with nitrogen and phosphorous cycling (Wang et al., 2022).

Shifts at the genus level in the most abundant taxa (microorganisms) across Phase I and Phase II are shown in Figure 5.6 and Figure 5.7, respectively. As expected, in both phases, artificial aeration caused the development of different microbial communities between systems (Silveira et al., 2022). After 27 weeks in Phase I, W-Ag-ENMs had a large stimulatory effect on the abundance of *Thiovirga* (a sulfur-oxidizing bacterium; Ito et al., 2005) increasing on average from 0.06% to 13.20 % in WA; whereas, CA only increased to 4.94%. Conversely, the addition of Ag^+ revealed no appreciable growth of the same genus in ionic aerated system. Ag^+ is known to complex with sulfur, forming Ag_2S, removing it from solution, and, as such, perhaps reduced the need for this particular genus. It was also noted that the relative abundance for the genus *Nocardioides* (a methylotrophic halotolerant actinobacterium; Meena et al., 2020) decreased in the INA and PNA systems and increase in CNA. The sensitivity of microbial communities to Ag-ENMs has been observed to be species dependant; specifically, in TW systems, ammonia oxidizing bacteria and nitrifying bacteria have been reported to be the most vulnerable to Ag-ENM stresses (Choi et al., 2008; Jiang et al., 2017).

In this study, the separation of the non-aerated Ag amended systems noted in the Phase II PCA plots can be attributed to the relative abundance of 6 specific genera (*Candidatus Kaiserbacteria*; *Candidatus Nomurabacteria*; *Candidatus Moranbacteria*; *C39* of the *Rhodocyclaceae* family; *SCGC AAAD11-D5*; and an unknown genus of the *Arcobacteraceae* family) in the interstitial water at week 9. Additionally, in Phase II, a large increase in the abundance of the genus *Parcubacteria* (putative fermenting heterotrophic organism, Coats et al., 2023) was observed only in CNA on average from 2.55% to 7.45%. The hormetic responses observed in TWs from sublethal concentrations of Ag-ENMs is thought to be either a result of niche filling (functional redundancies) within the overall microbial consortium or as an upregulation of nitrogen-cycling genes (Sarkar, 2022; Truu et al., 2022). The system design used in this study allows for the in-situ investigation of interstitial microbial communities during the exposure. These interstitial microbial communities are related to those found in the gravel-associated biofilm due to constant shear occurring, but are not wholly representative (Rajabzadeh et al., 2015). However, it is suggested that future studies directly examine the impacts of W-Ag-ENMs on TW biofilms. This would require dismantling of the experimental system (mesocosms in this case).

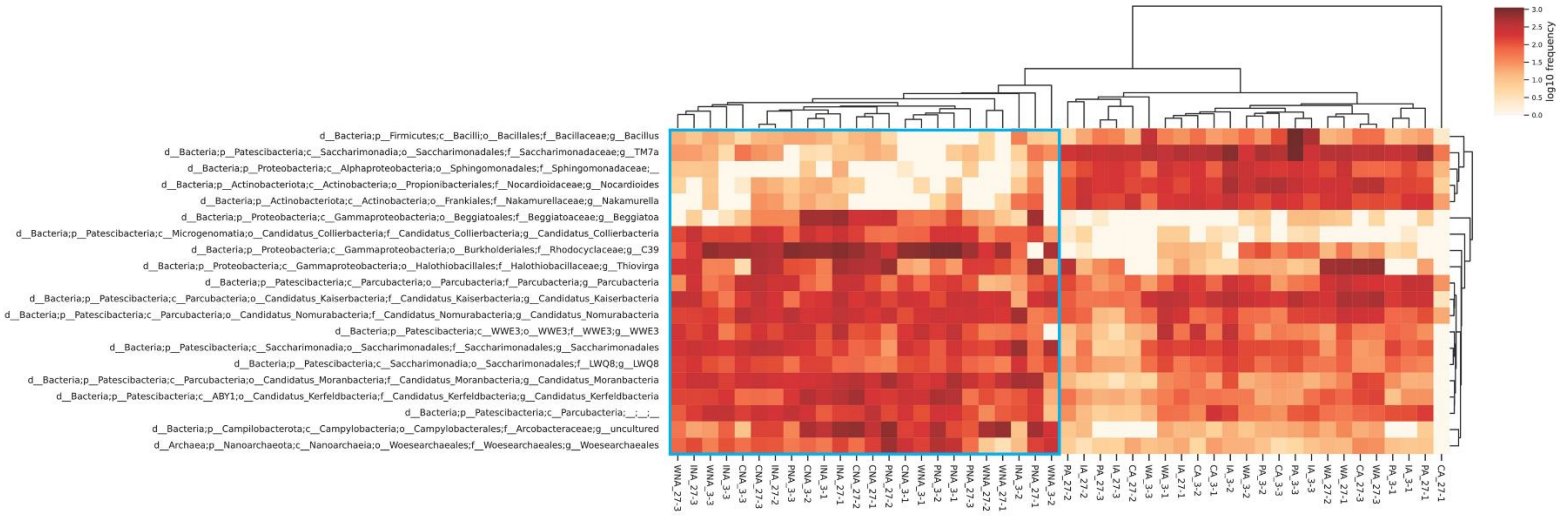

Figure 5.6: Taxonomy of the top 20 most abundant genera grouped based on the average Bray-Curtis distance metric for Phase I (A) and Phase II (B). The bottom corresponds to the weekly individual mesocosms where C= control, P = PVP, I=ionic, W = weathered for the different silver treatments is combined with A=aerated or NA=non-aerated to denoted the specific system. The number following the treatment abbreviation denotes the respective week the data was collected during each phase. On the frequency scale, the darker the color, the more abundant the genus in the sample. *Note: blue box identifies the non-aerated samples.

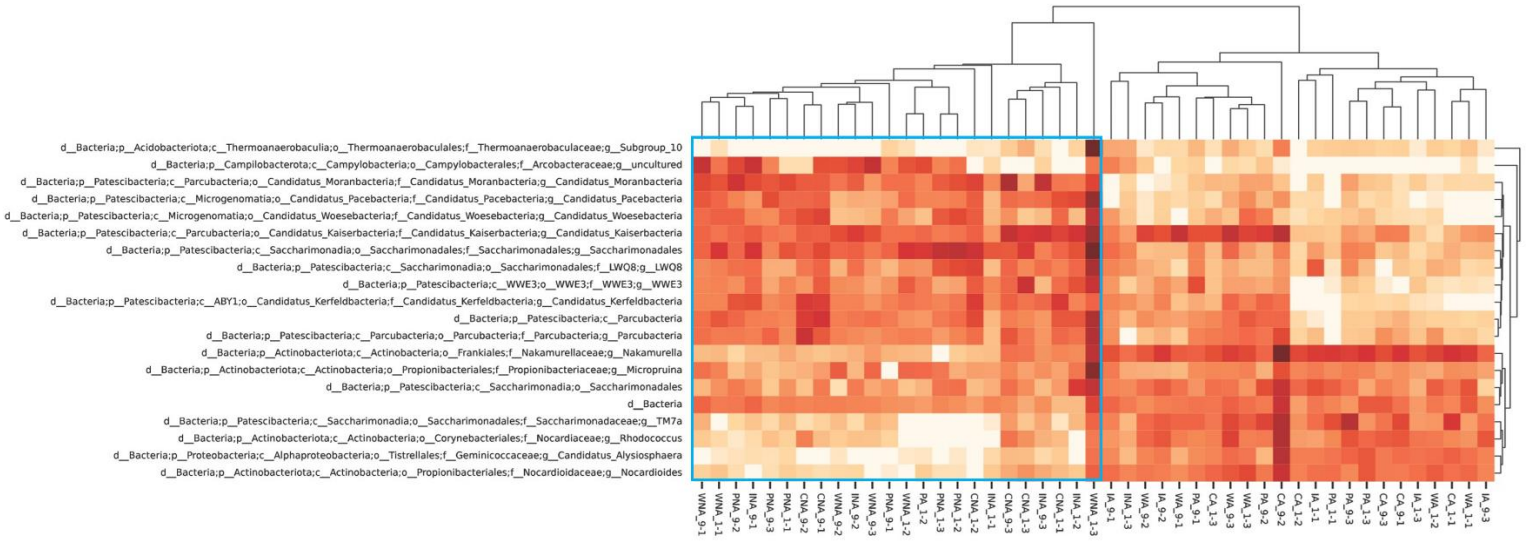

Figure 5.7: Taxonomy of the top 20 most abundant genera grouped based on the average Bray-Curtis distance metric for Phase I (A) and Phase II (B). The bottom corresponds to the weekly individual mesocosms where C= control, P = PVP, I=ionic, W = weathered for the different silver treatments is combined with A=aerated or NA=non-aerated to denoted the specific system. The number following the treatment abbreviation denotes the respective week the data was collected during each phase. On the frequency scale, the darker the color, the more abundant the genus in the sample. *Note: blue box identifies the non-aerated samples.

5.5 Conclusions

The is the first study to investigate the impacts of realistic weathered Ag-ENMs from commercial products along with pristine Ag-ENMs in established treatment wetland mesocosms over a total exposure period of 217-d. Following the addition of silver to the systems, the results showed that the doses of 0.1 to 1 mg Ag-ENM/L had little to no long-lasting impacts on the overall performance of the treatment wetland systems. While slight functional and structural shifts in the interstitial communities were noted during the exposure, there were no observable inhibitory effects from either Ag-ENM or ionic silver. However, in this study, a mix of sheared biofilm and interstitial water was used, which are not perfect representations of the fixed microbial regime. Future studies should examine the effects of incidental Ag-ENMs on biofilm matrices, both rhizospheric and media-bound.

5.6 CReDiT Authorship Contribution Statement

Anbareen J. Farooq: Conceptualization, Methodology, Investigation, Validation, Formal analysis, Writing - original draft, Visualization.**; Laura J. Ogilvie:** Investigation; Formal Analysis; Writing - original draft; **Dani Damasceno Silvera:** Formal analysis; **Vincent Gagnon:** Supervision; **Mark Button:** Formal analysis; **Sarah Wallace:** Formal analysis; **David J. Patch:** Formal analysis; **Iris Koch:** Writing – review & editing, Supervision; **Denis O'Carroll:** Conceptualization, Resources, Supervision, Funding Acquisition; **Kela P. Weber**: Conceptualization, Resources, Writing – review & editing, Supervision, Funding Acquisition.

6. The functional and structural shifts in biofilm bound microbial communities from addition of incidentally released silver nanomaterials in planted treatment wetland mesocosms

Anbareen J. Farooq[†], Dani Damasceno Silvera[§], Sarah Wallace[†], David Patch[†], Denis O'Carroll[‡], and Kela P. Weber[†*]

[†]Environmental Sciences Group, Department of Chemistry and Chemical Engineering, Royal Military College of Canada, Kingston, ON K7K 7B4, Canada

[‡]School of Civil and Environmental Engineering, UNSW Water Research Laboratory, University of New South Wales Sydney, Manly Vale, NSW, 2093, Australia

[§] University of Santa Catarina (UFSC), Campus Universitário, Trindade, CEP 88040-900. Florianópolis, SC, Brazil. daniele.ds@posgrad.ufsc.br

*Corresponding author: kela.weber@rmc.ca

6.1 Abstract

Treatment wetland (TW) systems are effective technologies for the removal of silver nanomaterials (Ag-ENMs), an antimicrobial agent, from incoming wastewater streams. However, there is growing concern regarding impairment to the TW performance as, upon entering, the Ag-ENMs are predominately found within the microbial biofilm, which plays an essential role in the pollutant degradation potential of these systems. While the impacts from pristine Ag-ENMs to the bound microbial communities have been investigated, little is known about the effects of true incidentally released Ag-ENMs from consumer products on these communities. In this study we examined the fate and effects on the gravel-associated and rhizospheric biofilm communities after a long-term exposure to incidental Ag-ENMs weathered from commercial textiles and a PVP-coated pristine Ag-ENM through a mesocosms deconstruction. Similar to previous studies, the majority of silver was found in the biofilm with up to 67% retain in the bottom 30 – 60 cm. The results show that the weathered Ag-ENMs caused functional and structural shifts in the rhizospheric and media bound biofilms in the aerated systems, while the non-aerated communities were largely unaffected. The water treatment of these systems was largely unaffected despite these shifts demonstrating the robustness of treatment wetlands.

Keywords: silver nanomaterials; treatment wetland; biofilm; metagenomics; fate

6.2 Introduction

For rural communities, decentralized biological wastewater treatment processes, such as treatment wetlands (TW), are far more prominent due to their low costs and reliable performance (Capodaglio et al., 2017). The wastewater treatment potential of TWs is mainly achieved through microbially mediated degradation of pollutants (Button et al., 2015). These microbes can be found in the interstitial water, but more so organize themselves within biofilm matrices adhering to plant roots (rhizospheric) or the substrate bed (media-bound) (Farooq et al., 2023a; Weber, 2016). The biofilm matrix, composed of extracellular polymeric substances (EPS), is considered a natural barrier, protecting the enclosed microbial communities from perturbations in a stable environment. (Flemming et al., 2016; Karygianni et al., 2020). Over time, the application of TWs has broadened from domestic wastewater to more complex contaminants from a wide range of areas, including nanomaterials (Ji et al., 2022).

Over the past two decades, with the rapid expansion of nanotechnology, engineered nanomaterials (ENMs) have been increasingly used in broad range of fields as a result of their enhanced physico-chemical properties that separates them to their bulk-scale counterparts (Chouhan and Chouhan, 2018; Horikoshi and Serpone, 2013). The estimated size of the global nanomaterial market reached around 8.0 billion USD in 2020 and is forecasted to grow at annual rate of 14.1%, projected until 2028 (Barhoum et al., 2022). ENMs can be classified a number of ways including by their elemental composition, the most popular type being silver nanomaterials (Ag-ENMs). Ag-ENMs are reported to account for 24 to 50% of the nanomaterial consumer products worldwide (Inshakova and Inshakov, 2017; Project on Emerging Nanotechnologies, 2023). These products include, but are not limited to, medical supplies, electronics, coatings, packaging, and textiles (Vance et al., 2015). Through the production, use, and eventually disposal of these nano-embedded products, there is the high potential for the release of incidental or "weathered" Ag-ENMs into wastewater streams (Li et al., 2013). Thus, as the widespread use of Ag-ENMs is directly related to their well documented antimicrobial properties, there is a significant concern regarding their potential toxic effects in systems like treatment wetlands where the pollutant removal is directly tied to the health of their microbial communities (Anees Ahmad et al., 2020; Kim et al., 2007).

While TW systems are effective at removing Ag-ENMs from wastewater streams containing them primarily within the soil layer or the biofilm matrix in gravel-based systems it is not without impacts to the internal microbial dynamics (Auvinen et al., 2017; Cao et al., 2018). Under the stress of Ag-ENMs, shifts in microbial structure have been observed with key functional bacteria such as ammonifers (*Pseudomonas*), nitrifiers (*Nitrosomonas* and *Nitrospira*), and denitrifiers (*Thauera* and *Dechloromas*) decreasing in abundance following the addition of Ag-ENMs (Liu et al., 2019). However, until now, all previous studies have primarily used pristine particles; however, the toxicity of Ag-ENMs towards different organisms is dependant on a number of factors, including size and shape (Choi and Hu, 2008; Gorka et al., 2015; Pal et al., 2007). Auclair & Gagné (2022) and Helmlinger et al. (2016) both noted that the spherical Ag-ENMs displayed a higher toxicity than any other form including prismatic or cubic particles. Characterization of incidental Ag-ENMs from consumer products has shown that they are released into wastewater streams in a variety as

nanoaggregates, nanoplates, and nanoparticles, all of different sizes different compositions, compared to their pristine Ag-ENM counterparts (Benn et al., 2010; Patch et al., 2021). Based on such different physicochemical properties from the pristine Ag-ENMs, may result in different effects on TW biofilms.

To date, the effects of incidentally released Ag-ENMs from commercial products remains largely unknown to TW biofilms as studies have focused on the impacts from pristine particles. In this study, following the exposure to artificially generated W-Ag-ENMs (detailed in Farooq et al. (2023)), TW mesocosms were destructively sampled for a comprehensive understanding of the impacts and fate of incidental Ag-ENMs to TW biofilms. The objectives of the present study were to (1) determine the distribution Ag-ENMs within the compartments of the TW mesocosm; (2) investigate the spatial structural and functional differences in TW wetland mesocosms following the addition of both pristine and incidentally released Ag-ENMs. To the authors knowledge this is the first work to assess the fate and impacts from realistic weathered Ag-ENMs in TW biofilms.

6.3 Materials and Methods

6.3.1 Silver Nanomaterials

The weekly suspensions of incidentally released, also referred to as weathered, Ag-ENMs (W-Ag-ENMs) used in this study were generated through the washing of physically weathered Lululemon's "T.H.E. Sock Silver" as described by Patch et al. (2021). The socks were used due to their high silver content (37 mg Ag/kg textile) from the incorporation of X-STATIC® fibres, which are nylon fibres that have an electrolytically deposited layer of Ag-ENMs (Gagnon et al., 2019). Polyvinylpyrrolidone (PVP) coated (PVP 0.2 wt%) silver nanoparticles (20-30 nm, Skyspring Nanomaterials, Inc, TX, USA) were used as a pristine control (P-Ag-ENMs). Weekly nanomaterial suspensions were obtained by dispersing the nanopowder in DI water using sonication (Fisher Scientific Model 505 Sonic Dismembrator, Fisher Scientific, NH, USA) at 50 Hz for 60 seconds. The average median diameter of the weekly suspensions of the P-Ag-ENM and W-Ag-ENM were 76.7±10.8 nm and 89.5 ± 40.4 nm, respectively, determined through single particle ICP-MS (Elan DRC II, Perkin Elmer, MA, USA).

6.3.2 Experimental Design

Re-circulating TW mesocosms (height: 0.61 m, diameter: 0.25 m) were built for each type of exposure: Ag-ENM (weathered and polyvinylpyrrolidone (PVP) coated), ionic silver (Ag^+ in the form of $AgNO_3$), and an unexposed control, both as aerated and non-aerated units in triplicate for a total of twenty-four systems. All mesocosms were filled with washed limestone pea gravel and planted with *Phalaris arundianacea*. Aerated systems were outfitted with individual aeration stones (6") connected to an EcoPlus Air 3 pump (Atlantic Pond Supply; Moncton, NB) by ½" Nalgene tubing. The systems were batch fed simulated wastewater (COD:N:P 100:5:1) as described by Weber & Legge (2011) every 7 days. The systems had already been in operation for just over a year prior to the silver exposure experiment, which lasted 455 days. In Phase I, Ag-ENMs and Ag^+ were directly added to affected system on a

weekly basis for a final in-situ concentrations 0.1 mg Ag/L for 189 days. After a recovery period of 238 days, the weekly dosage was increased to 1 mg Ag/L for 28 days in Phase II. These exposure experiments were based on the scenario of a release into a single home TW system. The TW mesocosm design and exposure experiment have been fully described in our previous study (Farooq et al., 2023b). Throughout the exposure, influent and effluent samples were taken to complete a mass balance of silver.

6.3.3 Nanomaterial Fate Analysis

Following both exposures, aboveground biomass was harvested and TW mesocosms were destructively sampled to investigate the Ag distribution within the systems. Each mesocosm was divided into three layers: 1) 0-10 cm, 2) 10-30 cm, and 3) 30-60 cm (Figure 6.1). Each layer was mixed together before gravel samples were retrieved for further analysis. Additionally, representative root samples, were collected from each layer; however, as most systems did not have root biomass in the lower third region, the two layers of 10-30 cm and 30-60 cm were combined for the rhizospheric biofilm samples. Representative biofilm samples for total silver analysis were extracted following the procedure as detailed in Section 6.3.4.1. Secondary gravel samples (25 g) were taken to determine organic content (volatile solids) following the methods described in Weber & Legge (2013) using a drying oven (105˚C) for 24h followed by a muffler furnace (550˚C) for 15min.

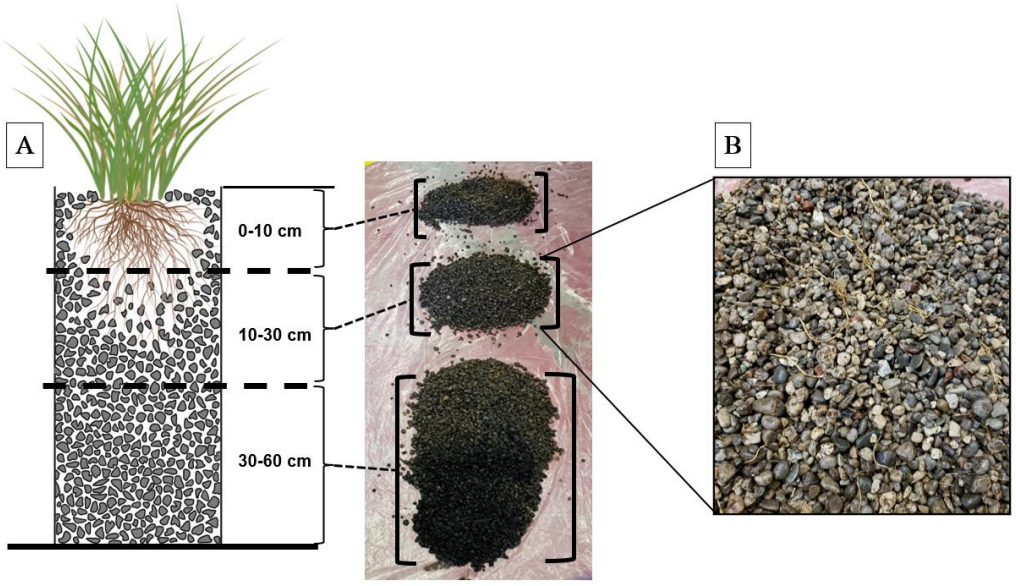

Figure 6.1: (A) Mesocosm schematic showing each layer taken during destructive sampling: 1) 0-10 cm, 2) 10-30 cm, 3) 30-60 cm. (B) A close up of the 10-30 cm layer showing the lower roots amongst the gravel media.

Samples of the weekly stock solutions, biofilm, plant tissue (shoot/leaves and roots), and effluent underwent heated acid digestion using an *aqua regia* solution (1:3 HNO_3 70% and HCl 35%) prior to analysis through inductively coupled plasma-mass spectrometry (ICP-MS) (Elan DRC II, Perkin Elmer, MA,USA). The subsequent mass balance was calculated as follows:

$$\sum_{i=1}^{n} C_{in_i} \times V_{in_i} = \sum_{j=1}^{3} m_{biofilm} + \sum_{j=1}^{2} m_{roots} + m_{leaves/shoots} + \sum_{i=1}^{n} C_{out_i} \times V_{out_i} \quad (1)$$

where C_{in_i} is the concentration of stock Ag, V_{in_i} the volume of stock suspension added, $m_{biofilm}$ is the Ag content in the biofilm, m_{roots} is the Ag content in the roots, $m_{leaves/shoots}$ is the Ag content in the leaves/shoots, C_{out_i} is the concentration of Ag in the effluent, and V_{out_i} the volume of the effluent; i is the week number; n is the total number of weeks of exposure; and j is the respective layer.

Representative plant tissue (root and shoot) and biofilm samples were sent for x-ray absorption near edge structure (XANES) analysis at the Canadian Light Source Inc. – Advanced Photon Source (CLS@APS) X-ray Science Division (XSD) on the bending magnet (BM) beamline, Sector 20, however concentrations in the samples were too low for effective analysis. Similarly, scanning electron microscopy with energy dispersive x-ray fluorescence (Quanta FEG 250 and EDAX Octane Elite, ThermoFisher Scientific, OR, USA) was used to detect and quantify the speciation of silver in the plant tissue and biofilm samples, but was unsuccessful.

6.3.4 Microbial Community Analysis

6.3.4.1 Microbial Detachment

Following the procedure as detailed in Weber & Legge (2010b), 25 g of pea gravel from each layer was shaken for 3h (Innova 4320 Refrigerated Incubator Shaker) in a 10mM phosphate buffer solution (pH 7 with 8.5 g/L NaCl) to detach the microbial communities. For the rhizospheric microbial communities, approximately 1.5 g of representative root material from 0-10 cm and 10-60 cm was used with the same protocol.

6.3.4.2 Community Level Physiological Profiling (CLPP)

Community Level Physiological Profiling (CLPP) was used to characterize the functional variation in richness and catabolic activity (measured as the average well colour development, AWCD) for interstitial and detached (gravel-associated and rhizospheric) biofilm samples using a 96 well BIOLOG ® EcoPlate (BIOLOG Inc., CA, USA). Each plate contains 31 different carbon substrates, and a blank well in triplicate. Together with the carbon substrate, each well contains tetrazolium violet, a redox dye indicator, and when a mixed microbial

community sample is inoculated into the well, the production of NADH via cell respiration reduces the tetrazolium dye to formazan. The colour development is tracked over the course of 96 hours with absorbance readings taken at every 4-hour mark by a microplate reader stacker (Eon Microplate Spectrophotometer, BioTek Instruments, Inc., VT, USA) at 595nm.

6.3.4.3 DNA Extraction and Sequencing

To assess microbial structural changes, 16S ribosomal RNA sequencing was conducted on the gravel and rhizospheric microbial communities as detailed in Silveira et al. (2022) and Farooq et al. (2023). Briefly, a total of 25 mL of the detached and 100 mL of interstitial microbial communities were collected for each sample and filtered separately through 0.22 µm filter paper (Millipore, Bedford, MA, USA) using a sterile vacuum filtration. DNA was extracted from the full filter using the FastDNA Spin Kit for Soil (MP Biomedicals, Santa Ana, CA, USA) following the manufacturer's protocol. The DNA concentrations were measured using a Qubit fluorometer and Qubit dsDNA HS assay kit (Invitrogen, ON, CAN).

The variable V3 and V4 regions of the 16S ribosomal RNA gene (16S rRNA) were amplified and purified from each sample following the Illumina 16S Metagenomic Sequencing Library Preparation guide (version B, Illumina Canada Ulc., Victoria, BC, Canada). Each sample was normalized to 4 nM, pooled, denatured, and diluted to 4 pM. Sequencing was performed using the MiSeq Reagent v3 600 cycle kit on the MiSeq (Illumina Canada Ulc., Victoria, BC, Canada) generating paired end 2 x 300 bp reads. A 10% spike in of the PhiX control library was added to monitor the quality of the sequencing run.

QIIME2 version 2021.11 (Caporaso et al., 2010) on VirtualBox (version 7.0) was used to analyze the 16S rRNA sequences. Demultiplexed fastq files were imported and reads were filtered, denoised, and merged with the removal of chimeras using DADA2 (Callahan et al., 2016). Reads were classified using the naive bayes classifier (Bokulich et al., 2018; Robeson et al., 2021) trained on the Silva 138 taxonomic database (99% OTU full length sequences; Quast et al., 2013). The median frequency was 25846 (min-max: 529-103886) reads and thus samples were rarefied to 7000 reads for diversity analyses. The align-to-tree-mafft-fasttree pipeline was used for phylogenetic dependent analyses. Multiple alpha diversity metrics were estimated including Shannon’s diversity index, observed OTUs, Faith’s phylogenetic diversity, and evenness. Multiple beta diversity metrics were estimated including Jaccard, Bray-Curtis, unweighted UniFrac, and weighted UniFrac distances.

6.3.5 Data Analysis

Analysis of the CLPP data was performed as described by Weber et al. (2007) and Weber and Legge (2010) to determine substrate richness and diversity. Richness represents the number of different carbon substrates utilized by a microbial community with absorbance greater than 0.25 AU. Whereas, the AWCD is based on the carbon substrates utilization pattern (CSUP) of a given sample. The time point 48 h was chosen to obtain the most variation within the data set while minimizing the number of over-saturated wells (absorbance units greater than 2.0) (Kela P. Weber and Legge, 2010). As suggested by Weber and Legge (2009), the carbon substrates can be divided into five groups (guilds), which include polymers, carbohydrates, carboxylic acids and acetic acids, amino acids, and amines/amides to better understand

specific functional differences in the microbial community (Table D.1). Additionally, a set of 10 of the 31 carbon sources (D-xylose, D-mannitol, 2-hydroxy benzoic acid, 4-hydroxy benzoic acid, D-malic acid, L-arginine, L-asparagine, L-phenylaline, L-serine, L-threonine) were identified as root exudates from based on a short literature survey (Badri and Vivanco, 2009; Campbell et al., 1997; Willig et al., 2000). Principal component analysis (PCA) was performed using the covariance matrix (n-1) of the CSUP data to further assess for functional differences between systems using XLSTAT statistical software (2023.1.2, Addinsoft). Datasets were subjected to Taylor series transformations based on assessment of normality, homoscedasticity and linear correlations following the recommendations of Weber et al. (2007). One-way ANOVA was used to identify differences between treatment means in individual measurements while post-hoc Tukey's tests were used to identify significantly different treatment groups. Post-hoc Dunnett's tests were used to identify treatments which significantly differed from the control (Dunnett, 1955).

PCA ordinations were also generated in XLSTAT using genera with abundances over 1% to compare the structural differences in the microbial communities within the for the aerated and non-aerated system sets. This was followed by Agglomerative Hierarchical Clustering (AHC) of the metagenomic data to further identify differences in the microbial communities using the Unweighted Pair Group Method with Arithmetic mean (UPGMA). One-way permutational analysis of variance (PERMANOVA) was performed in QIIME 2 with both beta diversity matrices Bray-Curtis and Euclidean distance to assess the differences in microbial composition among samples from different systems. The percent of reads in each sample matching to the top 20 abundant genera were plotted and compared among designs in a heatmap using an average Bray-Curtis metric. All alpha diversity indices and the beta diversity analysis were performed using QIIME 2 software (2019.10).

6.4 Results and Discussion

6.4.1 Distribution of Silver in Treatment Wetland Mesocosms

Overall, the mass balance revealed that while 88.2% to 99.0% (per drainage values) of the silver mass loaded was retained within the TW mesocosms, only 46% to 71% was recovered across treatments (Table 6.1). After destructively sampling the systems, the interior mesocosm walls retained some biofilm material; however, due to the size of the systems and time constraints, completing an acid wash extraction of the empty mesocosms was not feasible. This was likely a major contributor to poor closure of the mass balance. The aerated systems had higher release of Ag in the drained effluent compared to the non-aerated systems linked to the observed in quantities of TSS in the effluent as discussed in our previous study (Farooq et al., 2023b). Overall, the TWs were more effective at retaining W-Ag-ENMs compared to Ag^{+} and P-Ag-ENMs indicating that there could be a reduced potential of the discharged to the surrounding environment with respect to realistic particles entering wastewater streams.

Similar to previous TW studies, the media bound biofilm acted as the main internal sink trapping the majority (50+%) of Ag-ENMs and Ag^{+} within its EPS matrix and spatially, on a mass basis, the lower biofilm layer (30-60 cm) retained the largest percentage of silver.

(Auvinen et al., 2017; Liu et al., 2019). The subsequent preferential binding of silver to biofilms has been mainly attributed to the electrostatic attraction between positively charged Ag-ENMs and negatively charged biofilm (Desmau et al., 2018). A spatial analysis showed that the organic (biofilm) content had a uniform distribution in non-aerated systems across all treatments (Figure 6.2A, B, ANOVA, $p>0.05$). Interestingly, the aerated P-Ag-ENM system saw a significant (ANOVA, $p<0.05$) peak in organic content in the 10-30 cm layer compared to the other treatments, where the organics had a non-significant increase with depth (ANOVA, $p>0.05$). Correspondingly, silver was found in each layer for all treatments; yet, its subsequent distribution in the biofilm was uniform only for the Ag^+ amended systems under both aeration modes (Figure 6.2C, D). The non-aerated systems were observed to have significantly higher P-Ag-ENM in its upper biofilm layer (0-10 cm); whereas, higher fractions of silver (ug Ag/g organics) were preferentially bound in the lower layer (30-60 cm) of all the W-Ag-ENM systems.

Figure D.1 shows the total above and belowground biomass harvested from the TW mesocosms during deconstruction. Overall, the non-aerated systems had significantly higher biomass, particularly in the upper root layer (0-10 cm), compared to their aerated counterparts (ANOVA, $p<0.05$). Artificial aeration is known to negatively impact the development of plants, such as *Phragmites australis*, in TW systems resulting in stunted growth and finer root structures (Butterworth et al., 2016). A visual comparison of the *P. arundinacea* roots prior to deconstruction confirmed that the biomass of was far denser within the non-aerated mesocosms creating a thicker rhizospheric zone (Figure D.2). While the aerated systems had less biomass density, the root mass was noted to be more even distributed throughout the upper and lower layers of the wetland. Aeration is known to cause the elongation of roots, which can explain this spatial uniformity (Geisler, 1965).

While the uptake of Ag^+ by the roots was relatively uniform across all systems, depth profiles of the root tissues showed a significant difference between the aerated and non-aerated uptake of both types of Ag-ENMs (Figure 6.2E, F, ANOVA, $p<0.05$). Silver concentrations (mg Ag/ kg DW biomass) in non-aerated root tissues were 1.6 to 4 times higher on average for Ag-ENM treatments. Ag-ENMs are known to permeate into the plant biomass through the root cell wall pores depending on their size (Navarro et al., 2008a). The stunted roots noted in the aerated systems likely contributed to the poor uptake, filtering out more of the pristine and weathered Ag-ENMs.

Similar to previous studies, translocation of silver was limited into the aboveground plant, representing less than 1% of the total mass of silver loaded into the Ag systems (Auvinen et al., 2016; J. Huang et al., 2019c). While there was no significant difference in the aboveground biomass from the addition of silver, slightly lower amounts of shoots/leaves were harvested from P-Ag-ENM and Ag^+ systems compared to the control in the aerated mesocosms. Whereas, in non-aerated systems, both types of nanomaterials, in particular P-Ag-ENM, had lower average total biomass.

Unfortunately, speciation of the silver in the biofilm and plant tissue through XANES and SEM were not sensitive enough to collect useable data. In literature, Ag-ENMs are noted to transform once they enter into TW systems forming complexes through the interactions with ligands, such as sulfur or chloride (Levard et al., 2012). These chemical transformations, tend

to reduce the overall availability of silver to the surrounding environments and limit potential toxic effects.

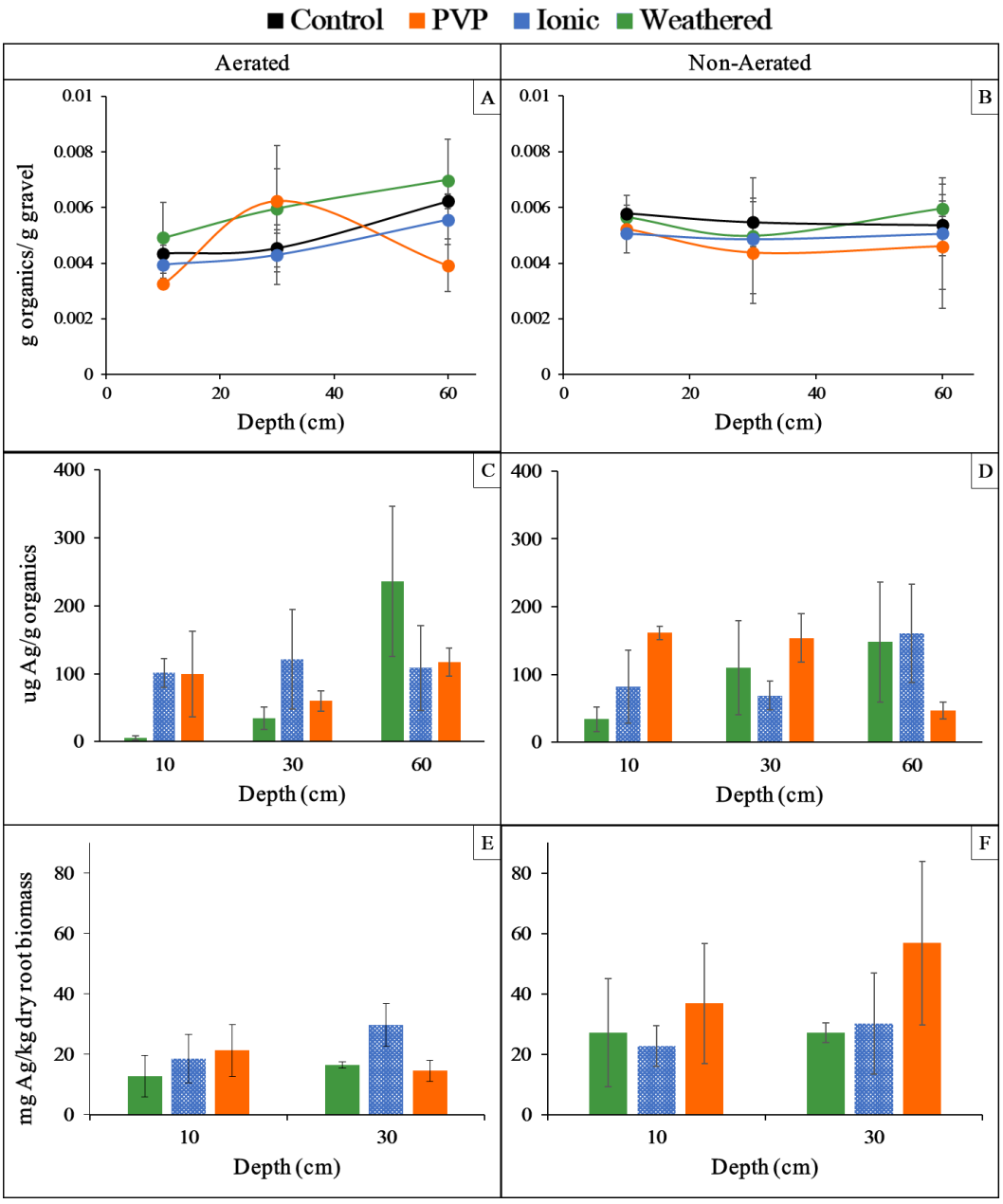

Figure 6.2: Spatial distribution of organic content within the gravel media (A,B), silver within the gravel media (C,D), and silver in the root biomass (E, F) within the treatment wetland mesocosms. Data points presented as means standard deviation (n=3).

Table 6.1: Distribution of silver in effluent, plants tissue and biofilm in TW mesocosms after 217-d exposure. Data points presented as means standard deviation (n=3, except for the aerated P-Ag-ENM where n=2).

	P-Ag-ENM		Ionic		W-Ag-ENM	
Location	*Aerated*	*Non-Aerated*	*Aerated*	*Non-Aerated*	*Aerated*	*Non-Aerated*
Above ground	<1%	<1%	<1%	<1%	<1%	<1%
Roots (0-10cm)	<1%	1.7 ± 0.8%	<1%	1.7 ± 0.1%	<1%	1.8 ± 0.8%
Roots (10-60cm)	<1%	1.1 ± 0.0%	<1%	<1%	<1%	1.1 ± 0.4%
Total Plants	0.5 ± 0.1%	3.0 ± 0.6%	0.3 ± 0.1%	1.9 ± 0.2%	0.5 ± 0.1%	3.0 ± 0.6%
Biofilm (0-10 cm)	6.3 ± 4.4%	14.5 ± 0.7%	5.2 ± 1.2%	5.5 ± 2.3%	0.4 ± 0.2%	3.2 ± 1.6%
Biofilm (10-30 cm)	11.3 ± 0.3%	21.9 ± 3.6%	19.6 ± 0.7%	8.1 ± 1.3%	5.6 ± 1.8%	13.9 ± 3.5%
Biofilm (30-60 cm)	16.6 ± 0.2%	16.9 ± 3.3%	28.5 ± 5.2%	28.0 ± 7.9%	50.2 ± 10.7%	49.9 ± 31.6%
Total Biofilm	36.4 ± 4.2%	53.3 ± 4.7%	53.2 ± 5.8%	41.5 ± 3.7%	59.8 ± 11.9%	67.0 ± 29.3%
Drainage	11.5 ± 0.9%	4.6 ± 0.7%	12.2 ± 2.2%	3.4 ± 0.3%	9.0 ± 4.5%	1.0 ± 0.2%
% Recovery	47.2 ± 6.8%	61.7 ± 1.7%	68.6 ± 11.8%	46.4 ± 6.8%	69.3 ± 7.5%	71.1 ± 28.9%

6.4.2 Functional Assessment of Microbial Communities

The catabolic activity, measured through AWCD, is presented for the interstitial, gravel-associated and rhizospheric microbial communities at each depth in Figure 6.3. In general, catabolic activity decreased with depth as seen for both gravel-associated and rhizospheric biofilm in line with the results of Weber & Legge (2013). Only the AWCD of the aerated and non-aerated gravel-associated biofilm from the W-Ag-ENM mesocosms was relatively constant with depth. Substrate richness was noted to followed similar trends with catabolic activity for both the aerated and non-aerated system (Figure S3A,B; S4A, B). Similar to previous studies, the interstitial microbial communities exhibited less activity compared to the detached gravel-associated biofilm communities in almost all systems (Lv et al., 2017; Weber and Legge, 2013). Notably, the interstitial bacteria of the W-Ag-ENMs mesocosms had comparable or higher levels of activity to those of the detached biofilm matrix. During the exposure, the addition of the W-Ag-ENMs in the wash water matrix stimulated the catabolic activity of the interstitial communities while the overall microbial activity, representative of the entire fixed microbial regime (included the biofilm), was unchanged (Farooq et al., 2023b).

Significant differences between treatments with respect to catabolic activity were observed in both the aerated and non-aerated systems (ANOVA, $p<0.05$). A Dunnet test indicated that the biofilm communities exposed to ionic silver (in the form of $AgNO_3$) had significantly reduced activity compared to the controls in the aerated systems for both the gravel-associated and rhizospheric biofilm at multiple depths (Figure 6.3A,C). Numerous studies have documented the toxic effects of ionic silver towards single organisms and large complex microbial communities through the generation of reactive oxygen species (Park et al., 2009; Asghari et al., 2012; Gray et al., 2022). However, in the upper layers of non-aerated systems, the addition of W-Ag-ENMs significantly lower the activity compared to the control in both types of detached biofilms (ANOVA, $p<0.05$).

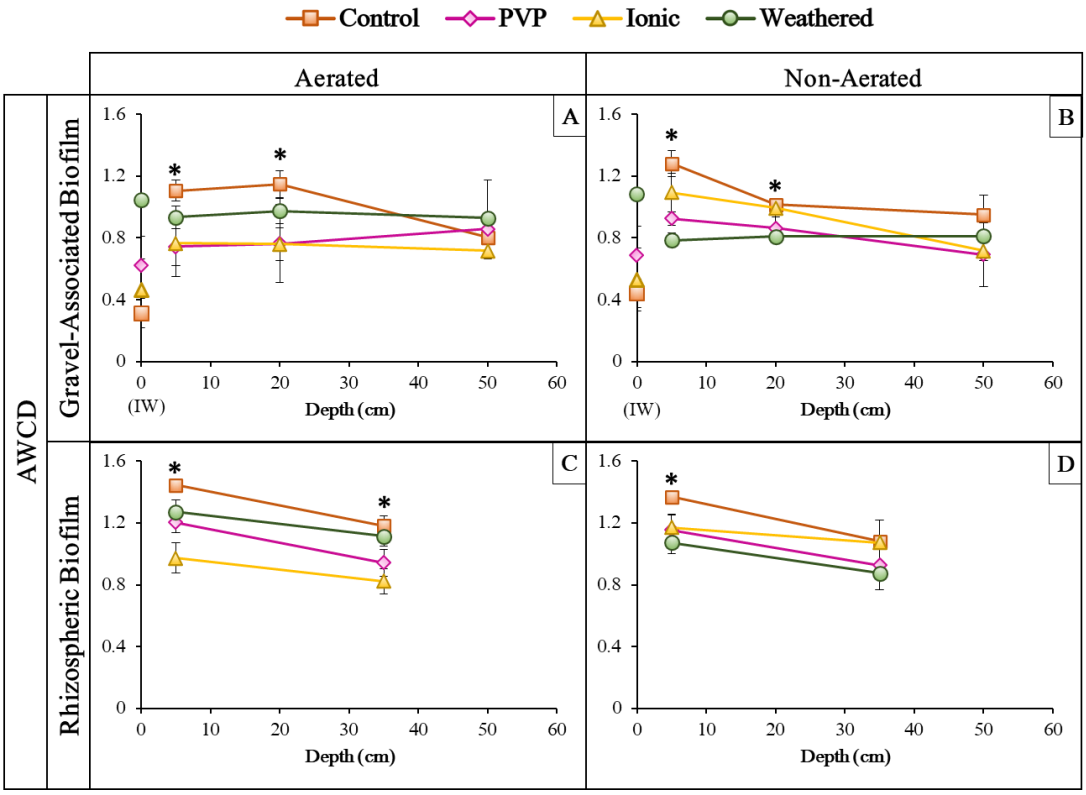

Figure 6.3: Depth profiles of the average well colour development for the gravel-associated (A,C) and rhizospheric (B,D) biofilm from the aerated (right) and (left) and non-aerated systems (right). Data points presented as means standard deviation (n=3). The asterisk (*) denotes significant differences between treatment at specific depth from a one-way ANOVA ($p<0.05$)

Principal component analysis (PCA) was used to examine the functional differences in the carbon source utilization patterns for both rhizospheric and gravel-associated biofilms (Figure 6.4A, B). The principal components (F1 and F2) describe 63.49% and 52.20% of the variance in aerated and non-aerated systems, respectively. For the aerated systems, the controls formed a separate grouping from the Ag^{+} and Ag-ENM amended systems indicating there was a clear difference in the functional potential of the microbial communities from the addition of silver regardless of sample location. A closer examination of the biplot, which overlays the specific carbons sources on the PCA, showed that the differentiation along the first principal component was primary related to the microbial communities' capacity to metabolize amine/amides (phenylethylamine) and amino acids (L-arginine, a known root exudate), which was reduced in the P-Ag-ENMs and Ag^{+} systems (Figure 6.4C). The carbon sources which influenced the separation of the controls from the silver treatments were three amino acids (L-threonine, L-phenylalanine and L-arginine) and a single carbohydrate (i-erythritol), the former of which are all known root exudates (Table D.1). Plants have been known to exude

chemicals from their roots which can alter the chemical and biological characteristics of the rhizosphere and, in turn, the associated rhizospheric microbial community (Whipps and Lynch, 1990). Root exudate will enhance the metabolic capabilities of a microbial community, but it is entirely plant specific (Button et al., 2016b). Moreover, different growing seasons plants will adapt their production of root exudate to recruit specific bacteria (G. Wang et al., 2022).

Interestingly, Echavarri-Bravo et al. (2015) noted the similar suppression in utilization of amino acids in a benthic estuarine microbial community 24h after the addition of a single 1 mg/L pulse of pristine Ag-ENMs. Though authors noted that the microbial communities had recovered from the one-time pulse after 120h. Button et al. (2016a) found observed no functional difference in CSUPs from addition of 0.1 mg/L of Ag^{+}, citrate coated and PVP-coated Ag-ENMs compared to the controls in TW microcosms biofilms. In the current experiment the biofilm had been chronically exposure to silver over a total 455 days (including a recovery period), which likely led to more permanent effects compared to the latter which only lasted 28 days.

In the case of the non-aerated systems, the metabolic functional patterns were found to be primarily influenced by spatial location along the F1 axis (Figure 6.4B). The stratification seen in this study is thought to be a result of the increase root biomass in the upper 0-10 cm enhancing the activity. Weber & Legge (2013) previously noted that rhizospheric biofilm have a disproportionately large catabolic activity as compared to gravel-associated biofilm a similar stratification with depth. Moreover, plants roots are known to mediate a small amount of oxygen transfer into TW systems (Bezbaruah and Zhang, 2003). In the case of *Phalaris*, it is estimated that the oxygen release from the roots can reach about 20% root volume creating a separate microenvironment and, in turn, microbial communities with a different metabolic function (Edwards et al., 2006). Specifically, the differentiation between groupings was attributed to the higher utilization of carboxylic and acetic acids from microbes in the top 10 cm of all systems (Figure 6.4D). Spatial functional variation has often been observed along flow paths and with depth in pilot-scale TW systems as more easily degradable compounds being are utilized first and microbial communities adapt towards more complex compound towards the effluent release points in larger scale systems (Button et al., 2015; Ruppelt et al., 2020; Silveira et al., 2022).

Moreover, in both plots, but more so in the aerated system, the W-Ag-ENMs systems were separately grouped from the other silver treatments and their controls indicating that the accumulation of incidental W-Ag-ENM cause different functional changes to TW than with pristine Ag-ENMs. The differentiation of the W-Ag-ENMs microbial communities in both the aerated and non-aerated systems was due to their enhanced utilization of two specific carboxylic and acetic acid carbon sources D-galactonic acid-γ-lactone and D-malic acid. Interestingly, researchers have identified D-galactonic acid-γ-lactone as a carbon source utilized to promote heavy metal (Cd, Cu, Pb and As) resistance to microbial communities in contaminated environments (Martínez-Toledo et al., 2021).

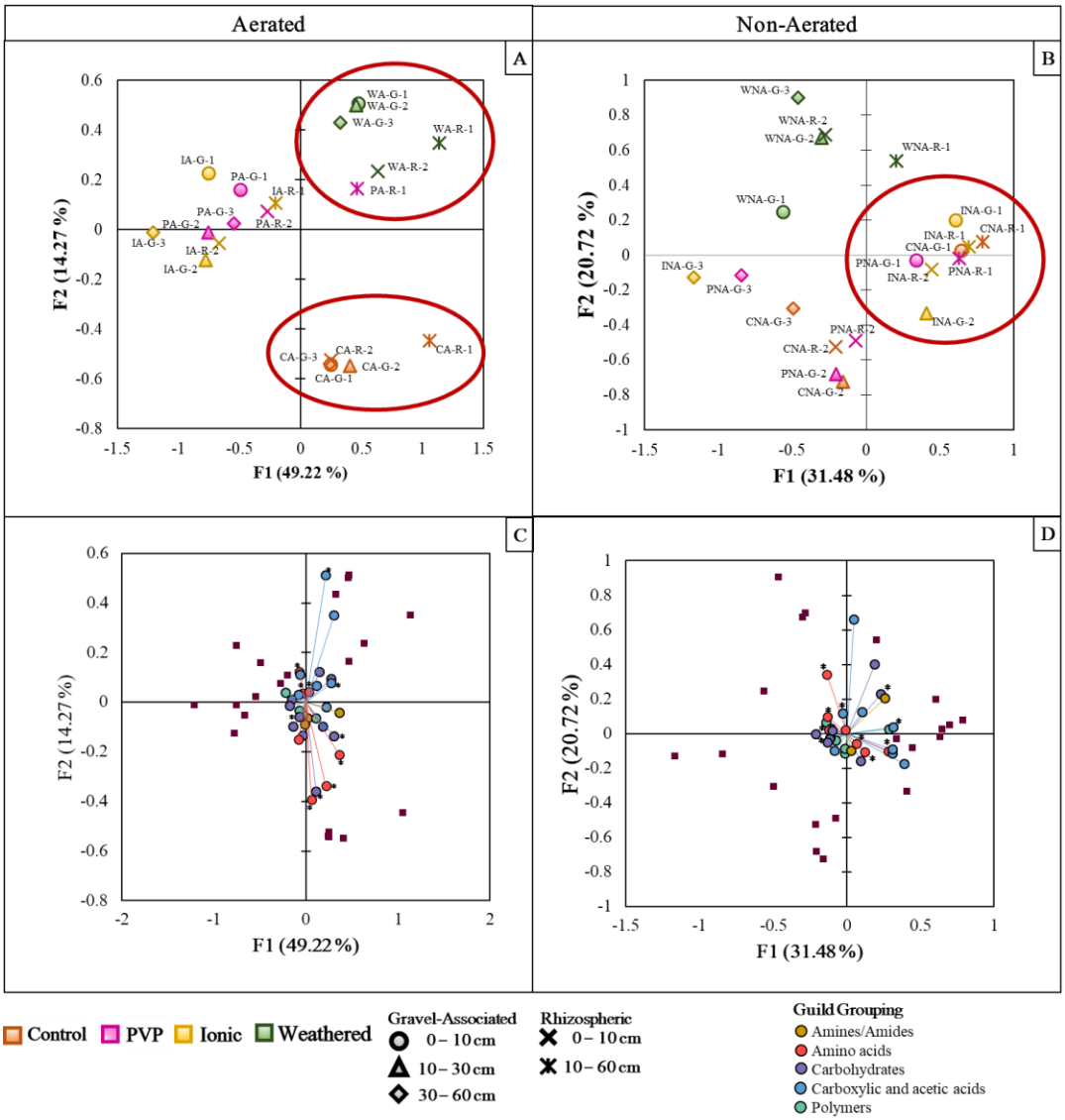

Figure 6.4: Principal component ordinations for Taylor transformed carbon source utilization patterns obtained from Biolog Ecoplates and associated biplots for aerated (A, C) and non-aerated (B,D) mesocosms; and associated biplots. C= control, P = PVP, I=ionic, W = weathered for the different silver treatments is combined with A=aerated or NA=non-aerated to denoted the specific system and G= gravel-associated biofilm or R=rhizospheric biofilm. The number following the treatment abbreviation denotes the respective sample the sample: 0 – 10 cm (1), 10 – 30 cm (2); 30 – 60 cm (3). Manual grouping based on observed visual differences were applied. For the biplots and * denote root exudate carbon sources.

6.4.3 Assessment of Microbial Community Structure

6.4.3.1 Structural Richness

To assess any structural changes in the microbial community from the uptake of Ag^+ and Ag-ENMs, 16S rRNA sequencing was performed on the detached rhizospheric and gravel-associated microbial communities. The alpha diversity metrics of species richness (measured as operational taxonomic units, OTUs) and Shannon diversity of the gravel-associated and rhizospheric microbial communities had no significant difference between silver amended systems and their respective controls for both the aerated and non-aerated mesocosms (ANOVA, $p>0.05$, Table D.2).

Though not statistically significant, the spatial trends in microbial richness for the aerated systems showed that the gravel-associated microbial communities of all silver treatments increased with depth towards the lower 30 – 60 cm region, opposite to the control (Figure S3C). From the mass balance on the silver amended mesocosm, the bottom 30 cm of the aerated systems also had the highest concentration of silver. One possible explanation from Yang & Alvarez (2015) who noted that sub-lethal concentration of silver caused an increase in the production of sugars and protein of the EPS biofilm matrix. This is typically attributed to a hormetic response and accompanies an upregulation in genes as a self-defence response (Sarkar, 2022).

In the case of the aerated rhizospheric biofilm, there was a noted increase in structural richness with depth for the microbial communities of the ionic, P-Ag-ENM and control mesocosms. (Figure S4C). Comparing the structural and the previously discussed functional richness metrics of the aerated rhizospheric biofilm shows opposing trends with depth. This suggests for these systems that as the microbial density increased with their corresponding functional ability declined. Conversely, for the W-Ag-ENM systems, the metabolic richness and structural richness remained relatively unchanged with depth for the rhizospheric bacteria.

6.4.3.2 Taxonomic Analysis

Taxonomic analysis revealed that the most abundant phyla identified through sequencing were *Proteobacteria*, *Actinobacteriota* (*Actinobacteria*), *Bacteroidota*, *Chloroflexi*, and *Planctomycetota*, cumulatively representing 76–91% and 73–86% across all aerated and non-aerated systems, respectively (Figure 6.5). The two largest phyla of *Actinobacteria* and *Proteobacteria,* which have been often associated with nitrogen and phosphorous cycling in TWs, showed no difference in relative abundance between treatments along the depth of the systems (Wang et al., 2022). Higher relative abundances of *Bacteroidota* were noted across all silver treatments in the aerated rhizospheric (7.2–13.3%) and gravel-associated (9.7-11.1%) biofilms compared to the controls (3.5-3.7%), at depths of both 10-30 cm and 30-60cm within the mesocosms. In addition, the aerated ionic exposure resulted in an average higher relative abundance of *Firmicutes* in rhizospheric biofilm, with 9.85% and 6.33% in the upper layer (0-10cm) and lower layers (10-60 cm) of the mesocosms, respectively, compared to 1.18% and 0.21% in the control. Notably, the non-aerated gravel-associated biofilm of the weathered, P-Ag-ENM and ionic silver treatments had higher average relative abundances of 5.0%, 4.1%, and 1.5%, respectively, of the archaeal phyla *Halobacteriota* in the lower layer (30-60 cm), compared to the control at 0.3% (Figure 6.5C). Specifically, this was linked to an increase in abundance of methanogens, *Methanosarcina*, and *Methanosaeta*, in the non-

aerated silver treatments (Mand and Metcalf, 2019; Smith and Ingram-Smith, 2007). Grosser et al. (2021) also noted an increase in the abundance of methanogens, specifically, *Methanosarcina,* stimulated by the addition of Ag-ENMs in anaerobic digesters.

Interestingly, there was a shift in "Other" phyla with depth, representing around 1-2% in the upper layer (0-10 cm), which increased to 4-5% of the bottom layer (30-60 cm) across all treatments in both the rhizospheric and gravel-associated biofilm. This suggests that the conditions at the bottom layer, across treatments, led to the development of more unique bacteria with depth.

A closer examination of the top 20 genera is shown in Figure D.5 and Figure D.6 for the aerated and non-aerated systems. While the non-aerated systems showed spatial variation in relative abundance of the top genera, no discernable differences from treatment were observed. Whereas, the differences of the microbial structure in the aerated systems were far more variable. Multivariate analysis of the beta diversity (abundance data) was performed to better visualize the microbial structural differences of rhizospheric and gravel-associated biofilm for the aerated and non-aerated systems across all treatments beyond the top 20 genera (Figure 6.6). In the case of the non-aerated systems, while there was a differentiation of both Ag-ENM microbial communities from the control along the F2 axis, the PCA plot along with the dendrogram based on Agglomerative Hierarchical Clustering (AHC) showed that the microbial communities were group by layer rather than treatment (Figure 6.6B and Figure D.**7**).

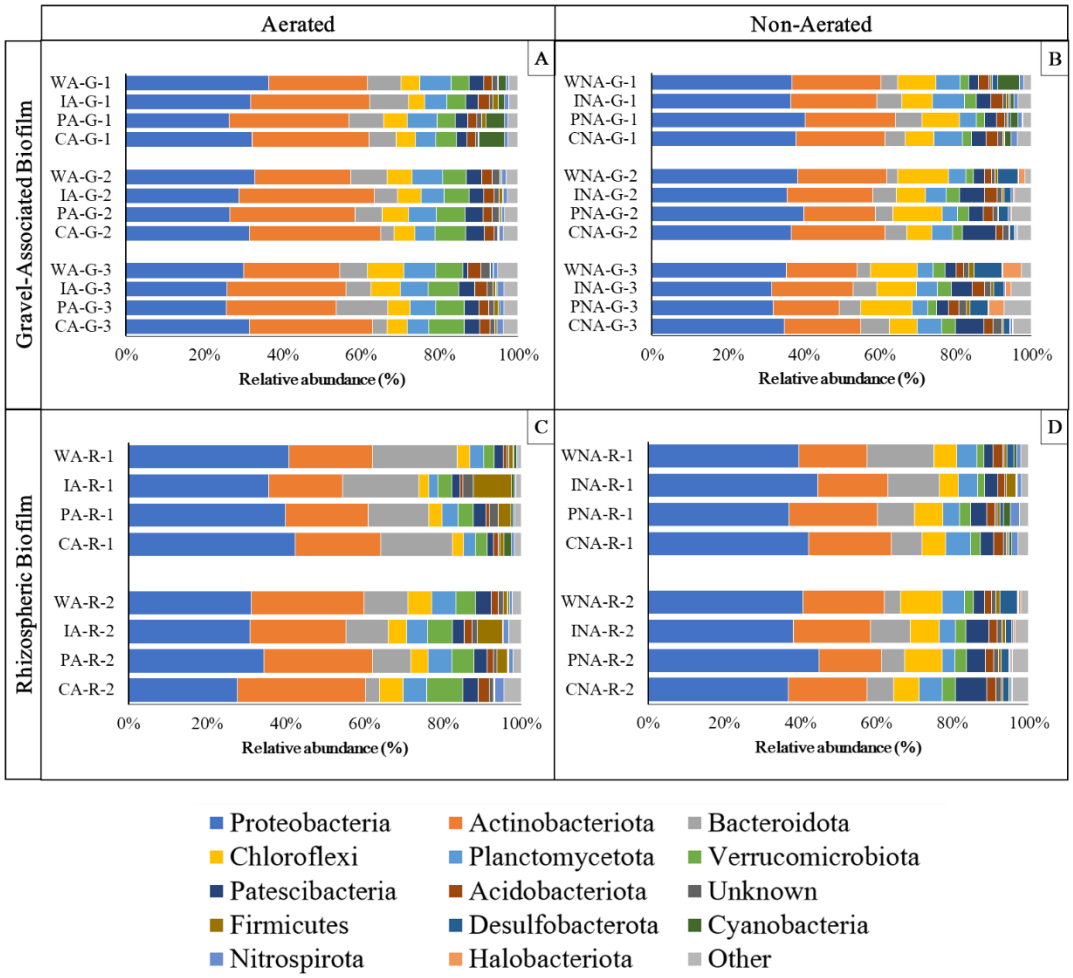

Figure 6.5: Average relative abundance of dominant phylum in aerated and non-aerated gravel-associated (A, B) and rhizospheric (C, D) biofilm. C= control, P = PVP, I=ionic, W = weathered for the different silver treatments is combined with A=aerated or NA=non-aerated to denoted the specific system and G= gravel-associated biofilm or R=rhizospheric biofilm to denote the specific system. The number following the treatment abbreviation denotes the respective sample the sample: 0-10 cm (1), 10-30 cm (2); 30-60 cm (3).

For the aerated systems, the differentiation along the first principal component (F1) was attributed to the spatial location in the TW mesocosm explaining 30.86% of the variance (Figure 6.6A). Similar to the CSUPs plots, the addition of W-Ag-ENMs cause a discernable shift in microbial structural composition grouping separately from the other treatments along F2 axis. The separation of the W-Ag-ENM microbial communities along the was primarily attributed to an increase in the genus *SM1A02* (novel anammox strain, Xie et al., 2021) bacteria of the phylum *Planctomycetota*, and a decrease in t*SBR1031* (hydrolytic acidifying bacteria, Quan et al., 2006) of the phylum *Chloroflexi* relative to the control. Due to the tight clustering of the remaining aerated systems, a second PCA plot was generated showing that

the ionic and P-Ag-ENMs treatments did cause a structural shift away from the controls (Figure 6.6C). The relative average abundances of both *Aeromonas* and *Bacillus* (denitrifying bacteria, Sarkar, 2022) were noted to be slightly higher in the top layer of the rhizospheric biofilm (0-10 cm) of the aerated ionic and P-Ag-ENM. Further differences were related several other smaller genera including *Bradyrhizobium* (nitrogen fixing bacteria, Beeckmans and Xie, 2015), and *Ellin6067* (anammox bacteria, Prosser et al., 2014), which had higher abundances in the lower layers of the control.

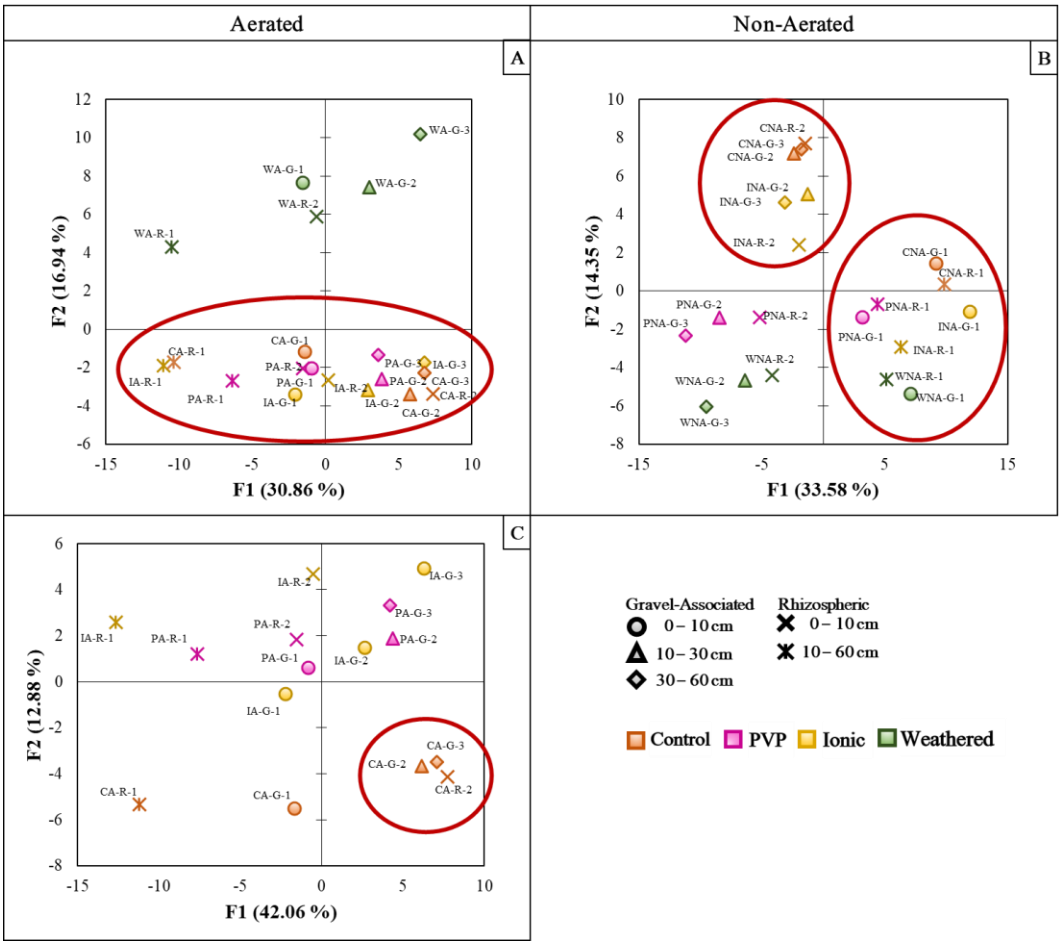

Figure 6.6: Principal component ordinations for averaged abundance data for genera for (A) aerated and (B) non-aerated systems; (C) A secondary PCA plot looking at the aerated genera data without the weathered treatment to visualize the differences. C= control, P = PVP, I=ionic, W = weathered for the different silver treatments is combined with A=aerated or NA=non-aerated to denoted the specific system and G= gravel-associated biofilm or R=rhizospheric biofilm to denote the specific system. The number following the treatment abbreviation denotes the respective sample the sample: 0-10 cm (1), 10-30 cm (2); 30-60 cm (3). Manual grouping based on observed visual differences were applied.

Overall, the addition of Ag+ and Ag-ENMs had a slightly stimulatory effect on the relative abundances of several genera including nitrogen cycling bacteria. Yang et al. (2013) noted that sublethal concentration of Ag-ENMs led to the upregulation in expression of nitrifying genes as a defense-response to the stress of Ag-ENMs. This has also been linked to niche-filling or functional redundancies in more diverse microbial communities exhibit a hormetic response under the stress of Ag-ENMs (Gray et al., 2022; Z. Zhang et al., 2018). While there was a shift in the microbial community structure and metabolic function in aerated systems; in our previous paper, which detailed the *in-situ* exposure (0.1 mg/L and 1 mg/L of Ag^{+} and Ag-ENMs), there were no detrimental changes in the overall treatment performance of the silver amended systems compared to the controls (Farooq et al., 2023b). This is line with Huang et al. (2019b) and Truu et al. (2022), who noted similar shifts in microbial structure, but no overall loss in treatment performance at concentrations of 0.2 mg/L and 0.1 mg/L Ag-ENMs, respectively. However, compared to Liu et al., (2023), applications of 1 mg/L of Ag-ENMs in batch-fed TWs resulted in immediate significant impairment of key enzymatic activities related to the carbon and nitrogen metabolisms in TW biofilms. In the current study, given that the systems were exposed through pulse loads of silver in two phases over a total period of 455 days, the biofilm resistance to the silver treatments may have increased over time (Alito and Gunsch, 2014).

6.5 Conclusions

In this study the effects and fate of weathered Ag-ENMs from commercial products on the rhizospheric and media-bound biofilm in TW were investigated. Overall, the aerated systems displayed a higher sensitivity to the presence of Ag-ENMs and silver ions compared to their non-aerated systems counterparts; while the weathered Ag-ENMs treatment led to both structural and functional differences in the microbial community compared to the control and to the other silver treatments. A significant difference in catabolic activity was observed in top layer of both the rhizospheric and gravel-associated biofilm. CSUPs patterns showed that the addition of silver reduced the ability to utilize root exudate (amino acids) for both rhizospheric and gravel-associated biofilms at all depths in the aerated systems; whereas in the non-aerated systems the metabolic functional patterns and microbial structure were found to be primarily influenced by depth. The shifts in microbial community structure and function, while interesting, do not represent a detrimental effect of silver on the TW mesocosms. Rather they are the result of the upregulation of specific genera as part of the observed system resilience and response to silver exposures.

6.6 Acknowledgements

The authors would like to thank Dr. Vincent Gagnon and Laura Ogilvie for their experimental design input; Chris Folkins, Sarah Denford, Blaire Coffey, and Patrick Garrett for their assistance with the dismantling of the mesocosm systems. Dr. Iris Kock for her assistance in running the samples This research used resources of the Advanced Photon Source, an Office of Science User Facility operated for the U.S. Department of Energy (DOE) Office of Science by Argonne National Laboratory and was supported by the U.S. DOE under Contract No. DE-

AC02-06CH11357, the Canadian Light Source and its funding partners (Sector 20 work), and DOE and MRCAT member institutions (Sector 10). We would like to thank Zou Finfrock and Debora Motta Meira, beamline scientists at Sector 20, for their support during the experiment, as well as Kirk Scheckel and Derek Peloquin for access to Sector 10, and for providing support with experiments at Sector 10

6.7 CReDiT Authorship Contribution Statement

Anbareen J. Farooq: Conceptualization, Methodology, Investigation, Validation, Formal analysis, Writing - original draft, Visualization.; ; **Dani Damasceno Silvera:** Formal analysis; **Sarah Wallace:** Formal analysis; **David J. Patch:** Formal analysis; **Denis O'Carroll:** Conceptualization, Resources, Supervision, Funding Acquisition; **Kela P. Weber**: Conceptualization, Resources, Writing – review & editing, Supervision, Funding Acquisition.

7. Principal Outcomes and Recommendations

The main objective of this thesis was to examine the fate and effects of incidental silver nanomaterials within planted treatment wetland mesocosms. To that end:

7.1.1 Objective A: Evaluate the current trends and relevancy of meso-scale treatment wetlands as a comparative system to the full-scale.

A comprehensive literature review was conducted using pairing of four key terms to gather relevant mesocosm scale TW research published until and including 2017. This literature search returned 3299 articles, which were then filtered against two sets of criteria: (1) the meso-scale of 10 – 1,000 L, and (2) the inclusion of at least 3 different water quality metrics in the article. This yielded a final total of 542 research papers from across 52 countries corresponding to 1486 unique designs between them. From these articles, information was extracted to analyze current trends within the treatment wetland field. In tandem, pollutant treatment data was also extracted to be compared to full-scale data.

Through the meta-analysis, a large increase in research output was noted over the period of 1992 –2017 as the mesocosm became more widely employed in the field due to its high flexibility in design. Additionally, the number of research topics were observed to diversify into increasingly niche areas, including investigation into microbial communities, which are the main driver of the TW wastewater potential; and emerging contaminants, such as nanomaterials. From the available data, a comparison of mesoscale and full-scale areal removal rate coefficients for BOD revealed that even though mesocosms are controlled systems, their overall performance, with respect to BOD, is comparable to full-scale TW systems with little difference between scales of operation.

7.1.2 Objective B: Characterize the morphological characteristics of treatment wetland biofilm to more accurately understand pollutant interactions.

Gravel-associated, rhizospheric, and detached biofilms were harvested from 3 different TW systems (two unplanted and one planted), to be imaged using conventional light microscopy, E-SEM, and Wet-SEM imaging techniques. Images revealed that biofilm morphology was heterogeneous in nature, differing from the fixed film structure model used in the TW field. Structures appeared as clustered aggregates, continuous films, and largely as 3D porous matrices with visible open channels. Additionally, larger organisms, such as amoebas and rotifers, were observed embedded within the biofilm structure. The pore size distribution, quantified in MATLAB and Image J, showed that pore diameters were predominately < 10 µm. Based on visual findings a new conceptual model was proposed to account for the microscale porous morphology of the biofilm matrix. It is postulated that the presence of the water channels will enhance the mass transport of dissolved oxygen and pollutants to the internal biofilm structure.

7.1.3 Objective C: Examine the in-situ impacts and removal of incidental silver nanomaterials in treatment wetland mesocosms.

Two separate in-situ exposures (0.1 mg/L and 1 mg/L) of weathered Ag-ENMs were conducted in both artificially aerated and non-aerated batch-fed subsurface flow wetland mesocosms alongside a pristine Ag-ENM and a positive ionic silver control exposure. Water quality and chemistry metrics showed no significant difference from the addition of any silver treatment. While the CSUPs and microbial structure of the interstitial microbial communities showed variation, the activity of the fixed biological regime (which included the microbes in the biofilm matrix) was not affected. Overall, there were no observable differences between the silver treatments and their respective controls demonstrating the robustness of the wetland systems.

7.1.4 Objective D: Assess the impacts and fate of incidental nanomaterials in treatment wetland biofilms.

Following the exposure study from Chapter 5, media-bound and rhizospheric biofilm samples were harvested spatially from each system to quantify the functional and structural changes in the microbial communities from the addition of the weathered Ag-ENMs. The mass balance revealed that the majority of silver recovered had been sequestered in the gravel-associated biofilm; in particular in the lower half of the mesocosms. A significant difference in catabolic activity was observed in top layer of both the rhizospheric and gravel-associated biofilm. CSUPs patterns showed that the addition of silver reduced the ability to utilize root exudate (amino acids) for both rhizospheric and gravel-associated biofilms at all depths in the aerated systems; whereas in the non-aerated systems the metabolic functional patterns were found to be primarily influenced by depth. Structural analysis of the microbial community showed some shifts likely due to niche filling and upregulation of specific genes as part of the resilient response to the silver exposures.

7.2 Scientific Contribution

The thesis presents the first ever exposure using realistic weathered Ag-ENMs in treatment wetlands systems. The particles themselves were artificially generated through a novel method to repeatably replicate human weathering of a textile. Moreover, the second exposure experiment required the development of a method to concentrate the artificially weathered Ag-ENMs while maintaining their size and shape distributions. This work was a comprehensive assessment of the silver kinetics, removal performance, water quality, and microbial health in both aerated and non-aerated systems. The subsequent fate study was also the first to quantify the fate and effects of realistic weathered Ag-ENMs in biofilm and also included a spatial resolution of the systems. This study also provided the first examination of the effects of Ag-ENMs on rhizospheric biofilm in TWs.

Moreover, this thesis contributed to the first comparison between mesocosm scale and full-scale treatment wetland systems. This was the first work to quantify the global state of mesoscale research through multiple metrics including focus area, types of analysis, and median size among others. Furthermore, the thesis contributes to the discussion of scalability

of research from mesocosm to full scale within the treatment wetland field through the comparison of global areal removal rate coefficients.

Finally, this thesis also contributes to the first known quantification of biofilm morphology in the treatment wetland field, as well as the first hydrated biofilm images obtained through Wet-SEM techniques. The analysis of the images led to the development of a new conceptual model, which ultimately will inform biokinetic modelling and will fundamentally change the way the treatment wetland field understands the transport of pollutants into and around the biofilm matrix.

7.3 Recommendations

This thesis used a multi-phasic approach to investigate the impacts and fate of incidentally released silver nanomaterials in treatment wetlands mesocosms, and provided a multi-level perspective on TWs. From the micro level of biofilm morphology, to the meso-level exposure studies, and finally to the global scale examining trends in the field at large.

Based on the knowledge gained in this thesis, recommendations for future work include:

1. Expand on the scalability discussion at the mesoscale comparing the removal rate coefficients of other key pollutants (including total nitrogen) to their full-scale counterparts.

2. Continue to quantify biofilm morphology from different treatment wetland designs under different operation regime to validate the conceptual model. Investigate the spatial distribution of microbial communities within the TW biofilm matrix using staining or fluorescent tagging to determine how the porous matrix affects their distribution. Investigating the flow regimes and pollutant transport mechanisms occurring within a range of biofilm pore sizes is also required

3. Investigate the addition of weathered Ag-ENMs during the start up phase of treatment wetland mesocosms

4. Examine the influence of different aeration modes on the toxicity of weathered Ag-ENMs to microbial communities

8. References

Abdelwahed, W., Degobert, G., Stainmesse, S., Fessi, H., 2006. Freeze-drying of nanoparticles: Formulation, process and storage considerations ☆. https://doi.org/10.1016/j.addr.2006.09.017

Ahn, C., Mitsch, W.J., 2002. Scaling considerations of mesocosm wetlands in simulating large created freshwater marshes. Ecol. Eng. 18, 327–342. https://doi.org/10.1016/S0925-8574(01)00092-1

Alhede, M., Qvortrup, K., Liebrechts, R., Høiby, N., Givskov, M., Bjarnsholt, T., 2012. Combination of microscopic techniques reveals a comprehensive visual impression of biofilm structure and composition. FEMS Immunol. Med. Microbiol. 65, 335–342. https://doi.org/10.1111/j.1574-695X.2012.00956.x

Alito, C.L., Gunsch, C.K., 2014. Assessing the effects of silver nanoparticles on biological nutrient removal in bench-scale activated sludge sequencing batch reactors. Environ. Sci. Technol. 48, 970–976. https://doi.org/10.1021/ES403640J/SUPPL_FILE/ES403640J_SI_001.PDF

Anees Ahmad, S., Sachi Das, S., Khatoon, A., Tahir Ansari, M., Afzal, M., Saquib Hasnain, M., Kumar Nayak, A., 2020. Bactericidal activity of silver nanoparticles: A mechanistic review. Mater. Sci. Energy Technol. 3, 756–769. https://doi.org/10.1016/J.MSET.2020.09.002

Asghari, S., Johari, S.A., Lee, J.H., Kim, Y.S., Jeon, Y.B., Choi, H.J., Moon, M.C., Yu, I.J., 2012. Toxicity of various silver nanoparticles compared to silver ions in Daphnia magna. J. Nanobiotechnology 10, 1–11. https://doi.org/10.1186/1477-3155-10-14/TABLES/3

Auclair, J., Gagné, F., 2022. Shape-Dependent Toxicity of Silver Nanoparticles on Freshwater Cnidarians. Nanomaterials 12, 12. https://doi.org/10.3390/NANO12183107/S1

Auffan, M., Rose, J., Wiesner, M.R., Bottero, J.Y., 2009. Chemical stability of metallic nanoparticles: A parameter controlling their potential cellular toxicity in vitro. Environ. Pollut. https://doi.org/10.1016/j.envpol.2008.10.002

Auvinen, H., Kaegi, R., Rousseau, D.P.L., Du Laing, G., 2017. Fate of Silver Nanoparticles in Constructed Wetlands—a Microcosm Study. Water. Air. Soil Pollut. 228. https://doi.org/10.1007/s11270-017-3285-9

Auvinen, H., Sepúlveda, V.V., Rousseau, D.P.L., Du Laing, G., 2016. Substrate- and plant-mediated removal of citrate-coated silver nanoparticles in constructed wetlands. Environ. Sci. Pollut. Res. 23, 21920–21926. https://doi.org/10.1007/s11356-016-7459-6

Aybar, M., Perez-Calleja, P., Li, M., Pavissich, J.P., Nerenberg, R., 2019. Predation creates

unique void layer in membrane-aerated biofilms. Water Res. 149, 232–242. https://doi.org/10.1016/j.watres.2018.10.084

Azodi, M., Sultan, Y., Ghoshal, S., 2016. Dissolution behavior of silver nanoparticles and formation of secondary silver nanoparticles in municipal wastewater by single-particle ICP-MS. Environ. Sci. Technol. 50. https://doi.org/10.1021/acs.est.6b03957

Badri, D. V., Vivanco, J.M., 2009. Regulation and function of root exudates. Plant. Cell Environ. 32, 666–681. https://doi.org/10.1111/J.1365-3040.2009.01926.X

Bakke, R., Olsson, P.Q., 1986. Biofilm thickness measurements by light microscopy. J. Microbiol. Methods 5, 93–98. https://doi.org/10.1016/0167-7012(86)90005-9

Bao, S., Liang, L., Huang, J., Liu, X., Tang, W., Yi, J., Fang, T., 2019. Removal and fate of silver nanoparticles in lab-scale vertical flow constructed wetland. Chemosphere 214. https://doi.org/10.1016/j.chemosphere.2018.09.110

Barhoum, A., García-Betancourt, M.L., Jeevanandam, J., Hussien, E.A., Mekkawy, S.A., Mostafa, M., Omran, M.M., Abdalla, M.S., Bechelany, M., 2022. Review on Natural, Incidental, Bioinspired, and Engineered Nanomaterials: History, Definitions, Classifications, Synthesis, Properties, Market, Toxicities, Risks, and Regulations. Nanomater. 2022, Vol. 12, Page 177 12, 177. https://doi.org/10.3390/NANO12020177

Bäuerlein, P.S., Emke, E., Tromp, P., Hofman, J.A.M.H., Carboni, A., Schooneman, F., de Voogt, P., van Wezel, A.P., 2017. Is there evidence for man-made nanoparticles in the Dutch environment? Sci. Total Environ. 576, 273–283. https://doi.org/10.1016/J.SCITOTENV.2016.09.206

Beeckmans, S., Xie, J.P., 2015. Glyoxylate Cycle. Ref. Modul. Biomed. Sci. https://doi.org/10.1016/B978-0-12-801238-3.02440-5

Benn, T., Cavanagh, B., Hristovski, K., Posner, J.D., Westerhoff, P., 2010. The release of nanosilver from consumer products used in the home. J. Environ. Qual. 39, 1875–1882. https://doi.org/10.2134/jeq2009.0363

Benn, T.M., Westerhoff, P., 2008. Nanoparticle silver released into water from commercially available sock fabrics. Environ. Sci. Technol. 42, 4133–4139. https://doi.org/10.1021/es7032718

Benton, T.G., Solan, M., Travis, J.M.J., Sait, S.M., 2007. Microcosm experiments can inform global ecological problems. Trends Ecol. Evol. 22, 516–521. https://doi.org/10.1016/J.TREE.2007.08.003

Bergmans, L., Moisiadis, P., Van Meerbeek, B., Quirynen, M., Lambrechts, P., 2005. Microscopic observation of bacteria: Review highlighting the use of environmental SEM. Int. Endod. J. 38, 775–788. https://doi.org/10.1111/j.1365-2591.2005.00999.x

Bezbaruah, A.N., Zhang, T.C., 2003. Performance of a constructed wetland with a

sulfur/limestone denitrification section for wastewater nitrogen removal. Environ. Sci. Technol. 37, 1690–1697. https://doi.org/10.1021/ES020912W/ASSET/IMAGES/LARGE/ES020912WF00006.JPEG

Blaser, S.A., Scheringer, M., MacLeod, M., Hungerbühler, K., 2008. Estimation of cumulative aquatic exposure and risk due to silver: Contribution of nano-functionalized plastics and textiles. Sci. Total Environ. 390, 396–409. https://doi.org/10.1016/j.scitotenv.2007.10.010

Bokulich, N.A., Kaehler, B.D., Rideout, J.R., Dillon, M., Bolyen, E., Knight, R., Huttley, G.A., Gregory Caporaso, J., 2018. Optimizing taxonomic classification of marker-gene amplicon sequences with QIIME 2's q2-feature-classifier plugin. Microbiome 6, 1–17. https://doi.org/10.1186/S40168-018-0470-Z/TABLES/3

Boltz, J.P., Smets, B.F., Rittmann, B.E., Van Loosdrecht, M.C.M., Morgenroth, E., Daigger, G.T., 2017. From biofilm ecology to reactors: A focused review. Water Sci. Technol. 75, 1753–1760. https://doi.org/10.2166/wst.2017.061

Boog, J., Nivala, J., Aubron, T., Wallace, S., van Afferden, M., Müller, R.A., 2014. Hydraulic characterization and optimization of total nitrogen removal in an aerated vertical subsurface flow treatment wetland. Bioresour. Technol. 162, 166–174. https://doi.org/10.1016/j.biortech.2014.03.100

Boudarel, H., Mathias, J.D., Blaysat, B., Grédiac, M., 2018. Towards standardized mechanical characterization of microbial biofilms: analysis and critical review. npj Biofilms Microbiomes 4. https://doi.org/10.1038/s41522-018-0062-5

Brix, H., 1994. Functions of Macrophytes in Constructed Wetlands. Water Sci. Technol. 29, 71–78. https://doi.org/10.2166/WST.1994.0160

Brix, H., 1993. Macrophyte-Mediated Oxygen Transfer in Wetlands: Transport Mechanisms and Rates, in: Constructed Wetlands for Water Quality Improvement. CRC Press, pp. 391–398. https://doi.org/10.1201/9781003069997-48

Buckman, J., Bankole, S.A., Zihms, S., Lewis, H., Couples, G., Corbett, P.W.M., 2017. Quantifying porosity through automated image collection and batch image processing: Case study of three carbonates and an aragonite cemented sandstone. Geosci. 7. https://doi.org/10.3390/geosciences7030070

Bundschuh, M., Filser, J., Lüderwald, S., McKee, M.S., Metreveli, G., Schaumann, G.E., Schulz, R., Wagner, S., 2018. Nanoparticles in the environment: where do we come from, where do we go to? Environ. Sci. Eur. https://doi.org/10.1186/s12302-018-0132-6

Busnardo, M.J., Gersberg, R.M., Langis, R., Sinicrope, T.L., Zedler, J.B., 1992. Nitrogen and phosphorus removal by wetland mesocosms subjected to different hydroperiods. Ecol. Eng. 1, 287–307. https://doi.org/10.1016/0925-8574(92)90012-Q

Butterworth, E., Richards, A., Jones, M., Brix, H., Dotro, G., Jefferson, B., 2016. Impact of aeration on macrophyte establishment in sub-surface constructed wetlands used for tertiary treatment of sewage. Ecol. Eng. 91, 65–73. https://doi.org/10.1016/J.ECOLENG.2016.01.017

Button, M., Auvinen, H., Van Koetsem, F., Hosseinkhani, B., Rousseau, D., Weber, K.P., Du Laing, G., 2016a. Susceptibility of constructed wetland microbial communities to silver nanoparticles: A microcosm study. Ecol. Eng. 97, 476–485. https://doi.org/10.1016/j.ecoleng.2016.10.033

Button, M., Nivala, J., Weber, K.P., Aubron, T., Müller, R.A., 2015. Microbial community metabolic function in subsurface flow constructed wetlands of different designs. Ecol. Eng. 80. https://doi.org/10.1016/j.ecoleng.2014.09.073

Button, M., Rodriguez, M., Brisson, J., Weber, K.P., 2016b. Use of two spatially separated plant species alters microbial community function in horizontal subsurface flow constructed wetlands. Ecol. Eng. 92, 18–27. https://doi.org/10.1016/j.ecoleng.2016.03.044

Calabrese, E.J., Baldwin, L.A., 2001. Hormesis: U-shaped dose responses and their centrality in toxicology. Trends Pharmacol. Sci. 22, 285–291. https://doi.org/10.1016/S0165-6147(00)01719-3

Callahan, B.J., McMurdie, P.J., Rosen, M.J., Han, A.W., Johnson, A.J.A., Holmes, S.P., 2016. DADA2: High-resolution sample inference from Illumina amplicon data. Nat. Methods 13, 581–583. https://doi.org/10.1038/nmeth.3869

Campbell, C.D., Grayston, S.J., Hirst, D.J., 1997. Use of rhizosphere carbon sources in sole carbon source tests to discriminate soil microbial communities. J. Microbiol. Methods 30, 33–41. https://doi.org/10.1016/S0167-7012(97)00041-9

Canette, A., Briandet, R., 2014. Microscopy: Confocal Laser Scanning Microscopy, in: Encyclopedia of Food Microbiology: Second Edition. Elsevier Inc., pp. 676–683. https://doi.org/10.1016/B978-0-12-384730-0.00214-7

Cao, C., Huang, J., Guo, Y., Yan, C., Xiao, J., Ma, Y.X., Liu, J., Guan, W., 2019. Long-term effects of environmentally relevant concentration of Ag nanoparticles on the pollutant removal and spatial distribution of silver in constructed wetlands with Cyperus alternifolius and Arundo donax. Environ. Pollut. 252. https://doi.org/10.1016/j.envpol.2019.05.144

Cao, C., Huang, J., Yan, C., Liu, J., Hu, Q., Guan, W., 2018. Shifts of system performance and microbial community structure in a constructed wetland after exposing silver nanoparticles. Chemosphere 199. https://doi.org/10.1016/j.chemosphere.2018.02.031

Cao, C., Huang, J., Yan, C., Ma, Y., Xiao, J., Zhang, X., 2021a. Comparative analysis of upward and downward vertical flow constructed wetlands on the nitrogen removal and functional microbes treating wastewater containing Ag nanoparticles. J. Environ.

Manage. 278. https://doi.org/10.1016/j.jenvman.2020.111573

Cao, C., Huang, J., Yan, C., Zhang, X., 2021b. Hydraulic flow direction alters impacts of AgNPs on pollutant removal and silver spatial distribution in vertical flow constructed wetlands. Environ. Sci. Pollut. Res. 28. https://doi.org/10.1007/s11356-021-15350-y

Cao, C., Huang, J., Yan, C., Zhang, X., Ma, Y., 2021c. Impacts of Ag and Ag2S nanoparticles on the nitrogen removal within vertical flow constructed wetlands treating secondary effluent. Sci. Total Environ. 777. https://doi.org/10.1016/j.scitotenv.2021.145171

Cao, C., Huang, J., Yan, C.N., 2022. Unveiling changes of microbial community involved in N and P removal in constructed wetlands with exposing to silver nanoparticles. J. Hazard. Mater. 432. https://doi.org/10.1016/j.jhazmat.2022.128642

Capodaglio, A.G., Callegari, A., Cecconet, D., Molognoni, D., 2017. Sustainability of decentralized wastewater treatment technologies. Water Pract. Technol. 12, 463–477. https://doi.org/10.2166/WPT.2017.055

Caporaso, J.G., Kuczynski, J., Stombaugh, J., Bittinger, K., Bushman, F.D., Costello, E.K., Fierer, N., Pẽa, A.G., Goodrich, J.K., Gordon, J.I., Huttley, G.A., Kelley, S.T., Knights, D., Koenig, J.E., Ley, R.E., Lozupone, C.A., McDonald, D., Muegge, B.D., Pirrung, M., Reeder, J., Sevinsky, J.R., Turnbaugh, P.J., Walters, W.A., Widmann, J., Yatsunenko, T., Zaneveld, J., Knight, R., 2010. QIIME allows analysis of high-throughput community sequencing data. Nat. Methods 2010 75 7, 335–336. https://doi.org/10.1038/nmeth.f.303

Chatterjee, S., Biswas, N., Datta, A., Dey, R., Maiti, P., 2014. Atomic force microscopy in biofilm study. Microscopy 63, 269–278. https://doi.org/10.1093/jmicro/dfu013

Chen, J., Liu, S.S., Wang, Y.J., Li, J., Liu, Y.S., Yang, F., Ying, G.G., 2021. Optimized constructed wetlands enhance the removal and reduce the risks of steroid hormones in domestic wastewater. Sci. Total Environ. 757. https://doi.org/10.1016/j.scitotenv.2020.143773

Chen, M., Mei, H., Qin, H., Yang, X., Guo, F., Chen, Y., 2023. Pyrite coupled with biochar alleviating the toxicity of silver nanoparticles on pollutants removal in constructed wetlands. Environ. Res. 219. https://doi.org/10.1016/j.envres.2022.115074

Chen, M.Y., Lee, D.J., Tay, J.H., Show, K.Y., 2007. Staining of extracellular polymeric substances and cells in bioaggregates. Appl. Microbiol. Biotechnol. 75, 467–474. https://doi.org/10.1007/s00253-006-0816-5

Choi, O., Deng, K.K., Kim, N.-J., Ross, L., Surampalli, R.Y., Hu, Z., Ross Louis, J., Surampalli, R.Y., Hu, Z., 2008. The inhibitory effects of silver nanoparticles, silver ions, and silver chloride colloids on microbial growth. Water Res. 42, 3066–3074. https://doi.org/10.1016/j.watres.2008.02.021

Choi, O., Hu, Z., 2008. Size dependent and reactive oxygen species related nanosilver toxicity to nitrifying bacteria. Environ. Sci. Technol. 42, 4583–4588. https://doi.org/10.1021/es703238h

Chouhan, N., Chouhan, N., 2018. Silver Nanoparticles: Synthesis, Characterization and Applications. Silver Nanoparticles - Fabr. Charact. Appl. https://doi.org/10.5772/INTECHOPEN.75611

Chyan, J.M., Senoro, D.B., Lin, C.J., Chen, P.J., Chen, I.M., 2013. A novel biofilm carrier for pollutant removal in a constructed wetland based on waste rubber tire chips. Int. Biodeterior. Biodegrad. 85, 638–645. https://doi.org/10.1016/j.ibiod.2013.04.010

Coats, E.R., Appel, F.J., Guho, N., Brinkman, C.K., Mellin, J., 2023. Interrogating the performance and microbial ecology of an enhanced biological phosphorus removal/post-anoxic denitrification process at bench and pilot scales. Water Environ. Res. 95, e10852. https://doi.org/10.1002/WER.10852

Collison, R.S., Grismer, M.E., 2013. Nitrogen and COD Removal from Domestic and Synthetic Wastewater in Subsurface-Flow Constructed Wetlands. Water Environ. Res. 85, 855–862. https://doi.org/10.2175/106143013x13736496909022

Colman, B.P., Espinasse, B., Richardson, C.J., Matson, C.W., Lowry, G. V., Hunt, D.E., Wiesner, M.R., Bernhardt, E.S., 2014. Emerging contaminant or an old toxin in disguise? Silver nanoparticle impacts on ecosystems. Environ. Sci. Technol. 48, 5229–5236. https://doi.org/10.1021/es405454v

Costerton, J.W., Lewandowski, Z., DeBeer, D., Caldwell, D., Korber, D., James, G., 1994. Biofilms, the customized microniche. J. Bacteriol. https://doi.org/10.1128/jb.176.8.2137-2142.1994

Danczak, R.E., Johnston, M.D., Kenah, C., Slattery, M., Wrighton, K.C., Wilkins, M.J., 2017. Members of the Candidate Phyla Radiation are functionally differentiated by carbon- and nitrogen-cycling capabilities. Microbiome 5, 112. https://doi.org/10.1186/S40168-017-0331-1/FIGURES/6

Davey, M.E., O'toole, G.A., 2000. Microbial Biofilms: from Ecology to Molecular Genetics. Microbiol. Mol. Biol. Rev. 64, 847–867. https://doi.org/10.1128/mmbr.64.4.847-867.2000

Davidovits, P., Egger, M.D., 1969. Scanning Laser Microscope. Nature 223, 831. https://doi.org/10.1038/223831a0

Davies, K.J., 2000. Oxidative stress, antioxidant defenses, and damage removal, repair, and replacement systems. IUBMB Life 50, 279–89. https://doi.org/10.1080/713803728

Decezaro, S.T., Wolff, D.B., Pelissari, C., Ramírez, R.J.M.G., Formentini, T.A., Goerck, J., Rodrigues, L.F., Sezerino, P.H., 2019. Influence of hydraulic loading rate and recirculation on oxygen transfer in a vertical flow constructed wetland. Sci. Total

Environ. 668, 988–995. https://doi.org/10.1016/J.SCITOTENV.2019.03.057

Desmau, M., Gélabert, A., Levard, C., Ona-Nguema, G., Vidal, V., Stubbs, J.E., Eng, P.J., Benedetti, M.F., 2018. Dynamics of silver nanoparticles at the solution/biofilm/mineral interface. Environ. Sci. Nano 5, 2394–2405. https://doi.org/10.1039/C8EN00331A

Donelli, G., 2014. Microbial Biofilms, Methods and Protocols Edited. Springer 1147. https://doi.org/10.1007/978-1-4939-0467-9

Dordio, A., Carvalho, A.J.P., 2013. Constructed wetlands with light expanded clay aggregates for agricultural wastewater treatment. Sci. Total Environ. 463–464, 454–461. https://doi.org/10.1016/j.scitotenv.2013.06.052

Dotro, G., Langergraber, G., Molle, P., Nivala, J., Puigagut, J., Stein, O., von Sperling, M., 2017. Treatment Wetlands, 7th ed. CSE: Centre for Science and Environment.

Dunnett, C.W., 1955. A Multiple Comparison Procedure for Comparing Several Treatments with a Control. J. Am. Stat. Assoc. 50, 1096–1121. https://doi.org/10.1080/01621459.1955.10501294

Dušek, J., Picek, T., Čížková, H., 2008. Redox potential dynamics in a horizontal subsurface flow constructed wetland for wastewater treatment: Diel, seasonal and spatial fluctuations. Ecol. Eng. 34, 223–232. https://doi.org/10.1016/J.ECOLENG.2008.08.008

Echavarri-Bravo, V., Paterson, L., Aspray, T.J., Porter, J.S., Winson, M.K., Thornton, B., Hartl, M.G.J., 2015. Shifts in the metabolic function of a benthic estuarine microbial community following a single pulse exposure to silver nanoparticles. Environ. Pollut. 201, 91–99. https://doi.org/10.1016/J.ENVPOL.2015.02.033

Edwards, K.R., Čižková, H., Zemanová, K., Šantrůčková, H., 2006. Plant growth and microbial processes in a constructed wetland planted with Phalaris arundinacea. Ecol. Eng. 27, 153–165. https://doi.org/10.1016/J.ECOLENG.2006.02.004

El Badawy, A.M., Scheckel, K.G., Suidan, M., Tolaymat, T., 2012. The impact of stabilization mechanism on the aggregation kinetics of silver nanoparticles. Sci. Total Environ. 429, 325–331. https://doi.org/10.1016/j.scitotenv.2012.03.041

El, S., Koraichi, S., Latrache, H., Hamadi, F., 2012. Scanning Electron Microscopy (SEM) and Environmental SEM: Suitable Tools for Study of Adhesion Stage and Biofilm Formation, in: Scanning Electron Microscopy. https://doi.org/10.5772/34990

Fabrega, J., Renshaw, J.C., Lead, J.R., 2009. Interactions of silver nanoparticles with Pseudomonas putida biofilms. Environ. Sci. Technol. 43, 9004–9009. https://doi.org/10.1021/es901706j

Fan, J., Zhang, B., Zhang, J., Ngo, H.H., Guo, W., Liu, F., Guo, Y., Wu, H., 2013.

Intermittent aeration strategy to enhance organics and nitrogen removal in subsurface flow constructed wetlands. Bioresour. Technol. 141, 117–122. https://doi.org/10.1016/J.BIORTECH.2013.03.077

Farooq, A.J., Chamberlain, M., Poonja, A., Mumford, K.G., Wallace, S., Weber, K.P., 2023a. Peaks, pores, and dragon eggs: Uncovering and quantifying the heterogeneity of treatment wetland biofilm matrices. Sci. Total Environ. 855, 158857. https://doi.org/10.1016/J.SCITOTENV.2022.158857

Farooq, A.J., Ogilvie, L., Silveira, D.D., Gagnon, V., Button, M., Wallace, S.J., Patch, D.J., Koch, I., O'Carroll, D.M., Weber, K.P., 2023b. Limited effects of incidental silver nanomaterials from commercial textiles on treatment wetland mesocosms. Prep.

Faulwetter, J.L., Gagnon, V., Sundberg, C., Chazarenc, F., Burr, M.D., Brisson, J., Camper, A.K., Stein, O.R., 2009. Microbial processes influencing performance of treatment wetlands: A review. Ecol. Eng. https://doi.org/10.1016/j.ecoleng.2008.12.030

Fernández, L.D., 2015. Source-sink dynamics shapes the spatial distribution of soil protists in an arid shrubland of northern Chile. J. Arid Environ. 113. https://doi.org/10.1016/j.jaridenv.2014.10.007

Flemming, H., Neu, T.R., Wozniak, D.J., Carolina, N., Decho, A., Kreft, J., Neu, T., Nielsen, P., Ro, U., Schooling, S., Szewzyk, U., Wolfaardt, G., 2016. The EPS Matrix : The " House of Biofilm Cells " 189, 7945–7947. https://doi.org/10.1128/JB.00858-07

Flemming, H.C., Baveye, P., Neu, T.R., Stoodley, P., Szewzyk, U., Wingender, J., Wuertz, S., 2021. Who put the film in biofilm? The migration of a term from wastewater engineering to medicine and beyond. npj Biofilms Microbiomes. https://doi.org/10.1038/s41522-020-00183-3

Flemming, H.C., Wingender, J., 2010. The biofilm matrix. Nat. Rev. Microbiol. https://doi.org/10.1038/nrmicro2415

Fonder, N., Headley, T., 2013. The taxonomy of treatment wetlands: A proposed classification and nomenclature system. Ecol. Eng. 51. https://doi.org/10.1016/j.ecoleng.2012.12.011

Gagnon, V., Button, M., Boparai, H.K., Nearing, M., O'Carroll, D.M., Weber, K.P., 2019. Influence of realistic wearing on the morphology and release of silver nanomaterials. Environ. Sci. Nano Nano 6, 411–424. https://doi.org/10.1039/C8EN00803E

Gagnon, V., Chazarenc, F., Comeau, Y., Brisson, J., 2007. Influence of macrophyte species on microbial density and activity in constructed wetlands. Water Sci. Technol. 56, 249–254. https://doi.org/10.2166/WST.2007.510

García, J., Ojeda, E., Sales, E., Chico, F., Píriz, T., Aguirre, P., Mujeriego, R., 2003. Spatial variations of temperature, redox potential, and contaminants in horizontal flow reed

beds. Ecol. Eng. 21, 129–142. https://doi.org/10.1016/J.ECOLENG.2003.10.001

Geisler, G., 1965. The Morphogenetic Effect of Oxygen on Roots. Plant Physiol. 40, 85. https://doi.org/10.1104/PP.40.1.85

Geranio, L., Heuberger, M., Nowack, B., 2009. The behavior of silver nanotextiles during washing. Environ. Sci. Technol. 43, 8113–8118. https://doi.org/10.1021/es9018332

Gorka, D.E., Osterberg, J.S., Gwin, C.A., Colman, B.P., Meyer, J.N., Bernhardt, E.S., Gunsch, C.K., DiGulio, R.T., Liu, J., 2015. Reducing Environmental Toxicity of Silver Nanoparticles through Shape Control. Environ. Sci. Technol. 49, 10093–10098. https://doi.org/10.1021/ACS.EST.5B01711/SUPPL_FILE/ES5B01711_SI_001.PDF

Gottschalk, F., Nowack, B., 2011. The release of engineered nanomaterials to the environment. J. Environ. Monit. 13, 1145–55. https://doi.org/10.1039/c0em00547a

Gottschalk, F., Sonderer, T., Scholz, R.W., Nowack, B., 2009. Modeled environmental concentrations of engineered nanomaterials (TiO2, ZnO, Ag, CNT, fullerenes) for different regions. Environ. Sci. Technol. 43, 9216–9222. https://doi.org/10.1021/es9015553

Gray, D.B., Gagnon, V., Button, M., Farooq, A.J., Patch, D.J., Wallace, S.J., Koch, I., O'Carroll, D.M., Weber, K.P., 2022. Silver nanomaterials released from commercial textiles have minimal impacts on soil microbial communities at environmentally relevant concentrations. Sci. Total Environ. 806, 151248. https://doi.org/10.1016/J.SCITOTENV.2021.151248

Grosser, A., Grobelak, A., Rorat, A., Courtois, P., Vandenbulcke, F., Lemière, S., Guyoneaud, R., Attard, E., Celary, P., 2021. Effects of silver nanoparticles on performance of anaerobic digestion of sewage sludge and associated microbial communities. Renew. Energy 171, 1014–1025. https://doi.org/10.1016/J.RENENE.2021.02.127

Hajipour, M.J., Fromm, K.M., Ashkarran, A.A., Jimenez De Aberasturi, D., Ruiz De Larramendi, I., Rojo, T., Serpooshan, V., Parak, W.J., Mahmoudi, M., 2012. Antibacterial properties of nanoparticles. Trends Biotechnol. https://doi.org/10.1016/j.tibtech.2012.06.004

Harcum, S.W., 2008. Purification of protein solutions, in: Biologically Inspired Textiles: A Volume in Woodhead Publishing Series in Textiles. Elsevier Inc., pp. 26–43. https://doi.org/10.1533/9781845695088.1.26

Helmlinger, J., Sengstock, C., Groß-Heitfeld, C., Mayer, C., Schildhauer, T.A., Köller, M., Epple, M., 2016. Silver nanoparticles with different size and shape: equal cytotoxicity, but different antibacterial effects. RSC Adv. 6, 18490–18501. https://doi.org/10.1039/C5RA27836H

Hendren, C.O., Mesnard, X., Dröge, J., Wiesner, M.R., 2011. Estimating production data for

five engineered nanomaterials as a basis for exposure assessment. Environ. Sci. Technol. 45, 2562–2569. https://doi.org/10.1021/es103300g

Hijosa-Valsero, M., Reyes-Contreras, C., Domínguez, C., Bécares, E., Bayona, J.M., 2016. Behaviour of pharmaceuticals and personal care products in constructed wetland compartments: Influent, effluent, pore water, substrate and plant roots. Chemosphere 145, 508–517. https://doi.org/10.1016/j.chemosphere.2015.11.090

Horikoshi, S., Serpone, N., 2013. Introduction to Nanoparticles, in: Microwaves in Nanoparticle Synthesis: Fundamentals and Applications. pp. 1–24. https://doi.org/10.1002/9783527648122.ch1

Hou, J., Wang, C., Rozenbaum, R.T., Gusnaniar, N., de Jong, E.D., Woudstra, W., Geertsema-Doornbusch, G.I., Atema-Smit, J., Sjollema, J., Ren, Y., Busscher, H.J., van der Mei, H.C., 2019. Bacterial Density and Biofilm Structure Determined by Optical Coherence Tomography. Sci. Rep. 9, 1–12. https://doi.org/10.1038/s41598-019-46196-7

Hu, B., Hu, S., Chen, Z., Vymazal, J., 2021. Employ of arbuscular mycorrhizal fungi for pharmaceuticals ibuprofen and diclofenac removal in mesocosm-scale constructed wetlands. J. Hazard. Mater. 409, 124524. https://doi.org/10.1016/J.JHAZMAT.2020.124524

Huang, H., Peng, C., Peng, P., Lin, Y., Zhang, X., Ren, H., 2019. Towards the biofilm characterization and regulation in biological wastewater treatment 1115–1129.

Huang, J., Cao, C., Liu, J., Yan, C., Xiao, J., 2019a. The response of nitrogen removal and related bacteria within constructed wetlands after long-term treating wastewater containing environmental concentrations of silver nanoparticles. Sci. Total Environ. 667. https://doi.org/10.1016/j.scitotenv.2019.02.396

Huang, J., Cao, C., Yan, C., Guan, W., Liu, J., 2018a. Comparison of Iris pseudacorus wetland systems with unplanted systems on pollutant removal and microbial community under nanosilver exposure. Sci. Total Environ. 624. https://doi.org/10.1016/j.scitotenv.2017.12.222

Huang, J., Cao, C., Yan, C., Liu, J., Hu, Q., Guan, W., 2017. Impacts of silver nanoparticles on the nutrient removal and functional bacterial community in vertical subsurface flow constructed wetlands. Bioresour. Technol. 243. https://doi.org/10.1016/j.biortech.2017.07.178

Huang, J., Cao, M., Ma, Y., Liu, J., Guan, W., 2022. Wastewater treatment performance and microbial community structure in the constructed wetland under double-pressureof low temperature and Ag NPs exposure. J. Southeast Univ. (English Ed. 38, 291–299. https://doi.org/10.3969/j.issn.1003-7985.2022.03.011

Huang, J., Xiao, J., Chen, M., Cao, C., Yan, C., Ma, Y., Huang, M., Wang, M., 2019b. Fate of silver nanoparticles in constructed wetlands and its influence on performance and

microbiome in the ecosystems after a 450-day exposure. Bioresour. Technol. 281. https://doi.org/10.1016/j.biortech.2019.02.013

Huang, J., Xiao, J., Guo, Y., Guan, W., Cao, C., Yan, C., Wang, M., 2020. Long-term effects of silver nanoparticles on performance of phosphorus removal in a laboratory-scale vertical flow constructed wetland. J. Environ. Sci. (China) 87. https://doi.org/10.1016/j.jes.2019.07.012

Huang, J., Yan, C., Cao, C., Peng, C., Liu, J., Guan, W., 2018b. Performance evaluation of Iris pseudacorus constructed wetland for advanced wastewater treatment under long-term exposure to nanosilver. Ecol. Eng. 116. https://doi.org/10.1016/j.ecoleng.2018.03.003

Huang, J., Yan, C., Liu, J., Guan, W., Singh, R.P., Cao, C., Xiao, J., 2019c. Feasibility study of vertical flow constructed wetland for tertiary treatment of nanosilver wastewater and temporal-spatial distribution of pollutants and microbial community. J. Environ. Manage. 245. https://doi.org/10.1016/j.jenvman.2019.04.128

Huang, Q., Wu, H., Cai, P., Fein, J.B., Chen, W., 2015. Atomic force microscopy measurements of bacterial adhesion and biofilm formation onto clay-sized particles. Sci. Reports 2015 51 5, 1–12. https://doi.org/10.1038/srep16857

Iasur-Kruh, L., Hadar, Y., Milstein, D., Gasith, A., Minz, D., 2010. Microbial population and activity in wetland microcosms constructed for improving treated municipal wastewater. Microb. Ecol. 59, 700–709. https://doi.org/10.1007/s00248-009-9611-z

Ilyas, H., Masih, I., 2017. The performance of the intensified constructed wetlands for organic matter and nitrogen removal: A review. J. Environ. Manage. 198, 372–383. https://doi.org/10.1016/J.JENVMAN.2017.04.098

Inshakova, E., Inshakov, O., 2017. World market for nanomaterials: Structure and trends, in: MATEC Web of Conferences. https://doi.org/10.1051/matecconf/201712902013

Islam, M.A., Jacob, M. V., Antunes, E., 2021. A critical review on silver nanoparticles: From synthesis and applications to its mitigation through low-cost adsorption by biochar. J. Environ. Manage. 281, 111918. https://doi.org/10.1016/J.JENVMAN.2020.111918

Ito, T., Sugita, K., Yumoto, I., Nodasaka, Y., Okabe, S., 2005. Thiovirga sulfuroxydans gen. nov., sp. nov., a chemolithoautotrophic sulfur-oxidizing bacterium isolated from a microaerobic waste-water biofilm. Int. J. Syst. Evol. Microbiol. 55, 1059–1064. https://doi.org/10.1099/IJS.0.63467-0

Janković, N.Z., Plata, D.L., 2019. Engineered nanomaterials in the context of global element cycles. Environ. Sci. Nano 6, 2697–2711. https://doi.org/10.1039/C9EN00322C

Ji, Z., Tang, W., Pei, Y., 2022. Constructed wetland substrates: A review on development, function mechanisms, and application in contaminants removal. Chemosphere 286,

131564. https://doi.org/10.1016/J.CHEMOSPHERE.2021.131564

Jiang, H.-S.S., Qiu, X.-N.N., Li, G.-B.B., Li, W., Yin, L.-Y.Y., 2014. Silver nanoparticles induced accumulation of reactive oxygen species and alteration of antioxidant systems in the aquatic plant Spirodela polyrhiza. Environ. Toxicol. Chem. 33, 1398–1405. https://doi.org/10.1002/etc.2577

Jiang, H.S., Yin, L., Ren, N.N., Xian, L., Zhao, S., Li, W., Gontero, B., 2017. The effect of chronic silver nanoparticles on aquatic system in microcosms. Environ. Pollut. 223, 395–402. https://doi.org/10.1016/J.ENVPOL.2017.01.036

Jizheng, P., Houhu, Z., Xuejun, L., Yong, L., Min, Z., Hongling, X., 2019. Enhanced nitrogen removal by the integrated constructed wetlands with artificial aeration. Environ. Technol. Innov. 14, 100362. https://doi.org/10.1016/J.ETI.2019.100362

Kadlec, R.H., Wallace, S.D., 2009. Treatment Wetlands, Second. ed, Treatment Wetlands, Second Edition. CRC Press.

Kaegi, R., Sinnet, B., Zuleeg, S., Hagendorfer, H., Mueller, E., Vonbank, R., Boller, M., Burkhardt, M., 2010. Release of silver nanoparticles from outdoor facades. Environ. Pollut. 158, 2900–2905. https://doi.org/10.1016/j.envpol.2010.06.009

Kaegi, R., Voegelin, A., Ort, C., Sinnet, B., Thalmann, B., Krismer, J., Hagendorfer, H., Elumelu, M., Mueller, E., 2013. Fate and transformation of silver nanoparticles in urban wastewater systems. Water Res. 47, 3866–3877. https://doi.org/10.1016/j.watres.2012.11.060

Kaegi, R., Voegelin, A., Sinnet, B., Zuleeg, S., Hagendorfer, H., Burkhardt, M., Siegrist, H., 2011. Behavior of metallic silver nanoparticles in a pilot wastewater treatment plant. Environ. Sci. Technol. 45, 3902–3908. https://doi.org/10.1021/es1041892

Karcz, J., Bernas, T., Nowak, A., Talik, E., Woznica, A., 2012. Application of lyophilization to prepare the nitrifying bacterial biofilm for imaging with scanning electron microscopy. Scanning 34, 26–36. https://doi.org/10.1002/sca.20275

Karygianni, L., Ren, Z., Koo, H., Thurnheer, T., 2020. Biofilm Matrixome: Extracellular Components in Structured Microbial Communities. Trends Microbiol. 28, 668–681. https://doi.org/10.1016/J.TIM.2020.03.016

Keller, A.A., Lazareva, A., 2013. Predicted Releases of Engineered Nanomaterials: From Global to Regional to Local. Environ. Sci. Technol. Lett. 1, 65–70. https://doi.org/10.1021/ez400106t

Keller, A.A., McFerran, S., Lazareva, A., Suh, S., 2013. Global life cycle releases of engineered nanomaterials. J. Nanoparticle Res. 15. https://doi.org/10.1007/s11051-013-1692-4

Kennedy, G., Mayer, T., 2002. Natural and Constructed Wetlands in Canada: An Overview.

Water Qual. Res. J. 37, 295–325. https://doi.org/10.2166/WQRJ.2002.020

Kim, B., Gwak, G., Hong, S., 2017. Review on methodology for determining forward osmosis (FO) membrane characteristics: Water permeability (A), solute permeability (B), and structural parameter (S). Desalination. https://doi.org/10.1016/j.desal.2017.08.006

Kim, J.S., Kuk, E., Yu, K.N., Kim, J.H., Park, S.J., Lee, H.J., Kim, S.H., Park, Y.K., Park, Y.H., Hwang, C.Y., Kim, Y.K., Lee, Y.S., Jeong, D.H., Cho, M.H., 2007. Antimicrobial effects of silver nanoparticles. Nanomedicine Nanotechnology, Biol. Med. 3, 95–101. https://doi.org/10.1016/j.nano.2006.12.001

Kim, J.W., Choi, H., Pachepsky, Y.A., 2010. Biofilm morphology as related to the porous media clogging. Water Res. 44, 1193–1201. https://doi.org/10.1016/j.watres.2009.05.049

Kirby, C.S., Dennis, A., Kahler, A., 2009. Aeration to degas CO2, increase pH, and increase iron oxidation rates for efficient treatment of net alkaline mine drainage. Appl. Geochemistry 24, 1175–1184. https://doi.org/10.1016/J.APGEOCHEM.2009.02.028

Klaine, S.J., Alvarez, P.J.J., Batley, G.E., Fernandes, T.F., Handy, R.D., Lyon, D.Y., Mahendra, S., McLaughlin, M.J., Lead, J.R., 2008. Nanomaterials in the environment: Behavior, fate, bioavailability, and effects. Environ. Toxicol. Chem. 27, 1825–1851. https://doi.org/10.1897/08-090.1

Krsmanovic, M., Biswas, D., Ali, H., Kumar, A., Ghosh, R., Dickerson, A.K., 2021. Hydrodynamics and surface properties influence biofilm proliferation. Adv. Colloid Interface Sci. 288, 102336. https://doi.org/10.1016/J.CIS.2020.102336

Kulshreshtha, N.M., Verma, V., Soti, A., Brighu, U., Gupta, A.B., 2022. Exploring the contribution of plant species in the performance of constructed wetlands for domestic wastewater treatment. Bioresour. Technol. Reports 18, 101038. https://doi.org/10.1016/J.BITEB.2022.101038

Kulthong, K., Srisung, S., Boonpavanitchakul, K., Kangwansupamonkon, W., Maniratanachote, R., 2010. Determination of silver nanoparticle release from antibacterial fabrics into artificial sweat. Part. Fibre Toxicol. 7. https://doi.org/10.1186/1743-8977-7-8

Kvítek, L., Panáček, A., Soukupová, J., Kolář, M., Večeřová, R., Prucek, R., Holecová, M., Zbořil, R., 2008. Effect of surfactants and polymers on stability and antibacterial activity of silver nanoparticles (NPs). J. Phys. Chem. C 112, 5825–5834. https://doi.org/10.1021/jp711616v

Laborda, F., Bolea, E., Jiménez-Lamana, J., 2014. Single particle inductively coupled plasma mass spectrometry: A powerful tool for nanoanalysis. Anal. Chem. 86, 2270–2278. https://doi.org/10.1021/ac402980q

Lazim, Z.M., Salmiati, S., Marpongahtun, M., Arman, Z., Ridza, M., Haniffah, M., Azman, S., Yong, L., Salim, M.R., 2023. Distribution of Silver (Ag) and Silver Nanoparticles (AgNPs) in Aquatic Environment. https://doi.org/10.3390/w15071349

Levard, C., Hotze, E.M., Lowry, G. V., Brown, G.E., 2012. Environmental transformations of silver nanoparticles: Impact on stability and toxicity. Environ. Sci. Technol. https://doi.org/10.1021/es2037405

Li, L., Hartmann, G., Döblinger, M., Schuster, M., 2013. Quantification of nanoscale silver particles removal and release from municipal wastewater treatment plants in Germany. Environ. Sci. Technol. 47, 7317–7323. https://doi.org/10.1021/es3041658

Li, L., Stoiber, M., Wimmer, A., Xu, Z., Lindenblatt, C., Helmreich, B., Schuster, M., 2016. To What Extent Can Full-Scale Wastewater Treatment Plant Effluent Influence the Occurrence of Silver-Based Nanoparticles in Surface Waters? Environ. Sci. Technol. 50, 6327–6333. https://doi.org/10.1021/ACS.EST.6B00694/SUPPL_FILE/ES6B00694_SI_001.PDF

Li, X., He, F., Wang, Z., Xing, B., 2022. Roadmap of environmental health research on emerging contaminants: Inspiration from the studies on engineered nanomaterials. Eco-Environment Heal. 1, 181–197. https://doi.org/10.1016/J.EEHL.2022.10.001

Liao, C., Li, Y., Tjong, S.C., 2019. Bactericidal and cytotoxic properties of silver nanoparticles. Int. J. Mol. Sci. https://doi.org/10.3390/ijms20020449

Lin, P.-C., Lin, S., Wang, P.C., Sridhar, R., 2013. Techniques for physicochemical characterization of nanomaterials. https://doi.org/10.1016/j.biotechadv.2013.11.006

Little, B., Wagner, P., Ray, R., Pope, R., Scheetz, R., 1991. Biofilms: An ESEM evaluation of artifacts introduced during SEM preparation. J. Ind. Microbiol. 8, 213–221. https://doi.org/10.1007/BF01576058

Liu, J., Hurt, R.H., 2010. Ion release kinetics and particle persistence in aqueous nano-silver colloids. Environ. Sci. Technol. 44, 2169–2175.

Liu, T., Guo, F., Chen, M., Zhao, S., Yang, X., He, Q., 2023. Silver nanoparticles disturb treatment performance in constructed wetlands: Responses of biofilm and hydrophyte. J. Clean. Prod. 385. https://doi.org/10.1016/j.jclepro.2022.135751

Liu, T., Lu, S., Wang, R., Xu, S., Qin, P., Gao, Y., 2020. Behavior of selected organophosphate flame retardants (OPFRs) and their influence on rhizospheric microorganisms after short-term exposure in integrated vertical-flow constructed wetlands (IVCWs). Sci. Total Environ. 710, 136403. https://doi.org/10.1016/J.SCITOTENV.2019.136403

Liu, X., Yang, X., Hu, X., He, Q., Zhai, J., Chen, Y., Xiong, Q., Vymazal, J., 2019. Comprehensive metagenomic analysis reveals the effects of silver nanoparticles on nitrogen transformation in constructed wetlands. Chem. Eng. J. 358.

https://doi.org/10.1016/j.cej.2018.10.151

Lorenz, C., Windler, L., von Goetz, N., Lehmann, R.P., Schuppler, M., Hungerbühler, K., Heuberger, M., Nowack, B., 2012. Characterization of silver release from commercially available functional (nano)textiles. Chemosphere 89, 817–824. https://doi.org/10.1016/j.chemosphere.2012.04.063

Lowry, G. V., Espinasse, B.P., Badireddy, A.R., Richardson, C.J., Reinsch, B.C., Bryant, L.D., Bone, A.J., Deonarine, A., Chae, S., Therezien, M., Colman, B.P., Hsu-Kim, H., Bernhardt, E.S., Matson, C.W., Wiesner, M.R., 2012. Long-term transformation and fate of manufactured Ag nanoparticles in a simulated large scale freshwater emergent wetland. Environ. Sci. Technol. 46, 7027–7036. https://doi.org/10.1021/es204608d

Lv, T., Carvalho, P.N., Zhang, L., Zhang, Y., Button, M., Arias, C.A., Weber, K.P., Brix, H., 2017. Functionality of microbial communities in constructed wetlands used for pesticide remediation: Influence of system design and sampling strategy. Water Res. 110, 241–251. https://doi.org/10.1016/j.watres.2016.12.021

Lydmark, P., Lind, M., Sörensson, F., Hermansson, M., 2006. Vertical distribution of nitrifying populations in bacterial biofilms from a full-scale nitrifying trickling filter. Environ. Microbiol. 8, 2036–2049. https://doi.org/10.1111/J.1462-2920.2006.01085.X

Ma, R., Levard, C., Judy, J.D., Unrine, J.M., Durenkamp, M., Martin, B., Jefferson, B., Lowry, G. V., 2014. Fate of Zinc Oxide and Silver Nanoparticles in a Pilot Wastewater Treatment Plant and in Processed Biosolids. Environ. Sci. Technol. 48, 104–112. https://doi.org/10.1021/es403646x

Malyan, S.K., Yadav, S., Sonkar, V., Goyal, | V C, Singh, O., Singh, R., Member, W., 2021. Mechanistic understanding of the pollutant removal and transformation processes in the constructed wetland system. https://doi.org/10.1002/wer.1599

Mand, T.D., Metcalf, W.W., 2019. Energy Conservation and Hydrogenase Function in Methanogenic Archaea, in Particular the Genus Methanosarcina . Microbiol. Mol. Biol. Rev. 83. https://doi.org/10.1128/MMBR.00020-19/FORMAT/EPUB

Markus, A.A., Parsons, J.R., Roex, E.W.M., de Voogt, P., Laane, R.W.P.M., 2015. Modeling aggregation and sedimentation of nanoparticles in the aquatic environment. Sci. Total Environ. 506–507, 323–329. https://doi.org/10.1016/j.scitotenv.2014.11.056

Martin, C., Pignon, F., Magnin, A., Meireles, M., Lelièvre, V., Lindner, P., Cabane, B., 2006. Osmotic compression and expansion of highly ordered clay dispersions. Langmuir 22, 4065–4075. https://doi.org/10.1021/la052605k

Martínez-Toledo, Á., González-Mille, D.J., García-Arreola, M.E., Cruz-Santiago, O., Trejo-Acevedo, A., Ilizaliturri-Hernández, C.A., 2021. Patterns in utilization of carbon sources in soil microbial communities contaminated with mine solid wastes from San Luis Potosi, Mexico. Ecotoxicol. Environ. Saf. 208, 111493. https://doi.org/10.1016/J.ECOENV.2020.111493

Massarsky, A., Trudeau, V.L., Moon, T.W., 2014. Predicting the environmental impact of nanosilver. Environ. Toxicol. Pharmacol. https://doi.org/10.1016/j.etap.2014.10.006

Matović, B., Bošković, S., 2007. Terminology for nanomaterials and nanotechnology. Metalurgija 13, 155–157.

McGillicuddy, E., Murray, I., Kavanagh, S., Morrison, L., Fogarty, A., Cormican, M., Dockery, P., Prendergast, M., Rowan, N., Morris, D., 2017. Silver nanoparticles in the environment: Sources, detection andecotoxicology. Sci. Total Environ. 575, 231–246. https://doi.org/10.1016/j.scitotenv.2016.10.041

Meena, K.K., Bitla, U.M., Sorty, A.M., Singh, D.P., Gupta, V.K., Wakchaure, G.C., Kumar, S., 2020. Mitigation of Salinity Stress in Wheat Seedlings Due to the Application of Phytohormone-Rich Culture Filtrate Extract of Methylotrophic Actinobacterium Nocardioides sp. NIMMe6. Front. Microbiol. 11, 501325. https://doi.org/10.3389/FMICB.2020.02091/BIBTEX

Meyer, D.E., Curran, M.A., Gonzalez, M.A., 2011. An examination of silver nanoparticles in socks using screening-level life cycle assessment. J. Nanoparticle Res. 13, 147–156. https://doi.org/10.1007/s11051-010-0013-4

Mitchell, E.A.D., Charman, D.J., Warner, B.G., 2008. Testate amoebae analysis in ecological and paleoecological studies of wetlands: Past, present and future, in: Biodiversity and Conservation. https://doi.org/10.1007/s10531-007-9221-3

Mitrano, D.M., Nowack, B., 2017. The need for a life-cycle based aging paradigm for nanomaterials: Importance of real-world test systems to identify realistic particle transformations. Nanotechnology. https://doi.org/10.1088/1361-6528/28/7/072001

Mitrano, D.M., Rimmele, E., Wichser, A., Erni, R., Height, M., Nowack, B., 2014. Presence of nanoparticles in wash water from conventional silver and nano-silver textiles. ACS Nano 8, 7208–7219. https://doi.org/10.1021/nn502228w

Mitsch, W.J., Gosselink, J.G., 2015. Wetlands, Fifth. ed.

Morones, J.R., Elechiguerra, J.L., Camacho, A., Holt, K., Kouri, J.B., Ramírez, J.T., Yacaman, M.J., 2005. The bactericidal effect of silver nanoparticles. Nanotechnology 16, 2346–2353. https://doi.org/10.1088/0957-4484/16/10/059

Morvannou, A., Forquet, N., Michel, S., Troesch, S., Molle, P., 2015. Treatment performances of French constructed wetlands: results from a database collected over the last 30 years. Water Sci. Technol. 71, 1333–1339. https://doi.org/10.2166/WST.2015.089

Mozhayeva, D., Engelhard, C., 2020. A critical review of single particle inductively coupled plasma mass spectrometry-A step towards an ideal method for nanomaterial characterization. J. Anal. At. Spectrom. https://doi.org/10.1039/c9ja00206e

Murphy, C., Rajabzadeh, A.R., Weber, K.P., Nivala, J., Wallace, S.D., Cooper, D.J., 2016. Nitrification cessation and recovery in an aerated saturated vertical subsurface flow treatment wetland: Field studies and microscale biofilm modeling. Bioresour. Technol. 209, 125–132. https://doi.org/10.1016/j.biortech.2016.02.065

Navarro, E., Baun, A., Behra, R., Hartmann, N.B., Filser, J., Miao, A.J., Quigg, A., Santschi, P.H., Sigg, L., 2008a. Environmental behavior and ecotoxicity of engineered nanoparticles to algae, plants, and fungi. Ecotoxicol. 2008 175 17, 372–386. https://doi.org/10.1007/S10646-008-0214-0

Navarro, E., Piccapietra, F., Wagner, B., Marconi, F., Kaegi, R., Odzak, N., Sigg, L., Behra, R., 2008b. Toxicity of silver nanoparticles to Chlamydomonas reinhardtii. Environ. Sci. Technol. 42, 8959–64. https://doi.org/10.1021/es801785m

Neu, T., Lawrence, J., 2015. Innovative techniques, sensors, and approaches for imaging biofilms at different scales. Trends Microbiol. 23, 233–242. https://doi.org/10.1016/j.tim.2014.12.010

Neu, T.R., Lawrence, J.R., 1997. Development and structure of microbial biofilms in river water studied by confocal laser scanning microscopy. FEMS Microbiol. Ecol. 24, 11–25. https://doi.org/10.1111/j.1574-6941.1997.tb00419.x

Neu, T.R., Swerhone, G.D.W., Lawrence, J.R., 2001. Assessment of lectin-binding analysis for in situ detection of glycoconjugates in biofilm systems. Microbiology 147, 299–313. https://doi.org/10.1099/00221287-147-2-299

Nielsen, P.H., Jahn, A., Palmgren, R., 1997. Conceptual model for production and composition of exopolymers in biofilms. Water Sci. Technol. 36, 11–19. https://doi.org/10.1016/S0273-1223(97)00318-1

Nivala, J., Murphy, C., Freeman, A., 2020. Recent Advances in the Application, Design, and Operations & Maintenance of Aerated Treatment Wetlands. Water 2020, Vol. 12, Page 1188 12, 1188. https://doi.org/10.3390/W12041188

Nivala, J., Murphy, C., Troesch, S., Wallace, S., Esser, D., 2014. Intensified and Modified Wetland Designs. Sustain. Sanit. Pract. 18, 15–20.

Nivala, J., Wallace, S., Headley, T., Kassa, K., Brix, H., van Afferden, M., Müller, R., 2013. Oxygen transfer and consumption in subsurface flow treatment wetlands. Ecol. Eng. 61, 544–554. https://doi.org/10.1016/J.ECOLENG.2012.08.028

Nowack, B., Krug, H.F., Height, M., 2011. 120 years of nanosilver history: Implications for policy makers. Environ. Sci. Technol. 45, 1177–1183. https://doi.org/10.1021/es103316q

Nowack, B., Mitrano, D.M., 2018. Procedures for the production and use of synthetically aged and product released nanomaterials for further environmental and ecotoxicity testing. NanoImpact. https://doi.org/10.1016/j.impact.2017.12.001

Nowack, B., Mueller, N.C., 2008. Exposure modeling of engineered nanoparticles in the environment. EMPA Act. https://doi.org/10.1021/es7029637

Nyvad, B., Fejerskov, O., 1987. Scanning electron microscopy of early microbial colonization of human enamel and root surfaces in vivo. Eur. J. Oral Sci. 95, 287–296. https://doi.org/10.1111/j.1600-0722.1987.tb01844.x

Odum, E.P., 1984. The Mesocosm. Bioscience 34, 558–562. https://doi.org/10.2307/1309598

Oopkaup, K., Truu, M., Nõlvak, H., Ligi, T., Preem, J.K., Mander, Ü., Truu, J., 2016. Dynamics of bacterial community abundance and structure in horizontal subsurface flow wetland mesocosms treating municipal wastewater. Water (Switzerland) 8, 457. https://doi.org/10.3390/w8100457

Ouellet-Plamondon, C., Chazarenc, F., Comeau, Y., Brisson, J., 2006. Artificial aeration to increase pollutant removal efficiency of constructed wetlands in cold climate. Ecol. Eng. 27, 258–264. https://doi.org/10.1016/j.ecoleng.2006.03.006

Pal, S., Tak, Y.K., Song, J.M., 2007. Does the antibacterial activity of silver nanoparticles depend on the shape of the nanoparticle? A study of the Gram-negative bacterium Escherichia coli. Appl. Environ. Microbiol. 73, 1712–1720. https://doi.org/10.1128/AEM.02218-06

Park, H.J., Kim, J.Y., Kim, J., Lee, J.H., Hahn, J.S., Gu, M.B., Yoon, J., 2009. Silver-ion-mediated reactive oxygen species generation affecting bactericidal activity. Water Res. 43, 1027–1032. https://doi.org/10.1016/J.WATRES.2008.12.002

Patch, D., Koch, I., Peloquin, D., O'Carroll, D., Weber, K., 2021. Development and validation of a method for the weathering and detachment of representative nanomaterials from conventional silver-containing textiles. Chemosphere 284, 131269. https://doi.org/10.1016/j.chemosphere.2021.131269

Pedescoll, A., Sidrach-Cardona, R., Sánchez, J.C., Bécares, E., 2013. Evapotranspiration affecting redox conditions in horizontal constructed wetlands under Mediterranean climate: Influence of plant species. Ecol. Eng. 58, 335–343. https://doi.org/10.1016/j.ecoleng.2013.07.007

Peters, R.J.B., van Bemmel, G., Milani, N.B.L., den Hertog, G.C.T., Undas, A.K., van der Lee, M., Bouwmeester, H., 2018. Detection of nanoparticles in Dutch surface waters. Sci. Total Environ. 621, 210–218. https://doi.org/10.1016/J.SCITOTENV.2017.11.238

Petrie, B., Barden, R., Kasprzyk-Hordern, B., 2015. A review on emerging contaminants in wastewaters and the environment: Current knowledge, understudied areas and recommendations for future monitoring. Water Res. 72, 3–27. https://doi.org/10.1016/j.watres.2014.08.053

Picioreanu, C., Van Loosdrecht, M.C.M., Heijnen, J.J., 1998. Mathematical modeling of

biofilm structure with a hybrid differential- discrete cellular automaton approach. Biotechnol. Bioeng. 58, 101–116. https://doi.org/10.1002/(SICI)1097-0290(19980405)58:1<101::AID-BIT11>3.0.CO;2-M

Pikal, M.J., Tang, X., 2004. Design of Freeze-Drying Processes for Pharmaceuticals: Practical Advice. Artic. Pharm. Res. https://doi.org/10.1023/B:PHAM.0000016234.73023.75

Project on Emerging Nanotechnologies, 2023. Consumer Products Inventory [WWW Document]. Proj. Emerg. Nanotechnologies. URL http://www.nanotechproject.tech/cpi (accessed 8.19.23).

Prosser, J.I., Head, I.M., Stein, L.Y., 2014. The family Nitrosomonadaceae. The Prokaryotes: Alphaproteobacteria and Betaproteobacteria 9783642301971, 901–918. https://doi.org/10.1007/978-3-642-30197-1_372/TABLES/3

Pulit-Prociak, J., Banach, M., 2016. Silver nanoparticles - A material of the future...? Open Chem. 14, 76–91. https://doi.org/10.1515/CHEM-2016-0005/ASSET/GRAPHIC/J_CHEM-2016-0005_FIG_004.JPG

Qiu, G., Wirianto, K., Sun, Y., Ting, Y.P., 2016. Effect of silver nanoparticles on system performance and microbial community dynamics in a sequencing batch reactor. J. Clean. Prod. 130, 137–142. https://doi.org/10.1016/J.JCLEPRO.2015.10.051

Quan, K., Hou, J., Zhang, Z., Ren, Y., Peterson, B.W., Flemming, H.C., Mayer, C., Busscher, H.J., van der Mei, H.C., 2021. Water in bacterial biofilms: pores and channels, storage and transport functions. https://doi.org/10.1080/1040841X.2021.1962802. https://doi.org/10.1080/1040841X.2021.1962802

Quan, Z.X., Im, W.T., Lee, S.T., 2006. Azonexus caeni sp. nov., a denitrifying bacterium isolated from sludge of a wastewater treatment plant. Int. J. Syst. Evol. Microbiol. 56, 1043–1046. https://doi.org/10.1099/IJS.0.64019-0

Quast, C., Pruesse, E., Yilmaz, P., Gerken, J., Schweer, T., Yarza, P., Peplies, J., Glöckner, F.O., 2013. The SILVA ribosomal RNA gene database project: improved data processing and web-based tools. Nucleic Acids Res. 41, D590. https://doi.org/10.1093/NAR/GKS1219

Rahman, M.E., Halmi, M.I.E. Bin, Samad, M.Y.B.A., Uddin, M.K., Mahmud, K., Shukor, M.Y.A., Abdullah, S.R.S., Shamsuzzaman, S.M., 2020. Design, Operation and Optimization of Constructed Wetland for Removal of Pollutant. Int. J. Environ. Res. Public Health 17. https://doi.org/10.3390/IJERPH17228339

Rai, M., Yadav, A., Gade, A., 2008. Silver nanoparticles as a new generation of antimicrobials. Biotechnol. Adv. 27, 76–83. https://doi.org/10.1016/j.biotechadv.2008.09.002

Rajabzadeh, A.R., Legge, R.L., Weber, K.P., 2015. Multiphysics modelling of flow dynamics, biofilm development and wastewater treatment in a subsurface vertical flow constructed wetland mesocosm. Ecol. Eng. 74, 107–116. https://doi.org/10.1016/j.ecoleng.2014.09.122

Ramprasad, C., Philip, L., 2018. Greywater treatment using horizontal, vertical and hybrid flow constructed wetlands. Curr. Sci. 114, 155–165. https://doi.org/10.18520/cs/v114/i01/155-165

Reidy, B., Haase, A., Luch, A., Dawson, K.A., Lynch, I., 2013. Mechanisms of silver nanoparticle release, transformation and toxicity: A critical review of current knowledge and recommendations for future studies and applications. Materials (Basel). 6, 2295–2350. https://doi.org/10.3390/ma6062295

Renslow, R.S., Marshall, M.J., Tucker, A.E., Chrisler, W.B., Yu, X.Y., 2017. In situ nuclear magnetic resonance microimaging of live biofilms in a microchannel. Analyst 142, 2363–2371. https://doi.org/10.1039/c7an00078b

Robeson, M.S., O'Rourke, D.R., Kaehler, B.D., Ziemski, M., Dillon, M.R., Foster, J.T., Bokulich, N.A., 2021. RESCRIPt: Reproducible sequence taxonomy reference database management. PLoS Comput. Biol. 17, e1009581. https://doi.org/10.1371/journal.pcbi.1009581

Ruppelt, J.P., Tondera, K., Wallace, S.J., Button, M., Pinnekamp, J., Weber, K.P., 2020. Assessing the role of microbial communities in the performance of constructed wetlands used to treat combined sewer overflows. Sci. Total Environ. 736. https://doi.org/10.1016/j.scitotenv.2020.139519

Sapsford, K.E., Tyner, K.M., Dair, B.J., Deschamps, J.R., Medintz, I.L., 2011. Analyzing nanomaterial bioconjugates: A review of current and emerging purification and characterization techniques. Anal. Chem. https://doi.org/10.1021/ac200853a

Sarkar, M., 2022. Effect of silver nanoparticles on nitrogen-cycling bacteria in constructed wetlands. Nanotechnol. Environ. Eng. https://doi.org/10.1007/s41204-021-00192-3

Sauvé, S., Desrosiers, M., 2014. A review of what is an emerging contaminant. Chem. Cent. J. 8, Article 15. https://doi.org/10.1186/1752-153X-8-15

Scherwass, A., Erken, M., Arndt, H., 2016. Grazing Effects of Ciliates on Microcolony Formation in Bacterial Biofilms. Microb. Biofilms - Importance Appl. https://doi.org/10.5772/63516

Schlafer, S., Meyer, R.L., 2017. Confocal microscopy imaging of the biofilm matrix. J. Microbiol. Methods. https://doi.org/10.1016/j.mimet.2016.03.002

Schneider, M., 2015. Investigation of the effects of emerging contaminants on microbial communities within different ecosystems. Beuth Hochschule für Technik Berlin.

Sheng, Z., Van Nostrand, J.D., Zhou, J., Liu, Y., 2018. Contradictory effects of silver nanoparticles on activated sludge wastewater treatment. J. Hazard. Mater. 341, 448–456. https://doi.org/10.1016/J.JHAZMAT.2017.07.051

Silveira, D.D., Farooq, A.J., Wallace, S.J., Lapolli, F.R., Nivala, J., Weber, K.P., 2022. Structural and functional spatial dynamics of microbial communities in aerated and non-aerated horizontal flow treatment wetlands. Sci. Total Environ. 838, 156600. https://doi.org/10.1016/J.SCITOTENV.2022.156600

Sinicrope, T.L., Langis, R., Gersberg, R.M., Busnardo, M.J., Zedler, J.B., 1992. Metal removal by wetland mesocosms subjected to different hydroperiods. Ecol. Eng. 1, 309–322. https://doi.org/10.1016/0925-8574(92)90013-R

Smith, K.S., Ingram-Smith, C., 2007. Methanosaeta, the forgotten methanogen? Trends Microbiol. 15, 150–155. https://doi.org/10.1016/j.tim.2007.02.002

Sondi, I., Salopek-Sondi, B., 2004. Silver nanoparticles as antimicrobial agent: A case study on E. coli as a model for Gram-negative bacteria. J. Colloid Interface Sci. 275, 177–182. https://doi.org/10.1016/j.jcis.2004.02.012

Sotiriou, G.A., Pratsinis, S.E., 2010. Antibacterial activity of nanosilver ions and particles. Environ. Sci. Technol. 44, 5649–5654. https://doi.org/10.1021/es101072s

Sousa, W.T.Z., Panitz, C.M.N., Thomaz, S.M., 2011. Performance of pilot-scale vertical flow constructed wetlands with and without the emergent macrophyte Spartina alterniflora treating mariculture effluent. Brazilian Arch. Biol. Technol. 54, 405–413. https://doi.org/10.1590/S1516-89132011000200024

Stark, L.R., Williams, F.M., Wenerick, W.R., Wuest, P.J., Urban, C., 1996. The Effects of Substrate Type, Surface Water Depth, and Flow Rate on Manganese Retention in Mesocosm Wetlands. J. Environ. Qual. 25, 97–106. https://doi.org/10.2134/jeq1996.00472425002500010013x

StatNano, 2023. Nanotechnology Products Database (NPD) [WWW Document]. URL https://product.statnano.com/ (accessed 8.19.23).

Steer, D., Fraser, L., Boddy, J., Seibert, B., 2002. Efficiency of small constructed wetlands for subsurface treatment of single-family domestic effluent. Ecol. Eng. 18, 429–440. https://doi.org/10.1016/S0925-8574(01)00104-5

Stefanakis, A., 2020. Constructed wetlands for sustainable wastewater treatment in hot and arid climates: Opportunities, challenges and case studies in the Middle East. Water (Switzerland). https://doi.org/10.3390/W12061665

Stefanakis, A., Akratos, C.S., Tsihrintzis, V.A., 2014. Constructed Wetlands Classification, in: Vertical Flow Constructed Wetlands. Elsevier, pp. 17–25. https://doi.org/10.1016/b978-0-12-404612-2.00002-7

Stewart, P.S., 2003. Diffusion in biofilms. J. Bacteriol. https://doi.org/10.1128/JB.185.5.1485-1491.2003

Stewart, P.S., Murga, R., Srinivasan, R., de Beer, D., 1995. Biofilm structural heterogeneity visualized by three microscopic methods. Water Res. 29, 2006–2009. https://doi.org/10.1016/0043-1354(94)00339-9

Stewart, R.I.A., Dossena, M., Bohan, D.A., Jeppesen, E., Kordas, R.L., Ledger, M.E., Meerhoff, M., Moss, B., Mulder, C., Shurin, J.B., Suttle, B., Thompson, R., Trimmer, M., Woodward, G., 2013. Mesocosm Experiments as a Tool for Ecological Climate-Change Research. Adv. Ecol. Res. 48, 71–181. https://doi.org/10.1016/B978-0-12-417199-2.00002-1

Stoodley, P., Dodds, I., De Beer, D., Scott, H.L., Boyle, J.D., 2005. Flowing biofilms as a transport mechanism for biomass through porous media under laminar and turbulent conditions in a laboratory reactor system. Biofouling 21, 161–168. https://doi.org/10.1080/08927010500375524

Stoodley, P., Sauer, K., Davies, D.G., Costerton, J.W., 2002. Biofilms as complex differentiated communities. Annu. Rev. Microbiol. 56, 187–209. https://doi.org/10.1146/annurev.micro.56.012302.160705

Stottmeister, U., Wießner, A., Kuschk, P., Kappelmeyer, U., Kästner, M., Bederski, O., Müller, R.A., Moormann, H., 2003. Effects of plants and microorganisms in constructed wetlands for wastewater treatment, in: Biotechnology Advances. Elsevier Inc., pp. 93–117. https://doi.org/10.1016/j.biotechadv.2003.08.010

Stowell, R., Ludwig, R., Colt, J., Tchoba, G., 1981. Concepts in Aquatic Treatment System Design. J. Environ. Eng. Div. 107, 919–940. https://doi.org/10.1061/JEEGAV.0001225

Suarez, C., Persson, F., Hermansson, M., 2015. Predation of nitritation–anammox biofilms used for nitrogen removal from wastewater. FEMS Microbiol. Ecol. 91, 124. https://doi.org/10.1093/FEMSEC/FIV124

Sun, C., Hu, K., Mu, D., Wang, Z., Yu, X., 2022. The Widespread Use of Nanomaterials: The Effects on the Function and Diversity of Environmental Microbial Communities. Microorganisms 10. https://doi.org/10.3390/MICROORGANISMS10102080

Syafiuddin, A., Salmiati, S., Hadibarata, T., Kueh, A.B.H., Salim, M.R., Zaini, M.A.A., 2018. Silver Nanoparticles in the Water Environment in Malaysia: Inspection, characterization, removal, modeling, and future perspective. Sci. Reports 2018 81 8, 1–15. https://doi.org/10.1038/s41598-018-19375-1

Talebian, S., Rodrigues, T., Das Neves, J., Sarmento, B., Langer, R., Conde, J., 2021. Facts and Figures on Materials Science and Nanotechnology Progress and Investment. ACS Nano 15, 15940–15952. https://doi.org/10.1021/ACSNANO.1C03992/ASSET/IMAGES/MEDIUM/NN1C039

92_0009.GIF

Tang, J., Wu, Y., Esquivel-Elizondo, S., Sørensen, S.J., Rittmann, B.E., 2018. How Microbial Aggregates Protect against Nanoparticle Toxicity. Trends Biotechnol. 36, 1171–1182. https://doi.org/10.1016/J.TIBTECH.2018.06.009

Tao, W., Wang, J., 2009. Effects of vegetation, limestone and aeration on nitritation, anammox and denitrification in wetland treatment systems. Ecol. Eng. 35, 836–842. https://doi.org/10.1016/J.ECOLENG.2008.12.003

Tavanaei, A., Salehi, S., 2015. Pore, throat, and grain detection for rock SEM images using digital watershed image segmentation algorithm. J. Porous Media 18, 507–518. https://doi.org/10.1615/JPorMedia.v18.i5.40

Thuptimdang, P., Limpiyakorn, T., Khan, E., 2017. Dependence of toxicity of silver nanoparticles on Pseudomonas putida biofilm structure. Chemosphere 188, 199–207. https://doi.org/10.1016/J.CHEMOSPHERE.2017.08.147

Tian, R., Ning, D., He, Z., Zhang, P., Spencer, S.J., Gao, S., Shi, W., Wu, L., Zhang, Y., Yang, Y., Adams, B.G., Rocha, A.M., Detienne, B.L., Lowe, K.A., Joyner, D.C., Klingeman, D.M., Arkin, A.P., Fields, M.W., Hazen, T.C., Stahl, D.A., Alm, E.J., Zhou, J., 2020. Small and mighty: Adaptation of superphylum Patescibacteria to groundwater environment drives their genome simplicity. Microbiome 8, 1–15. https://doi.org/10.1186/S40168-020-00825-W/FIGURES/5

Truu, M., Ligi, T., Nõlvak, H., Peeb, A., Tiirik, K., Devarajan, A.K., Oopkaup, K., Kasemets, K., Kõiv-Vainik, M., Kasak, K., Truu, J., 2022. Impact of synthetic silver nanoparticles on the biofilm microbial communities and wastewater treatment efficiency in experimental hybrid filter system treating municipal wastewater. J. Hazard. Mater. 440, 129721. https://doi.org/10.1016/J.JHAZMAT.2022.129721

Tyroller, L., Rousseau, D.P.L., Santa, S., García, J., 2010. Application of the gas tracer method for measuring oxygen transfer rates in subsurface flow constructed wetlands. Water Res. 44, 4217–4225. https://doi.org/10.1016/j.watres.2010.05.027

Valiei, A., Kumar, A., Mukherjee, P.P., Liu, Y., Thundat, T., 2012. A web of streamers: Biofilm formation in a porous microfluidic device. Lab Chip 12, 5133–5137. https://doi.org/10.1039/c2lc40815e

Vance, M.E., Kuiken, T., Vejerano, E.P., McGinnis, S.P., Hochella, M.F., Hull, D.R., 2015. Nanotechnology in the real world: Redeveloping the nanomaterial consumer products inventory. Beilstein J. Nanotechnol. 6, 1769–1780. https://doi.org/10.3762/bjnano.6.181

Vauthier, C., Cabane, B., Labarre, D., 2008. How to concentrate nanoparticles and avoid aggregation? Eur. J. Pharm. Biopharm. 69, 466–475. https://doi.org/10.1016/j.ejpb.2008.01.025

Vera, I., Araya, F., Andrés, E., Sáez, K., Vidal, G., 2014. Enhanced phosphorus removal from sewage in mesocosm-scale constructed wetland using zeolite as medium and artificial aeration. Environ. Technol. (United Kingdom), Environ. Technol. (UK) 35, 1639–1649. https://doi.org/10.1080/09593330.2013.877984

Verma, V., 2018. Silver Nanoparticles Market Size By Application, Industry Analysis Report, Regional Outlook, Growth Potential, Price Trends, Competitive Market Share & Forecast, 2018 - 2024 [WWW Document]. Glob. Information,Inc. URL https://www.giiresearch.com/report/gmi555348-silver-nanoparticles-market-size-by-application.html

Vymazal, J., 2023. Thirty years of constructed wetlands for municipal wastewater treatment in the Czech Republic. Ecol. Eng. 194. https://doi.org/https://doi.org/10.1016/j.ecoleng.2023.107054

Vymazal, J., 2013. Emergent plants used in free water surface constructed wetlands: A review. Ecol. Eng. 61, 582–592. https://doi.org/10.1016/j.ecoleng.2013.06.023

Vymazal, J., 2011. Constructed Wetlands for Wastewater Treatment: Five Decades of Experience. Environ. Sci. Technol. 45, 61–69. https://doi.org/10.1021/es101403q

Vymazal, J., 2010. Constructed Wetlands for Wastewater Treatment. Water 2010, Vol. 2, Pages 530-549 2, 530–549. https://doi.org/10.3390/W2030530

Vymazal, J., 2009. The use constructed wetlands with horizontal sub-surface flow for various types of wastewater. Ecol. Eng. 35, 1–17. https://doi.org/10.1016/J.ECOLENG.2008.08.016

Vymazal, J., 2005. Horizontal sub-surface flow and hybrid constructed wetlands systems for wastewater treatment. Ecol. Eng. 25, 478–490. https://doi.org/10.1016/j.ecoleng.2005.07.010

Vymazal, J., Kröpfelová, L., 2008. Wastewater treatment in constructed wetlands with horizontal sub- surface flow, Environmental Pollution.

Vymazal, J., Zhao, Y., Mander, Ü., 2021. Recent research challenges in constructed wetlands for wastewater treatment: A review. Ecol. Eng. 169, 106318. https://doi.org/10.1016/j.ecoleng.2021.106318

Wagner, M., Taherzadeh, D., Haisch, C., Horn, H., 2010. Investigation of the mesoscale structure and volumetric features of biofilms using optical coherence tomography. Biotechnol. Bioeng. 107, 844–853. https://doi.org/10.1002/bit.22864

Walker, J.T., Mackerness, C.W., Rogers, J., Keevil, C.W., 1995. Heterogeneous Mosiac Biofilm – A Haven for Waterborne Pathogens, in: Microbial Biofilms. Cambridge University Press, pp. 196–204. https://doi.org/10.1017/CBO9780511525353.013

Wang, G., Jin, Z., Wang, X., George, T.S., Feng, G., Zhang, L., 2022. Simulated root

exudates stimulate the abundance of Saccharimonadales to improve the alkaline phosphatase activity in maize rhizosphere. Appl. Soil Ecol. 170, 104274. https://doi.org/10.1016/J.APSOIL.2021.104274

Wang, H.X., Xu, J.L., Sheng, L.X., Liu, X.J., 2018. A Review of Research on Substrate Materials for Constructed Wetlands. Mater. Sci. Forum 913, 917–929. https://doi.org/10.4028/WWW.SCIENTIFIC.NET/MSF.913.917

Wang, J., Long, Y., Yu, G., Wang, G., Zhou, Z., Li, P., Zhang, Y., Yang, K., Wang, S., 2022. A Review on Microorganisms in Constructed Wetlands for Typical Pollutant Removal: Species, Function, and Diversity. Front. Microbiol. 13, 845725. https://doi.org/10.3389/FMICB.2022.845725

Ward, C.S., Pan, J.F., Colman, B.P., Wang, Z., Gwin, C.A., Williams, T.C., Ardis, A., Gunsch, C.K., Hunt, D.E., 2019. Conserved Microbial Toxicity Responses for Acute and Chronic Silver Nanoparticle Treatments in Wetland Mesocosms. Environ. Sci. Technol. 53. https://doi.org/10.1021/acs.est.8b06654

Weber, K.P., 2016. Microbial community assessment in wetlands for water pollution control: Past, present, and future outlook. Water (Switzerland) 8, 503. https://doi.org/10.3390/w8110503

Weber, K.P., Gagnon, V., 2014. Microbiology in Treatment Wetlands. Sustain. Sanit. Pract. Outcomes from UFZ Wetl. Work. Spec. Issue 25–30.

Weber, K.P., Gehder, M., Legge, R.L., 2008. Assessment of changes in the microbial community of constructed wetland mesocosms in response to acid mine drainage exposure. Water Res. 42, 180–188. https://doi.org/10.1016/j.watres.2007.06.055

Weber, K.P., Grove, J.A., Gehder, M., Anderson, W.A., Legge, R.L., 2007. Data transformations in the analysis of community-level substrate utilization data from microplates. J. Microbiol. Methods 69. https://doi.org/10.1016/j.mimet.2007.02.013

Weber, K.P., Legge, R.L., 2013. Comparison of the catabolic activity and catabolic profiles of rhizospheric, gravel-associated and interstitial microbial communities in treatment wetlands. Water Sci. Technol. 67, 886–893. https://doi.org/10.2166/wst.2012.637

Weber, K.P., Legge, R.L., 2011. Dynamics in the bacterial community-level physiological profiles and hydrological characteristics of constructed wetland mesocosms during start-up. Ecol. Eng. 37, 666–677. https://doi.org/10.1016/j.ecoleng.2010.03.016

Weber, Kela P., Legge, R.L., 2010. Community-level physiological profiling. Methods Mol. Biol. 599, 263–281. https://doi.org/10.1007/978-1-60761-439-5_16

Weber, Kela P, Legge, R.L., 2010. Method for the detachment of culturable bacteria from wetland gravel. J. Microbiol. Methods 80, 242–250. https://doi.org/10.1016/j.mimet.2010.01.006

Weber, K.P., Petersen, E.J., Bissegger, S., Koch, I., Zhang, J., Reimer, K.J., Rehmann, L., Slawson, R.M., Legge, R.L., O'Carroll, D.M., 2014. Effect of gold nanoparticles and ciprofloxacin on microbial catabolism: A community-based approach. Environ. Toxicol. Chem. 33, 44–51. https://doi.org/10.1002/etc.2412

Whipps, J.M., Lynch, J.M., 1990. Carbon economy. Rhizosph. 59–97.

Wießner, A., Kappelmeyer, U., Kuschk, P., Kästner, M., 2005. Influence of the redox condition dynamics on the removal efficiency of a laboratory-scale constructed wetland. Water Res. 39, 248–256. https://doi.org/10.1016/j.watres.2004.08.032

Willig, S., Varanini, Z., Nannipieri, P., 2000. Types, Amounts, and Possible Functions of Compounds Released into the Rhizosphere by Soil-Grown Plants. Rhizosph. 35–56. https://doi.org/10.1201/9780849384974-8

Wimpenny, J., Manz, W., Szewzyk, U., 2000. Heterogeneity in biofilms. FEMS Microbiol. Rev. https://doi.org/10.1016/S0168-6445(00)00052-8

Wu, S., Austin, D., Liu, L., Dong, R., 2011. Performance of integrated household constructed wetland for domestic wastewater treatment in rural areas. Ecol. Eng. 37, 948–954. https://doi.org/10.1016/J.ECOLENG.2011.02.002

Xie, F., Zhao, B., Cui, Y., Ma, X., Li, D., Yue, X., 2021. Enhancing nitrogen removal performance of anammox process after short-term pH and temperature shocks by coupling with iron-carbon micro-electrolysis. J. Clean. Prod. 289, 125753. https://doi.org/10.1016/J.JCLEPRO.2020.125753

Xiu, Z.M., Zhang, Q.B., Puppala, H.L., Colvin, V.L., Alvarez, P.J.J., 2012. Negligible particle-specific antibacterial activity of silver nanoparticles. Nano Lett. 12, 4271–4275. https://doi.org/10.1021/NL301934W/SUPPL_FILE/NL301934W_SI_001.PDF

Yang, C., Wang, B., Wang, H., He, Z., Pi, Y., Zhou, J., Liang, T., Chen, M., He, T., Fu, T., 2022. Removal of organochlorine pesticides and metagenomic analysis by multi-stage constructed wetland treating landfill leachate. Chemosphere 301. https://doi.org/10.1016/j.chemosphere.2022.134761

Yang, Y., Alvarez, P.J.J., 2015. Sublethal Concentrations of Silver Nanoparticles Stimulate Biofilm Development. Environ. Sci. Technol. Lett. 2, 221–226. https://doi.org/10.1021/ACS.ESTLETT.5B00159

Yang, Y., Wang, J., Xiu, Z., Alvarez, P.J.J., 2013. Impacts of silver nanoparticles on cellular and transcriptional activity of nitrogen-cycling bacteria. Environ. Toxicol. Chem. 32, 1488–1494. https://doi.org/10.1002/ETC.2230

Yonathan, K., Mann, R., Mahbub, K.R., Gunawan, C., 2022. The impact of silver nanoparticles on microbial communities and antibiotic resistance determinants in the environment. Environ. Pollut. 293, 118506. https://doi.org/10.1016/J.ENVPOL.2021.118506

Zhang, H., Wang, X.C., Zheng, Y., Dzakpasu, M., 2023. Removal of pharmaceutical active compounds in wastewater by constructed wetlands: Performance and mechanisms. J. Environ. Manage. 325, 116478. https://doi.org/10.1016/J.JENVMAN.2022.116478

Zhang, L., Lyu, T., Zhang, Y., Button, M., Arias, C.A., Weber, K.P., Brix, H., Carvalho, P.N., 2018. Impacts of design configuration and plants on the functionality of the microbial community of mesocosm-scale constructed wetlands treating ibuprofen. Water Res. 131, 228–238. https://doi.org/10.1016/j.watres.2017.12.050

Zhang, P., Chen, Y.P., Qiu, J.H., Dai, Y.Z., Feng, B., 2019. Imaging the Microprocesses in Biofilm Matrices. Trends Biotechnol. 37, 214–226. https://doi.org/10.1016/j.tibtech.2018.07.006

Zhang, X., Bishop, P.L., Kupferle, M.J., 1998. Measurement of polysaccharides and proteins in biofilm extracellular polymers. Water Sci. Technol. 37, 345–348. https://doi.org/10.1016/S0273-1223(98)00127-9

Zhang, Z., Gao, P., Li, M., Cheng, J., Liu, W., Feng, Y., 2016. Influence of Silver nanoparticles on nutrient removal and microbial communities in SBR process after long-term exposure. Sci. Total Environ. 569–570, 234–243. https://doi.org/10.1016/j.scitotenv.2016.06.115

Zhang, Z.Z., Cheng, Y.F., Xu, L.Z.J., Bai, Y.H., Jin, R.C., 2018. Anammox granules show strong resistance to engineered silver nanoparticles during long-term exposure. Bioresour. Technol. 259, 10–17. https://doi.org/10.1016/J.BIORTECH.2018.03.024

Zhao, Y.Q., Sun, G., Allen, S.J., 2004. Anti-sized reed bed system for animal wastewater treatment: A comparative study. Water Res. 38, 2907–2917. https://doi.org/10.1016/j.watres.2004.03.038

Zhu, H., Yan, B., Xu, Y., Guan, J., Liu, S., 2014. Removal of nitrogen and COD in horizontal subsurface flow constructed wetlands under different influent C/N ratios. Ecol. Eng. 63, 58–63. https://doi.org/10.1016/J.ECOLENG.2013.12.018

Zurita, F., Del Toro-Sánchez, C.L., Gutierrez-Lomelí, M., Rodriguez-Sahagún, A., Castellanos-Hernandez, O.A., Ramírez-Martínez, G., White, J.R., 2012. Preliminary study on the potential of arsenic removal by subsurface flow constructed mesocosms. Ecol. Eng. 47, 101–104. https://doi.org/10.1016/j.ecoleng.2012.06.018

A. Appendix A

Supplemental Information

Evolution of the mesocosm: Informing treatment wetland research across the globe

Anbareen J. Farooq[†], Jacques Brisson[ǂ], Scott Wallace[§], and Kela P. Weber[†*]

[†]Environmental Sciences Group, Department of Chemistry and Chemical Engineering, Royal Military College of Canada, Kingston, ON K7K 7B4, Canada

[ǂ] Institut de Recherche en Biologie Végétale (IRBV), Département des Sciences Biologiques, Université de Montréal, Montréal, Québec H2X 1Y4, Canada

[§]Naturally Wallace Consulting LLC, Pilot Mountain, North Carolina 27041, USA

*Corresponding author: kela.weber@rmc.ca

Table A.1: C* values for HSSF systems (from Kadlec and Wallace (2009))

Treatment	P	C_i (mg/L)	C* (mg/L)
Tertiary	3	0-30	1
Secondary	3	30-100	5
Primary	3	100-200	10
Super	3	>200	15

Table A.2: C* values for VF systems (adapted from Kadlec and Wallace (2009))

Treatment	P	C_i (mg/L)	C* (mg/L)
Tertiary	2	3-30	2
Secondary	2	30-100	2
Primary	2	100-200	2
Super	2	>200	2

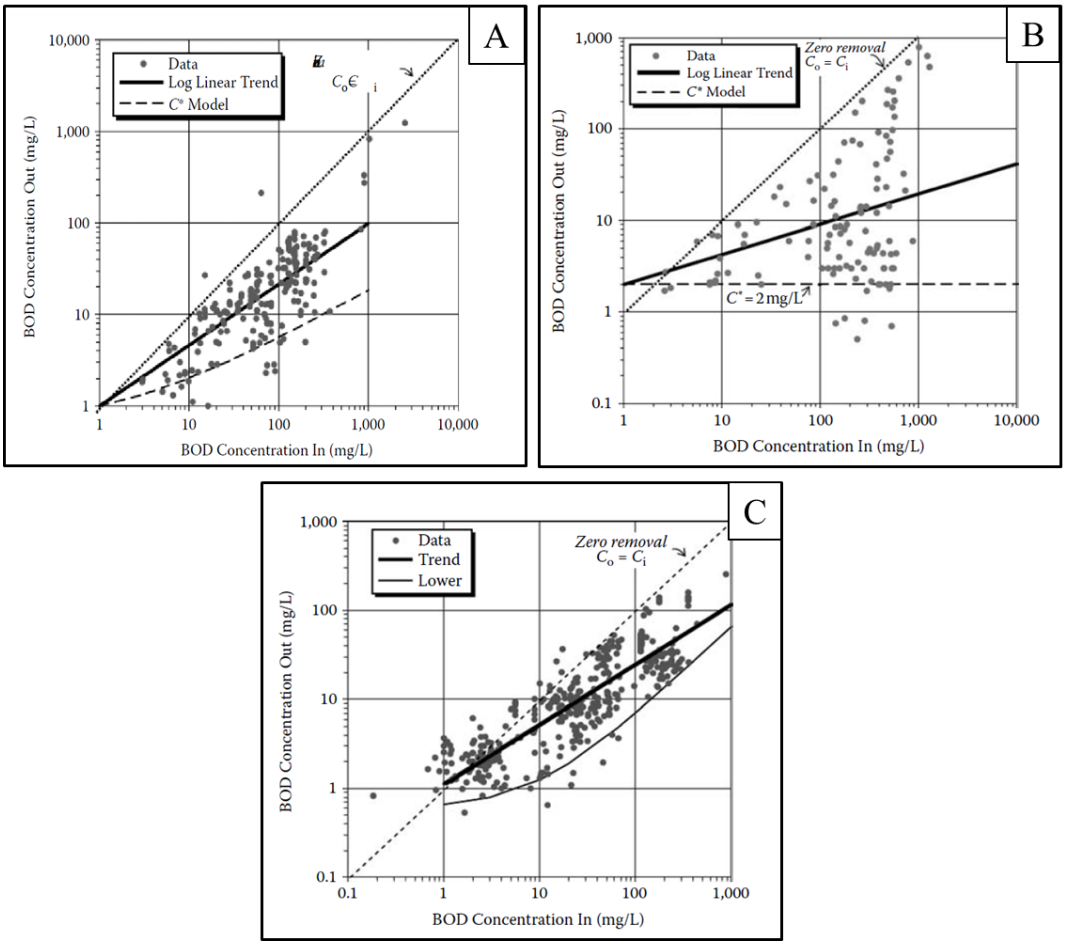

Figure A.1: Input–output concentration for BOD in **(A)** 202 HSSF wetlands; **(B)** 62 VF wetlands; **(C)**138 FWS wetlands. There is one data point per wetland, covering the entire period of record. The lower bound curve, excluding 5% of the lowest values, is C*. The central tendency is described through a log-linear regression for each dataset. Graphs retrieved from Chapter 8 of Kadlec and Wallace (2009).

B. Appendix B

Supplemental Information

Peaks, pores, and dragon eggs: Uncovering and quantifying the heterogeneity of treatment wetland biofilm matrices

Anbareen J. Farooq†, Mhari Chamberlain†, Arman Poonja†, Kevin Mumford‡, Scott Wallace§ and Kela P. Weber†*

†Environmental Sciences Group, Department of Chemistry and Chemical Engineering, Royal Military College of Canada, Kingston, ON K7K 7B4, Canada

‡ Department of Civil Engineering, Queen's University, Kingston, Ontario, K7L 3N6

§Naturally Wallace Consulting LLC, Pilot Mountain, North Carolina 27041, USA

*Corresponding author: kela.weber@rmc.ca

Table B.1: Water Chemistry Data

Sample	Water Temperature (ºC)	Conductivity (µS/cm)	Dissolved Oxygen (mg/L)	pH	ORP (mV)	NH_4 (mg/L)
Inlet	11.1 ± 4.8	647.5 ± 76.5	7.1±0.5	6.3±0.3	86.3±10.0	12.5±0.7
Non-aerated (Day 4)	22.5 ± 0.5	732.0 ± 26.2	0.3±0.03	6.6±0.1	-248.2±4.1	15.8±1.9
Aerated (Day 4)	22.1 ± 0.8	771.3 ± 23.2	6.1±0.6	7.4±0.1	90.6±2.2	5.1±0.2

Table B.2: Breakdown of sampling strategy across all phases

Phase	Material	Analysis	Aerated Unplanted M1	Non-Aerated Planted M2	Non-Aerated Unplanted M3
I	Detached Biofilm	Light Microscopy	✓		✓
		SEM	✓		✓
II	Gravel-Associated Biofilm	SEM	✓		✓
III	Rhizospheric Biofilm	SEM		✓	

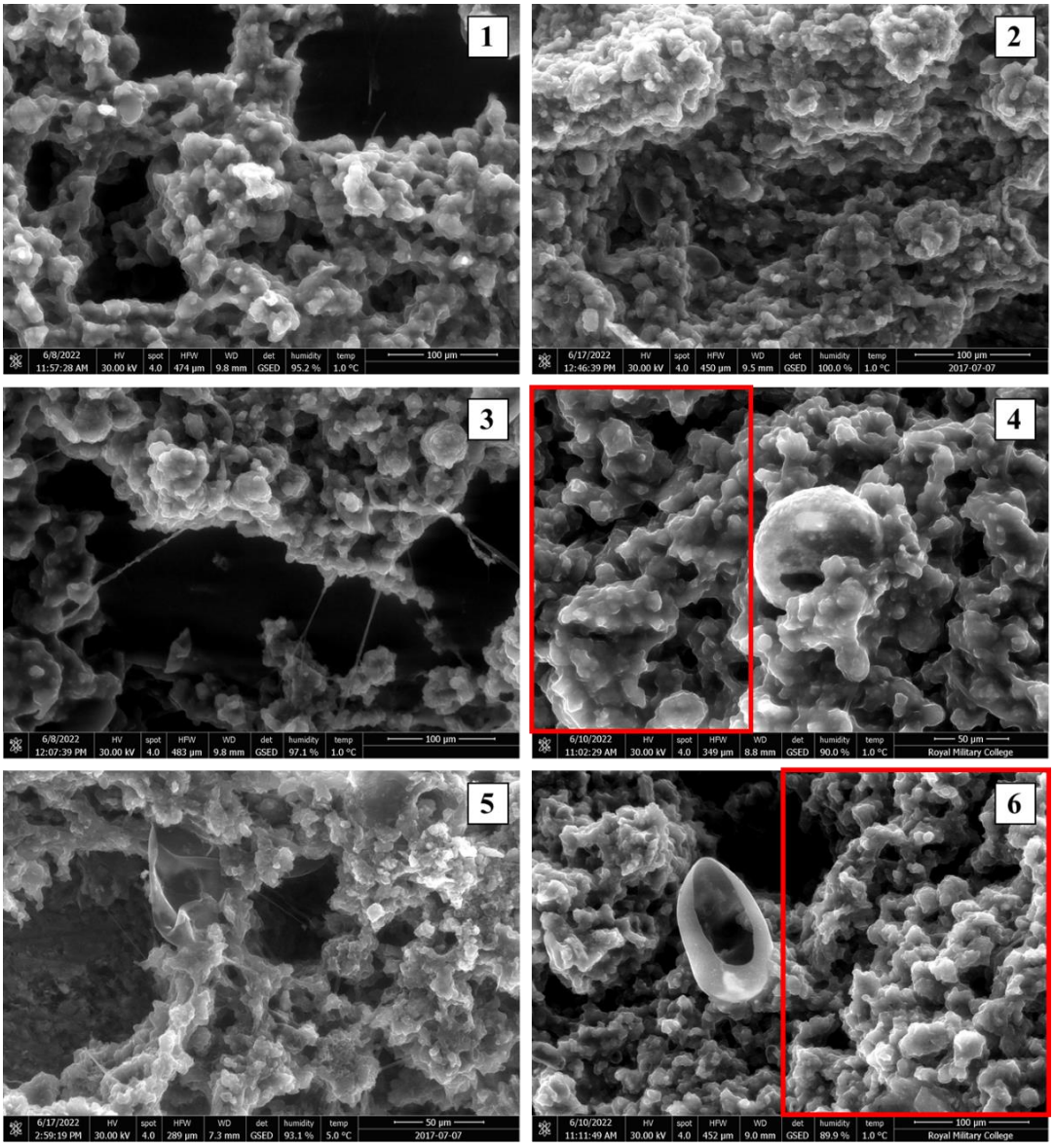

Figure B.1: Representative Wet-SEM images of detached and gravel-associated biofilm taken for pore distribution analysis. Micrographs 4 and 6 were cropped for analysis to focus on the biofilm morphology.

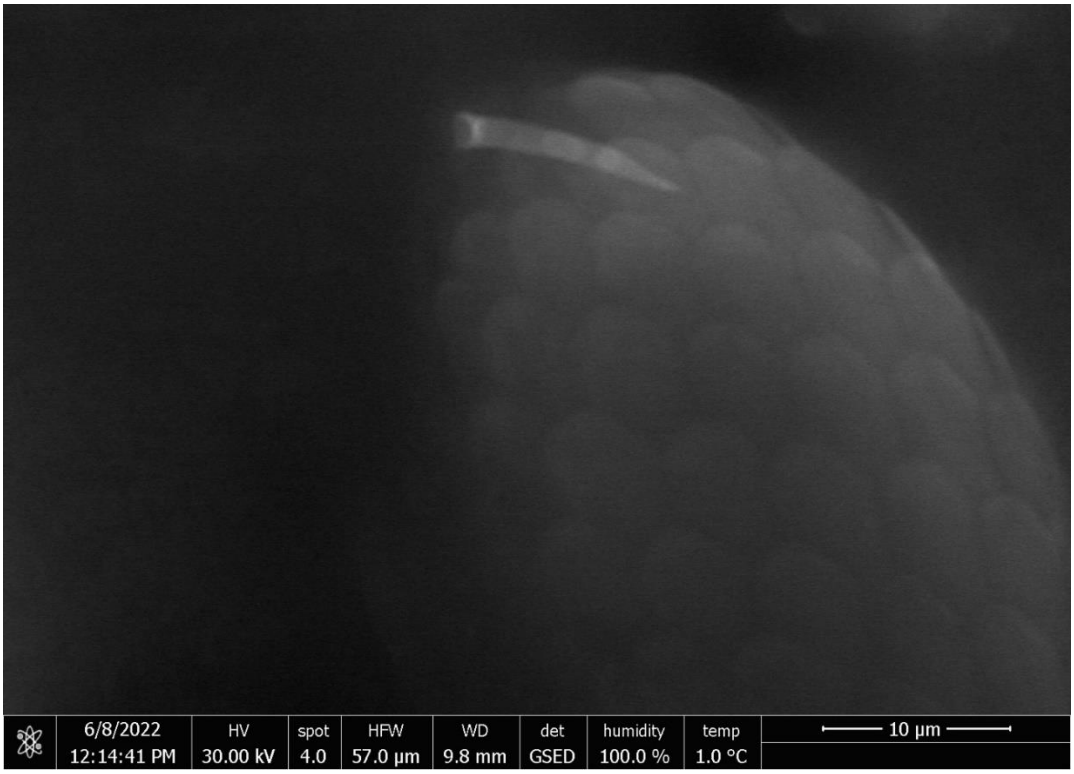

Figure B.2: Close-up Wet-SEM image of morphological shell of testate amoeba embedded within the biofilm matrix.

C. Appendix C

Supplemental Information

Limited effects of incidental silver nanomaterials from commercial textiles on treatment wetland mesocosms

Anbareen J. Farooq†, Laura Ogilvie, Dani Damasceno Silvera, Vincent Gagnon, Mark Button, Sarah Wallace, David Patch, Iris Koch, Denis O'Carroll, and Kela P. Weber†*

†Environmental Sciences Group, Department of Chemistry and Chemical Engineering, Royal Military College of Canada, Kingston, ON K7K 7B4, Canada

*Corresponding author: kela.weber@rmc.ca

C.1 Ex-Situ Screening Test

C.1.1 Nanomaterial Selection and Preparation

A range of pristine silver nanoparticles were use in this study including polyvinylpyrrolidone (PVP) coated (99.95 % Ag, 20 to 30 nm, SkySpring Nanomaterials Inc.), citrate stabilized (20 nm, Sigma-Aldrich), uncoated (99.95 % Ag, 20 to 30 nm, SkySpring Nanomaterials Inc.) and carboxymethyl cellulous (CMC) coated silver nanoparticles (3.7 g/L in 1 % CMC solution, 20 to 30 nm, provided by The University of Western Ontario, London, Canada. Synthesis involved the combination of CMC and $AgNO_3$ in the presence of sodium borohydride ($NABH_4$) as described in Weber et al. (2014).

For each nanoparticle type, stock solutions were prepared the day prior to the ex-situ experiment. All stock suspensions concentrations were 200 mg/L except for the citrate-coated Ag-ENM, which, due to limited availability, were 20 mg/L. The stock solutions were prepared in deionized water (dH2O) to reduce impact on the microbial matrix after which they sonicated for 30 minutes (Tabletop Ultrasonic Cleaner, FS140H, Fisher Scientific, Waltman, MA, USA). Total and dissolved Ag content of the stock suspensions were confirmed through ICP-MS analysis (Section 2.3). Characterization of dissolved vs particulate silver content of each stock suspension are presented in Figure C**.1**. The ionic silver (as $AgNO_3$) stock solution had a small fraction of particulates (< 10%), which can be attributed to instrument error. CMC-coated Ag-ENMs reported around 50% dissolved ionic silver content, which is likely an artifact of the synthesis process. Citrate-stabilized, PVP-coated, uncoated, and sulphidized nanoparticles as well as the sock wash solution contained negligible dissolved silver.

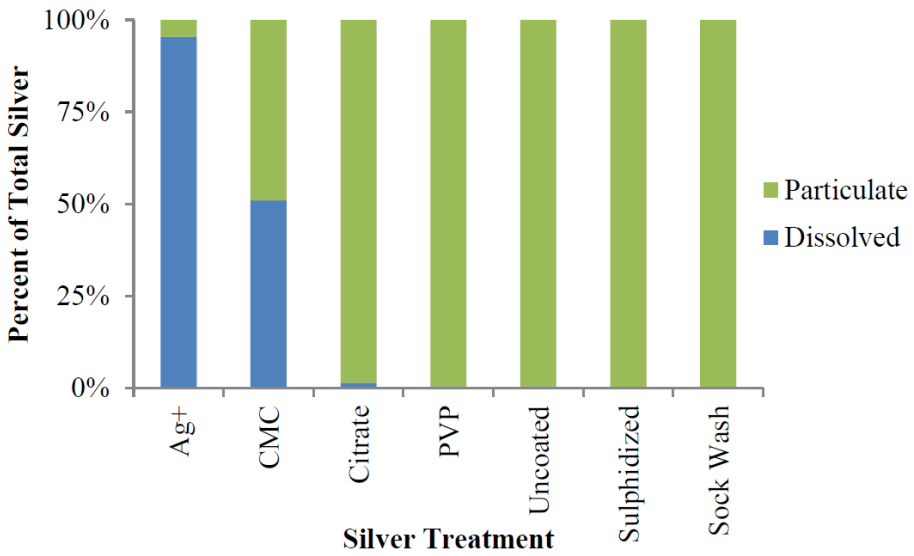

Figure C.1: Particulate versus dissolved (ionic) fraction of silver contained in the stock solutions of each silver treatment mixed in deionized water. Dissolved defined here as <10 kDa molecular weight cut-off. Each bar represents the value from a single sample; replicates were not performed for this analysis

C.1.2 Experimental Design

A total of 100 mL of pore water containing interstitial bacteria from six aerated and six non-aerated TW mesocosms was collected 24h after weekly wastewater loading to create composite samples for each set of mesocosms. Each composite interstitial water mix was lightly agitated to ensure complete mixing of the water/microbial community before a total of 20 mL was dispensed into 29 different 50-mL c-tubes. The interstitial microbial communities were amended with silver to create dose responses curve for each type of nanoparticle at concentrations of 0.1 mg/L, 0.25 mg/L, 0.5 mg/L, 1 mg/L, 5 mg/L, and 10 mg/L (Table C.1).

Table C.1: Concentrations evaluated for ex-situ silver nanoparticle (and ionic silver) exposures on constructed wetland interstitial water microbial communities. An "X" depicts a concentration which was used.

Silver Nanoparticle Type	**Concentration (mg/L)**					
	0.1	**0.25**	**0.5**	**1**	**5**	**10**
Ag+	X	X	X	X	X	X
PVP	X	X	X	X	X	X
Citrate	X	X	X	X		
CMC	X	X	X	X	X	X
Uncoated	X	X	X	X	X	X

Prior to spiking, original Ag stock suspensions prior were diluted to ensure the same volumes of nanoparticle solution and wetland water were combined at each concentration. Due to availability limitations the 5 mg/L and 10 mg/L concentrations had to be omitted for the citrate coated Ag-ENMs. Ag-spiked samples were lightly agitated to ensure proper mixing before being inoculated onto individual BIOLOG EcoPlates™ for CLPP analysis (Section 5.3.5.1). A time point of 40h was selected for the calculations of microbial activity (measured through AWCD).

C.1.3 Results

Dose response curves for the overall catabolic function (AWCD) for the interstitial microbial communities from aerated mesocosms are displayed in Figure C**.2**A. For all silver treatments the AWCD decreased with increasing silver load. Complete inhibition of microbial community catabolic activity was observed at 0.1 mg Ag/L, the lowest concentration tested, for Ag^{+} and CMC-coated Ag-ENMs, and at 5 mg Ag/L for PVP-coated and uncoated Ag-ENMs. The high susceptibility of the aerated microbes is thought to be a results of the O_2 enrich interstitial water, which would readily oxidize the Ag-ENMs into Ag^{+} ions (Liu and Hurt, 2010). Many studies have linked Ag-ENM toxicities to the release of Ag^{+} ions rather than the Ag-ENMs themselves (Liao et al., 2019; Navarro et al., 2008b).

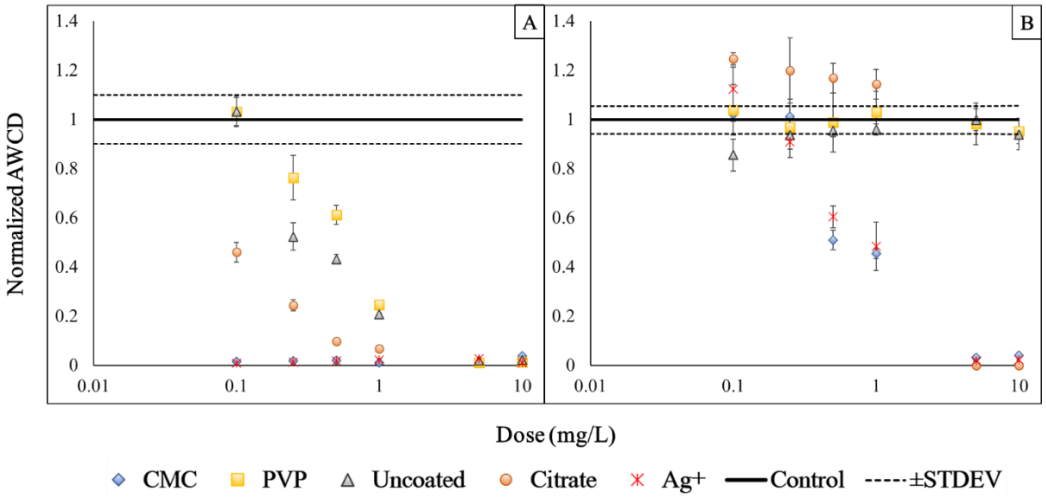

Figure C.2: Dose-response curves for interstitial microbial communities from aerated (A) and non-aerated (B) treatment wetlands. Data points are the means ± standard deviation of triplicate measurements from a single plate. All AWCD data has been normalized their respective control system, which is presented by the solid black line. Hashed lines represent ±1 standard deviation from the average control AWCD. The x-axis is represented in the log scale.

In comparison, the toxicity observed in the non-aerated microbial communities was considerably lower than their aerated counterparts due to the limited dissolved oxygen content (Figure C.2B; Table C.4). While there was a similar trend of decreasing catabolic activity with increasing Ag concentration, this only was observed for the CMC-coated Ag-ENMs and Ag^+ spiked microbial communities. Complete inhibition of the non-aerated microbial communities was not observed for Ag^+ and CMC-coated Ag NPs until a concentration of 10 mg Ag/L compared to 0.1 mg Ag/L in the aerated systems. Moreover, little to no effect was observed from citrate stabilized, uncoated, and PVP-coated Ag-ENMs. Instead, a mild positive effect was observed from the citrate-stabilized Ag-ENMs, which is attributed to the microbial communities' ability to metabolize the citrate coating as an additional source of carbon (Weber and Gagnon, 2014).

The large effect observed by CMC-coated particles is likely an artifact of the synthesis process and residual ionic silver that remains in solution. Schneider (2015) used the same particles for their ecotoxicity screening of Canadian soils and natural wetlands. The author found similar effects between Ag^+ and CMC-coated Ag-ENMs; however complete inhibition was observed to begin at the much lower concentrations of 0.1 mg Ag/L and 0.5 mg Ag/L for Ag^+ and CMC-coated Ag-ENMs, respectively. This may imply an increased resistance to silver in the CW microbial community versus those from a natural wetland.

Based on these results, PVP-coated Ag-ENMs were selected as the pristine nanomaterial for the *in-situ* experiment as they were observed to have the slowest rate of inhibition of the aerated microbial communities that could be tracked over a long-term experimental study in comparison to incidentally released Ag-ENMs.

C.2 Concentration Method Development

Researchers have noted that the quantity of weathered Ag-ENMs released from commercial products tend to be too small to achieve large volumes of high concentrated suspensions. Previous studies have found that Ag-ENMs released from textiles reach, on average, approximately 2 mg Ag/L in a total volume of no more than 0.3-L of tap water (Gagnon et al., 2019; Kulthong et al., 2010; Mitrano and Nowack, 2017). Additionally, successive washings of the same textile showed a sharp decline in the amount of silver released compared to the initial wash. This low yield has proved to be a crucial limitation on the scale at which realistic weathered silver nanomaterials are used in ecotoxicological research (Nowack and Mitrano, 2018).

Freeze-drying or lyophilization, is a process by which water is removed from a frozen sample by sublimation and desorption under vacuum. It has often been employed in nanotechnology to improve the long-term stability of nanomaterials by transforming the suspension into a shelf-stable solid without introducing impurities (Abdelwahed et al., 2006). This process occurs in three stages: controlled freezing, primary drying, and secondary drying. Ice sublimation occurs during primary drying and water is desorbed under secondary drying (Pikal and Tang, 2004). However, for larger scales, depending on the capabilities of the freeze-dryer, this process can take weeks to achieve the amount of Ag-ENMs needed.

Dialysis is a common technique used for the purification of nanomaterial or protein suspensions, but has rarely been thought of in the context of concentrating low nanomaterial content suspensions (Harcum, 2008; Sapsford et al., 2011). By using a high molecular weight polymer solution, osmotic stress can be applied to another solution contained in a semi-permeable membrane. The pressure difference will cause the water to displace across the membrane into the polymer solution until it reaches equilibrium concentrating the in-bag suspension (Kim et al., 2017; Martin et al., 2006). This work endeavoured to develop a method using dialysis to increase the concentration of the weathered Ag-ENM in a reliable and efficient manner while maintaining the original nanomaterial characteristics.

C.2.1 Dialysis Procedure

The dialysis methodology for the weathered nanomaterials was modified from Vauthier et al. (2008), in which the authors applied dialysis in concentrating pristine pharmaceutical nanoparticles. Three fresh W-Ag-ENM solutions were prepared following the as protocol in Section 5.3.2.2. A total of 30 mL of each nanomaterial suspension was added in to a 0.3 m section of dialysis tubing (FisherSci Regenerated Cellulose Membrane, MWCO 12,000-14,000) and sealed, in triplicate. The bag was then submerged in a 100 mL of a 100 g/L solution of polyethylene glycol (PEG, MW 20, 000). The dialysis was performed at room temperature in a 0.5-L rectangular basin. Dialysis bags were removed at either 17h or 24h and the final solution was re-suspended in 5 mL of DI water. The solution was probe sonicated (Fisherbrand™ Model 505 Sonic Dismembrator) at 20 kHz for 60 seconds prior to characterization. Concentration factors (C_f) were calculated as the ratio of the initial and final concentrations of the W-Ag-ENM suspension.

C.2.2 Nanomaterial Characterization

Total silver concentration, size distribution and average median particle size were determined through ICP-MS and spICP-MS in triplicate for each run (as detailed in Section 5.3.3) to characterize both pre- and post-dialysis nanomaterial suspensions. Additionally, complementary size distribution analysis was performed using serial filtration/ICP-MS (0.5 um, 0.45 um, 0.2 um, and 10 kDa) to compare to previous studies (Mitrano et al., 2014). Scanning electron microscopy with energy dispersive x-ray fluorescence (SEM/EDX) was used to compare pre- and post-dialysis Ag-ENM morphology (Quanta FEG 250 and EDAX Octane Elite, ThermoFisher Scientific, OR, USA) in environmental mode at 100 Pa. Nanomaterial suspensions were pooled together for each run and collected via vacuum filtration onto a 0.025 nm cellulose filter, which was then mounted on the SEM sample holder stub with carbon tape for analysis.

C.2.3 Results

Table C.2 presents the characteristics of the nanomaterial suspensions before and after dialysis for each run. The dialysis method proved to be successful at consistently achieving high concentration factors, 30-40, within a 24-h period across all 3 runs. Between the 17h and 24h time points there was only a slight improvement in C_f, indicating that the osmotic equilibrium may not have been reached. Despite this, it is recommended that an earlier retrieval time point should be selected as the dialysis bag had flattened and folded over by 17h, which could have impeded the process.

Table C.2: Nanomaterial suspension characteristics pre- and post-dialysis concentration

Concentration (mg Ag/L)			
	Run 1	*Run 2*	*Run 3*
Total Dialysis Duration (h)	17	24	24
Original Wash	3.6 ± 0.1	5.2 ± 0.3	1.65 ± 0.2
Post-Dialysis	117.4 ± 10.8	201.5 ± 8.2	56.7 ± 33.3
C_f	32	38	34
Average Median Size (nm)			
Original Wash	57 ± 9	-	83 ± 2
Post-Dialysis	55 ± 4	-	73 ± 6

Over the same time period, the average median size of the suspensions determined showed no significant change from the dialysis method only a slight shift smaller size. The complementary size filter fractionation, performed on Run 2 and Run 3, using successive MW cut-off filters shows that the dialysis method was able to completely remove the ionic silver fraction (<0.001 um) leaving only particulate Ag in suspension for both runs (Figure C.3A). As a result, when processing the spICP-MS data any interference of the ionic silver fraction

is removed, which, in turn, lowered the method cut-off of ~60 nm to ~50 nm. The 1-200 nm fraction, i.e. the nanomaterials, showed a relatively similar proportion accounting for up to 47% of the particles in both the pre- and post-dialysis suspensions. It should be noted that Mitrano et al. (2014) found that this technique underestimated the smaller particulate Ag-ENMs as roughly 50% of Ag was lost across the filter skewing the proportions towards large particles. While the size-distribution determined through spICP-MS showed a similar result with no major shifts after dialysis (Figure C.3B, C), the majority of particles (>70%) were observed to between 50-100 nm with few larger particles compared to the filter fractionation. For spICP-MS, as Ag-ENMs travels through the instrument, corresponding peaks are detected from the brief interactions of the plasma with the small amount ions from the particle (Laborda et al., 2014). It is assumed each peak represents a single particle and the intensity of each peak is proportional to the elemental mass. A fundamental limitation of this highly sensitive technique is the dwell time (duration of the peak) that is milliseconds in length (Mozhayeva and Engelhard, 2020). Any interruption can cause coincident particles that would create bias in the final results and, as such, should be paired with complimentary techniques such as SEM.

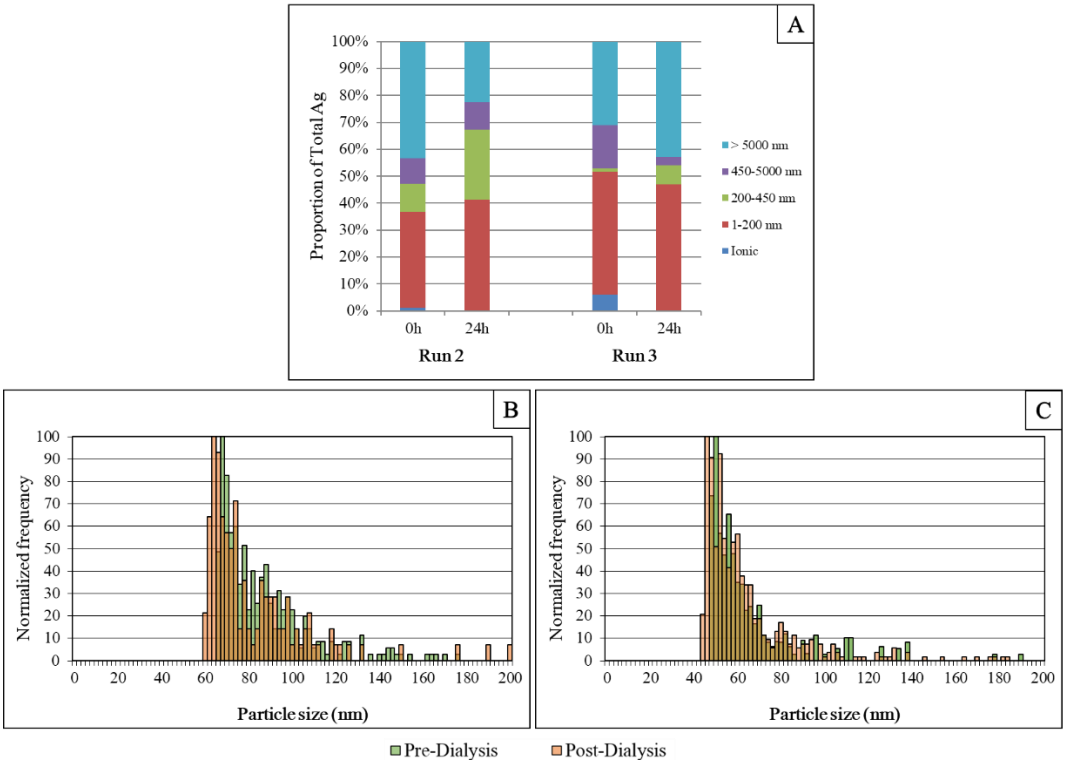

Figure C.3: Size distribution of Ag ENMs suspensions pre-and post-dialysis through (A) serial filtration for Run 2 and Run 3; (B) spICP-MS for Run 3; and (C) spICP-MS for Run 1.

Similar to Gagnon et al. (2019), SEM images of pre-dialysis nanomaterial suspensions showed that the incidentally nanomaterial suspensions are comprised of a mix of ionic silver, nanoplates, spherical nanoparticles and irregular nano-aggregates (images not shown). Following dialysis, the wide variety of morphologies and sizes distributions were not observed to change from the parent suspension (Figure C.4). Even as the osmotic pressure forcing particles closer together, little to no aggregation was observed in the SEM images in line with the results of Vauthier et al. (2008) with respect to pristine nanoparticles. Across all runs, nanoplates were microns in length and width, but had an average thickness of 85.2 ± 30.8 nm.

Compared to other "dewatering" techniques, such as freeze-drying, dialysis proved to be a highly efficient and reliable method to concentrate the incidentally released Ag-ENMs through the removal of water from the suspension while retaining the same relative size and morphology throughout the process. Based on these results, this experiment was scaled-up to dialyzed W-Ag-ENMs suspensions for Phase II-B of the exposure.

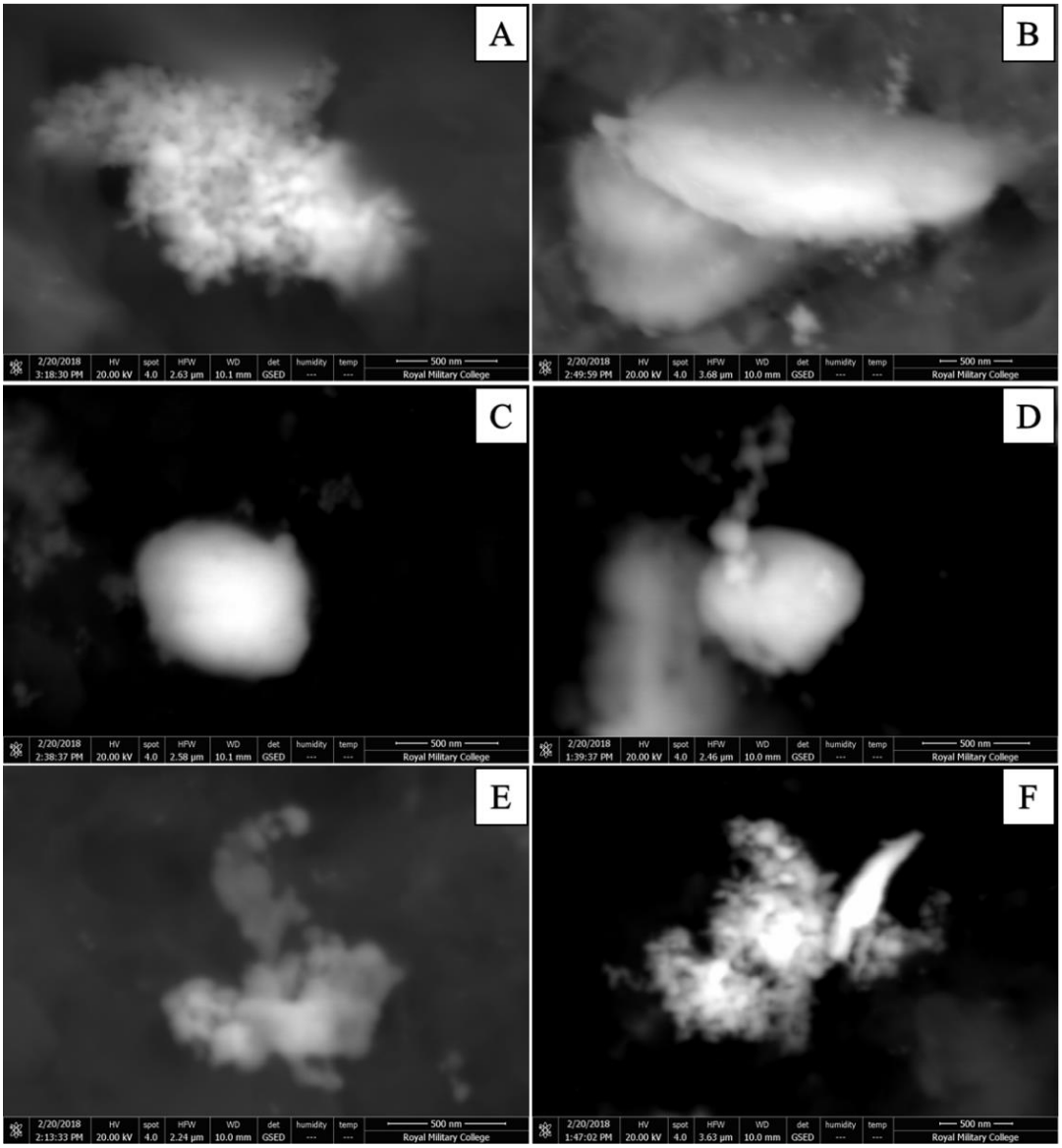

Figure C.4: Representative SEM imaging of released silver nanomaterials post-dialysis including nanosheets (A.B); spherical particles (C,D); nanoaggregates (E,F)

C.3 Materials and Methods

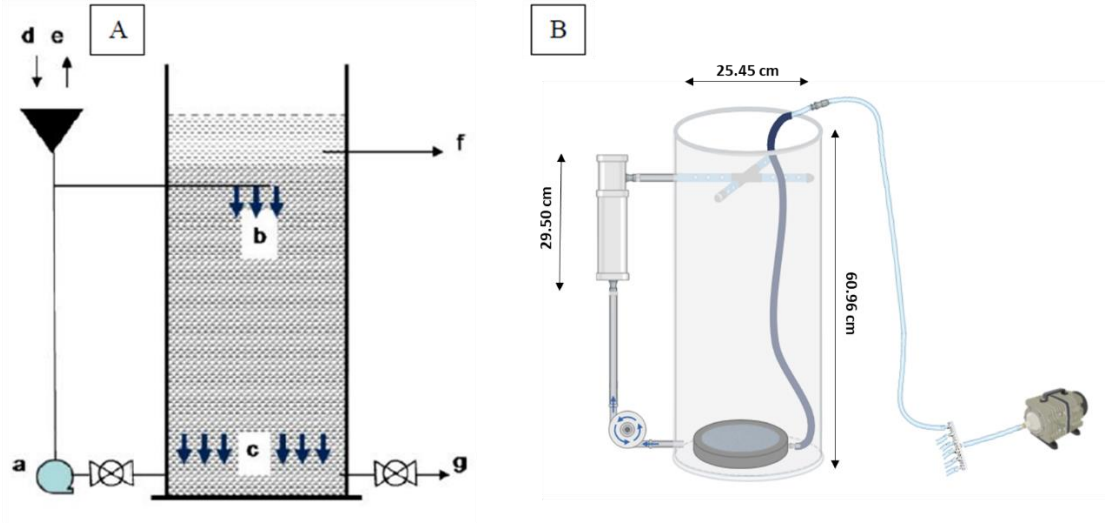

Figure C.5: (A) Mesocosm schematic: Water is continuously circulated by the pump (a) and distributed into the mesocosm (b) water flows vertically through the mesocosm and is collected at the bottom (c). A port has been affixed to the mesocosm near the water inlet. **(B)** Biorender of the mesocosm detailing the build with aeration stone.

Figure C.6: Full set-up of planted TW mesocosms

C.3 Supplemental Results

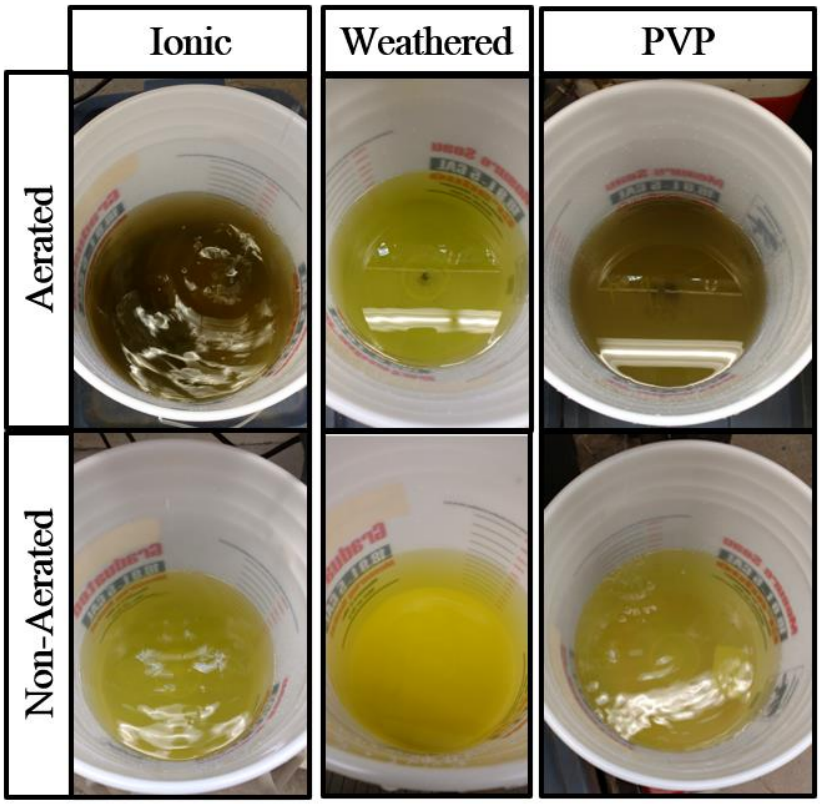

Figure C.7: Representative effluent images from TW mesocosms during Phase I

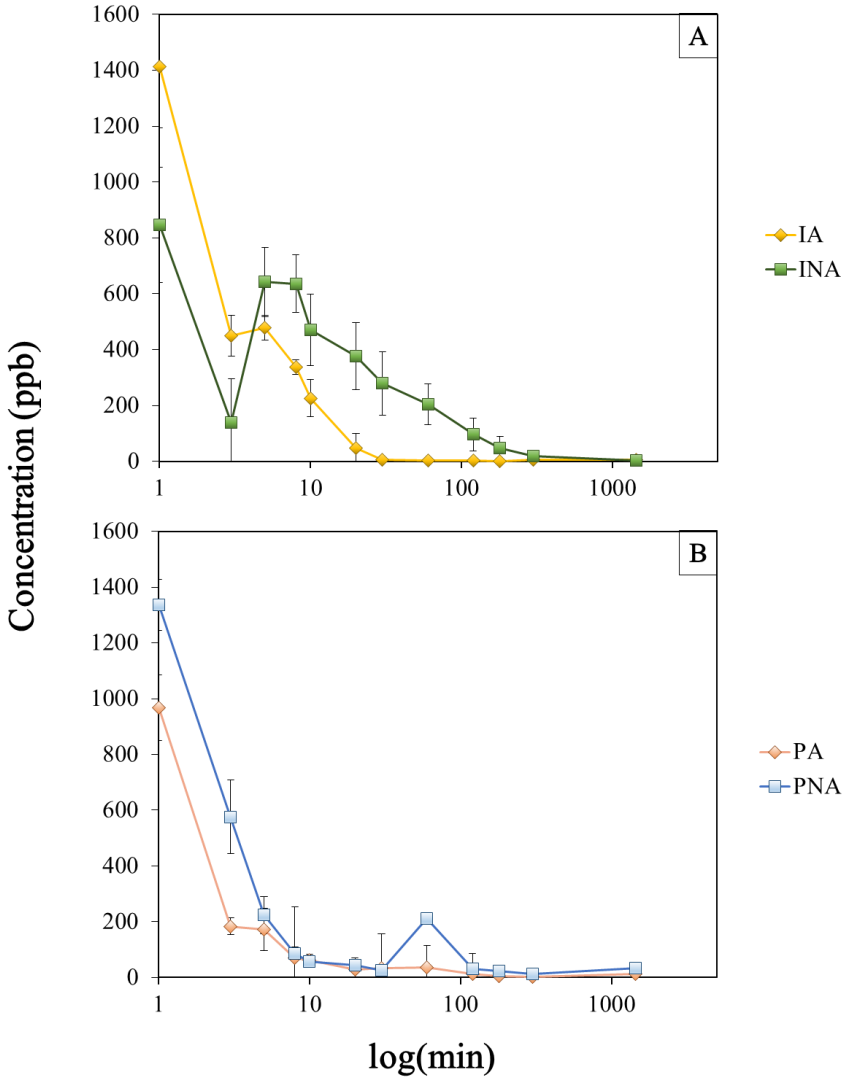

Figure C.8: Average silver concentration in treatment wetland mesocosm amended with (A) ionic silver, (IA= ionic aerated, INA = Ionic Non-Aerated); and (B) PVP-coated Ag-ENMs (PA=PVP aerated, PNA=PVP Non-Aerated) in Phase II. Data points are represented as means ± standard deviation (n=4)

Table C.3: Physicochemical characteristics of TW mesocosms under 0.1 mg Ag/L exposure. Data is presented as mean ± standard deivations of bi-weekly measurements (n=42 per treatment)

Treatment	T (°C)	ET (L/d)	pH	EC (uS/cm)	DO (mg/L)	TOC (mg/L)	TN (mg/L)	NH_4 (mg/L)	NO_3 (mg/L)	ORP (mV)
Influent	20.6 ± 5.4	-	7.0 ± 0.3	786.3 ± 102.5	6.3 ± 1.7	244.4 ± 43.7	63.2 ± 10.5	9.6 ± 3.6	56.4 ± 12.5	156.6 ± 77.1
Aerated - Day 4										
CA	22.7 ± 1.5	0.3 ± 0.1	7.5 ± 0.2	710.7 ± 43.7	7.4 ± 1.2	9.1 ± 2.4	37.9 ± 10.8	3.4 ± 1.5	34.3 ± 10.8	98.8 ± 42.0
PA	22.8 ± 1.7	0.3 ± 0.1	7.5 ± 0.2	707.0 ± 50.7	7.2 ± 1.5	9.7 ± 3.6	39.9 ± 10.5	3.4 ± 1.6	36.2 ± 10.5	97.4 ± 45.4
IA	22.8 ± 1.6	0.3 ± 0.1	7.5 ± 0.1	708.1 ± 45.9	6.8 ± 1.3	10.2 ± 5.9	41.0 ± 8.2	3.4 ± 1.6	37.2 ± 8.1	96.0 ± 41.1
WA	22.6 ± 1.6	0.4 ± 0.1	7.6 ± 0.2	703.5 ± 45.9	7.0 ± 1.1	10.8 ± 3.6	35.0 ± 12.9	3.3 ± 1.6	31.3 ± 13.2	96.9 ± 42.7
Non-Aerated - Day 4										
CNA	22.6 ± 1.6	0.5 ± 0.2	6.9 ± 0.1	712.6 ± 55.8	0.1 ± 0.2	14.0 ± 4.3	2.8 ± 2.5	2.7 ± 2.2	0.2 ± 0.5	-194.1 ± 52.5
PNA	22.8 ± 1.7	0.5 ± 0.2	6.9 ± 0.1	718.6 ± 61.7	0.1 ± 0.1	14.4 ± 4.0	3.9 ± 3.3	3.4 ± 2.6	0.5 ± 1.7	-195.3 ± 50.6
INA	22.7 ± 1.6	0.6 ± 0.3	6.9 ± 0.1	704.1 ± 59.6	0.1 ± 0.2	13.5 ± 4.3	3.2 ± 3.1	2.7 ± 2.5	0.6 ± 1.6	-187.7 ± 46.0
WNA	22.5 ± 1.6	0.6 ± 0.2	7.0 ± 0.1	708.0 ± 53.9	0.1 ± 0.2	17.5 ± 6.1	2.6 ± 2.2	2.2 ± 1.8	0.3 ± 0.9	-184.9 ± 45.7

Table C.4: Physicochemical characteristics of TW mesocosms during Phase II-A following recovery period. Data is presented as mean ± standard deivations of bi-weekly measurements (n=15 per treatment)

Treatment	T (°C)	ET (L/d)	pH	EC (uS/cm)	DO (mg/L)	TOC (mg/L)	TN (mg/L)	NH_4 (mg/L)	NO_3 (mg/L)	ORP (mV)
Influent	26.5 ± 1.6	-	7.5 ± 0.1	913.1 ± 96.12	5.0 ± 1.0	316.3 ± 31.4	78.6 ± 7.5	13.5 ± 1.7	61.0 ± 9.1	165.4 ± 74.6
Aerated - Day 4										
CA	21.3 ± 2.3	0.3 ± 0.1	8.5 ± 0.1	688.4 ± 94.5	7.4 ± 0.9	18.4 ± 17.5	45.6 ± 10.4	5.6 ± 0.6	39.9 ± 10.7	157.9 ± 48.2
PA	21.3 ± 2.4	0.3 ± 0.1	8.3 ± 0.1	717.8 ± 82.8	6.0 ± 1.1	29.7 ± 19.5	44.4 ± 18.2	5.7 ± 0.3	38.6 ± 18.1	157.5 ± 48.1
IA	21.0 ± 2.3	0.3 ± 0.1	8.3 ± 0.2	688.8 ± 103.8	7.0 ± 1.2	16.3 ± 8.1	42.5 ± 10.9	6.1 ± 0.2	36.4 ± 10.7	159.1 ± 49.7
WA	21.1 ± 2.3	0.3 ± 0.1	8.1 ± 0.5	751.8 ± 85.9	7.2 ± 1.1	27.6 ± 18.2	49.6 ± 12.3	6.1 ± 0.1	43.5 ± 12.4	158.1 ± 49.4
Non-Aerated - Day 4										
CNA	21.7 ± 2.3	0.7 ± 0.2	7.5 ± 0.1	710.8 ± 62.9	0.1 ± 0.1	13.3 ± 6.2	3.1 ± 2.8	3.1 ± 2.8	B.D.L.	-52.2 ± 46.1
PNA	21.4 ± 2.4	0.5 ± 0.1	7.3 ± 0.1	739.2 ± 68.4	0.1 ± 0.2	28.4 ± 8.4	4.5 ± 3.3	4.5 ± 3.3	B.D.L.	-140.8 ± 21.6
INA	21.3 ± 2.5	0.6 ± 0.2	7.4 ± 0.1	728.1 ± 55.7	0.2 ± 0.2	16.5 ± 6.6	3.1 ± 2.5	3.1 ± 2.5	B.D.L.	-48.9 ± 52.9
WNA	21.3 ± 2.4	0.5 ± 0.1	7.4 ± 0.1	712.8 ± 27.3	0.2 ± 0.2	19.1 ± 16.3	4.4 ± 3.4	4.3 ± 3.2	0.1 ± 0.2	-98.9 ± 63.8

Table C.5: Physicochemical characteristics of TW mesocosms during Phase II- B under 1 mg Ag/L exposure. Data is presented as mean ± standard deviations of bi-weekly measurements (n=12 per treatment)

Treatment	T (°C)	ET (L/d)	pH	EC (uS/cm)	DO (mg/L)	TOC (mg/L)	TN (mg/L)	NH_4 (mg/L)	NO_3 (mg/L)	ORP (mV)
Influent	25.6 ±6.7	-	7.7 ± 0.1	855.3 ± 126.6	5.3 ± 1.6	268.5 ± 30.6	58.6 ± 3.41	11.9 ± 1.4	47.7 ± 3.5	187.9 ± 15.5
Aerated - Day 4										
CA	21.5 ± 1.8	0.3 ± 0.1	8.5 ± 0.1	692.2 ± 32.6	7.5 ± 0.4	7.6 ± 1.5	35.7 ± 9.0	3.5 ± 2.7	30.4 ± 9.2	201.8 ± 21.5
PA	21.3 ± 1.8	0.3 ± 0.1	8.3 ± 0.1	648.5 ± 66.6	6.1 ± 1.5	16.8 ± 17.9	40.0 ± 3.6	3.6 ± 2.7	34.6 ± 3.4	206.7 ± 10.6
IA	21.4 ± 1.8	0.3 ± 0.1	8.4 ± 0.2	665.4 ± 55.3	6.5 ± 0.9	10.4 ± 6.0	39.9 ± 6.7	3.6 ± 2.7	34.5 ± 6.8	198.9 ± 24.1
WA	21.0 ± 2.0	0.3 ± 0.1	8.6 ± 0.2	630.2 ± 86.0	7.5 ± 0.3	36.2 ± 16.4	4.2 ± 5.2	1.3 ± 1.9	2.1 ± 3.3	199.2 ± 16.4
Non-Aerated - Day 4										
CNA	21.6 ± 1.8	0.7 ± 0.2	7.5 ± 0.0	715.8 ± 43.6	0.2 ± 0.1	10.7 ± 3.8	0.9 ± 0.4	0.6 ± 0.6	B.D.L.	-44.5 ± 50.1
PNA	21.6 ± 1.7	0.6 ± 0.1	7.3 ± 0.1	704.6 ± 61.4	0.2 ± 0.1	12.7 ± 9.0	2.3 ± 1.8	1.5 ± 1.9	B.D.L.	-83.4 ± 28.6
INA	21.7 ± 1.8	0.6 ± 0.1	7.5 ± 0.1	684.7 ± 39.7	0.2 ± 0.1	9.5 ± 2.5	0.9 ± 0.8	0.6 ± 0.8	B.D.L.	-37.2 ± 51.5
WNA	21.7 ± 1.8	0.5 ± 0.1	7.3 ± 0.1	734.0 ± 72.4	0.2 ± 0.1	113.3 ± 53.4	2.6 ± 1.0	1.7 ± 1.6	B.D.L.	-100.1 ± 24.3

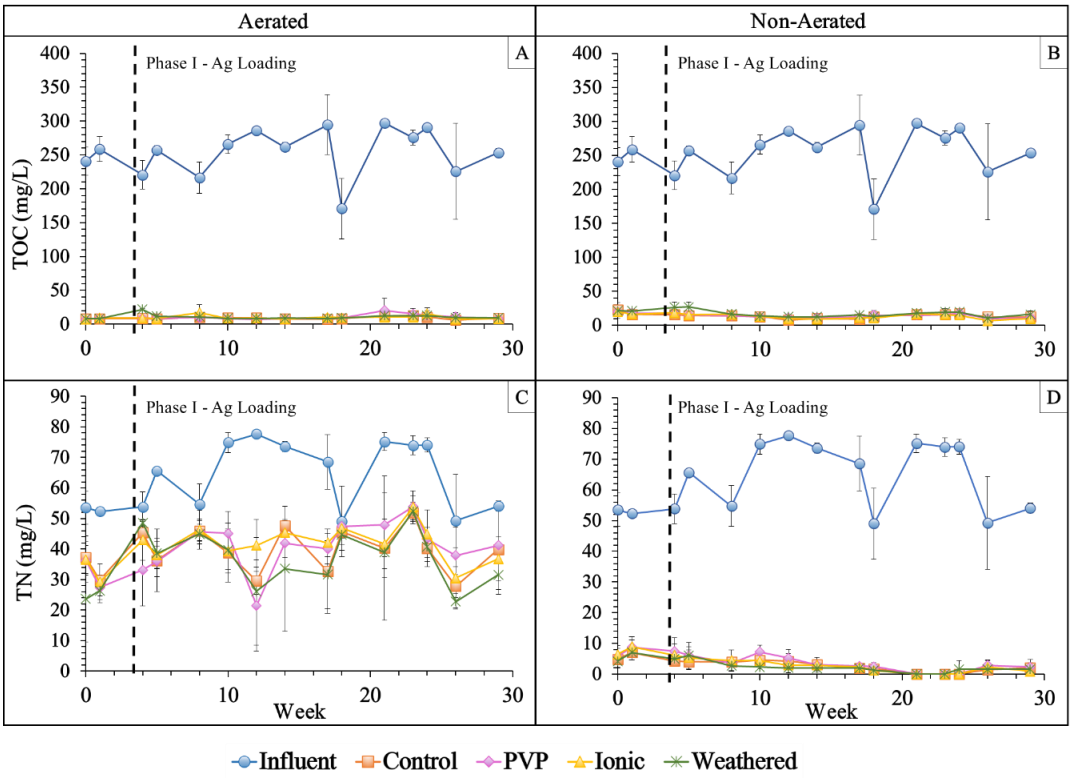

Figure C.9: Average TOC and TN influent and *in-situ* Day 4 concentration in Aerated (A,C) and Non-aerated (B,D) systems during Phase I. Data points are presented as means ± standard deviation, n = 3.

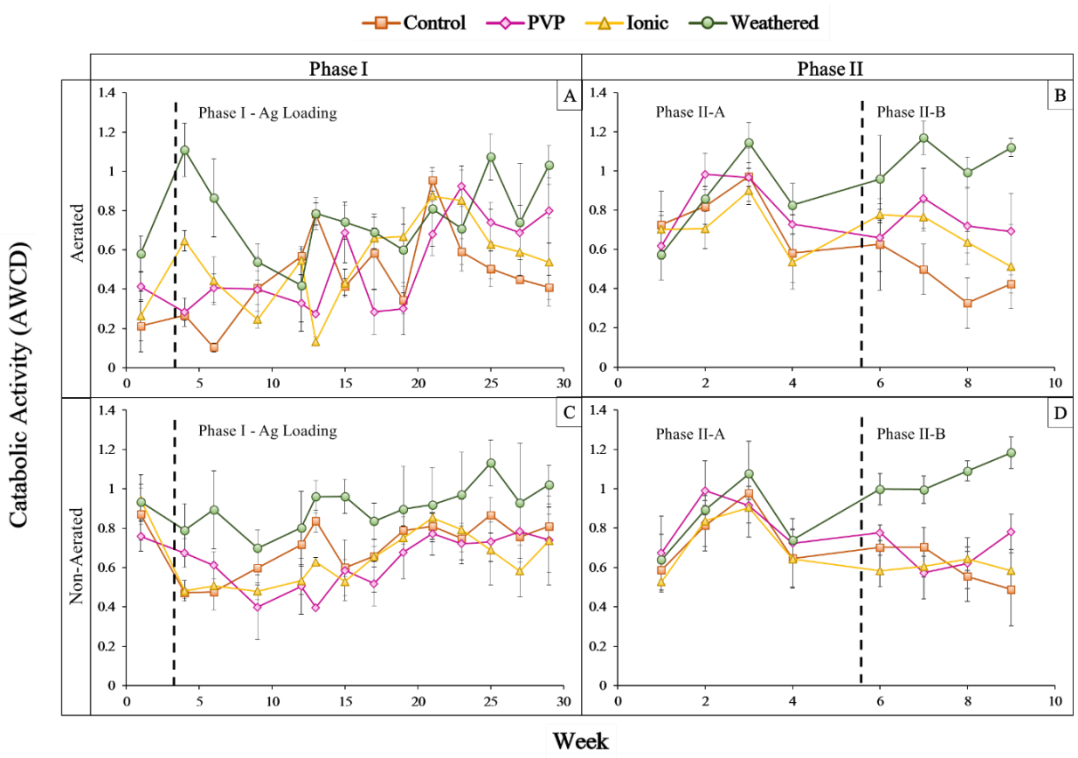

Figure C.10: Weekly catabolic activity (measured as average well colour development) of Phase I (left) and Phase II (right) for the aerated (A, B) and non-aerated (C, D) systems. Data points are means ± standard deviation (n=3).

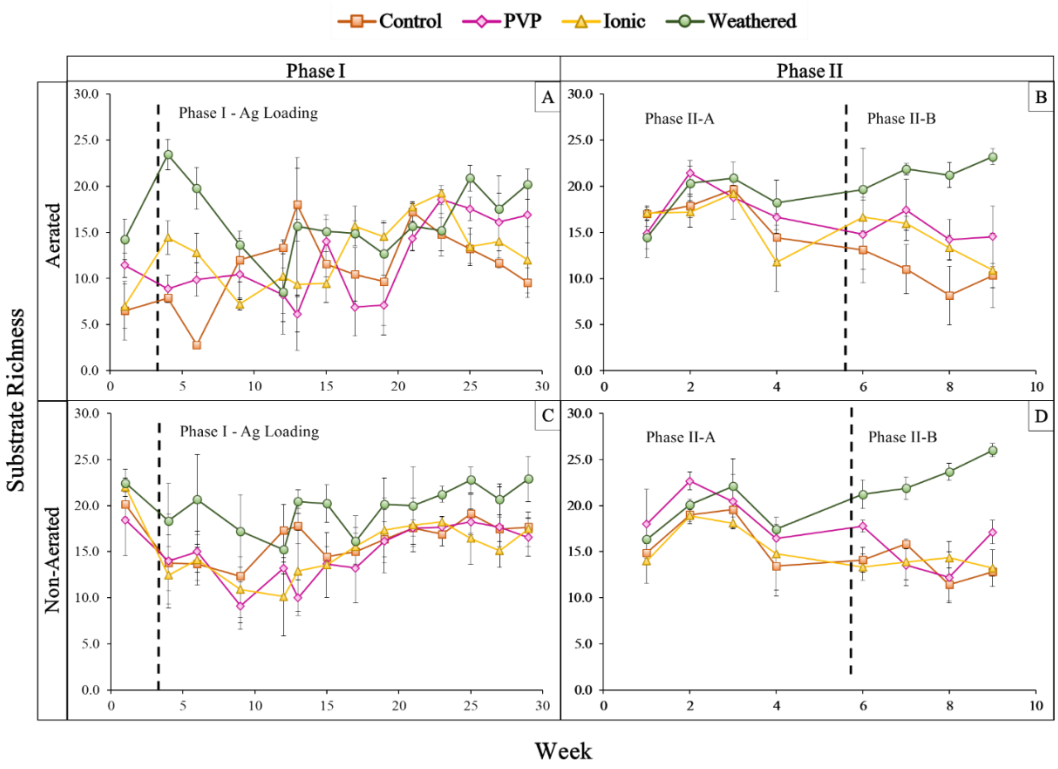

Figure C.11: Weekly substrate richness of Phase I (left) and Phase II (right) for the aerated (A, B) and non-aerated (C, D) systems. Data points are means ± standard deviation (n=3).

Table C.6: Numbers of rRNA sequences analyzed, and the alpha diversity indices measured for microbial populations at the start and end of Phase I and Phase II. Values are averages from replicate systems (n=3).

Treatments	Week	Raw reads	Effective reads [(a)]	Normalized reads	Microbial richness (OTU)	Microbial diversity (Shannon index)
Phase I						
CA	3	71987	29045	8000	880	8.06
	27	76093	24301	8000	536	6.87
PA	3	74519	30589	8000	781	7.50
	27	55044	18708	8000	513	6.82
IA	3	90988	38042	8000	820	7.52
	27	74845	22161	8000	669	7.43
WA	3	95812	34762	8000	825	7.56
	27	78795	33223	8000	616	6.98
ANOVA	Between systems (p-value)				NS	NS
CNA	3	73992	29266	8000	379	6.30
	27	77495	31554	8000	423	6.38
PNA	3	101379	38832	8000	466	6.52
	27	69922	29456	8000	396	5.78
INA	3	63503	24966	8000	354	5.84
	27	73426	30737	8000	411	6.16
WNA	3	63230	21486	8000	354	5.77
	27	50545	19012	8000	339	5.69
ANOVA	Between systems (p-value)				NS	NS
Phase II						
CA	1	61744	22646	10000	643	7.23
	9	625568	174739	10000	1093	7.94
PA	1	94515	28591	10000	647	6.99
	9	91618	37932	10000	899	7.70
IA	1	63435	18227	10000	682	7.29
	9	66810	26881	10000	735	7.96
WA	1	85438	29692	10000	742	7.39
	9	121441	40927	10000	903	7.50
ANOVA	Between systems (p-value)				NS	NS
CNA	1	68265	28262	10000	527	6.46
	9	125358	50280	10000	773	6.92
PNA	1	102137	33646	10000	750	6.80
	9	78952	31503	10000	709	6.56
INA	1	71627	22268	10000	650	6.91
	9	93026	33447	10000	777	7.05
WNA	1	578938	228458	10000	889	7.29
	9	120170	42020	10000	795	6.86
ANOVA	Between systems (p-value)				NS	NS

(a) Low-quality reads and chimaera removed

D. Appendix D

Supplemental Information

The functional and structural shifts from addition of incidentally released silver nanomaterials in planted treatment wetland mesocosms

Anbareen J. Farooq[†], Dani Damasceno Silvera[§], Sarah Wallace[†], David Patch[†], Denis O'Carroll[‡], and Kela P. Weber[†*]

[†]Environmental Sciences Group, Department of Chemistry and Chemical Engineering, Royal Military College of Canada, Kingston, ON K7K 7B4, Canada

[‡]School of Civil and Environmental Engineering, UNSW Water Research Laboratory, University of New South Wales Sydney, Manly Vale, NSW, 2093, Australia

[§] University of Santa Catarina (UFSC), Campus Universitário, Trindade, CEP 88040-900. Florianópolis, SC, Brazil. daniele.ds@posgrad.ufsc.br

*Corresponding author: kela.weber@rmc.ca

Table D.1: Carbon source guild groupings for community level physiological profiling. Highlighted carbon sources were identified as root exudates based on the following references: (1) Badri and Vivanco, (2009), (2) Campbell et al. (1997), and/or (3) Willig et al. (2000).

No.	Carbon source	Guild	Reference for root exudates
0	water (blank)	N/A	N/A
1	pyruvic acid methyl ester	carbohydrates	
2	Tween 40	polymers	
3	Tween 80		
4	α-cyclodextrin		
5	glycogen		
6	D-cellobiose	carbohydrates	
7	α-D-lactose		
8	β-methyl-D-glucoside		
9	D-xylose		Reference (1) and (2)
10	i-erythritol		N/A
11	D-mannitol		Reference (1) and (2)
12	N-acetyl-D-glucosamine		N/A
13	D-glucosaminic acid	carboxylic and acetic acids	
14	glucose-1-phosphate	carbohydrates	
15	D-, L-α-glycerol phosphate		
16	D-galactonic acid-γ-lactone	carboxylic and acetic acids	
17	D-galacturonic acid		
18	2-hydroxy benzoic acid		Reference (1) and (2)
19	4-hydroxy benzoic acid		Reference (2) and (3)
20	γ-hydroxybutyric acid		N/A
21	itaconic acid		
22	α-ketobutyric acid		
23	D-malic acid		Reference (1) and (2)
24	L-arginine	amino acids	Reference (2) and (3)
25	L-asparagine		
26	L-phenylalanine		
27	L-serine		
28	L-threonine		
29	glycyl-l-glutamic acid		N/A
30	phenylethylamine	amines/amides	
31	putrescine		

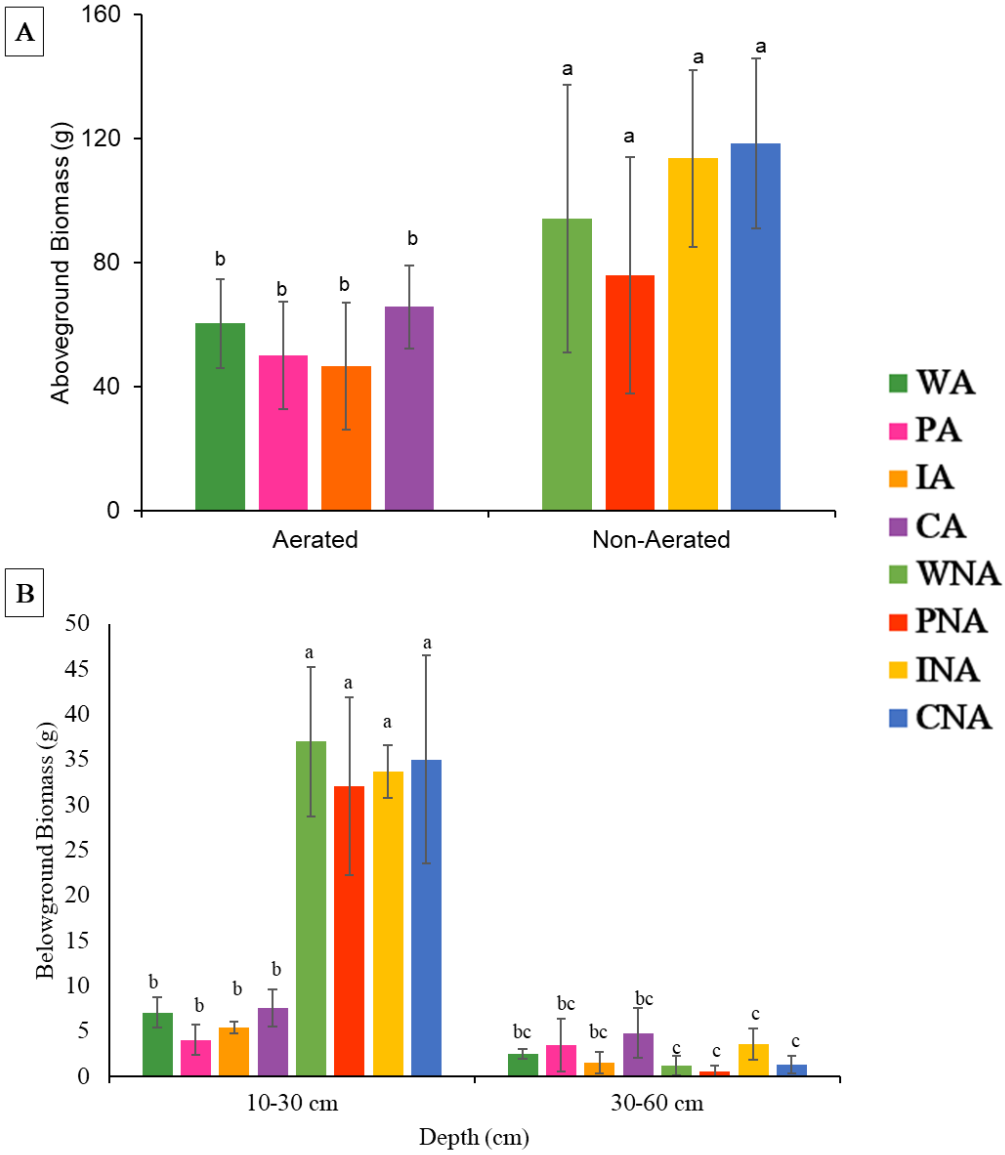

Figure D.1: Total plant biomass harvested from both aboveground (A) and belowground (B) regions of the TW mesocosms. Statistical different grouping identified through a post-hoc Tukey test were noted using different letters ($p<0.05$). Data points presented as means standard deviation (n=3 for the silver treatments and n=2 for the controls).

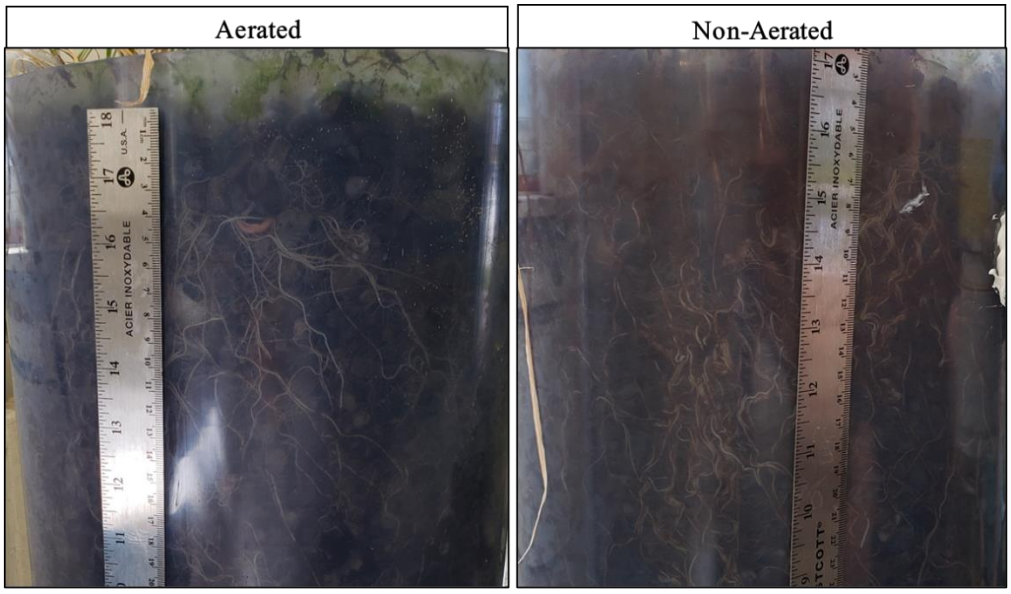

Figure D.2: Images of roots in aerated (left) and non-aerated (right) systems prior to deconstruction.

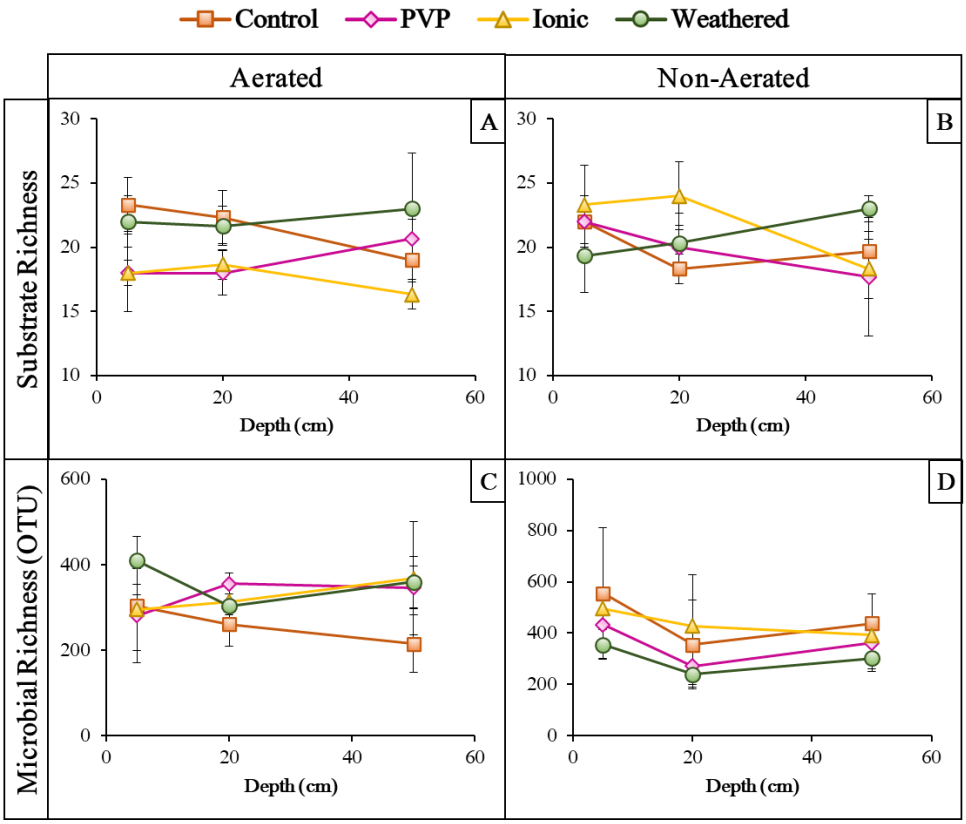

Figure D.3: Depth profile of the functional and structural microbial richness for the gravel-associated biofilm for the aerated (A,C) and non-aerated (B,D) systems. Data points presented as means standard deviation (n=3 for the silver treatments and n=2 for the controls for replicate systems).

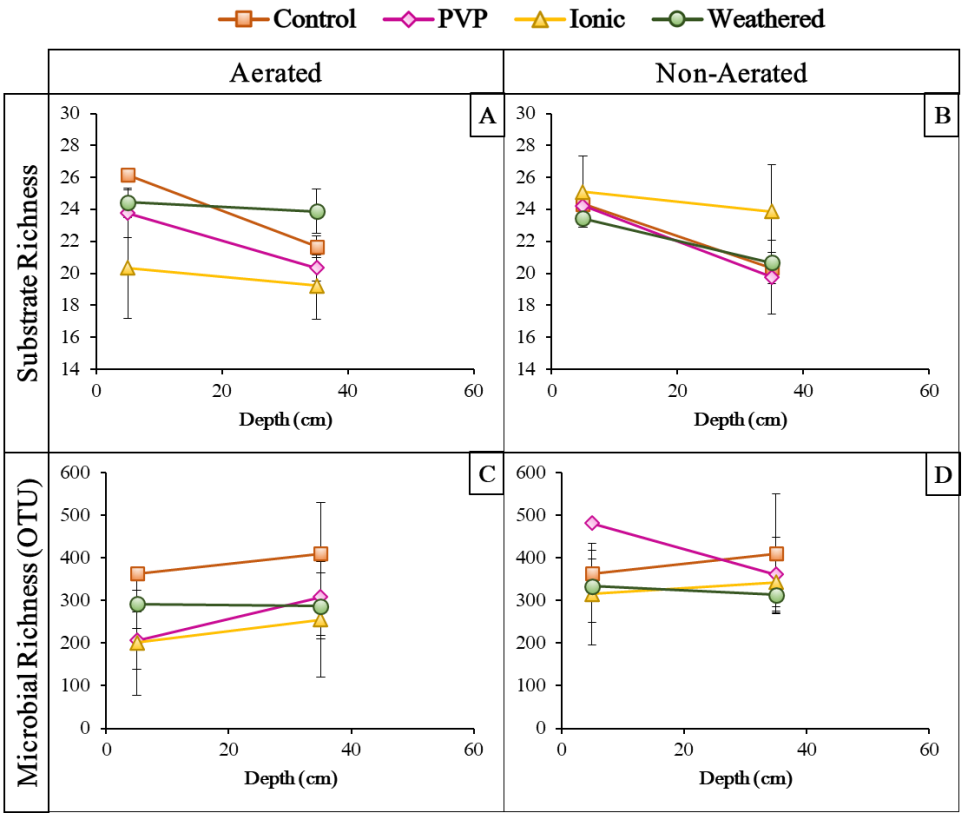

Figure D.4: Depth profile of the functional and structural microbial richness for the rhizopheric-associated biofilm for the aerated (A,C) and non-aerated (B,D) systems. Data points presented as means standard deviation (n=3 for the silver treatments and n=2 for the controls for replicate systems).

Table D.2: Average numbers of rRNA sequences analyzed, and the alpha diversity indices measured for microbial populations. C= control, P = PVP, I=ionic, W=weathered for the different silver treatments is combined with A=aerated or NA=non-aerated and G= gravel-associated biofilm or R= rhizospheric biofilm to denoted the specific system. The number following the treatment abbreviation denotes the respective depth the sample was collected.

Treatments	Raw reads	Effective reads [(a)]	Normalized reads	Microbial richness (OTU)	Microbial diversity (Shannon index)
CA-G-1	54510	28457	7000	304	7.13
CA-G-2	48548	26507	7000	262	6.74
CA-G-3	37815	18430	7000	216	6.58
IA-G-1	56851	31394	7000	296	6.91
IA-G-2	80282	39241	7000	314	6.89
IA-G-3	75017	39680	7000	369	7.30
WA-G-1	88108	45050	7000	410	7.58
WA-G-2	57999	29360	7000	304	7.17
WA-G-3	56149	29158	7000	360	7.56
PA-G-1	45510	24902	7000	282	7.02
PA-G-2	68335	37144	7000	355	7.18
PA-G-3	62538	34515	7000	347	7.26
CNA-G-1	129060	66129	7000	556	8.00
CNA-G-2	66433	35119	7000	356	7.07
CNA-G-3	75970	41891	7000	438	7.57
INA-G-1	67742	37926	7000	495	8.10
INA-G-2	84672	49289	7000	428	7.44
INA-G-3	61918	33885	7000	393	7.50
WNA-G-1	49013	27022	7000	355	7.52
WNA-G-2	47498	23668	7000	239	6.74
WNA-G-3	48812	26852	7000	302	7.05
PNA-G-1	70250	38683	7000	434	7.76
PNA-G-2	42418	21555	7000	272	6.91
PNA-G-3	58540	30051	7000	362	7.42
CA-R-1	83114	45237	7000	342	7.22
CA-R-2	57948	27087	7000	269	6.77
IA-R-1	60022	30901	7000	201	5.94
IA-R-2	41210	22009	7000	256	6.58
WA-R-1	74609	40255	7000	292	7.04
WA-R-2	49687	27247	7000	287	6.97
PA-R-1	46169	23401	7000	207	6.19
PA-R-2	98414	50902	7000	308	6.82

CNA-R-1	52504	28938	7000	364	7.46
CNA-R-2	64446	36375	7000	411	7.45
INA-R-1	57339	31073	7000	315	6.93
INA-R-2	65260	34089	7000	343	7.15
WNA-R-1	50492	27913	7000	333	7.36
WNA-R-2	50841	28756	7000	313	7.09
PNA-R-1	88947	49160	7000	482	7.73
PNA-R-2	63823	32662	7000	362	7.20
ANOVA	Between systems (p-value)			NS	NS

(a) Low-quality reads and chimaera removed

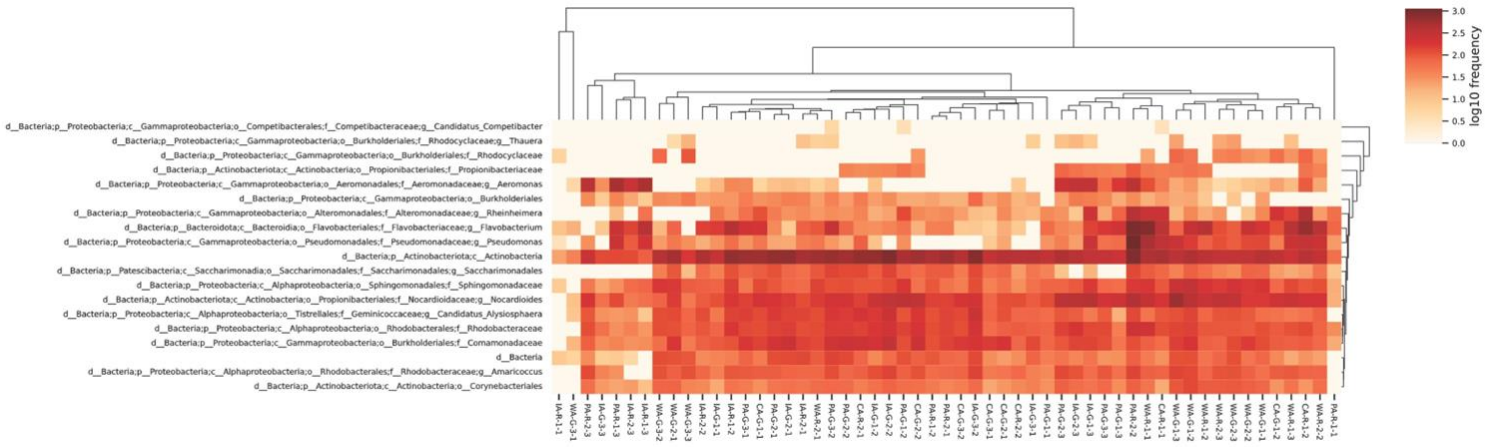

Figure D.5: Taxonomy of the top 20 most abundant genera grouped based on the average Bray-Curtis distance metric for the aerated systems. The bottom corresponds to the weekly individual mesocosms where C= control, P = PVP, I=ionic, W=weathered for the different silver treatments is combined with A=aerated or NA=non-aerated and G= gravel-associated biofilm or R= rhizospheric biofilm to denoted the specific system. The number following the treatment abbreviation denotes the respective depth the sample was collected.

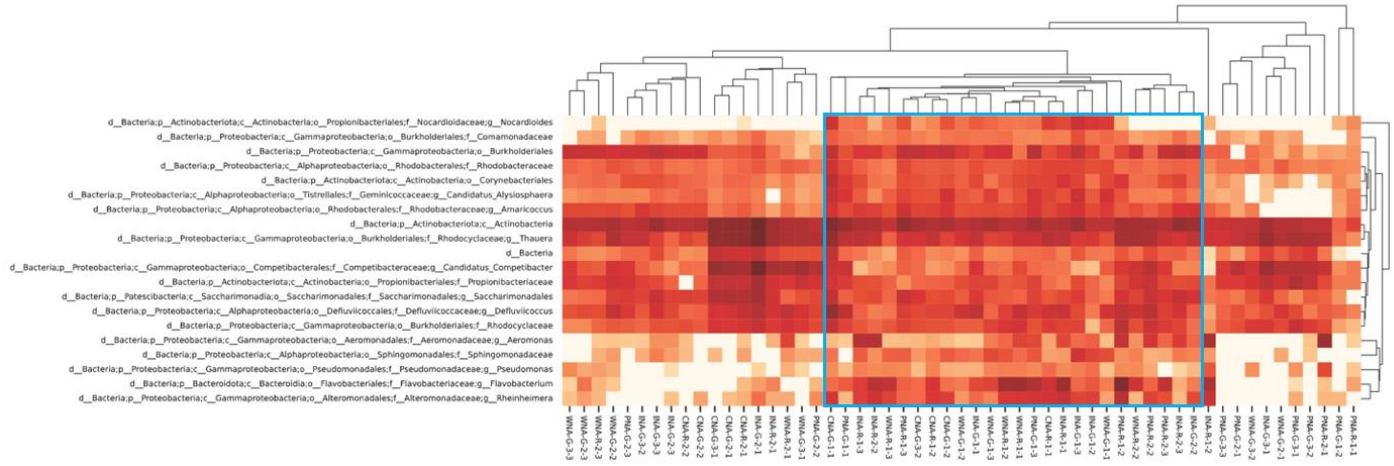

Figure D.6: Taxonomy of the top 20 most abundant genera grouped based on the average Bray-Curtis distance metric for the aerated systems. The bottom corresponds to the weekly individual mesocosms where C= control, P = PVP, I=ionic, W=weathered for the different silver treatments is combined with A=aerated or NA=non-aerated and G= gravel-associated biofilm or R= rhizospheric biofilm to denoted the specific system. The number following the treatment abbreviation denotes the respective depth the sample was collected. *the blue box denotes the samples from the top 0-10cm.

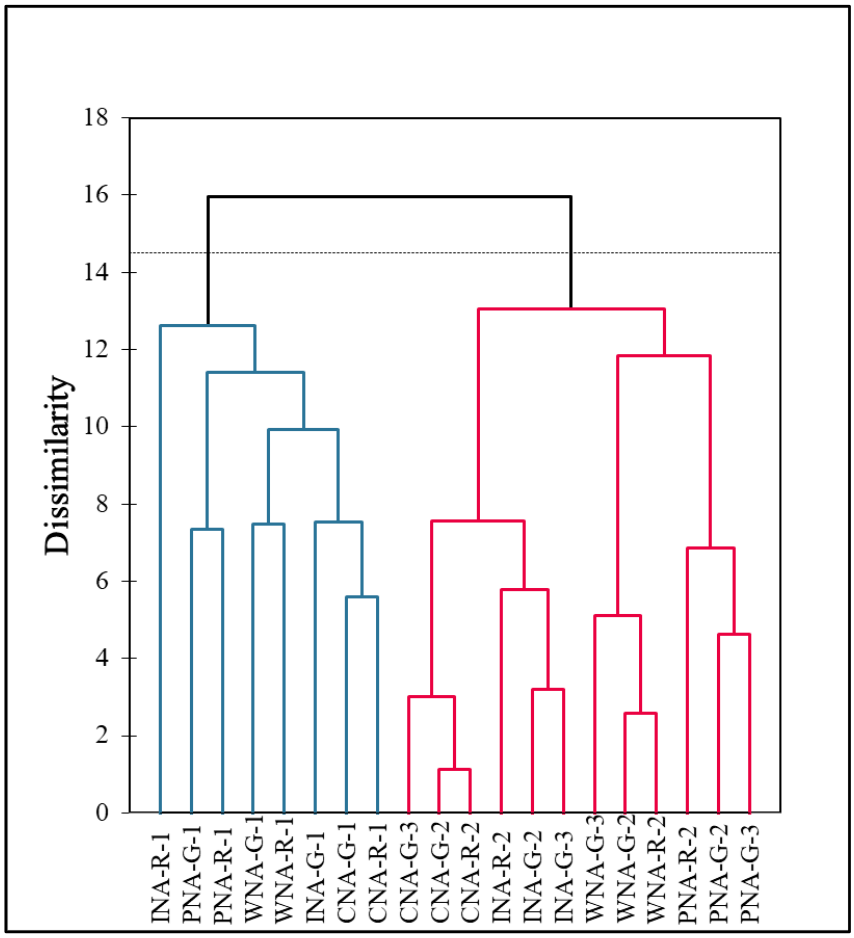

Figure D.7: Agglomerative hierarchical clustering analysis dendrogram of non-aerated genera abundance data. C= control, P = PVP, I=ionic, W = weathered for the different silver treatments is combined with A=aerated or NA=non-aerated to denoted the specific system and G= gravel-associated biofilm or R=rhizospheric biofilm to denote the specific system. The number following the treatment abbreviation denotes the respective sample the sample: 0-10 cm (1), 10-30 cm (2); 30-60 cm (3).